Titulo: Development of design specifications for strengthening deteriorated concrete bridge elements using externally applied FRP sheets.
Estudiante: Alfredo Maria Ceci.
Tutor: Prof. Joan Ramon Casas.

El refuerzo flexional de vigas en hormigon armado con FRP (fibre-reinforced polymer) se ha convertido, en la ultima decada, en unos de los metodos mas utilizados para aumentar la resistencia maxima de una estructura. Este fenomeno puede ser dividido en dos grupos: el primero que se manifesta por la presencia de una elevada tension cerca las extremidades del plato de FRP; el otro que esta causado por la formacion de una fisura intermedia en la viga. Para prevenir este fenomeno, muchos autores propusieron modelos para calcular el maximo valor de carga que la viga reforzado puede aguantar.

Este trabajo esta dividido en dos partes. En la primera, se ha estudiado el fenomeno de la despegatura del material compuesto (FRP) desde una viga en hormigon armado. Han sido considerados la manera de fallo llamada “end debonding” y otra conoscida con el nombre de “intermediate crack induced debonding”: tres diferentes database han sido creados reunendo los datos experimentales encontrados en literatura. El primero representa ensayos de hormigon con FRP testados para examinar la despegatura entre FRP y hormigon. El segundo database reunen vigas en hormigon armado que fallan por end debonding. El ultimo incluye diferentes tipologia de experimentos sobre vigas para analizar el fenomeno del intermediate crack induced debonding. Estos datos se han dividido en differentes grupo para analizar la diferencia entre los tipos de materiales y entre las differentes maneras de applicacion.

Se han encontrado diecinueve modelos que analizan la despegatura del FRP desde un ensayo de hormigon. Estos se pueden dividir en tres grupos: los modelos que tienen en cuenta una longitud de anclaje efectiva, los modelos que tienen en cuenta la longitud de ancaje real y los que son independientes de la longitud de anclaje. A través de una comparacion de los valores de bias (valor medio dividido por el valor nominal) y el coeficiente de variacion (COV), se ha demonstrado que los modelos propuestos no son buenos y aplicandolos a las vigas el resultado es aun peor.

Trece modelos han sido utilizados para calcular la carga de fallo por “end debonding” en vigas de hormigon armado renforzados con FRP; estos modelos se pueden dividir en tres grupos: modelos que tienen en cuenta la capacidad ultima a cortante de la viga, modelos que tienen en cuenta dientes de hormigon y modelos que analizan el comportamiento tensional entre FRP y hormigon. No todos los modelos desarrollan hipotesis mecanicas. Los modelos que consideran la capacidad ultima a cortante de la viga utilizan un sistema de calibraccion utilizando database de datos y esto puede dar una valutaccion no correcta de la carga de fallo. En muchos casos los autores no querian dar una exsata valutacion de la carga ultima, sino dar un valor seguro, es decir un valor analitico mas pequeno de lo experimental. Colotti et al. propuso un modelo, desarrollando hipotesis mecanicas, que permite de evaluar diferentes maneras de fallo que pueden interesar una viga con renfuerzo. El modelo que da los mejores valores de bias y coeficiente de variacion es lo de Casas y Pascual que tiene en cuenta interaccion entre hormigon, resina y FRP. La mayoria de los modelos no consideran importante el comportamiento de la resina y por eso mucho autores no dan informaciones sobre eso. Una ventaja del modelo de Casas y Pascual es que se puede utilizar para analizar el fenomeno del “intermediate induced debonding” tambien. Para convalidar la bondad del modelo, han sido coleccionados experimentos de vigas que fallan para “intermediate crack induced dedonding. El modelo de Casas y Pascual ha sido comparado con el modelo de Wu y Niu y se ha demonstrado como el primer modelo sea el mejor.

En la segunda parte del trabajo,se ha desarrollado la calibracion de factores de seguridad para utilizarlos en el proyecto de renfuerzos de viga en hormigon armado. Se han ulitizado diferentes tipologia de puentes, en hormigon armado y en hormigon pretensado, para tener en cuenta la mayoria de las estructuras en España. A través de la simulaccion de Monte Carlo, se han calibrado los factore de seguridad para obtener un indice de fiabilidad igual a 3,5 para un tiempo de proyecto de 50 años. Analizando los datos, se ha decidido de dividir la analisis en dos partes: los factores de seguridad para los puentes reforzado con fibras de carbono aplicadas en obra y puentes reforzado con fibras de carbono aplicadas con platos prefabricados.

Title: Development of design specifications for strengthening deteriorated concrete bridge elements using externally applied FRP sheets.

Student: Alfredo Maria Ceci.

Thesis Advisor: Prof. Joan Ramon Casas.

Bonding of a fibre-reinforced polymer (FRP) plate to the tension face of a beam has become a frequent strengthening method in the last decade. A large number of studies reported premature failures by debonding of FRP plates from the RC beams. These can be classified into two type: those associated with high interfacial stresses near the ends of the bonded plate; and those induced by a flexural or flexural-shear crack away from the plate ends. To prevent these phenomena, several models has been proposed to determine the maximum tensile load in FRP at failure.

This work was divided into two steps. In the first part, it was studied the phenomenon of debonding in RC beams reinforced with FRP plates. The end debonding failure mode and intermediate crack-induced debonding failure mode were taken into account: three different databases were created collecting the data from the available tests. The first one represents the concrete prism specimens tested in order to study the end debonding failure mode. The second database collects the flexural beam tests, four point bending test, done to study the behavior of FRP reinforcement at the end of plate. The last database which includes four point bending tests, three point bending tests and one point loading tests has been created to examine the intermediate crack-induced debonding. These data were divided in different groups to study the difference between each material and applied methodology.

Were found nineteen models based on the prism tests. These can be divided in three groups: the models considering effective bond length, models not considering the effective bond length and models independent of effective bond length. Basing the comparison on the values of bias (the ratio of the mean to the nominal value) and coefficient of variation (COV), it was demonstrated that the models proposed are not very good, and applying then to the beam tests the results made worse. To predict the failure load in the RC beams reinforced with FRP, thirteen models were found divided into three groups: shear capacity based models, concrete tooth based models, interfacial stress based models. Not all models are based on mechanical criteria. The shear capacity based models were calibrated on a particular database and could give a incorrect prediction for RC beams outsides these databases. In many case the authors did not want to predict correctly the load of failure, but put all data in the safe side with an analytical load lower than the experimental. Colotti et al. proposed a model based on mechanical criterion that predicts different modes of failure for the RC beam strengthened. The model which gave the best values of bias and coefficient of variation (COV) is the Casas and Pascual model considering the interaction between FRP, the resin and the concrete. Not many authors based their models on the interfacial behavior and a restricted number of beam tests presents information on the resin's characteristics. One of the advantage of Casas and Pascual model is that it can be used to predict the intermediate crack-induced debonding too. To test the goodness of the model for this mode of failure, beam tests failed for intermediate crack-induced debonding were collected. Casas and Pascual model was compared with Wu and Niu model and the first one results better to predict the phenomenon.

In the second part of this work, the calibration of partial safety factors to be used in the design of strengthening with CFRP was carried out, taking into account some real structures. Different typologies of bridges, reinforced and postensioned concrete were considered, in order to cover the most common structural schemes found in Spanish roadways. Trough the Monte Carlo simulation were calibrated the safety factor to obtain a reliability index equal to \$3,5\$ for a time design of 50 years. Was decided to separate the analysis into two groups: safety factors for bridges reinforced with carbon wet lay-up and carbon prepeg sheets.

Acknowledgements

First of all I would like to express my sincerest gratitude to Prof. Joan Ramon Casas for his guidance and expertise in an experience of a thesis abroad; the proposed theme, his availability and his patience towards my continuous doubts and requests were fundamental for the good outcome of this academic and human experience. I hope I have met all his expectations.

I would like to thank Prof. Michel Ghosn, who, during his stays in Barcelona, has given me wise suggestions in order to improve and complete the last part of my work. The time spent together gave me the opportunity to reflect and develop new ideas and hypothesis.

If I was given the possibility to do my thesis abroad I owe it to Prof. Mario Paolo Petrangeli. He was an important point of reference for me in Rome and helped me in identifying which professor I should to contact.

I wish to thank all the professors and the students with whom I had the pleasure to exchange views ad opinions; particularly my friend Stefano Ballerini with whom I shared all my doubts, disappointments, joys, courses, projects, exams, entire days and nights at the university.

I would also like to thank my family for giving me the possibility and the serenity to conduct my studies and follow my academic interests, supporting me during difficult moments without ever expecting more than I could give.

Albert and Monica gave me invaluable human support during these months. I knew I could count on them day by day and they represented my family while I was away from home. During this experience I cannot forget Joan for the many days spent together at the library and Patrice who actually represented for me a small portion of Rome in Barcelona.

Contents

Chapter 1

Introduction and objective

1.1 History of FRP

While bricks of mud and straw have been used in construction for thousands of years, modern composites have emerged as a construction material just in the past 50 years. In the early 1900's, scientists increased their experimentation and development of innovative new materials. Invented originally by accident by Owens-Corning ("Fibreglass"), FRP research was then encouraged heavily by the defense industry during World War II. Used heavily in aerospace and naval applications, their high strength-to-weight ratio and excellent corrosion resistance created numerous advantages for their use. In the decades to follow, FRP materials flourished in the aerospace, marine, electrical, automotive, sporting, and corrosion-resistance industries. After some experimentation using composites as reinforcement in concrete structures in the 1950's, the usage of FRPs in the construction industry experienced a revival in the 1980's. In 1986, the world's first highway bridge using composite reinforcing tendons was built in Germany, and in 1991 the first FRP bridge repair took place in Switzerland. Since then, FRP bridge decks, FRP-prestressed concrete bridges, and all-FRP bridges have been constructed around the world.

1.2 FRP system

FRP materials are essentially composite materials that consist of strong fibres set in a resin matrix. The fibres (usually glass, carbon or aramid) generally carry the bulk of the applied loads in the system, providing strength and stiffness in their longitudinal direction. Meanwhile, the resin matrix (generally epoxies, polyesters, vinyl esters or phenolics) bonds the fibres together and to the surface on which they are being applied. The matrix also acts to transfer stresses between the individual

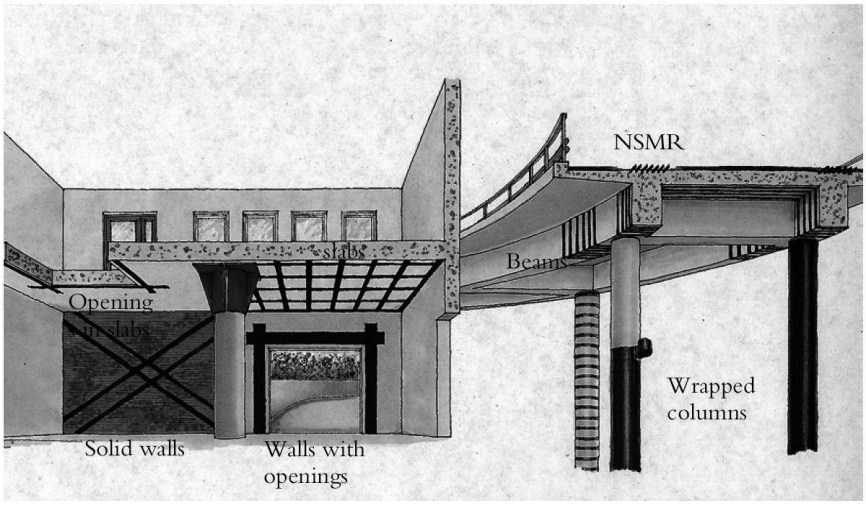

Figure 1.1: Applied FRP to structural elements (from Sas, 2008 [47]).

fibres, thus providing a more desirable distribution of stresses, while protecting the fibres from the environment and abrasion. The emergence of FRPs in the civil engineering industry has been driven by their numerous advantages over steel and concrete, including: high strength-to-weight ratio, resistance to corrosion, light weight & flexibility (easy installation), electromagnetic neutrality (GFRP and AFRP), low thermal conductivity (GFRP and AFRP).

Despite their outstanding benefits, many in the construction industry have been somewhat reluctant to accept them into everyday use, citing various disadvantages such as cost, brittle failure, and susceptibility to high temperatures. While their higher initial material costs may detract consumers, their longer lifespan means that their life-cycle costs are comparable to some of the traditional construction materials. FRPs are sometimes avoided due to their brittle behavior, experiencing sudden and explosive failure modes which are undesirable in structures. While this may be the case, the failure strain of FRP is larger than the yielding strain of steel, providing additional warning to those using the structure. Their susceptibility to high temperatures and fire has hindered their use for enclosed structures, which is why the majority of their use to date has occurred in bridges and other outdoor applications. Finally, many in the structural engineering field have been hesitant to use FRPs because they are either unfamiliar with how to use them, or they feel as though there is a lack of knowledge regarding their long-term durability. With large amounts of research having taken place over the past 20 years, and with the results looking promising, it may just be a matter of time before the construction

community is compelled to accept these new products.

1.2.1 Sheet system

The typical sheet system consists of epoxy primer, putty, dry or preimpregnated fibre and a resin system. The installation is preceded by the concrete surface preparation as described above. The primer is applied afterwards and in case of large unevenness the putty is used to level the surface. The following step involves the application of a thin layer of low viscosity epoxy adhesive to the concrete surface. The carbon fibre sheet is rolled and easily stretched over the impregnated surface. The possible air voids from the contact area are removed with the help of a roller and a new layer of adhesive is applied. The sheets used usually have a width of $200 - 400mm$ and a weight of $200 - 400g/m^2$. The most used sheets are made of unidirectional fabrics but bi-directional weaves are also used. Because sheets can be modelled to almost any geometrical shape they can be used for rounded sections or where full wrapping is needed.

1.2.2 Laminate system

The laminate systems have the following components: primer, adhesive and a composite laminate. While the primer can be similar to the one used for the sheet system and has the role of enhancing the bond of the adhesive to the concrete surface, the adhesive is different. Here, a high viscosity filled paste is used such as epoxy adhesive applied in a thickness of 1-2 mm. The laminates have a thickness of 1.2 mm and can be obtained in different widths: 50, 70, 100, 150 mm or other requested dimensions. Theoretically the length can be unlimited but for practical reasons such as transport or handling they are distributed in pieces not longer than 20 m. The installation of the laminate system is less time consuming than the sheets system and involves the application of the primer, followed by the application of the adhesive on the laminate with a slightly thicker thickness in the longitudinal axes. The next step is to apply the laminate on the surface (usually with a roller) with enough pressure that the adhesive thickness has a constant thickness over the entire surface. This system is appropriate for flat surfaces such as beams, walls and slabs.

1.3 Flexural Strengthening with FRPs

As previously stated, FRP sheets and plates have proven to be an excellent material for strengthening and rehabilitating in-situ concrete. In applications with concrete beams, the fabric or plate is simply bonded to the tensile face of the beam using an epoxy adhesive. This application of FRP to the tension face of a concrete beam

or slab has multiple benefits, including: increased service and ultimate flexural capacity, increased post-cracking stiffness, finer and more evenly distributed cracks.

It is clear that flexural strengthening of reinforced concrete beams has a great deal of potential, however, in order to be used more confidently by the civil engineer, a more complete understanding of the behavior of the strengthened beam needs to be acquired.

Crucial to this understanding are the modes of failure of the beam. Hollaway and Teng [30] proposed that there are six main failure mechanisms for reinforced concrete beams strengthened flexurally with FRPs, as shown in Figure 2-1.

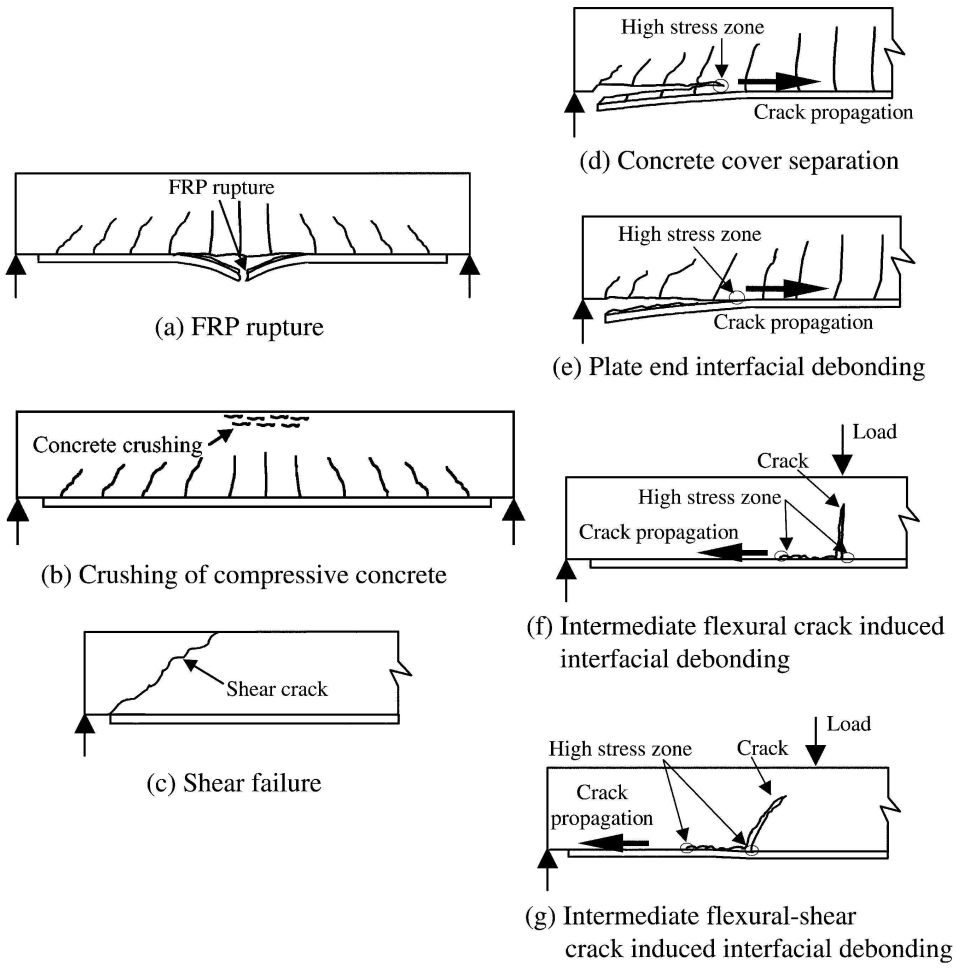

Figure 1.2: Failure modes of RC beams flexurally-strengthened with an FRP soffit plate (from Teng et al., [58]).

Failure modes 1-3 are somewhat similar to those experienced by unstrengthened beams, while modes 4-6 are specific to FRP strengthened beams and are considered premature failure modes. It is generally desirable to achieve FRP rupture or concrete crushing, given that the materials would be used to a greater degree of their potential. As a result, there has already been considerable research done on how to predict and avoid premature failure, especially the debonding failure modes (5) and (6). With added research, improved epoxy resins used for bonding, and innovative methods to provide mechanical anchorage for the FRP, engineers are learning how to avoid these premature failures in their strengthened beams.

With an increasing amount of experimentation and testing having taken place on reinforced concrete beams strengthened with FRPs, there have been various efforts to amalgamate numerous studies in order to announce some of the generally accepted conclusions. Meanwhile, the majority of the studies also experienced a failure of the beams due to debonding at the concrete-FRP interface. One of the main conclusions was that the research to date had neglected to really look at the strengthening or repair of beams that had been exposed to sustained loading or previous damage. It was also suggested that in order to maintain certain amounts of deformation prior to failure, the quantity of FRP applied should be limited with respect to the internal steel reinforcement and debonding should be avoided with the use of special anchorage details.

Although extensive research has been carried out on the performance of FRP systems an a number of models have been proposed to provide design guidelines for its application, the occurrence of premature debonding failure in which the strengthened member fails before the FRP strips achieve their full tensile strength is unpreventable when significant amount of FRP is used and if no additional restraining measures are taken. Four types of premature failure modes were commonly observed in the experiments on flexurally strengthened members. They are cover separation, plate end interfacial debonding, intermediate (flexural or flexural-shear) crack (IC) induced interfacial debonding, and critical diagonal crack (CDC) induced interfacial debonding. The debonding failure can be generally classified into two types. The first involves high interfacial stresses at the plate end, such as separation and plate end interfacial debonding, and the second is caused by a flexural or flexural-shear crack appearing on the intermediate tension side of the flexural members, such as CDC and IC interfacial debonding.

A number of researchers have attempted to install anchorage at the FRP plate end to delay or prevent plate end debonding failure. A marginal increase in the load capacity was presented in the plated beams with U plate end anchorage compared to those without one.

1.4 Objective

This work presents two different objectives. In the first part it was collected all proposed models used to prevent the phenomenon of debonding of FRP from the RC beams, and they were divided into two groups: the models which predicted the end debonding load and the models which predicted the intermediate crack induced debonding load; applying them to the collected databases it will be compare the goodness of each models and will be find the better one. All models will be compared on the same database, divided the experimental data for kind of material and application methodology, to do a significant statistical analysis and to decide the actual best model. The comparison will be focused on the different behavior between the different material (carbon, glass and aramid) and the two types of application (wet lay-up and prepeg plates). It will be demonstrated that the models could be good or not depending on the group taking into account. In the second part it will be proposed some partial safety factors to apply in concrete bridge elements design. The aim of this calibration, applying the American safety format, is to proposed some safety factors based on a statistical analysis covering a significant range of existing bridge decks. The calibration was done following the Monte Carlo procedure on eight different bridges (four reinforced concrete bridges and four postensioned concrete bridges). In order to determine an appropriate range of geometries to represent the existing strucutres, they were selected bridges having spans ranging from 10m to 56m, continuous and simply supported structures, four different cross sectional shape (girder, slab, box-girder, box-girder built by the balanced cantilever method). The safety factor were calibrated to obtain a reliability index equal to $3,5$ for a time design of 50 years.

Chapter 2

Debonding strength models

2.1 Existing models for bond behavior in plated RC beams

A search of the existing literature has found thirteen debonding strength models. Eight of them have been developed for FRP-plated RC beams in the past few years. Another five models have been developed for plate end debonding occurs either by concrete cover separation or in the concrete adjacent to the adhesive-to-concrete interface. Although the different mechanical properties of the bonded plate are expected to play a significant role, strength models can be expected to be applicable to different types of plates if the geometrical and material properties of plate are properly included. It is thus not unreasonable to expect that models developed for steel plated beams may well be applicable to FRP-plated beams, with modifications if necessary.

The existing debonding strength models can be classified into three categories based on their approaches, as done by Smith and Teng [52, 53]: shear capacity models, concrete tooth models and interfacial stress based model. It is worth noting that all the models developed specifically for FRP-strengthened RC beams follow the interfacial stress based approach. On the other hand, three of the five models specifically developed for steel plated beams follow either the shear capacity approach or a combined approach.

In their paper, Smith and Teng [52], reported eight existing models divided into three groups.

2.1.1 Shear capacity based models

The common feature of these models is that the debonding failure strength is related to the shear strength of the concrete with no or only partial contribution of the steel shear reinforcement. The debonding strength is generally given as the shear force acting at the plate end, with or without taking into account the effect of any coexistent moment. As interfacial stresses between the plate and the beam need not be evaluated, the required calculations are generally simple.

Jansze (1997) [52] proposed a plated end debonding strength model for steel plated beams but the background information to the model is not available to the authors. Only the final form of the model with general comments is available where it is stated that Jansze model [52] was based on the initiation of shear cracking in an RC beam without the contribution of shear reinforcement. The critical shear force in the RC beam at the plate end to cause debonding $V_{db,end}$ is given as follows:

$$V_{db,end} = \tau_{PES} b d \tag{2.1}$$

where $\rho_s = A_s/bd$ is the ratio of steel tension reinforcement, A_s the area of steel tension reinforcement, b the section width and d the effective depth of the section.

$$\tau_{PES} = 0,18 \sqrt[3]{3\frac{d}{B_{mod}}} \left(1 + \sqrt{\frac{200}{d}}\right) \sqrt[3]{100\rho_s f'_c} \tag{2.2}$$

$$B_{mod} = \sqrt[4]{\frac{\left(1 - \sqrt{\rho_s}\right)^2}{\rho_s} d a^3} \tag{2.3}$$

Here, B is the shear span and B_{mod} a modified shear span . If B_{mod} as defined by Eq.2.3 is greater than the actual shear span should be given by $(B_{mod} + B)/2$. Jansze model [52] appears to be invalid for soffit plates terminated at the support as B_{mod} becomes zero and Eq.2.2 predicts that debonding is never possible.

Ahmed and van Germert (1999) [52] modified Jansze model [52] to be suitable for use with FRP-plated RC beams. Ahmed and van Gemert model [52] is given as follows:

$$V_{db,end} = \left(\tau_{PES} + \Delta\tau_{mod}\right) b d \tag{2.4}$$

where:

$$\Delta\tau_{mod} = \tau_{PES} bd \left(\frac{S_s}{I_s b_{frp}} - \frac{S_{frp}}{I_{frp} b_a} \right) + 6188,5 \left(\frac{\tau - 4,121}{bd} \right) \tag{2.5}$$

$$\tau = \left(0,15776\sqrt{f'_c} + \frac{17,2366\rho_s d}{B} \right) + 0,9\frac{A_{sv} f_{sv}}{sb} \tag{2.6}$$

where τ_{PES} is given by the Eq.2.2, S_{frp} and S_s are the first moment of area of the FRP plate, and that of an equivalent steel plate about the neutral axis of a cracked plated section transformed to concrete, where the equivalent steel plate is one that has the same total tensile capacity and width as that of the FRP plate, but with an equivalent thickness determined assuming that the yield stress of steel is $550MPa$, I_{frp} and I_s are the second moments of area of a cracked plated section transformed to concrete with a FRP plate and an equivalent steel plate respectively, and b_{frp} and b_a are the widths of the FRP and adhesive respectively. The stirrup spacing is denoted by s, while A_{sv} and f_{yv} are the cross sectional area and the yield stress of the steel stirrups respectively. For all practical purposes b_a is equal to b_{frp}.

The modification given in Eqs.2.5 and 2.6 appear to rely on determining the difference in the interfacial shear stress between the RC beam and the plate as a result of replacing a steel plate with an FRP plate. This difference $\Delta\tau_{mod}$ is then added to the shear stress τ_{PES} in Eq.2.2 where the shear stress is determined over a fictitious shear span of length B_{mod}. The increase in shear strength offered by the shear reinforcement is also included as seen in Eq.2.6.

2.1.2 Concrete tooth models

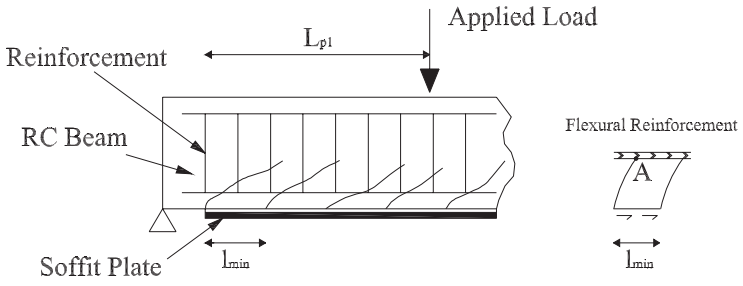

Figure 2.1: Concrete tooth model. Cracked beam and concrete tooth between two adjacent flexural cracks.

Concrete tooth models make use of the concept of a concrete "tooth" between two adjacent cracks deforming like a cantilever under the action of horizontal shear

stresses at the base of the beam (Fig.2.1). Debonding is deemed to occur when these shear stresses lead to tensile stresses at the root of the "tooth" that exceed the tensile strength of the concrete. The stress in the soffit plate at the debonding can then be determined by defining an effective length for the plate for end anchorage over which a uniform shear stress is assumed.

The concept of a concrete tooth was first described in Zhang et al. (1995) [69]. Based on this concept, Zhang et al. [69] and Raoof and Zhang (1997) [42] developed a strength model to predict concrete cover separation failures in steel plated beams. Minimum and maximum crack widths (l_{min} and l_{max} respectively) are determined which lead to lower and an upper bound stress in the plate to cause debonding respectively and the width of these cracks differ by a factor of two ($l_{max} = 2l_{min}$). The minimum width of a crack l_{min}, termed the minimum stabilized cracking spacing, is given by:

$$l_{min} = \frac{A_e f_{ct}}{u(\Sigma O_{bars} + b_{frp})} \tag{2.7}$$

where A_e is the area of concrete in tension, u the steel-to-concrete average bond strength, ΣO_{bars} the total perimeter of the tension reinforcing bars. It is assumed that $u = 0,28\sqrt{f_{cu}}$ (in MPa) and $f_{ct} = 0,36\sqrt{f_{cu}}$ (in MPa) where f_{cu} is the concrete cube compressive strength. For the case of an RC beam with a single layer of steel tension reinforcement, A_e is twice the distance from the centroid of the tension reinforcement to the base of the RC beam multiplied by the width of the RC beam.

Ignoring interaction between adjacent teeth and assuming elastic behavior, the required shear stress to cause failure of a tooth can be determined. Failure of the tooths occurs when the stress at point A (Fig.2.1) exceeds the tensile strength of the concrete. The tensile stress at point A, σ_A, can be determined from

$$\sigma_A = \frac{M_A}{I_A}\left(\frac{I}{2}\right) \tag{2.8}$$

where $M_A = \tau l b_{frp} h'$ and $I_A = b_{frp} l^3/12$. Here, l is the crack spacing (minimum or maximum), h' the net height of concrete cover measured form the based of the steel tension reinforcement to the base of the concrete beam, τ the shear stress at the interface between the concrete and the soffit plate, I_A the second moment of area of the tooth, and M_A the moment at the base of the tooth.

Substitution of M_A and I_A into Eq.2.8 and assuming that at the instant of plate debonding $\sigma_A = f_{ct}$, the shear stress at the interface between the concrete and the steel plate based on a minimum stabilized crack spacing can be determined as

follows. In this tooth theory, all teeth in the end anchorage zone are assumed to fail simultaneously at debonding.

$$\tau_{min} = \frac{f_{ct} l_{min}}{6h'} \frac{b}{b_{frp}}$$

The minimum stress in the soffit plate $\sigma_{s,min}$ required to cause flexural cracking and failure of a tooth covering the minimum stabilized crack spacing can then be determined as follows:

$$\sigma_{s(min)} = 0,154 \frac{L_p h_1 b^2 \sqrt{f_{cu}}}{h' b_{frp} t_{frp} (\Sigma O_{bars} + b_{frp})} \tag{2.9}$$

where L_p is an effective length of soffit plate for end anchorage, and h_1 is the distance from the centroid of the tension reinforcement to the base of the RC beam. This model has been applied only to simply-supported beams subject to three or four point bending, for which the limiting stress or Eq.2.9 was compared to the stress in the soffit plate directly under a point load to check the possibility of debonding. It is not clear how this model should be applied to beams subject to other loading condition (e.g. uniformly distributed load), but it is not unreasonable to choose the section of maximum moment in the beam for an assessment.

In Zhang et al. [69], the effective length for end anchorage was taken as the length of the soffit plate in the shear span (in Fig2.1 this is indicated as L_{p1}). In Raoof and Zhang [42], it was recommended that the effective length for end anchorage be the smaller of the length of the soffit plate in the shear span L_{p1}, and the following length L_{p2} which were calibrated against test data of steel plated RC beams that failed by plate end debonding:

$$L_{p2} = l_{min} \left(21 - 0,25 l_{min}\right) \quad , \quad l_{min} \leq 72mm \tag{2.10}$$

$$L_{p2} = 3 l_{min} \quad , \quad l_{min} > 72mm \tag{2.11}$$

Only the modified effective length for plate end anchorage as proposed by Raoof and Zhang [42] is considered as this is the more recent tooth model derived by this research group for steel plated RC beams.

Once the stress in the plate is known, the moment to cause separation of the plate, at the same location as the stress, can be calculated using a conventional section analysis with the assumption of plane section bending in accordance with Zhang et al. [69] with the tensile strength of concrete taken into account. A lower

and an upper bound bending moment are determined as a consequence of the assumed minimum (l_{min}) and maximum (l_{max}) stabilized crack spacings differing by a factor of two.

For a simply supported beam under four point bending with the plate positioned in the constant moment region, Raoof and Zhang [42] specified that the effective length should be obtained from Eq.2.10 as the length of the plate in the shear span L_{p1} is zero.

Wang and Ling (1998) [52] proposed a modification to Zhang et al. [69] tooth model to make it suitable for FRP strengthened beams. This involved modifying the average bond strength between the concrete and the plate, leading to the following formula for the minimum crack spacing:

$$l_{min} = \frac{A_e f_{ct}}{u_s \Sigma O_{bars} + u_{frp} b_{frp}} \tag{2.12}$$

where $u_s = 0,313\sqrt{f'_c}$ is the average bond strength between the steel tension reinforcement and the concrete and is the same as that used by Zhang et al. (1995) [69] assuming $f'_c = 0,8 f_{cu}$, while u_{frp} is the average bond shear strength between the FRP and the concrete and was taken as 1,96MPa.

Once the minimum stabilized crack spacing is determined the remainder of the analysis is essentially the same as that given in Zhang et al. [69] although the effective length for end anchorage was taken by Wang and Ling to be the total plate length in the shear span. In Wang and Ling model [52], the tensile strength of concrete was not included in the section analysis for relating the bending moment in the beam to the stress in the plate. Similar to the model of Zhang et al. [69], an upper bound solution of Wang and Ling model [52] is obtainable by replacing their minimum crack spacing (Eq.2.12) with a maximum crack spacing which is twice the former.

Raoof and Hassanen (2000) [43] also modified Zhang et al. model [69] for application to FRP plated beams. Two expression were presented by them for the effective length of the FRP plate for end anchorage with two corresponding values for the bond strength between the FRP and the concrete. Two new models thus resulted from these modifications. They are referred to herein as Raoof and Hassanen [43] model I and model II.

In Raoof and Hassanen model I [43], Eq.2.7 is retained to calculate the minimum stabilized crack spacing. The effective length of the FRP plate for end anchorage is taken to be the smaller of the plate length in the shear span (L_{p1} in Fig.2.1) and the following lengths which were calibrated which test data of FRP plated RC beams reported to have failed by plate end debonding:

$$L_{p2} = l_{min}(1,16 - 0,17l_{min}) \quad , \quad l_{min} \leq 56,5mm \tag{2.13}$$
$$L_{p2} = 4l_{min} \quad , \quad l_{min} > 40mm \tag{2.14}$$

In Raoof and Hassanen model II [43], the bond strength between the FRP plate and the concrete is specified as $0,8MPa$, while the bond strength between the steel tension reinforcement and the concrete is still the same as that originally specified in Zhang et al. [69]. The effective length of the FRP plate for end anchorage is defined as the smaller of the plate length in the shear span and the following lengths which were calibrated with test data of FRP plate RC beams reported to have failed by plate end debonding using the new value of FRP to concrete bond strength:

$$L_{p2} = l_{min}(11,6 - 0,17l_{min}) \quad , \quad l_{min} \leq 56,5mm$$
$$L_{p2} = 2l_{min} \quad , \quad l_{min} > 56,5mm$$

Once stabilized crack spacing and the effective length of FRP plate for end anchorage are determined, the remainder of the analysis is the analysis is the same as that given in Zhang et al. [69].

2.1.3 Interfacial stress based models

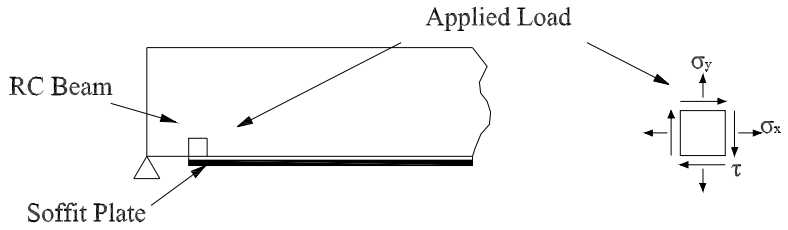

Figure 2.2: Stresses acting on a concrete element adjacent to the plate end.

A popular and logical assumption is that concrete cover separation or plate end interfacial debonding is due to high interfacial stresses at the end of the soffit

plate. Fig.2.2 shows the stresses acting on an element of concrete adjacent to the end of the adhesive layer where τ and σ_y denote the shear and transverse normal (peeling) stresses respectively while σ_x is the longitudinal stress. Interfacial stress based debonding strength models generally make use of interfacial stresses from an existing closed form solution and a concrete failure criterion.

Ziraba et al. (1995) [70] proposed two debonding strength models for steel plated RC beams, one for predicting plate end interfacial debonding and the other for predicting concrete cover separation which are termed Ziraba et al. [70] model I and II respectively.

In the model I, the Mohr-Coulomb failure criterion is used to define the critical stress state at plate end interfacial debonding:

$$\tau + \sigma_y \tan\phi \leq C \tag{2.15}$$

where τ and σ_y are the peak interfacial shear and normal stresses at the plate end, C the coefficient of cohesion, and ϕ the angle of internal friction. The peak interfacial shear and normal stresses are given by

$$\tau = \alpha_1 f_{ct} \left(\frac{C_{R1} V_0}{f'_c} \right)^{5/4} \tag{2.16}$$

$$\sigma_y = \alpha_2 C_{R2} \tau \tag{2.17}$$

where

$$C_{R1} = \left[1 + \left(\frac{K_a}{E_{frp} b_{frp} t_{frp}} \right)^{1/2} \frac{M_0}{V_0} \right] \frac{b_{frp} t_{frp}}{I_{trc,frp} b_a} (d_{frp} - x_{trc,frp})$$

$$C_{R2} = t_{frp} \left(\frac{K_n}{4 E_{frp} I_{frp}} \right)^{1/4}$$

where C_{R1} and C_{R2} are obtained from Roberts' analytical solution for interfacial shear and normal stresses, while α_1 and α_2 are empirical multipliers calibrated from numerical studies for RC beams retrofitted with steel plates. The shear stiffness K_a and the normal stiffness K_n of the adhesive layer are given by

$$K_a = \frac{G_a b_a}{t_a}$$

$$K_n = \frac{E_a b_a}{t_a}$$

with E_a, G_a,b_a and t_a being the modulus of elasticity, shear modulus, width and thickness of the adhesive layer respectively. $I_{trc,frp}$ is the second moment of area of the cracked plated section transformed into FRP, $x_{trc,frp}$ is the neutral axis depth of this transformed cracked section (distance from the compression face to the neutral axis), I_{frp} the second moment of area of the FRP plate alone, d_{frp} the distance from the compression face of the RC beam to the centroid of the FRP plate, and M_0 and V_0 the bending moment and shear force respectively at the plate end. Substitution of Eqs.2.16 and 2.17 into Eq. 2.15 gives an expression for the shear force in the beam, at the plate end, to cause plate end interfacial debonding:

$$V_{bd,end} = \frac{f'_c}{C_{R1}} \left[\frac{C}{\alpha_1 f_{ct}(1 + \alpha_2 C_{R2} \tan\phi)} \right]^{4/5}$$

This relationship is subject to the constraint of $a/h < 3$ where h is the depth of the RC beam. The following values for α_1, α_2 and ϕ were specified in Ziraba et al. [70]: $\alpha_1 = 35$, $\alpha_2 = 1,1$ and $\phi = 28°$. In Ziraba et al. [70] two values of C were used for specific numerical examples, namely $2,68MPa$ and $5,36MPa$ although the criteria used for the selection of these values were not made clear. Ziraba et al. [70] suggested that C lie between $4,80MPa$ and $9,50MPa$ based on experimental and numerical findings. For the present study C has been taken as $7,15MPa$ which is an average of the values given in Ziraba et al. [70].

In the model II, Ziraba et al. [70] modified the ACI code prediction of the shear capacity of an RC beam into the following equation where k is the efficiency factor of steel shear reinforcement:

$$V_{db,end} = (V_c + kV_s) \tag{2.18}$$

where V_c and V_s are the contributions of concrete and steel shear reinforcement to the shear capacity of an RC beam respectively and are given in their paper by

$$V_c = 1/6(\sqrt{f'_c} + 100\rho_s)bd$$
$$V_s = (A_{sv} f_{yv} d)/s$$

In Eq.2.18, k is an empirically derived stirrup efficiency factor to adjust the contribution of the steel stirrups and is related to the peak interfacial normal stress at the plate end. Based on a regression analysis of the test results of fourteen steel plated RC beams which failed by concrete cover separation, Ziraba et al. [70] proposed that

$$k = 2,4e^n \text{ and } n = -0,08C_{R1}C_{R2} \times 10^6$$

2.1.4 Smith and Teng model

Oehlers model

Oehlers thought this models (1992) [38] for steel plates but it's possible to apply it to FRP-strengthened beams too.

It is a shear capacity based model and the debonding failure strength is related to the shear strength of the concrete with no contribution of the steel shear reinforcement. The debonding strength is given as the shear force acting at the plate end, with or without taking into account the effect of any coexistent moment. As interfacial stresses between the plate and the beam need not be evaluated.

The flexural capacity of externally plated reinforced concrete beams can be determined from existing ultimate strength methods of analysis by considering the plate to act as part of the reinforcement. As the plate is not enclosed by the concrete, it's necessary to study a possibility of premature failure due to separation between the plate and the concrete that it's called peeling.

The peeling can be induced by shear forces and by flexural forces. Oehlers and Moran (1992) showed that flexural peeling occurs when the moment applied to the end of the plate is given by this equation:

$$M_{db,f} = \frac{(E_c I_{tr,c}) f_{ct}}{0,474 E_{frp} t_{frp}}$$

where $M_{db,f}$ is the moment at the end of the plate that is applied to the plated section; E_c and E_{frp} are the moduli of elasticity of the concrete and the FRP, respectively; $I_{tr,c}$ the cracked second moment of area of the plated section transformed to concrete; f_{ct} is Brazilian tensile strength of concrete; t_{frp} is the depth of plate. The value 0,474 is a constant which represents the mean value; if it needs the characteristic value it replaces by 0,901, which gives the 5% characteristic value for use in design. The flexural peeling occurs at a curvature of $f_{ct}/\left(0,474 E_s t_{frp}\right)$.

It can be seen, from many test results, that the amount of stirrups present in a beam increased the shear strength by up to a factor of almost six, the load at which peeling occurred did not increase. The shear peeling is a function of the shear strength of the beam without stirrups. The shear capacity of the concrete in the RC beam alone, based on experimental observations, is:

$$V_{db,s} = V_c = \left[1,4 - (d/2000)\right] bd \left(\rho_s f'_c\right)^{1/3} \tag{2.19}$$

where $\rho_s = A_s/bd$ is the ratio of steel tension reinforcement, A_s the area of steel tension reinforcement, b the section width and d the effective depth of the section.

The above expression for V_c, the shear capacity in the beam, is that given by the Australian concrete code and it is a requirement that $1,4 - (d/2000) \geq 1,1$.

The peeling depends on interaction between the shear load V_p and the moment M_p. When $M/V \rightarrow \infty$, peeling occurs when $M_p = M_{up}$, and when $M/V \rightarrow 0$, peeling occurs when $V_p = V_{uc}$, where V_{uc} is the shear strength of the beam without stirrups. The failure envelope can be used as a design equation as follows:

$$\frac{M_{db,end}}{M_{db,f}} + \frac{V_{db,end}}{V_{db,s}} \leq 1,17$$

where $M_p \leq M_{up}$ and $V_p \leq V_{uc}$.

In terms of the shear force at the plate end, the previous equation can be rearranged to read

$$V_{db,end} = \frac{1,17}{\frac{a}{M_{db,f}} + \frac{1}{V_{db,s}}}$$

where a is the distance from the support to the nearer end of the soffit plate, and $V_{db,end}a \leq M_{db,f}$, $V_{db,end} \leq V_{db,s}$

Oehlers (1992) [38] model is more conservative for wet lay-up plates than for pultruded plates. Concrete cover failures are also generally more conservatively predicted than plate end interfacial debonding failures.

Proposed model

Smith and Teng (2002) [53] presented a large test database containing the test results of 59 beams to have failed by plate end debonding.

The test data have been grouped into three sets, the first set for failure by concrete cover separation (44 results), the second set for failure by plate end interfacial debonding (8 results), the third set for failure by a mixed concrete cover separation and interfacial debonding mode (7 results); in addition are shown test results which have failed by plate end interfacial debonding in the adhesive.

Reference	Beam specimen	b (mm)	h (mm)	d (mm)	d' (mm)	f'_c (MPa)	a (mm)	B (mm)	L (mm)
I	C	152	305	251	0	39,8	203	914	2438
	D	152	305	251	0	39,8	203	914	2438
	G	152	305	251	0	43,0	0	914	2438
	I	152	305	251	0	42,4	203	914	2438
	M	152	305	251	0	42,4	0	914	2438
II	B2	100	100	84	16	42,4	20	300	900
	B4	100	100	84	16	42,4	20	300	900
	B6	100	100	84	16	42,4	20	300	900
III	$1A_u$	100	100	84	16	47,3	20	300	900
	$1B_u$	100	100	84	16	47,3	20	300	900
	$1B_{2u}$	100	100	84	16	47,3	20	300	900
	$1C_u$	100	100	84	16	47,3	20	300	900
	$2B_u$	100	100	84	16	47,3	20	340	900
	$2C_u$	100	100	84	16	47,3	20	340	900
IV	B1u,1.0	100	100	84	16	43,2	20	300	900
	B2u,1.0	100	100	84	16	43,2	20	300	900
	B1u,2.3	130	230	206	25	37,6	40	844	2200
V	DF.2	125	225	193	32	46,0	50	500	1500
	DF.3	125	225	193	32	46,0	50	500	1500
	DF.4	125	225	193	32	46,0	50	500	1500
	AF3	125	225	193	32	46,0	100	500	1500
	CF2-1	125	225	193	32	46,0	100	500	1500
	CF3-1	125	225	193	32	46,0	100	500	1500
	CF4-1	125	225	193	32	46,0	100	500	1500
VI	VR5	120	250	214	34	33,6	75	783	2350
	VR6	120	250	214	34	33,6	75	783	2350
	VR7	120	250	214	34	33,6	75	783	2350
	VR8	120	250	214	34	33,6	75	783	2350
	VR9	120	250	214	34	33,6	75	783	2350
	VR10	120	250	214	34	33,6	75	783	2350
VII	P_2	150	300	257	0	40,0	200	933	2800
	P_3	150	300	257	0	40,0	200	933	2800
	P_4	150	300	257	0	40,0	200	933	2800
	P_5	150	300	257	0	40,0	200	933	2800
VIII	2	150	250	205	45	35,4	350	500	1500
	6	150	250	205	45	39,9	200	500	1500
	7	150	250	205	45	37,6	350	500	1500

Table 2.1: Smith and Teng Database [53]: beams failed for concrete cover separation. I) Ritchie et al. (1991); II) Quantrill et al. (1996); III) Garden et al. (1997); IV) Garden et al. (1998); V) Ahmed et al. (1999); VI) Ahmed et al. (1999); VII) Beber et al. (1999); VIII) David et al. (1999).

Beam specimen	E_s (GPa)	f_y (MPa)	A_s (mm^2)	n.-ϕ (tension)	E'_s (GPa)	f'_y (MPa)	A'_s (mm^2)
C	200	414	253	2-12,7	0	0	0
D	200	414	253	2-12,7	0	0	0
G	200	414	253	2-12,7	0	0	0
I	200	414	253	2-12,7	0	0	0
M	200	414	253	2-12,7	0	0	0
B2	215	350	85	3-6	215	350	57
B4	215	350	85	3-6	215	350	57
B6	215	350	85	3-6	215	350	57
$1A_u$	215	350	85	3-6	215	350	57
$1B_u$	215	350	85	3-6	215	350	57
$1B_{2u}$	215	350	85	3-6	215	350	57
$1C_u$	215	350	85	3-6	215	350	57
$2B_u$	215	350	85	3-6	215	350	57
$2C_u$	215	350	85	3-6	215	350	57
B1u,1.0	215	350	85	3-6	215	350	57
B2u,1.0	215	350	85	3-6	215	350	57
B1u,2.3	220	556	236	3-10	220	556	101
DF.2	185	568	151	3-8	195	553	57
DF.3	185	568	151	3-8	195	553	57
DF.4	185	568	151	3-8	195	553	57
AF3	185	568	101	2-8	195	553	57
CF2-1	185	568	129	2-8,1-6	195	553	57
CF3-1	185	568	151	3-8	195	553	57
CF4-1	183	586	207	2-10,1-8	195	553	57
VR5	200	565	157	2-10	200	738	57
VR6	200	565	157	2-10	200	738	57
VR7	200	565	157	2-10	200	738	57
VR8	200	565	157	2-10	200	738	57
VR9	200	565	157	2-10	200	738	57
VR10	200	565	157	2-10	200	738	57
P_2	200	500	308	2-14	0	0	0
P_3	200	500	308	2-14	0	0	0
P_4	200	500	308	2-14	0	0	0
P_5	200	500	308	2-14	0	0	0
2	231	537	157	2-10	231	537	157
6	231	537	157	2-10	231	537	157
7	231	537	157	2-10	231	537	157

Table 2.2: Smith and Teng Database [53]: beams failed for concrete cover separation.

Beam specimen	E_{vs} (GPa)	f_{yv} (MPa)	A_{sv} (mm^2)	s (mm)	E_a (GPa)	t_a (mm)
C	200	414	99	102	8500	2,0
D	200	414	99	102	8500	2,0
G	200	414	99	102	8500	2,0
I	200	414	99	102	8500	2,0
M	200	414	99	102	8500	2,0
B2	215	350	14	50	11560	2,0
B4	215	350	14	50	11560	2,0
B6	215	350	14	50	11560	2,0
$1A_u$	215	350	14	51	11560	2,0
$1B_u$	215	350	14	51	11560	2,0
$1B_{2u}$	215	350	14	51	11560	2,0
$1C_u$	215	350	14	51	11560	2,0
$2B_u$	215	350	14	51	11560	2,0
$2C_u$	215	350	14	51	11560	2,0
B1u,1.0	215	350	14	51	8600	2,0
B2u,1.0	215	350	14	51	8600	2,0
B1u,2.3	220	350	57	150	8600	2,0
DF.2	195	553	57	100	7200	-
DF.3	195	553	57	100	7200	-
DF.4	195	553	57	100	7200	-
AF3	195	553	57	71	7200	-
CF2-1	195	553	57	71	7200	-
CF3-1	195	553	57	71	7200	-
CF4-1	195	553	57	71	7200	-
VR5	200	738	57	110	8500	-
VR6	200	738	57	110	8500	-
VR7	200	738	57	110	8500	-
VR8	200	738	57	110	8500	-
VR9	200	738	57	110	8500	-
VR10	200	738	57	110	8500	-
P_2	200	0	57	140	8500	1,0
P_3	200	0	57	140	8500	1,0
P_4	200	0	57	140	8500	1,0
P_5	200	0	57	140	8500	1,0
2	231	537	157	100	3260	0,37
6	231	537	157	100	3260	0,37
7	231	537	157	100	3260	0,37

Table 2.3: Smith and Teng Database [52]: beams failed for concrete cover separation.

Beam specimen	Type	E_{frp} (GPa)	f_{frp} (MPa)	t_{frp} (mm)	b_{frp} (mm)	V_{exp} (kN)
C	G-P	11,72	161	4,76	152	55,4
D	G-P	11,72	161	4,76	151	59,6
G	G-P	10,34	184	4,19	152	62,9
I	G/C-P	27,58	319	4,06	150	50,6
M	C-P	117,90	1489	1,27	152	72,1
B2	G-P	49	1078	1,2	80	17,0
B4	G-P	49	1078	1,6	60	17,5
B6	C-P	118,5	987	1,2	80	20,4
$1A_u$	C-P	111	1273	0,5	90	19,8
$1B_u$	C-P	111	1273	0,7	65	18,3
$1B_{2u}$	C-P	111	1273	0,7	65	18,2
$1C_u$	C-P	111	1273	1,0	45	16,0
$2B_u$	C-P	111	1273	0,7	65	17,0
$2C_u$	C-P	111	1273	1,0	45	17,8
B1u,1.0	C-P	111	1414	0,82	67	18,3
B2u,1.0	C-P	111	1414	0,82	67	16,0
B1u,2.3	C-P	115	1284	1,28	90	50,2
DF.2	C-W	240	3500	0,167 (2)	75	60,3
DF.3	C-W	240	3500	0,167 (3)	75	60,0
DF.4	C-W	240	3500	0,167 (4)	75	62,8
AF3	C-W	240	3500	0,167 (2)	75	48,3
CF2-1	C-W	240	3500	0,167 (2)	75	52,4
CF3-1	C-W	240	3500	0,167 (2)	75	59,1
CF4-1	C-W	240	3400	0,167 (2)	75	70,1
VR5	C-W	230	3400	0,11 (4)	120	51,1
VR6	C-W	230	3400	0,11 (4)	120	50,3
VR7	C-W	230	3400	0,11 (7)	120	62,1
VR8	C-W	230	3400	0,11 (7)	120	62,0
VR9	C-W	230	3400	0,11 (10)	120	64,8
VR10	C-W	230	3400	0,11 (10)	120	68,5
P_2	C-P	150	2400	1,2	100	68,0
P_3	C-P	150	2400	1,2	100	71,1
P_4	C-P	150	2400	2,4	100	78,0
P_5	C-P	150	2400	2,4	100	79,5
2	G-W	19,72	259	1,32	150	53,0
6	G-W	19,72	259	1,32	150	63,1
7	G-W	19,72	259	1,32	150	53,9

Table 2.4: Smith and Teng Database [52]: beams failed for concrete cover separation.

Reference	Beam specimen	b (mm)	h (mm)	d (mm)	d' (mm)	f'_c (MPa)	a (mm)	B (mm)	L (mm)
a)									
IX	A3	150	300	250	0	51,7	0	1065	2130
	A8	150	300	250	0	51,7	0	1065	2130
	C2	150	300	250	0	51,7	0	1065	2130
X	A950	120	150	120	34	25,7	190	440	1330
	A1100	120	150	120	34	25,7	115	440	1330
	A1150	120	150	120	34	25,7	90	440	1330
	B2	120	150	120	34	35,7	115	440	1330
b)									
XI	B	205	455	400	55	35,0	155	1983	4575
II	B3	100	100	84	16	42,4	20	300	900
XII	SB1	200	300	252	48	51,2	150	1300	3600
	SB2	200	300	252	48	52,0	200	1300	3600
	SB3	200	300	252	48	52,0	300	1300	3600
	MB1	200	300	252	48	56,0	150	1300	3600
	HB1	200	300	252	48	56,0	150	1300	3600
	FB1	200	300	252	48	51,2	150	1300	3600
c)									
III	$2A_u$	100	100	84	16	47,3	20	340	900
	$3A_u$	100	100	84	16	47,3	20	400	900
	$3B_u$	100	100	84	16	47,3	20	400	900
	$3C_u$	100	100	84	16	47,3	20	400	900
XIII	B7	75	150	131	22	37,0	10	650	1500
XI	4	150	250	205	45	36,2	200	500	1500
	5	150	250	205	45	40,6	50	500	1500
d)									
XIV	1B	200	200	152	48	48,0	1	914	2742
	1C	200	200	152	48	48,0	1	914	2742
	2B	200	200	152	48	48,0	1	914	2742
	2C	200	200	152	48	48,0	1	914	2742
	2D	200	200	152	48	48,0	1	914	2742
	3B	200	200	152	48	48,0	1	914	2742
	3C	200	200	152	48	48,0	1	914	2742
	3D	200	200	152	48	48,0	1	914	2742

Table 2.5: Smith and Teng Database [53]: a) beams failed for concrete cover separation; b) beams failed for plate end interfacial debonding; c) beams failed for mixed mode debonding; d) beams failed for plate end interfacial debonding. II) Quantrill et al. (1996); III) Garden et al. (1997); XI) Hau (1999); X) Tumialan et al. (1999); XI) Saadatmanesh and Ehsani (1991); XII) T*äl*jsten (1999); XIII) Juvandes et al. (1998); XIV) Ross et al. (1999)

Beam specimen	E_s (GPa)	f_y (MPa)	A_s (mm^2)	n.-ϕ (tension)	E'_s (GPa)	f'_y (MPa)	A'_s (mm^2)
a)							
A3	207	427	792	4-15,9	0	0	0
A8	207	427	792	4-15,9	0	0	0
C2	207	427	792	4-15,9	0	0	0
A950	200	384	236	3-10	200	400	57
A1100	200	384	236	3-10	200	400	57
A1150	200	384	236	3-10	200	400	57
B2	200	466	628	2-20	200	400	57
b)							
B	200	456	1013	2-25,4	200	456	253
B3	215	350	85	3-6	215	350	57
SB1	200	527	402	2-16	200	527	402
SB2	200	527	402	2-16	200	527	402
SB3	200	527	402	2-16	200	527	402
MB1	200	527	402	2-16	200	527	402
HB1	200	527	402	2-16	200	527	402
FB1	200	527	402	2-16	200	527	402
c)							
2A$_u$	215	350	85	3-6	215	350	57
3A$_u$	215	350	85	3-6	215	350	57
3B$_u$	215	350	85	3-6	215	350	57
3C$_u$	215	350	85	3-6	215	350	57
B7	200	190	14	2-3	200	470	151
4	231	537	157	2-10	231	537	157
5	231	537	157	2-10	231	537	157
d)							
1B	200	410	143	2-9,5	200	410	143
1C	200	410	143	2-9,5	200	410	143
2B	200	410	253	2-12,7	200	410	143
2C	200	410	253	2-12,7	200	410	143
2D	200	410	253	2-12,7	200	410	143
3B	200	410	396	2-15,9	200	410	143
3C	200	410	396	2-15,9	200	410	143
3D	200	410	396	2-15,9	200	410	143

Table 2.6: Smith and Teng Database [53]: a) beams failed for concrete cover separation; b) beams failed for plate end interfacial debonding; c) beams failed for mixed mode debonding; d) beams failed for plate end interfacial debonding.

Beam specimen	E_{vs} (GPa)	f_{yv} (MPa)	A_{sv} (mm^2)	s (mm)	E_a (GPa)	t_a (mm)
a)						
A3	207	0	143	125	2000	-
A8	207	0	143	125	2000	-
C2	207	0	143	250	2000	-
A950	200	400	57	50	12800	1,5
A1100	200	400	57	50	12800	1,5
A1150	200	400	57	50	12800	1,5
B2	200	400	57	50	12800	1,5
b)						
B	200	456	253	150	8500	1,5
B3	215	350	14	50	11560	2,0
SB1	200	527	157	75	8500	2,1
SB2	200	527	157	75	8500	2,4
SB3	200	527	157	75	8500	3,0
MB1	200	527	157	75	8500	2,4
HB1	200	527	157	75	8500	2,1
FB1	200	527	157	75	8500	0,4
c)						
2A$_u$	215	350	14	51	11560	2,0
3A$_u$	215	350	14	51	11560	2,0
3B$_u$	215	350	14	51	11560	2,0
3C$_u$	215	350	14	51	11560	2,0
B7	200	190	14	60	10250	2,5
4	200	190	14	60	3260	0,37
5	200	190	14	60	3260	0,37
d)						
1B	200	410	143	102	8500	2,0
1C	200	410	143	102	8500	2,0
2B	200	410	143	102	8500	2,0
2C	200	410	143	102	8500	2,0
2D	200	410	143	102	8500	2,0
3B	200	410	143	102	8500	2,0
3C	200	410	143	102	8500	2,0
3D	200	410	143	102	8500	2,0

Table 2.7: Smith and Teng Database [53]: a) beams failed for concrete cover separation; b) beams failed for plate end interfacial debonding; c) beams failed for mixed mode debonding; d) beams failed for plate end interfacial debonding.

Beam specimen	Type	E_{frp} (GPa)	f_{frp} (MPa)	t_{frp} (mm)	b_{frp} (mm)	V_{exp} (MPa)
a)						
A3	C-W	230	3400	0,165 (3)	150	86,1
A8	C-W	230	3400	0,165 (3)	75	98,2
C2	C-W	230	3400	0,165 (3)	150	79,3
A950	C-P	181	3140	1,2	80	28,1
A1100	C-P	181	3140	1,2	80	28,7
A1150	C-P	181	3140	1,2	80	29,5
B2	C-P	181	3140	1,2	80	65,1
b)						
B	G-P	37,23	400	6,0	152	125,0
B3	G-P	49	1078	1,2	30	12,3
SB1	C-P	155	2400	1,4	120	71,4
SB2	C-P	155	2400	1,4	120	75,5
SB3	C-P	155	2400	1,4	120	73,9
MB1	C-P	210	2000	1,4	120	79,6
HB1	C-P	300	1400	1,4	100	80,1
FB1	C-W	95	1800	2,4	150	74,4
c)						
$2A_u$	C-P	111	1273	0,5	90	19,3
$3A_u$	C-P	111	1273	0,5	90	19,5
$3B_u$	C-P	111	1273	0,7	65	17,3
$3C_u$	C-P	111	1273	1,0	45	15,4
B7	C-P	150	2400	1,2	50	12,5
4	G-W	19,723	259	1,32	150	65,4
5	G-W	19,723	259	2,64	150	79,4
d)						
1B	C-P	138	2206	0,45	200	40,1
1C	C-P	138	2206	0,45	200	35,6
2B	C-P	138	2206	0,45	200	49,0
2C	C-P	138	2206	0,45	200	35,6
2D	C-P	138	2206	0,45	200	40,1
3B	C-P	138	2206	0,45	200	54,5
3C	C-P	138	2206	0,45	200	54,1
3D	C-P	138	2206	0,45	200	54,3

Table 2.8: Smith and Teng Database [53]: a) beams failed for concrete cover separation; b) beams failed for plate end interfacial debonding; c) beams failed for mixed mode debonding; d) beams failed for plate end interfacial debonding.

Smith and Teng [53] noted that no interaction appears to exist between the moment and the shear force, and the shear force at failure is always grates than $V_{db,s}(V_c)$ as predicted by Eq.2.19. As a result, the following simple debonding strength model was proposed by Smith and Teng:

$$V_{db,end} = \eta V_c$$

This equation with $\eta = 1,5$ and with V_c given by Eq.2.19

In practical application debonding failure occurs in the use of strong adhesive. It is necessary to limit the range of applicability of the model to that of the collected data by the authors in terms of the magnitude of the moment at the plate end. It is suggested that the above proposed model can only be used when $M_{db,end}/M_u \leq 0.67$ as this approximates the upper limit of the test data.

Advantages of the model

This new model has a number of advantages over all the models assessed in the previous section and is recommended for use in design. These include:

- the model was calibrated with a large and reliable test database of FRP-strengthened beams and provides a suitable lower bound for design use;
- the model is simpler to apply as the shear capacity of the concrete in the RC beam is either known or has to be evaluated in flexural strengthening design so little extra work is required for checking plate end debonding;
- V_c may be evaluated according to any national or international design code, and this facilitates the inclusion of the model in any national code on FRP strengthening
- the model gives designers a better intuitive feel of the possibility of plate end debonding as it is directly related to this shear capacity of the concrete in the beam, particularly when steel shear reinforcement is not present as often is the case for slabs.
- this model is the best proposal available for design use, the predicted debonding strength, being only 40% higher than the shear capacity of the concrete, can become a limiting factor to FRP flexural strengthening of beams.

Category	Model	Average	COV	No.tests
Shear capacity				
based models:	Oehlers (1992)	2,35	21%	44
	Jansze (1997)	1,50	30%	39
	Ahmed and Van Gemert (1999)	1,15	21%	39
	Smith and Teng (2002) ($V_{bd,end}$=1,4V_c)	1,67	21%	44
	Smith and Teng (2002) ($V_{bd,end}$=1,5V_c)	1,56	21%	44
Concrete tooth				
models:	Raoof and Zhang (1997): Lower	1,47	36%	44
	Raoof and Zhang (1997): Upper	1,06	29%	44
	Wang and Ling (1998): Lower	1,20	29%	44
	Wang and Ling (1998): Upper	0,88	18%	44
	Raoof and Hassanen I (2000): Lower	1,61	41%	44
	Raoof and Hassanen I (2000): Upper	1,13	38%	44
	Raoof and Hassanen II (2000): Lower	1,57	38%	44
	Raoof and Hassanen II (2000): Upper	1,09	32%	44
Interfacial stress				
based models:	Ziraba et al. I (1994)	4,89	74%	44
	Ziraba et al. II (1995)	1,63	34%	44

Table 2.9: Test-to-predicted debonding strength ratios for failure by concrete cover separation: pultruded and wet lay-up plate [53].

Category	Model	Average	COV	No.tests
Shear capacity based models:	Oehlers (1992)	2,25	24%	59
	Jansze (1997)	1,41	33%	54
	Ahmed and Van Gemert (1999)	1,08	27%	53
	Smith and Teng (2002) ($V_{bd,end}$=1,4V_c)	1,60	24%	59
	Smith and Teng (2002) ($V_{bd,end}$=1,5V_c)	1,49	24%	59
Concrete tooth models:	Raoof and Zhang (1997): Lower	1,44	33%	59
	Raoof and Zhang (1997): Upper	1,04	27%	59
	Wang and Ling (1998): Lower	1,14	30%	59
	Wang and Ling (1998): Upper	0,87	19%	59
	Raoof and Hassanen I (2000): Lower	1,55	38%	59
	Raoof and Hassanen I (2000): Upper	1,09	35%	59
	Raoof and Hassanen II (2000): Lower	1,49	37%	59
	Raoof and Hassanen II (2000): Upper	1,05	31%	59
Interfacial stress based models:	Ziraba et al. I (1995)	4,36	79%	59
	Ziraba et al. II (1994)	1,57	33%	59

Table 2.10: Test-to-predicted debonding strength ratios for all plate end failures: pultruded and wet lay-up plate [53].

2.1.5 Teng and Yao model

The significant factors governing flexural debonding failure can be deduced as follows. A bonded plate is forced to deform with the original RC beam. This composite action leads to interfacial stresses at the plate-beam interface and at the steel bars-concrete cover interface. Provided the FRP plate is sufficiently wide relative to the beam, flexural debonding occurs along the latter interface when it can no longer resist the stresses induced by this composite action. The axial and bending rigidities of both the cracked RC section and the bonded plate are important parameter that determine the magnitudes of stresses at this interface. The cover thickness of concrete is also important as it affects the stresses at the steel bars-concrete interface for a given tensile force in the soffit plate. Furthermore, the width ratio between the plate and the RC beam is important as it affects directly the interfacial stresses between the plate and the concrete, and determines whether plate end interfacial debonding instead of concrete cover separation is critical. Based on these considerations and the knowledge that the debonding moment cannot exceed the ultimate moment of the unplated section, a detailed analysis was conducted by Teng and Yao [60, 61, 30] to identify the effect of each of the parameters that is likely to have a significant bearing on the flexural debonding strength. This analysis led to the following predictive model for flexural debonding of a plate end located in a pure bending region:

$$M_{db,f} = \frac{0,488 M_{u,0}}{(\alpha_{flex}\alpha_{axial}\alpha_w)^{1/9}} \tag{2.20}$$

where α_{flex}, α_{axial} and α_w are three dimensionless parameters defined respectively by:

$$\alpha_{flex} = \frac{(EI)_{c,frp} - (EI)_{c,0}}{(EI)_{c,0}} \tag{2.21}$$

$$\alpha_{axial} = \frac{E_{frp} t_p}{E_c d}$$

and

$$\alpha_w = \frac{b}{b_{frp}} \ , \ \frac{b}{b_{frp}} \leq 3 \tag{2.22}$$

where $(EI)_{c,frp}$ and $(EI)_{c,0}$ are the flexural rigidities of the cracked section with and without a soffit plate, respectively, $E_{frp}t_{frp}$ is the axial rigidity per unit width of the soffit plate, d is the effective depth of the beam, and $M_{u,0}$ is the theoretical ultimate moment of the unplated section which is also the upper bound of the flexural debonding moment $M_{db,f}$. It is obvious that α_{flex} reflects the effect of the contribution of the soffit plate to the flexural rigidity of the cracked section, α_{axial} reflects the effect of the axial rigidity ratio, and α_w reflects the effect of the width ratio. The limitation imposed on the width ratio reflects the limitation of the test data. These parameters indirectly reflect the effects of several other parameters. For example, the effects of concrete strength and steel tension reinforcement ratio are included in the theoretical ultimate moment of the unplated section $M_{u,0}$.

Eq.2.20 is a best-fit expression of the results of eighteen tests conducted by the authors, with the limitation that $M_{db,f}$ does not exceed $M_{u,0}$.

The shear debonding strength can be represented by the debonding shear force $V_{db,s}$ at a plate end located in a region of (nearly) zero moment. The debonding shear force lies between the shear resistance contributed by the concrete of the unplated beam and the full shear capacity of the plated beam. Therefore, the following equation is proposed to predict the shear debonding strength:

$$V_{db,s} = V_c + V_{frp} + \varepsilon_{v,e}\overline{V}_s \tag{2.23}$$

where V_c, V_{frp} and $\overline{V}_s$ are the contributions of the concrete, the soffit plate, and the internal shear reinforcement to the shear capacity of the beam, respectively, and $\overline{V}_s$ is the shear force carried by the steel shear reinforcement per unit strain, that is

$$\overline{V}_s = A_{sv}E_{sv}d_e/s_v$$

where A_{sv}, E_{sv} and s_v are the total cross-sectional area of the two legs of each stirrup, the elastic modulus and the longitudinal spacing of the stirrups, respectively. In Eq.2.23, $\varepsilon_{v,e}$ is the strain in the steel shear reinforcement, referred to here as the effective strain, and this effective strain may be well below the yield strain of the steel shear reinforcement at debonding failure.

Eight tests on plated RC beams in which the critical plate end distance was not greater than 50 mm were analysed to establish an expression for the effective strain $\epsilon_{v,e}$. In deducing the experimental values of $\epsilon_{v,e}$, the value of $V_c + V_{frp}$ was found from a corresponding plated beam which had no internal steel shear reinforcement and failed by CDC debonding (critical diagonal crack), with due adjustment to account for the differences in the geometry and the concrete strength using Oehlers

et al. prestress model (2004). Based on this analysis, the best-fit expression for $\epsilon_{v,e}$ is given by

$$\varepsilon_{v,e} = \frac{10}{(\alpha_{flex}\alpha_E\alpha_t\alpha_w)^{1/2}} \tag{2.24}$$

where α_{flex} and α_w are given by the Eqs.2.21 and 2.22, while the other two dimensionless parameters are defined by:

$$\alpha_E = \frac{E_{frp}}{E_c}$$

and

$$\alpha_t = \left(\frac{t_{frp}}{d}\right)^{1,3}$$

It may be noted that α_{axial} is now separated into α_E and α_t to better reflect the trends of the test results. Otherwise, the effective strain is assumed to depend similarly on the parameters which are important for flexural debonding. This assumption is based on the observation that shear debonding generally occurs after the formation of a significant shear crack which greatly increases the curvature near the plate end. That is, the development of a cover separation failure, following the formation of a significant shear crack, also depends on the stresses required at the steel bars-concrete interface to maintain curvature compatibility between the RC beam and the bonded plate.

The interfacial stresses between the concrete and the plate are directly related to the shear force and the bending moment in the beam at the plate end. This interaction between plate end shear and bending has been shown to be significant for FRP-plated RC beams, the authors proposed an interaction equation based on their test results as follows:

$$\left(\frac{V_{db,end}}{0,85V_{db,s}}\right)^2 + \left(\frac{M_{db,end}}{0,85M_{db,f}}\right)^2 = 1,0$$

where $V_{db,end}$ and $M_{db,end}$ are the plate end shear force and the plate end moment at debonding, respectively.

For practical applications of the proposed model for shear debonding, the expression of V_c can be replace by the corresponding expression in any national code

for concrete structures, while V_{frp} can be ignored. These simplifications yield more conservative predictions for most of the test result. The formulae for V_c used are listed below:

From ACI code,

$$\frac{V_c}{bd} = 0,158\sqrt{f'_c} + 17,2\left(\rho_s \frac{d}{B}\right).$$

From the British code,

$$\frac{V_c}{bd} = 0,79\left(\frac{100A_s}{bd}\right)^{1/3}\left(\frac{400}{d}\right)^{1/4}\left(\frac{f_{cu}}{25}\right)^{1/3}.$$

From the Australian code,

$$V_c = \left(1,4 - \frac{d}{2000}\right) bd\left(\rho_s f'_c\right)^{1/3}$$

2.1.6 Colotti et al. model

Colotti et al. (2004) [18] collected the results of 103 RC beam tests reported in literature (Tabs.2.11-2.16): of these, 15 beams were strengthened with steel plates, 69 beams with CFRP, and 19 beams with GFRP laminates. The beams differ in terms of geometry, concrete strength, and amount and strength of internal steel reinforcement (both longitudinal and transverse) and with a wide range of geometrical and mechanical characteristics.

The proposed model is based on truss analogy. Such a truss model has four significant advantages:

- The truss model approach is widely used in conventional RC beam design, and engineers can easily understand the engineering basis of the model;
- Linear-elastic models do not reflect the state of stress at failure of plated beams. Elastoplastic behavior of materials can be easily incorporated in the truss model;
- The failure behavior of conventional RC beams is generally not controlled by bond forces along the internal reinforcement. With plated beams, the potential debonding of the plate plays a dominant role in the failure process.

Reference	Beam specimen	b (mm)	h (mm)	d' (mm)	d'' (mm)	f'_c (MPa)	l_a (mm)	a (mm)
a	BF2	200	450	33	-	36,5	1180	1250
	BF3	200	450	33	-	34,9	1180	1250
	BF4	200	450	33	-	30,8	1180	1250
	BF5	200	450	33	-	37,4	1180	1250
	BF8	200	450	33	-	39,4	1180	1250
	BF9	200	450	33	-	33,7	1180	1250
b	A4	200	200	30	30	33,0	550	700
	A5	200	200	30	30	33,0	550	700
	B2	300	400	44	44	30,0	1000	1100
	B3	300	400	44	44	30,0	1000	1100
c	$1A_u$	100	100	10	10	57,9	300	300
	$2A_u$	100	100	10	10	57,9	340	340
	$3A_u$	100	100	10	10	57,9	400	400
	$1B_u$	100	100	10	10	57,9	300	300
	$1B2_u$	100	100	10	10	57,9	300	300
	$2B_u$	100	100	10	10	57,9	340	340
	$3B_u$	100	100	10	10	57,9	400	400
	$1C_u$	100	100	10	10	57,9	300	300
	$2C_u$	100	100	10	10	57,9	340	340
	$3C_u$	100	100	10	10	57,9	400	400
d	1U1.0	100	100	10	10	44,8	280	300
	2U1.0	100	100	10	10	44,8	280	300
	3U1.0	100	100	10	10	44,8	320	340
	4U1.0	100	100	10	10	44,8	380	400
	5U1.0	100	100	10	10	44,8	380	400
	1U2.3	130	230	13	15	39,0	805	845
	1U4.5	145	230	13	15	39,0	1485	1525
e	1B	200	200	40	40	54,8	914	914
	2B	200	200	40	40	54,8	914	914
	3B	200	200	40	40	54,8	914	914
	4B	200	200	40	40	54,8	914	914
	5B	200	200	40	40	54,8	914	914
	6B	200	200	40	40	54,8	914	914
f	A1.1	140	300	30	30	24,9	914	1800
	A3.1	140	300	30	30	24,9	1750	1800
g	B6	100	100	12	12	44,0	1750	300

Table 2.11: Colotti et al. database [18]. Properties of test beams with bonded CFRP laminates. a) Matthys (2000); b) Arduini et al. (1997); c) Garden et al. (1997); d) Garden et al. (1998); e) Ross et al. (1999); f) Spadea et al. (1997); g) Quantrill et al. (1996a). d'' and l_a are the bottom concrete cover and the plate length from the end plate to load point, respectively.

Beam specimen	E_s (GPa)	f_y (MPa)	A_s (mm^2)	A'_s (mm^2)	ϕ_l (mm)	f_{yv} (MPa)	A_{sv} (mm^2)	s (mm)
BF2	200	590	804	-	14	560	100,5	100
BF3	200	590	804	-	16	560	100,5	100
BF4	200	590	804	-	16	560	100,5	100
BF5	200	590	804	-	16	560	100,5	100
BF8	200	590	402	-	16	560	100,5	100
BF9	200	590	402	-	16	560	100,5	100
A4	200	540	308	308	14	540	56,5	150
A5	200	540	308	308	14	540	56,5	150
B2	200	340	398	266	13	340	100,5	100
B3	200	340	398	266	13	340	100,5	100
$1A_u$	215	350	85	56,5	6	350	14	50
$2A_u$	215	350	85	56,5	6	350	14	50
$3A_u$	215	350	85	56,5	6	350	14	50
$1B_u$	215	350	85	56,5	6	350	14	50
$1B2_u$	215	350	85	56,5	6	350	14	50
$2B_u$	215	350	85	56,5	6	350	14	50
$3B_u$	215	350	85	56,5	6	350	14	50
$1C_u$	215	350	85	56,5	6	350	14	50
$2C_u$	215	350	85	56,5	6	350	14	50
$3C_u$	215	350	85	56,5	6	350	14	50
1U1.0	215	350	85	56,5	6	350	14	50
2U1.0	215	350	85	56,5	6	350	14	50
3U1.0	215	350	85	56,5	6	350	14	50
4U1.0	215	350	85	56,5	6	350	14	50
5U1.0	215	350	85	56,5	6	350	14	50
1U2.3	220	556	236	100,5	10	410	56,5	150
1U4.5	220	556	226	100,5	12	410	56,5	150
1B	200	410	142	142	10	410	142,0	102
2B	200	410	259	142	13	410	142,0	102
3B	200	410	400	142	16	410	142,0	102
4B	200	410	567	142	19	410	142,0	102
5B	200	410	774	142	22	410	142,0	102
6B	200	410	1019	142	26	410	142,0	102
A1.1	200	435	402	402	16	435	56,5	150
A3.1	200	435	402	402	16	435	25,1	150
B6	200	350	85	56,5	6	350	14	50

Table 2.12: Colotti et al. database [18]. Properties of test beams with bonded CFRP laminates. ϕ_l represents the diameter of longitudinal bars.

Beam specimen	E_{frp} (GPa)	f_{frp} (MPa)	t_{frp} (mm)	b_{frp} (mm)	V_{exp} (MPa)
BF2	159	3200	1,2	100	185
BF3	159	3200	1,2	100	186
BF4	159	3200	1,2	100	184,2
BF5	159	3200	1,2	100	177,4
BF8	159	3200	1,2	100	111,3
BF9	233	3500	0,2	100	95,8
A4	167	2906	1,3	150	55
A5	167	2906	2,6	150	45
B2	400	3000	0,17	300	85
B3	400	3000	0,51	90	114
$1A_u$	111	1273	0,5	90	19,8
$2A_u$	111	1273	0,5	90	19,3
$3A_u$	111	1273	0,5	65	19,5
$1B_u$	111	1273	0,7	65	18,3
$1B2_u$	111	1273	0,7	65	18,2
$2B_u$	111	1273	0,7	65	17
$3B_u$	111	1273	0,7	45	17,3
$1C_u$	111	1273	1	45	16
$2C_u$	111	1273	1	45	17,8
$3C_u$	111	1273	1	67	15,4
1U1.0	111	1414	0,82	67	18,3
2U1.0	111	1414	0,82	67	16
3U1.0	111	1414	0,82	67	17
4U1.0	111	1414	0,82	67	17,3
5U1.0	111	1414	0,82	90	17,3
1U2.3	115	1284	1,28	90	50,2
1U4.5	115	1284	1,28	200	30
1B	138	2206	0,45	200	40
2B	138	2206	0,45	200	49
3B	138	2206	0,45	200	54,5
4B	138	2206	0,45	200	53,8
5B	138	2206	0,45	200	73,4
6B	138	2206	0,45	200	84,5
A1.1	152	2400	1,2	80	43,4
A3.1	152	2400	1,2	80	37,4
B6	1185,5	987	1,2	80	20,4

Table 2.13: Colotti et al. database [18]. Properties of test beams with bonded CFRP laminates.

Reference	Beam specimen	b (mm)	h (mm)	d' (mm)	d'' (mm)	f'_c (MPa)	l_a (mm)	B (mm)
h	I	152	305	48	-	40,0	280	914
	L	152	305	48	-	40,0	711	914
	M	152	305	48	-	43,2	914	914
i	B.7	75	150	20	20	37,0	914	650
	B.11	75	150	20	20	36,0	640	650
l	AF.2	125	225	25	25	41,0	450	500
	AF.2-1	125	225	25	25	41,0	300	500
	AF.3	125	225	25	25	41,0	350	500
	AF.4	125	225	25	25	41,0	400	500
	DF.1	125	225	25	25	42,0	450	500
	DF.2	125	225	25	25	42,0	450	500
	DF.3	125	225	25	25	40,5	450	500
	DF.4	125	225	25	25	40,5	450	500
	BF.2-1	125	225	25	25	41,0	450	500
	BF.3-1	125	225	25	25	41,0	450	500
	CF.2-1	125	225	25	25	43,0	450	500
	CF.3-1	125	225	25	25	43,0	400	500
	CF.4-1	125	225	25	25	43,0	400	500
	EF.1-1	125	225	25	25	46,0	400	500
	EF.3-1	125	225	25	25	38,0	450	500
	EF.4-1	125	225	25	25	33,0	450	500
	FF.2-2	125	225	25	25	39,5	450	500
	FF.2-3	125	225	25	25	39,5	630	500
	FF.3-2	125	225	25	25	38,5	630	500
	FF.3-4	125	225	25	25	38,5	810	500
m	A00	100	150	21	21	28,6	810	600
	A15	100	150	21	21	31,4	600	600
	A25	100	150	21	21	29,7	600	600
	A40	100	150	21	21	31,4	600	600
	A60	100	150	21	21	28,6	600	600
	A75	100	150	21	21	28,5	600	600
	A90	100	150	21	21	30,1	600	600

Table 2.14: Colotti et al. database [18]. Properties of test beams with bonded CFRP laminates. h) Ritchie et al. (1991); i) Juvandes et al. (1998); l) Ahmed (2000); m) Tan and Mathivoli (1999). d'' and l_a are the bottom concrete cover and the plate length from the end plate to load point, respectively.

Beam specimen	E_s (GPa)	f_y (MPa)	A_s (mm^2)	A'_s (mm^2)	ϕ_l (mm)	f_{yv} (MPa)	A_{sv} (mm^2)	s (mm)
I	200	414	253	-	13	414	99	102
L	200	414	253	-	13	414	99	102
M	200	414	253	-	13	414	99	102
B.7	200	190	14	151	3	190	14	60
B.11	200	190	14	151	3	190	14	61
AF.2	185	568	100,5	56,5	8	553	56,5	71
AF.2-1	185	568	100,5	56,5	8	553	56,5	71
AF.3	185	568	100,5	56,5	8	553	56,5	71
AF.4	185	568	100,5	56,5	8	553	56,5	71
DF.1	185	568	150,8	56,5	8	553	56,5	100
DF.2	185	568	150,8	56,5	8	553	56,5	100
DF.3	185	568	150,8	56,5	8	553	56,5	100
DF.4	185	568	150,8	56,5	8	553	56,5	100
BF.2-1	185	568	100,5	56,5	8	553	56,5	167
BF.3-1	185	568	100,5	56,5	8	553	56,5	100
CF.2-1	185	568	128,8	56,5	8	553	56,5	71
CF.3-1	185	568	150,8	56,5	8	553	56,5	71
CF.4-1	185	568	207,3	56,5	10	553	56,5	71
EF.1-1	185	568	150,8	56,5	8	553	56,5	100
EF.3-1	185	568	150,8	56,5	8	553	56,5	100
EF.4-1	185	568	150,8	56,5	8	553	56,5	100
FF.2-2	185	568	150,8	56,5	8	553	56,5	100
FF.2-3	185	568	150,8	56,5	8	553	56,5	100
FF.3-2	185	568	150,8	56,5	8	553	56,5	100
FF.3-4	185	568	150,8	56,5	8	553	56,5	100
A00	200	500	157	56,5	10	500	56,5	75
A15	200	500	157	56,5	10	500	56,5	75
A25	200	500	157	56,5	10	500	56,5	75
A40	200	500	157	56,5	10	500	56,5	75
A60	200	500	157	56,5	10	500	56,5	75
A75	200	500	157	56,5	10	500	56,5	75
A90	200	500	157	56,5	10	500	56,5	75

Table 2.15: Colotti et al. database [18]. Properties of test beams with bonded CFRP laminates. ϕ_l represents the diameter of longitudinal bars.

Beam specimen	E_{frp} (GPa)	f_{frp} (MPa)	t_{frp} (mm)	b_{frp} (mm)	V_{exp} (MPa)
I	27,6	319	4,06	150	50,6
L	54,5	614	1,27	152	61,4
M	117,9	1489	1,27	152	72,02
B.7	150	2400	1,2	50	12,5
B.11	150	2400	1,2	50	6,7
AF.2	240	3500	0,33	75	41,5
AF.2-1	240	3500	0,33	75	42,9
AF.3	240	3500	0,33	75	48,3
AF.4	240	3500	0,33	75	55,5
DF.1	240	3500	0,17	75	59,0
DF.2	240	3500	0,33	75	60,3
DF.3	240	3500	0,50	75	60,0
DF.4	240	3500	0,67	75	62,8
BF.2-1	240	3500	0,33	75	45,0
BF.3-1	240	3500	0,33	75	52,0
CF.2-1	240	3500	0,33	75	52,4
CF.3-1	240	3500	0,33	75	59,0
CF.4-1	240	3500	0,33	75	70,0
EF.1-1	240	3500	0,33	75	65,9
EF.3-1	240	3500	0,33	75	59,5
EF.4-1	240	3500	0,33	75	60,3
FF.2-2	240	3500	0,33	75	47,8
FF.2-3	240	3500	0,50	75	53,0
FF.3-2	240	3500	0,33	75	35,6
FF.3-4	240	3500	0,67	75	45,0
A00	230	3400	0,22	100	27,5
A15	230	3400	0,22	100	24,7
A25	230	3400	0,22	100	24,3
A40	230	3400	0,22	100	24,7
A60	230	3400	0,22	100	26,0
A75	230	3400	0,22	100	21,9
A90	230	3400	0,22	100	19,8

Table 2.16: Colotti et al. database [18]. Properties of test beams with bonded CFRP laminates.

Conventional truss model, which ignore any load transfer by bond, are therefore not applicable to plated beams. However, the truss model can be easily modified to incorporate the load transfer by bond, and can therefore provide a consistent model to reflect the various modes of failure observed in tests with plated beams;

- Because of the nature of the model, the truss analogy is equally valid for all plated beams whether the strengthening plate is made of steel, CFRP or GFRP.

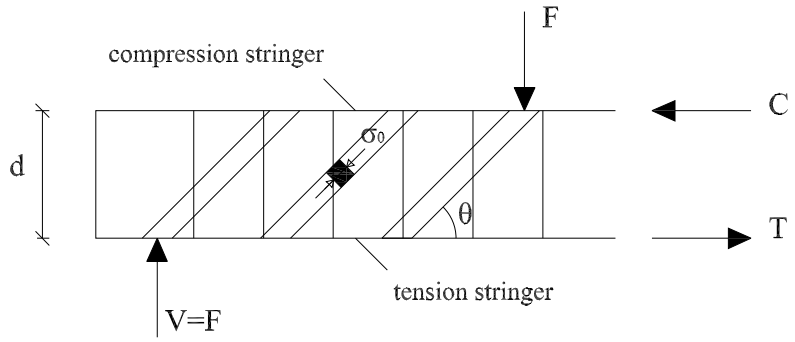

Figure 2.3: Truss analogy model for strengthened reinforced concrete.

The load-carrying capacity of an RC beam with externally bonded plates can be determined with reference to a scheme based on the truss analogy model. In this approach a beam is seen as a plane truss with an upper and a lower chord (compression concrete and tensile reinforcement, respectively) and web elements (diagonal concrete struts and transverse steel stirrups) as shown in Fig.2.3. The following assumptions are made:

- The distance d is assumed to be equal to the effective depth of the section;
- Perfectly plastic behavior is assumed for the materials and for the bond at the plate-concrete interface. In particular, the cylinder strength of concrete f'_c is provided with an effectiveness factor ν, introduced to take into account its limited ductility: $f_c = \nu f'_c$;
- The internal shear reinforcement is formed of closely spaced vertical stirrups whose effect can be represented by a unit length force $p_s = A_t f_t / s$, where A_t,

f_t, and s are the cross-sectional area, the tensile stress, and the spacing of stirrups, respectively;

- The concrete strut in the web is subject to a uniaxial compressive stress state σ_c inclined at an angle θ with respect to the beam axis; this state of stress is not active in the areas near the load and support reaction points where the regions are assumed to be unstressed;

- The external strengthening plate is treated like conventional reinforcement, and perfect bonding is assumed between the plate and the concrete.

- To take the force transfer mechanism for bonding and the associated debonding mechanism into account, the bonding force U is assumed to represent the plane stress flow at the plate-concrete interface. At the ultimate stage, the distribution of the bonding forces between plate and concrete is assumed to be uniform.

- When the bond mechanism is the failure criterion, the contribution of internal longitudinal bars at the ultimate state is neglected. The dowel action of the reinforcement and the aggregate interlock effects are also neglected.

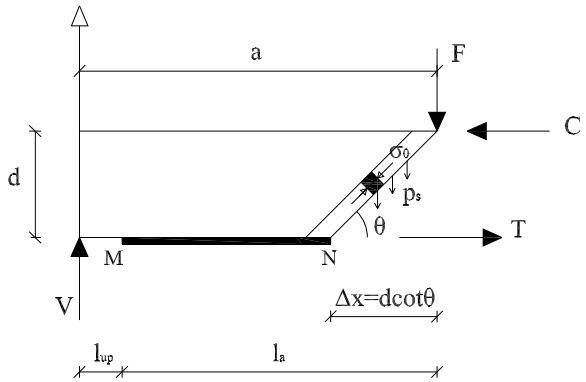

Figure 2.4: Free body diagram for truss analogy model.

Now consider a simply supported RC beam, strengthened in flexure with a plate/laminate bonded to the tension face and subject to two concentrated forces applied symmetrically at a distance a from the support (Fig.2.4). With reference to an x-y axis system, the statically admissible tension field can be shown to be

$$\begin{aligned}\sigma_x &= -\sigma_c \cos^2\theta \\ \sigma_y &= -\sigma_c \sin^2\theta + \frac{p_s}{b} \\ \tau_{xy} &= -\sigma_c \sin\theta\cos\theta\end{aligned}$$

From the boundary conditions at the upper and lower edges of the beam and on the basis of the definition of bond force per unit length, the bond strength U can be expressed as

$$U = \frac{dT}{dx} = \tau_{xy} b = \tau_b b_m \tag{2.25}$$

where τ_b and b_m indicate the bond stress at the plate-concrete interface and the effective width of the plate-adhesive interface, respectively.

It is then possible to establish the following relationships between stresses:

$$\begin{aligned}p_s &= U\tan\theta \\ \sigma_c &= \frac{U}{b}\frac{\cot^2\theta + 1}{\cot\theta}\end{aligned}$$

Fulfillment of the plasticity conditions requires that:

$$\begin{aligned}T &\leq T_y = A_s f_{sy} + A_p f_{pu} \\ p_s &\leq p_y = \frac{A_t f_{ty}}{s} \\ -f_c &\leq \sigma_c \leq 0\end{aligned}$$

where A_s, A_p are the cross-sectional area of internal longitudinal steel reinforcement and bonded plate/laminate, respectively; f_{sy}, f_{ty} are yield stress of longitudinal and transverse reinforcement; and f_{pu} is the yield (or rupture) stress of bonded plate/laminate.

The equilibrium conditions in the x-y directions and the moment equilibrium condition require:

$$C - T = 0 \tag{2.26}$$

$$V = \int_{x_n}^{x_0} (x_0 - x) p_s dx = 0 \tag{2.27}$$

$$M = Va - \int_{x_n}^{x_0} (x_0 - x) p_s dx - Td = 0 \tag{2.28}$$

Plate-debonding failure mode

From the cinematic point of view, the mechanism associated with this failure mode is characterized by slippage of the plate in the shear span (Fig.2.4). The bond strength at ultimate along the plate will have reached the value U_y and the stirrups which cross the cracking trajectory will have reached their yield limit p_y. These conditions lead to:

$$U = U_y \quad \text{for} \quad x_m \leq x \leq x_n \tag{2.29}$$

$$p_s = p_y \quad \text{for} \quad x_n \leq x \leq x_0 \tag{2.30}$$

By substituting eq.2.29 into eq.2.25 and integrating between the limits of cracking trajectory, it is possible to obtain

$$T = U_y \left(x_n - x_m\right) = U_y \left(l_a - \Delta x\right) \tag{2.31}$$

where $\Delta x = (x_0 - x_n) = d \cot \theta$; and l_a is the plate length in the shear span (Fig.2.4).

Substitution of eq.2.30 and eq.2.31 into eq.2.27 and eq.2.28 gives the ultimate load for the bond failure mode:

$$V = p_y d \left[\phi + \alpha - \sqrt{(\phi + \alpha)^2 - 2\phi\beta}\right], \quad p_y > 0 \tag{2.32}$$

where the terms α, β and ϕ are defined by $\alpha = a/d$, ratio of shear span to beam effective depth; $\beta = l_a/d$, ratio of plate length in shear shear span to beam effective depth; and $\phi = U_y/p_y$, ratio of bond strength to stirrup strength.

Eq.2.32 thus represents the debonding failure load of a plated beam.

Shear failure mode

Failure mode related to crushing of the concrete web and/or yielding of stirrups:

$$V = \frac{bdf_c}{2}\left[\sqrt{1+\alpha^2} - \alpha\right] + p_y d\alpha \qquad \text{for} \qquad 0 \leq \frac{p_y}{bf_c} \leq \frac{\sqrt{1+\alpha^2} - \alpha}{2\sqrt{1+\alpha^2}}$$

$$V = \sqrt{p_y bd^2 f_c \left(1 - \frac{p_y}{bf_c}\right)} \qquad \text{for} \qquad \frac{\sqrt{1+\alpha^2} - \alpha}{2\sqrt{1+\alpha^2}} \leq \frac{p_y}{bf_c} \leq 0,5$$

$$V = \frac{bdf_c}{2} \qquad \text{for} \qquad \frac{p_y}{bf_c} > 0,5$$

Tension/concrete crushing failure mode

Failure mode related to yielding of longitudinal and transverse reinforcement (beams with shear reinforcement) or related to crushing of the concrete web and/or yielding of longitudinal reinforcement (beams without shear reinforcement):

$$V = p_y d\left[\sqrt{\frac{2T_y}{p_y d}+\alpha^2}-\alpha\right] \qquad \text{for} \qquad \frac{p_y}{bf_c} > \frac{\sqrt{1+\alpha^2}-\alpha}{2\sqrt{1+\alpha^2}} \tag{2.33}$$

$$V = \frac{bdf_c}{2}\left[\sqrt{\frac{4T_y}{bdf_c}\left(1-\frac{T_y}{bdf_c}\right)+\alpha^2}-\alpha\right] \qquad \text{for} \qquad \frac{p_y}{bf_c} \leq \frac{\sqrt{1+\alpha^2}-\alpha}{2\sqrt{1+\alpha^2}},\ T_y \leq 0,5bdf_c$$

$$V = \frac{bdf_c}{2}\left[\sqrt{1+\alpha^2}-\alpha\right] \qquad \text{for} \qquad \frac{p_y}{bf_c} \leq \frac{\sqrt{1+\alpha^2}-\alpha}{2\sqrt{1+\alpha^2}},\ T_y > 0,5bdf_c$$

Plate rupture-flexural failure mode

The failure mode related to FRP tensile rupture, yielding of longitudinal steel reinforcement, and/or concrete crushing in compression (flexural failure mode) is well-established, and the failure load is then given by

$$V = \frac{M_u}{a} \tag{2.34}$$

Where M_u definition is taking by ACI440 [1]:

$$M_u = A_s f_s\left(d-\frac{\beta_1 c}{2}\right)+\psi_p A_{frp}E_{frp}\varepsilon_{frp}\left(h-\frac{\beta_1 c}{2}\right)$$

with

$$\varepsilon_p = \varepsilon_{cu}\left(\frac{h-c}{c}\right)-\varepsilon_{bi} \leq k_m\varepsilon_{pu}$$

The term k_m is a factor that is meant to limit the strain in the FRP reinforcement to prevent debonding or delamination. For this factor, on the basis of the experience of engineers designing bonded FRP systems, the following assumption is suggested:

$$k_m \begin{cases} 1-\frac{nE_{frp}t_{frp1}}{428000} & for \quad nE_{frp}t_{frp1} \leq 214000N/mm \\ \\ \frac{107000}{nE_{frp}t_{frp1}} & for \quad nE_{frp}t_{frp1} > 214000N/mm \end{cases}$$

Where n is the number of plies of FRP reinforcement; t_{p1} is the nominal thickness of one ply of the FRP reinforcement; and ε_{bi} is the strain in the concrete substrate at the time of the FRP installation.

The actual load-carrying capacity of a plated beam is then determined by the minimum value obtained from Eq.2.32 to Eq.2.34. More appropriately, because the mechanism associated with the bond failure involves both the slipping of the plate and the yielding of the stirrups, Eq.2.32 is, in practice, valid for beams with shear reinforcement.

Limiting bond strength

A key parameter of the model proposed here is represented by the limiting bond strength value of U_y, which should reflect the average behavior of the plate-adhesive-concrete interface.

The mechanical properties of the plate-adhesive-concrete interface are somewhat difficult to characterize and analyze with respect to the mechanical properties of their single constituent materials. In practice, bond failure in a plated beam can appear in two ways: as debonding of the plate from the concrete surface or as failure of the concrete cover between the plate and the internal reinforcing bars.

In Colotti et al. model [18] the limiting bond strength U_y for these two cases is evaluated as follows.

In the first case, the limiting bond strength in this case is derived from experimental results obtained from a series of pull-out tests collected by Swamy (1986). The limiting bond strength is then given by

$$U_y = b_m \left[2,77 + 0,06 \left(f'_c - 20\right)\right] \quad \text{for} \quad f'_c > 20MPa \tag{2.35}$$

For the value of the effective width of the plate-adhesive interface, b_m, a mean value between the beam and plate width is assumed: $b_m = (b + b_{frp})/2$.

In the second case, a simple strut-and-tie approach, as shown below, has been adopted here for a theoretical evaluation of U_y in this case.

Consider a concrete portion between two consecutive cracks. From the static point of view, this simple concrete element can be considered as a portion of plate subjected to in-plane shear forces along the boundary, which can be idealized by means of a strut-and-tie model, as shown in Fig.2.5. From equilibrium conditions:

$$N_t = \Delta T \tan\theta_c \tag{2.36}$$

where N_t, ΔT and θ_c are clearly defined in Fig.2.5.

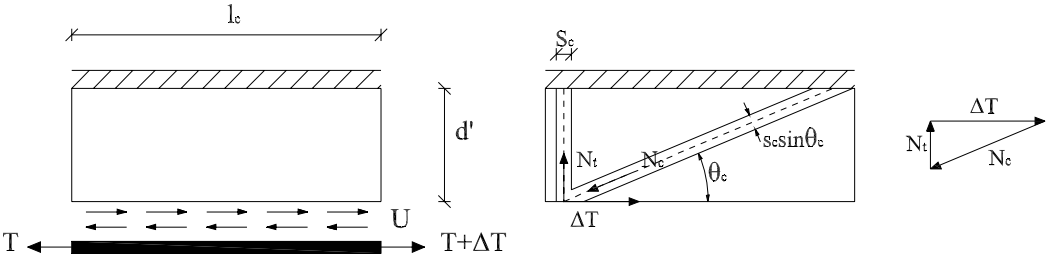

Figure 2.5: Strut and tie model to evaluation of bond strength.

In the ultimate state, setting

$$\Delta T = U_y l_c \quad \text{and} \quad N_t = f_t' s_c b$$

Eq.2.36 leads to

$$U_y = \frac{f_t' s_c b}{d'} \tag{2.37}$$

where f_t' is the tensile strength of the concrete; and s_c is the width of the tie-element, assumed as a fraction of the crack spacing size l_c.

The effective bond strength is the minimum calculated value given by Eq.2.35 and Eq.2.37

Numerical investigation

In the numerical investigation, for the Colotti et al. model [18], the following assumptions were made: $d = 0,9h$, $\nu_c = 0,7$, $s_c = l_c/5$. Furthermore, the tensile strength of concrete f_t' and the crack spacing size l_c, according to Eurocode2 [11] were assumed to be $f_t' = 1,3 \times 0,3 f_c^{2/3}$(MPa), $l_c = 50 + 0,25 k_1 k_2 \phi_1 / \rho_r$, with $k_1 = 0,8$,$k_2 = 0,5$, $\rho_r = A_s/(2,5bd)$, and ϕ_1 is the diameter of longitudinal bars.

Colotti et al. [18] model gives a small range of experimental/theoretical mean values, of 0,69-1,30 for CFRP plated beams and 0,85-1,32 for beams strengthened with GFRP plates. The model gives a good prediction of experimental data tests in Colotti et al.'s paper [18]. Bearing in mind that the properties of the concrete cannot be uniquely modeled, it is fair to state that the structural mechanics aspects of the proposed theory based on the truss model approach are derived entirely from basic engineering principles. It is considers all the possible failure mechanisms of plated RC beams, and in particular, it incorporates the potential debonding if the externally bonded plate which plays a dominant role in the failure process of

Category	Average	COV	No.tests
Bonded steel plates	1,03	14%	15
Bonded CFRP plates	1,02	15%	68
Bonded GFRP plates	1,02	10%	19

Table 2.17: Comparison between experimental and analytical results [18].

all plated beams. The model is thus applicable to all externally bonded beams irrespective of whether the bonded plate is made of steel of FRP.

The significant advantage of the structural model is that it can predict the mode of failure of the strengthened beam. It is recognized that there are discrepancies between the mode of failure identified by the theory and that reported in literature. This is due to the complex and confusing forms of cracking in the beams at failure.

2.1.7 Casas and Pascual model

Simplified model for a single crack

Many experimental tests have demonstrated the importance of the stiffness of the bonding resin. Starting from Harmon et al. model [29] that accounts for the properties of the bond layer, the concrete strength, the FRP stifness and the extent of flexural cracking, Casas and Pascual [13] proposed a new model, easy to apply, to predict the end debonding and the intermediate crack induced debonding tensile force in FRP sheet. The simplification is based on the fact that for concrete elements with large cross-sections depth, the distance between bending cracks is much larger than the effective bond length of the FRP (L_e). Thus, the condition at a crack is independent of the situation in closer cracks and therefore similar to the conditions of a bond characterization test.

Debonding occurs when the maximum shear stress reaches the allowable stress, namely τ_{max}. Then, the force per unit width in the FRP is:

$$T_u = \tau_{max} L_e$$

where

$$\tau_{max} = \eta \sqrt{f'_c}$$

f'_c is the compressive strength of concrete and η is a coefficient to be determined experimentally so as to best fit the data, equal to 0,996. L_e is the effective bond

length, when the stiffness of the strengthened concrete element is much higher than the FRP stiffness, defined as:

$$L_e = \sqrt{\frac{k_{frp}}{g_b}}$$

where k_f is the axial stiffness per unit length of the FRP, obtained from the Young's modulus and the thickness

$$k_{frp} = E_{frp} t_{frp}$$

g_b is the shear joint stiffness of concrete plus adhesive resin, expressed as

$$g_b = \frac{g_a g_c}{g_a + g_c}$$

The shear stiffness for resin and concrete g_a, g_c are, respectively

$$g_a = \frac{G_a}{t_a}$$
$$g_c = \frac{G_c}{t_{ce}}$$

G_a and G_c are the shear modulus of the resin and concrete. Poisson coefficients for concrete and resin are taken as $0,50$ and $0,38$ respectively. t_a is the resin thickness used in the application of the repair and t_{ce} is the concrete thickness that can be estimated as (in mm)

$$t_{ce} = b_{frp} + 50,8 \leq h/2$$

b_{frp} and h are the width of the FRP and the cross.section depth respectively, expressed in mm.

Simplified model for multiple cracks

In the case of multiple cracks, the distribution of shear stresses in the interface between two consecutive cracks will be, as shown in Fig.2.1.7, the sum of the shear stress distributions generated at each crack section. The failure criteria in the case

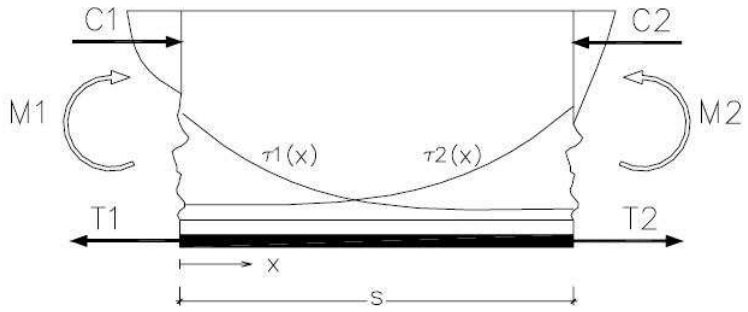

Figure 2.6: Distribution of shear stress in the concrete-FRP interface due to multiple cracking (from Casas and Pascual, 2007 [13]).

of beams can be expressed similarly to the model for single crack multiplied by the coefficient β.

$$T_u = \beta \tau_{max} L_e$$

This coefficient represents the increase in strength that concrete elements with surface-mounted FRP and multiple cracks may have when compared to elements with a single crack. β summarized all information concerning mechanical properties and thickness of the materials, influence of cracking and load sequence up to failure. It is equal to

$$\beta = \frac{\xi_1}{1 - \xi_2 \xi_3}$$

The coefficients ξ_1 and ξ_2 are defined by the following functions:

$$\xi_1 = \frac{e^{s/L_e} - e^{-s/L_e}}{e^{s/L_e} + e^{-s/L_e}}$$
$$\xi_2 = \frac{2}{e^{s/L_e} + e^{-s/L_e}}$$

where s is the distance between consecutive cracks. A reasonable estimate of the crack spacing is half of the effective depth of the concrete member, d ($s \simeq d/2$).

The simplified model is based on the shape of the diagram moment-tension in the FRP. The typical shape of this curve is presented in Fig2.1.7. The two different

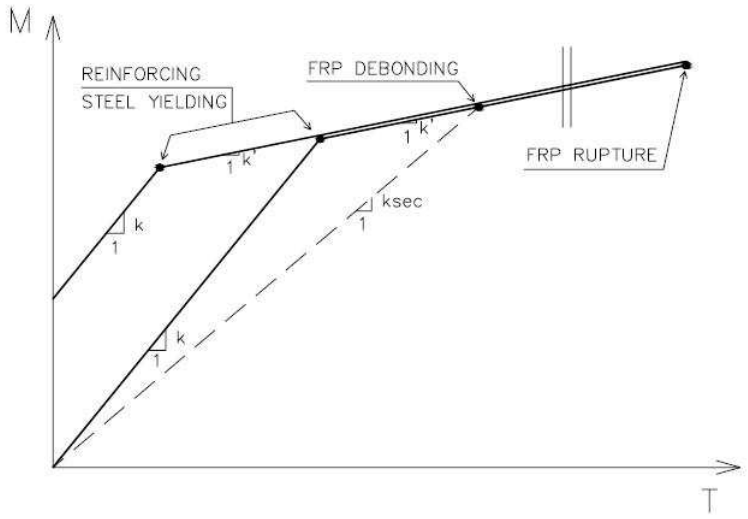

Figure 2.7: Relationship moment-tension in the FRP. Definition of k, k' and k_{sec} (from Casas and Pascual, 2007).

parts at the beginning depend on the level of the bending moment in the cross-section when the FRP is applied. As seen, the relationship may be idealized as a bilinear behavior and the slopes of the linear (k) and post-yielding (k') do not depend on the level of load at the moment of repair. Assuming debonding occurs in the post-yielding state, and that both M_1 and M_2 are in the second part of the M-T diagram, then $k' = \frac{M_1 - M_2}{T_1 - T_2}$ and the value of ξ_3 can be expressed as:

$$\xi_3 = 1 - \theta \frac{k}{k'}(1 - r)$$

where $r = M_2/M_1$ and $\theta = k_{sec}/k = 2/3$ is the ratio between the secant slope of the diagram M-T in section 1 at the moment of debonding (M_1/T_1) and the slope in the linear part. r is the ratio between the bending moment M_2 at a distance $d/2$ of the section of interest and the bending moment at this section M_1 obtained in a linear-elastic analysis.

2.2 Existing models for bond behavior in prism specimens

Various models readily available in different studies were collected by Toutanji et al. [62] to predict the bond strength of FRP-to-concrete bonded specimens. Eleven models were categorized as empirical models that are based directly on the regression of test date: fracture mechanics based models and design proposals that were generally based on some simple assumption. Another five models are based on average bond stress. And the last one is a model based on interface fracture energy and tension stiffness of FRP sheets.

2.2.1 Models considering effective bond length

Chen and Teng (2001) [16] based their model on the nonlinear fracture mechanics (NLFM) solution developed by Yuan and Wu (1999) for predicting bond strength and effective bond length, given as

$$P_u = 0,427\beta_p\beta_L\sqrt{f'_c}b_{frp}L_e$$

where

$$L_e = \sqrt{\frac{E_{frp}t_{frp}}{\sqrt{f'_c}}} \qquad \beta_p = \sqrt{\frac{2 - b_{frp}/b}{1 + b_{frp}/b}}$$

and

$$\beta_L = \begin{cases} 1 & if \quad L \geq L_e \\ \sin\frac{\pi L}{2L_e} \end{cases}$$

They also modified the above expression to propose a model that can be used for ultimate strength design as

$$P_u = 0,315\beta_p\beta_L\sqrt{f'_c}b_{frp}L_e$$

Maeda et al. (1997) [62] introduced a model based on the concept of effective bond length L_e

$$P_u = b_f L_e \left(110,2 \times 10^{-6} E_{frp}t_{frp}\right)$$

where

$$L_e = e^{6,13-0,58 \ln E_{frp}t_{frp}} \ (mm); \quad E_{frp}t_{frp} \ (GPa\,mm)$$

The bond length L was used in place of effective bond length to calculated the load when $L < L_e$.

Khalifa et al. (1998) [33] based their model on the guidelines of the Maeda et al. [62] model and proposed the inclusion of concrete compressive strength factor

$$P_u = b_{frp}L_e \left[\frac{110,2}{10^6} \left(\frac{f'_c}{42} \right)^{2/3} E_{frp}t_{frp} \right]$$

Neubauer and Rostasy (1997) [62] modified the Holzenkämpfer (1994) bond strength model proposed for steel strengthened concrete using nonlinear fracture mechanics as follow:

$$P_u = \begin{cases} 0,64k_{frp}b_{frp}\sqrt{E_{frp}t_{frp}f_{ctm}} & if \quad L \geq L_e \\ 0,64k_{frp}b_{frp}\sqrt{E_{frp}t_{frp}f_{ctm}}\frac{L}{L_e}\left(2 - \frac{L}{L_e}\right) & if \quad L < L_e \end{cases}$$

where

$$L_e = \sqrt{\frac{E_{frp}t_{frp}}{2f_{ctm}}} \quad \text{and} \quad G_f = c_f f_{ctm}$$

They reported the average value of $0,204$ for c_f, with a standard deviation of $0,053$ for 51 specimens from the results of double shear tests conducted on CFRP-to-concrete bonded joints. f_{ctm} is defined as the concrete surface tensile strength, but since it is not available in the reported data, concrete splitting tensile strength f_{ct} is used in its place.

The Niedermeier (1996) [62] model was a modification of the Holzenkämpfer model as shown

$$P_u = \begin{cases} 0,78b_{frp}\sqrt{2G_f E_{frp}t_{frp}} & if \quad L \geq L_e \\ 0,78b_{frp}\sqrt{2G_f E_{frp}t_{frp}}\frac{L}{L_e}\left(2 - \frac{L}{L_e}\right) & if \quad L < L_e \end{cases}$$

where

$$L_e = \sqrt{\frac{E_{frp}t_{frp}}{4f_{ctm}}} \quad \text{and} \quad G_f = c_f k_{frp}^2 f_{ctm}\ (Nmm/mm^2)$$

and

$$k_f = \sqrt{1,125\frac{2 - b_{frp}/b}{1 + b_{frp}/400}}$$

Lu et al. (2005) [34] proposed a model on the basis of interfacial fracture energy regardless of the shape of the bond-slip curve.

They defined the bond length factor β_l as per the Neubauer and Rostasy [62] definition. The analytical solution for effective bond length L_e was equal to:

$$P_u = \beta_l b_{frp}\sqrt{2E_{frp}t_{frp}G_f}$$

where

$$\beta_l = \begin{cases} 1 & for \quad L > L_e \\ \frac{L}{L_e}\left(2 - \frac{L}{L_e}\right) & for \quad L \leq L_e \end{cases}, \qquad G_f = 0,308\beta_w^2\sqrt{f_{ct}}$$

$$\beta_w = \sqrt{\frac{2,25 - b_{frp}/b}{1,25 + b_{frp}/b}}$$

$$L_e = a + \frac{1}{2\lambda_1} ln \frac{\lambda_1 + \lambda_2 tan(\lambda_2 a)}{\lambda_1 - \lambda_2 tan(\lambda_2 a)}, \quad \lambda_1 = \sqrt{\frac{\tau_{max}}{s_o E_{frp} t_{frp}}}, \quad \lambda_2 = \sqrt{\frac{\tau_{max}}{(s_{frp} - s_o) E_{frp} t_{frp}}}$$

$$a = \frac{1}{\lambda_2}\sin^{-1}\left[0,99\sqrt{\frac{s_{frp} - s_o}{s_{frp}}}\right], \quad \tau_{max} = 1,50\beta_w f_{ct}$$

$$s_o = 0,0195\beta_w f_{ct}, \quad s_{frp} = \frac{2G_f}{\tau_{max}}$$

The Sato model (2003) [62] is based on FRP thickness, stiffness and concrete compressive strength

$$P_u = (b_{frp} + 2\Delta b)L_e(2,68f_c'^{0,2}t_{frp}E_{frp} \times 10^{-5})$$

where

$$L_e = 1,89(E_{frp}t_{frp})^{0,4} \quad \text{provided} L_e \leq L$$

and $\Delta b = 3,7mm$, i.e., working width of concrete.
The Iso model (2003) [62] is directly a function of concrete compressive strength

$$P_u = b_{frp}L_e\left(0,93f_c'^{0,44}\right)$$

where

$$L_e = 0,125\left(E_{frp}t_{frp}\right)^{0,57} \quad \text{provided} \quad L_e \leq L$$

The Yang et al.(2001) [62] model is based on concrete tensile strength, but another noticeable factor is that it considers the effective bond length L_e as a constant equal to $100mm$

$$P_u = \left(0,5 + 0,08\sqrt{\frac{E_{frp}t_{frp}}{100f_{ct}}}\right) L_e b_{frp}(0,5f_{ct})$$

2.2.2 Models not considering effective bond length

Tanaka (1996) [62] defined a simple empirical model in terms of the average bond shear stress at failure, where the bond length L is in mm

$$P_u = b_{frp}L(6,13 - \ln L)$$

Hiroyuki and Wu (1997) [62] had a similar empirical model, where the bond length L is in cm

$$P_u = b_{frp}L\left(5,88L^{-0,669}\right)$$

Brosens and van Germet (1997) [62] proposed a simple design rule based on very few parameters

$$P_u = 0,5 b_{frp} L f_{ctm}$$

Since the concrete surface tensile strength f_{ctm} is not available in the reported data, concrete splitting tensile strength f_{ct} is used in its place.

Izumo (2003) [62] proposed two different expressions for carbon and aramid fiber sheets separately

$$P_u = (3,8 f_c'^{2/3} + 15,2) L b_{frp} t_{frp} E_{frp} \times 10^{-3}; \qquad \text{for carbon fiber sheets}$$

$$P_u = (3,4 f_c'^{2/3} + 69) L b_{frp} t_{frp} E_{frp} \times 10^{-3}; \qquad \text{for aramid fiber sheets}$$

Adhikary and Mutsuyoshi (2001) [62] presented a simple expression for bond strength that is directly a function of concrete compression strength

$$P_u = b_{frp} L (0,25 f_c'^{2/3})$$

2.2.3 Models independent of bond length

Täljsten (1996) [55, 57] model is based on nonlinear fracture mechanics analysis.

$$P_u = \sqrt{\frac{2 E_{frp} t_{frp} G_f}{1 + \alpha_T}} b_{frp}$$

where

$$\alpha_T = \frac{E_{frp} t_{frp}}{E_c t}$$

As the expression for G_f is not known from the source, to calculate the fracture energy is applied a simple bilinear relationship between the variation of fracture energy and concrete strength proposed by Zhao (2005) [62], give as

$$G_f = \begin{cases} 0,014 f_c' & if \quad 0 \leq f_c' \leq 46,2 MPa \\ 0,65 & if \quad f_c' \geq 46,2 MPa \end{cases}$$

Yuan and Wu (1999) [62, 67] used a linear elastic fracture mechanics for predicting their model. They proposed a similar equation as Täljsten [55] but with modification that included the width ratio of FRP to concrete

$$P_u = \sqrt{\frac{2E_{frp}t_{frp}G_f}{1+\alpha_Y}}b_{frp}$$

where

$$\alpha_Y = \frac{b_{frp}E_{frp}t_{frp}}{bE_ct}$$

Dai et al. (2005) [19] conducted a series of single-lap pullout tests to determine the local bond stress-slip relationship of FRP-concrete interface. They proposed the bond strength based on interfacial fracture energy and FRP stiffness as

$$P_u = (b_{frp} + 2\Delta b)\sqrt{2E_{frp}t_{frp}G_f}$$

where

$$G_f = 0,524f_c^{0,236}\ (N/mm)$$

The value of the working width of concrete $\Delta b = 3,7mm$ is based on experimental analysis.

The comparison of models is based on parameters involving statistical functions like average value, standard deviation and coefficient of variation of the experimental to predicted bond strength ratio . Toutanji et al. [62] collected an experimental data that consists of 351 concrete primes bonded with FRP plates tested in single and double shear tests, from experimental studies by Zhao, Maeda et al., Adhikary and Mutsuyoshi, Sharma et al., Seracino, Yao et al., Fuquan et al., Bizindavyi and Neale, Chajes et al., Taljsten, Tan, Zhao et al., Takeo et al., Ren, Ueda et al., Wu et al., Kamiharako et al. and Nakaba et al..

Models for bond behavior	Average	COV	No. tests
Chen and Teng (2001)	1,167	28%	351
Chen and Teng modified (2001)	1,581	28%	351
Maeda et al. (1997)	1,076	34%	351
Khalifa et al. (1998)	1,253	34%	351
Neubauer and Rostasy (1997)	0,891	29%	351
Niedermeier (1996)	1,370	30%	351
Lu et al. (2005)	1,221	29%	351
Sato, JCI (2003)	0,780	50%	351
Iso, JCI (2003)	1,086	33%	351
Yang et al. (2001)	1,189	33%	351
Tanaka (1996)	2,081	55%	345
Hiroyuki and Wu (1997)	2,101	47%	351
Brosens and van Germet (1997)	1,392	53%	351
Izumo, JCI (2003)	0,739	62%	215
Adhikary and Mutsuyoshi (2001)	0,843	56%	351
Taljsten (1996)	1,314	33%	351
Yuan and Wu (1999)	1,311	32%	351
Dai et al. (2005)	0,673	29%	351

Table 2.18: Experimental to predicted bond-strength ratios [62].

Chapter 3

Analysis of flexural tests data

3.1 Selection criteria for constructing a test database

To compare the debonding strength models explained in the previous chapter, it was created a large database which included many plated reinforced concrete beams tested from 1991 to 2007.

It was assembled with clear selection criteria. For inclusion in this database, the following requirements must be met:

- failure of the beam was by plate end debonding;
- the FRP plate was neither prestressed nor anchored in any form at its ends;
- the beam never experienced loading before being loaded to debonding failure;
- sufficient details for various geometric and material parameters were provided to enable the results to be used with confidence.

The only geometric and material properties assumed in the database, if it not available in the reported data, are depth of concrete cover which is assumed be 10% of the overall beam depth which is similar to the average of the different cover depths used for other beams in the database, and modulus of elasticity of steel reinforcement ($200GPa$). The concrete characteristics were calculated using the ACI 318-95 code expressions. For the elastic modulus of concrete E_c (in MPa) and the splitting tensile strength of concrete f_{ct} (in MPa) were adopted which are related to the concrete cylinder compressive strength f'_c in (MPa) as follows:

$$E_c = 4730\sqrt{f'_c} \tag{3.1}$$

$$f_{ct} = 0,53\sqrt{f'_c} \tag{3.2}$$

For beams with only the concrete cube compressive strength f_{cu} reported, the concrete cylinder strength was taken to be $0,8 f_{cu}$.

For beams with pultruded plates, the adhesive layer thickness was sometimes not reported. In such cases, the thickness of the adhesive layer was assumed to be 2 mm, a value similar to the average of those reported for the remaining beams with pultruded plates.

For beams strengthened with FRP plates constructed in a wet lay-up process, the thickness of the FRP plate vs the thickness of the adhesive, was generally not available. The adhesive layer thickness were worked out using the following formulas for a single layer of FRP:

$$t_a = \frac{t_{frp,g} - t_{sheet}}{2}$$
$$t_{frp} = t_a + t_{sheet}$$

Based on the assumptions that the sheet sits in the middle of the adhesive, and the sheet and the outside form the plate. For the latter cases, t_a was assumed to be 0,42 mm based on measurements of plates samples formed from carbon fiber sheet by wet lay-up in the authors' laboratory, and the FRP plate thickness, t_{frp}, was worked out from the previous equation for a single layer of FRP. For cases where the FRP plate was formed from a number of layers, the total plate thickness was found by multiplying the single layer thickness by the number of layers by assuming that the adhesive thickness between two sheets is t_a.

Due to this additional uncertainty with wet lay-up plates, test data of beams with wet lay-up plates and those with pultruded plates are appropriately differentiated from each other in comparisons.

If the elastic modulus of the adhesive was not reported, it was assumed to be 8500 MPa, a value close to the average of the values reported for the other cases of the database (an average of 8697 MPa from 37 tests of Smith and Teng database [53]).

In the database was reported the RC beam details where b, h, d, d', f'_c, f_{cu},E_c and f_{ct} denote the width of RC beam, overall depth of RC beam, distance from beam compression face to centroid of steel tension reinforcement, distance from beam compression face to centroid of steel compression reinforcement, concrete cylinder compressive, cube compressive strength, modulus of elasticity of concrete, and concrete cylinder splitting tensile strength respectively. Then was reported the reinforcement properties, where E_s, E'_s and E_{yv} denote the moduli of elasticity of the steel tension reinforcement, steel compression reinforcement and steel shear reinforcement (stirrups only) respectively while f_y, f'_y and f_{yv} denote the corresponding yield strength and A_s, A'_s, A_{sv} the corresponding cross-sectional areas. The reinforcement material

properties E_a, t_a, E_{frp}, f_{frp}, t_{frp}, b_{frp} and a denote the modulus of elasticity of adhesive, thickness of adhesive layer, modulus of elasticity of FRP, tensile strength of FRP in the main fiber direction, FRP thickness, FRP width, and the distance from the support to the nearer end of the soffit plate. Also it was given the details of loading configuration and the failure load where B, L and V_{exp} represent the distance form the support to the nearer applied load, the span of the beam and the experimental shear force at the plate end to cause debonding.

The database collected 161 beams tested under four-point bending and reported by 34 authors. The tests including 14 glass fiber reinforced polymer beams and 147 carbon fiber reinforced polymer beams. The data are divided by material and bonded form (prepeg systems and wet lay-up system).

In the sequent paragraphs are going to have applied:Jasze model, Ahmed and van Gemert model, Wang and Ling model reported by Smith and Teng [52, 53], Smith and Teng model [53], Colotti et al. model [18], Teng and Yao model [61], Casas and Pascual model [13], Ziraba et al. model [70], Raoof and Zhang model [42], Raoof and Hassanen model [43] explained in the previous chapter, to 90 C-W data, 57 C-P data, 7 G-W data, 7 G-P data.

The comparison between the different model was done with the following values: "average of difference", Bias and COV, where:

$$\text{Difference} = \frac{V_{an} - V_{exp}}{V_{exp}} \ [\%] \tag{3.3}$$

$$\text{Bias} = \frac{\overline{V_{exp}}}{V_{an}} \tag{3.4}$$

$$\text{COV} = \sqrt{\frac{1}{N}\sum_{1}^{N}\left(\frac{x_i}{\mu} - 1\right)^2} \ [\%] \tag{3.5}$$

where N is the total number of tests, x_i and μ are the single value of bias and the average of bias, respectively.

3.2 Jansze model

Jansze model [52] was proposed for steel plated beams and the predictions of failure load for FRP plated beams are characterized by an high difference from the experimental load. No all data can be used, when the soffit plates terminate at the support (a=0) the model is not valid. Only one C-P plated beam is not valid for this model, 14 C-W plated beams and one G-P plated beam.

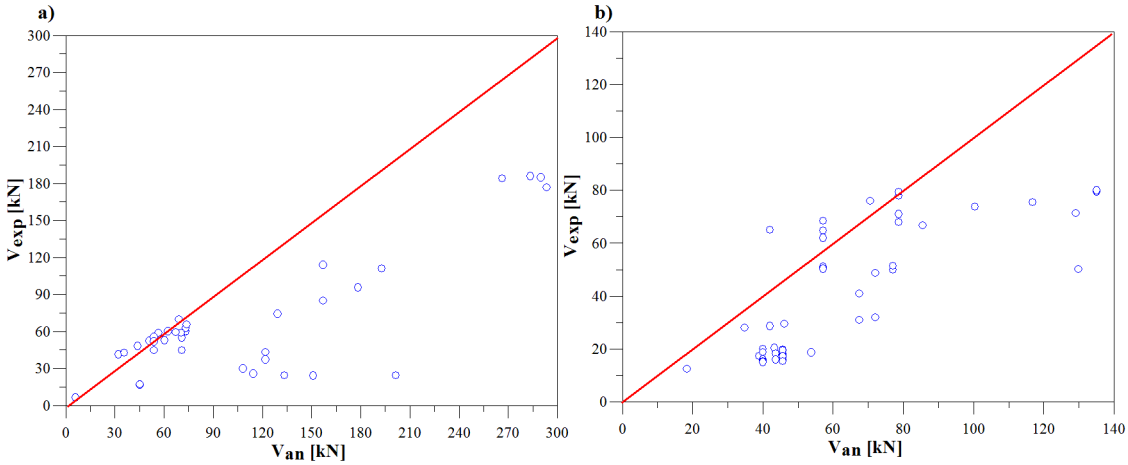

Figure 3.1: Test results vs predictions of Jansze model [52]. a)CFRP wet lay-up system (77 valid tests); b)CFRP prepeg system (50 valid tests).

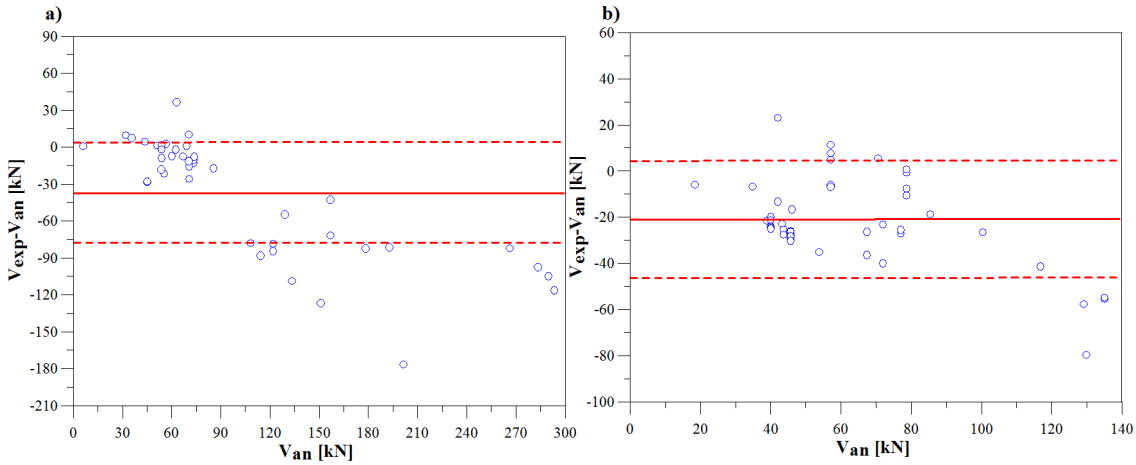

Figure 3.2: Difference between test results and analytical vs predictions of Jansze model [52]. a)CFRP wet lay-up system μ=-35,4kN, σ=37,9kN (77 valid tests); b)CFRP prepeg system μ=-21,4kN, σ=18,4kN (50 valid tests).

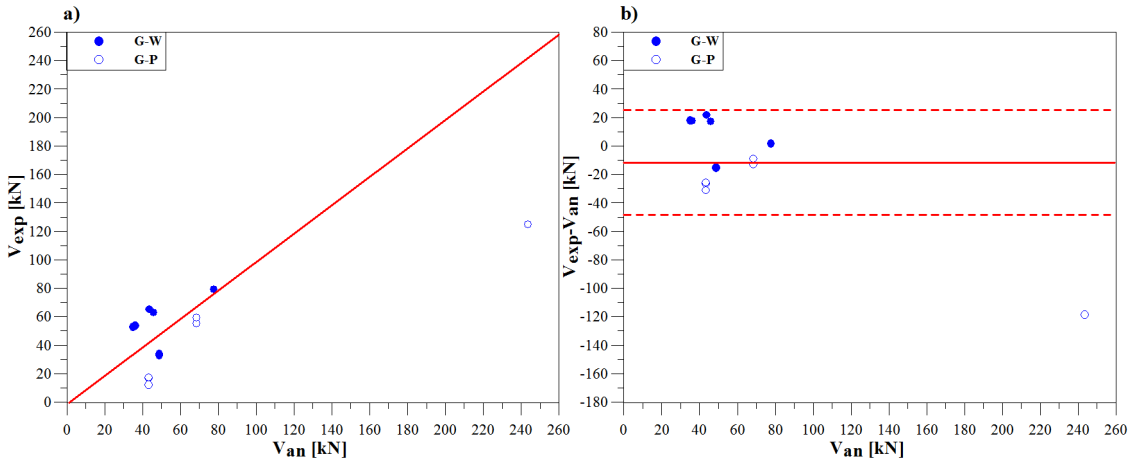

Figure 3.3: a)Test results vs predictions of Jansze model [52], GFRP wet lay-up system (7 valid tests) and GFRP prepeg system (6 valid tests);b)Difference between test results and analytical vs predictions of Jansze model [52] μ=-13,6kN, σ=35,2kN

The Ross beam tests [53] have the FRP plates that terminate at $1mm$ to the support. Calculating the critical shear forces causing debonding, they are too high to be considered in the comparison between experimental and analytical load. In this case, it was considered that the FRP plates terminate at the support and B_{mod} becomes zero.

The Jansze model [52] is valid on more than 90% of data tests.

	Average of difference	Bias	COV	n. of tests
C-W	$77,8\%$	$0,68$	$44,0\%$	77
C-P	$82,1\%$	$0,64$	$43,1\%$	50
G-W	$5,7\%$	$1,18$	$29,7\%$	7
G-P	$114,2\%$	$0,55$	$40,1\%$	6

Table 3.1: Comparison between experimental and analytical results calculated with Jansze model [52].

As seen in Tab.3.1, this model presents a significantly dispersion of tests results vs predictions values (Fig3.1 and Fig.3.3). In some cases the analytical failure loads are greater than the experimental loads. This means that the beam fails due to a load lower than the design load. The averages of the differences demonstrate that the model is not able to predict correctly the critical load force. The RC beams reinforced with CFRP prepeg system present a bias of $0,64$ and a COV equal to

$43,1\%$. While the C-W group has an higher uncertainly of result being COV $44,03\%$ and a bias of $0,68$. Regarding GFRP sheets, beams reinforced with GFRP applied with wet-lay up system are characterized by good value of coefficient of dispersion, equal to $29,7\%$ an a bias of $1,18$; not good is the prediction of GFRP prepeg system reinforcement being the COV as high as CFRP sheets, $40,1\%$ and a bias equal to $0,55$.

Taking into account Fig.3.2 and Fig.3.3b, the difference between the experimental value of failure load and the analytical value presents an high dispersion and the majority of point are set in unsafe side ($V_{exp} > V_{an}$). Jansze model, applied to C-W data, gave an average of difference between V_{exp} and V_{an} equal to $-35,44kN$ and a standard deviation of $37,9kN$; while C-P group is characterized by an average value closer to zero, being $-21,41kN$ and σ equal to $18,4kN$. Considering all beams reinforced with glass sheets, results that μ is equal to $-13,6kN$ and σ is equal to $35,17kN$.

3.3 Ahmed and van Gemert model

Ahmed and van Gemert [62] modified the Jansze model [62] to be suitable for use with FRP-plated RC beams.

The authors introduced an equivalent steel plate that has the same total tensile capacity and width as that of FRP plate, but with an equivalent thickness determined assuming that the yield stress of steel is $550MPa$.

$$s_{s,eq} = \frac{A_{frp}}{b_{frp}} \frac{f_{frp}}{f_y}$$

This equivalent steel plate is needed to calculate the increment of shear force in FRP plate $\Delta\tau_{mod}$. This correction can be positive or negative and it depends principally on the plate characteristics.

The number of valid tests is the same of Jansze model [52] because Ahmed and van Gemert [52] used the validity condition of the previous model. For this reason it was used the same hypothesis about Ross data [53].

As seen in Fig.3.4 and Fig.3.5, the model predicted a good values of bias but the predictions are characterized by high dispersion. The beams reinforced with wet-lay up system presented a bias of $0,67$ and a coefficient of variation of $47,0\%$. The bias of C-P group is closer to unity being $0,82$ but COV is higher than C-W group data. Both C-P and C-W data present an average of prediction failure load lower than real load being μ equal to $-36,7kN$ and $-17,1kN$ for C-W and C-P, respectively. Standard deviation is higher in beams reinforced with carbon sheets applied with

	Average of difference	Bias	COV	n. of tests
C-W	69,2%	0,67	47,0%	77
C-P	51,3%	0,82	68,3%	50
G-W	20,0%	1,27	13,5%	7
G-P	79,6%	0,72	53,1%	6

Table 3.2: Comparison between experimental and analytical results calculated with Ahmed and van Gemert model [52].

wet-lay up system than beam reinforced with prepeg carbon sheets being equal to $42,8kN$ and $25,0kN$ for C-W and C-P, respectively.

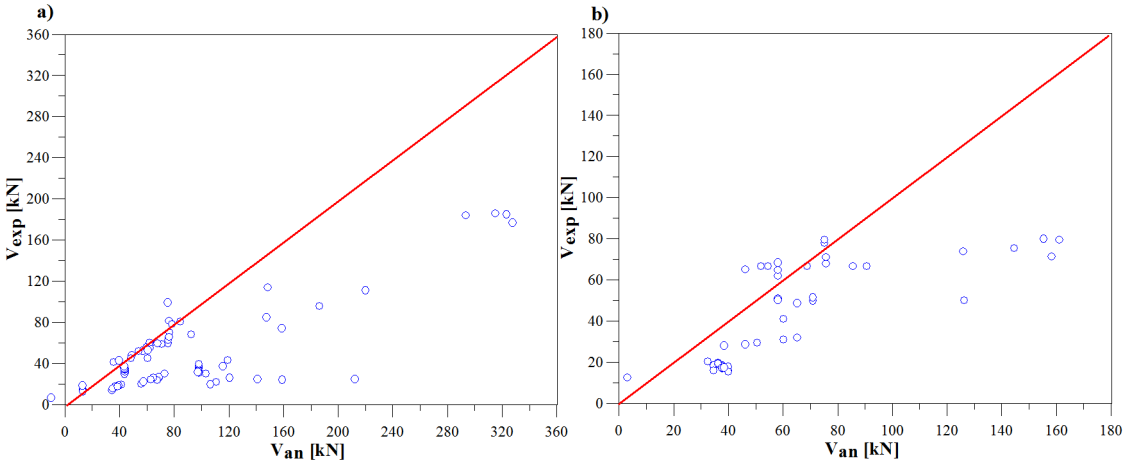

Figure 3.4: Test results vs predictions of Ahmed and Van Gemert model [52]. a)CFRP wet lay-up system (77 valid tests); b)CFRP prepeg system (55 valid tests).

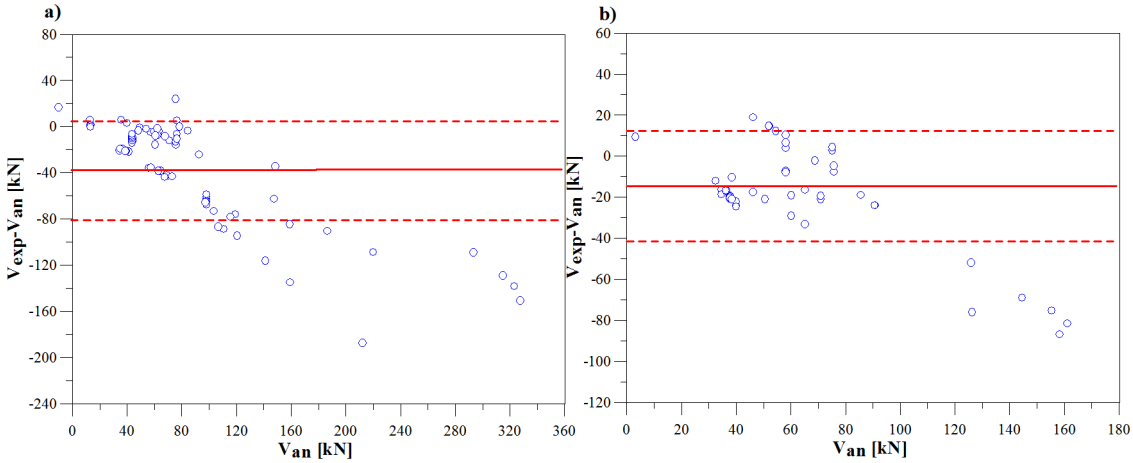

Figure 3.5: Difference between test results and analytical vs predictions of Ahmed and Van Gemert model [52]. a)CFRP wet lay-up system μ=-36,7kN, σ=42,8kN (77 valid tests); b)CFRP prepeg system μ=-17,1kN, σ=25,0kN (55 valid tests).

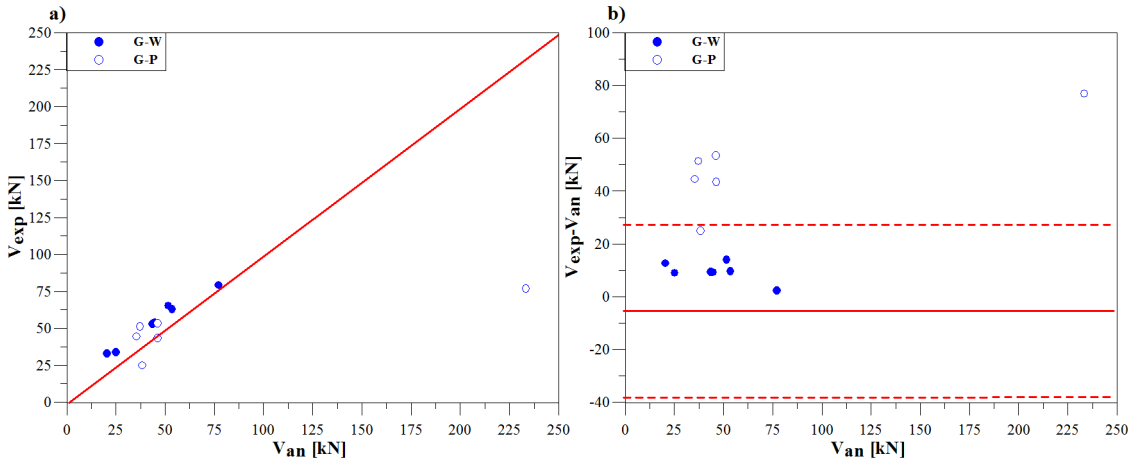

Figure 3.6: a)Test results vs predictions of Ahmed and Van Gemert model [52], GFRP wet lay-up system (7 valid tests) and GFRP prepeg system (6 valid tests);b)Difference between test results and analytical vs predictions of Ahmed and Van Gemert model [52] μ=-6,4kN, σ=32,3kN.

In Fig.3.6 are represented the prediction of load failure of beams glass sheets, wet-lay up and prepeg. The model is good for G-W data where gives the lower value of COV being $13,5\%$ and a bias of $1,27$; while G-P group is characterized by a bias equal to $0,72$ and a COV equal to $53,1\%$. In this case, the majority of data are set in safe side, this means that the predict failure load is lower than experimental failure load. The average of P_{exp}-P_{an} is equal to $-6,36kN$ and the standard deviation is equal to $32,3kN$.

Comparison between Ahmed and van Gemert model and Jansze model

Comparing the two model, the modification done to use FRP-plated RC beams improves the analytical prediction. The average of V_{exp}/V_{an} is closer to the unit than Jansze model [52], although the coefficient of variation is higher.

Neither Jansze model [52] nor Ahmed and van Gemert model [52] depend on the bonding system. In the first one, the C-W data present a greater dispersion than the C-P data; while in the second model the prediction of debonding load in C-W data are more accurate. The C-P predictions should be better than the C-W prediction with less uncertainty. This is due to the better application system that reduce the weakness of bond. Both models are not good for design purpose because the value test results vs predictions are presented above and under the red line and the high dispersion of the data reduced the reliability of these models.

3.4 Smith and Teng model

The first step was to calculate the flexural debonding moment at the end of the plate $M_{db,f}$. To do this it needs define the cracked second moment of area of the plated section transformed to concrete $I_{tr,c}$. The moment of inertia about the neutral axis is:

$$I_{tr,c} = \frac{by_n^3}{12} + by_n\left(\frac{y_n}{2}\right)^2 + n_s A'_s\left(y_n - d'\right)^2 + n_s A_s\left(d - y_n\right)^2 + n_{frp}A_{frp}\left(d_{frp} - y_n\right)^2 \tag{3.6}$$

where y_n is the neutral axis, n_s is the modular ratio of elasticity between steel and concrete E_s/E_c, n_{frp} is the modular ratio of elasticity between FRP and concrete E_{frp}/E_c, d_{frp} is the distance from beam compression face to centroid of FRP reinforcement and A_{frp} is FRP reinforcement area.

The neutral axis was calculated as follows:

$$y_n = \frac{\varepsilon_c}{\varepsilon_c + \varepsilon_{frp}} d_{frp} \tag{3.7}$$

where ε_c is the compressive strain in the concrete taken as $3,5‰$, ε_{frp} is tensile strain in the FRP, calculated as:

$$\varepsilon_{frp} = \frac{f_{frp}}{E_{frp}}$$

The authors limited the range of applicability of the model, it is suggested that their model can only used when $M_{db,end}/M_u \leq 0,67$; where $M_{db,end}$ and M_u are the moment applied at the end of the plate and the flexural strength of the section, respectively, as follows:

$$M_{db,end} = V_{exp} \cdot a \tag{3.8}$$

$$M_u = A_s f_y d + A_{frp}\varepsilon_{frp}E_{frp}d_{frp} - \frac{\alpha\beta^2 f'_c y_n^2 b}{2} - A'_s\varepsilon'_s E_s d' \tag{3.9}$$

where the terms α and β are parameters defining a rectangular stress block in the concrete equivalent to non linear distribution of stress. If concrete crushing is the controlling mode of failure (before or after steel yielding), α and β can be taken as the values associated with the Whitney stress block ($\alpha = 0,85$ and β from section

10.2.7.3 of ACI318-05). If FRP rupture, cover delamination, or FRP debonding occur, the Whitney stress block will give reasonably accurate results.

The delamination occurs when:

$$\frac{M_{db,end}}{M_{db,f}} + \frac{V_{db,end}}{V_{db,s}} \geq 1,17$$

where $V_{db,end}$ is the shear force at the plate end as follows:

$$V_{db,s} = \eta\,[1,4 - d/2000]\,bd\,\left[\rho_s f'_c\right]^{1/3} \tag{3.10}$$

The value of η could be different by 1,5 like the authors demonstrated. It was examined the effects of the change of η on the Smith and Teng database [53].

η	No. of valid tests	Bias	COV
1,4	59	1,65	25,5%
1,5	48	1,61	23,0%

Table 3.3: Comparison between $\eta = 1,4$ and $\eta = 1,5$ using Smith and Teng model [53].

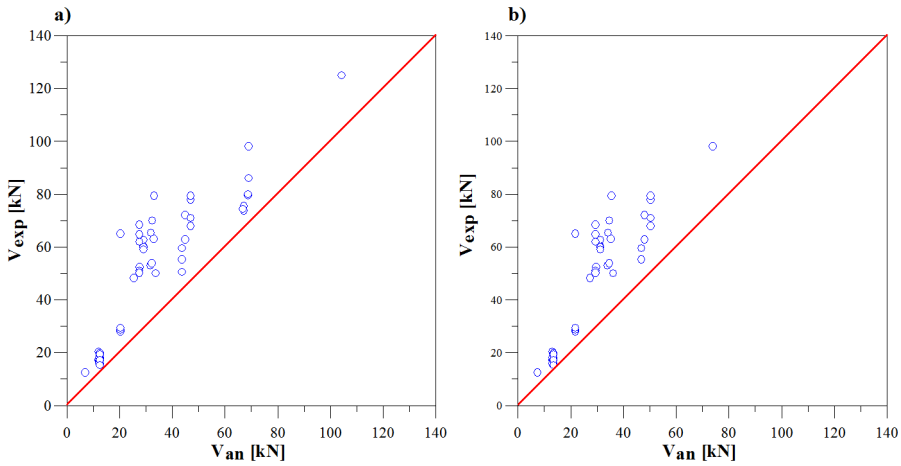

Figure 3.7: Comparison between $\eta = 1,4$ and $\eta = 1,5$.

With a smaller value of η it obtained more valid tests with a greater value of COV (coefficient of variation). It was chosen to use $\eta = 1,4$ to obtained a greater

	Average of difference	Bias	COV	n. of tests
C-W	35,7%	1,66	27,0%	69
C-P	34,7%	1,62	26,8%	39
G-W	28,9%	1,52	24,3%	3
G-P	25,6%	1,35	6,5%	6

Table 3.4: Comparison between experimental and analytical results calculated with Smith and Teng model [53].

database for this model with 59 of 67 valid tests. It caused a greater dispersion of values, $25,5\%$ and it is recommended (by the authors too) in practical design [53].

The Smith and Teng model [53] can predict if the beam fails due to debonding, but doesn't give information about different failure modes. Taking into account all data, 42 beams don't fail for debonding, in the 75% of cases, the model prediction is correct.

It was considered all data and were divided in four groups: C-W, C-P, G-W, G-P. The valid tests are 69 for C-W plates, 39 for C-P plates, 3 for G-W plates and 6 for G-P plates.

In the comparison plots, Fig3.8 and Fig.3.10a, it is showed that all values are above the red line that represents the condition $V_{exp} = V_{an}$. This means that the experimental shear force needed to delaminate FRP plates is greater than the analytical.

As reported is Tab.3.4, there isn't great difference between the failure loads predict in C-P and C-W group. The COV value is equal to $26,8\%$ for beams reinforced with prepeg carbon plate and in wet lay-up applied sheets is equal to $27,0\%$; the bias is higher than unity being $1,62$ and $1,66$ for C-P and C-W group, respectively. Taking into account the difference between the experimental load and the analytical, as seen in Fig.3.9, all values are set over the zero line and presented a lower value of σ than Jansze model [52] and Ahmed and Van Gemert model [52] being $21,6kN$ and $12,9kN$ for C-W and C-P group, respectively; while the average values are equal to $-21,3kN$ and $-16,2kN$ for C-W and C-P data, respectively.

The best prediction results to be for prepeg glass sheets where the COV is equal to $6,5\%$ and bias is equal to $1,35$. The G-W analytical results are similar to predictions of beams reinforced with carbon sheets; the coefficient of variation is equal to $24,3\%$, while the bias is $1,52$. Considering glass sheets all together, the average of difference between experimental and analytical failure load id equal to $13,7kN$. All prediction values are higher than experimental results being σ equal to $8,2kN$.

The goodness of model is represented by a low dispersion of data and a their position is the safe side (where $V_{an} < V_{exp}$). There isn't a difference quality of prediction between prepeg and wet lay-up sheets because it was used the same model. This model starts from a calibration of different tests without any mechanical approach, these is the reason of the limitation on moment applied that the authors used. The model should be improve using more data for the calibration. It doesn't give information about another mode of failure.

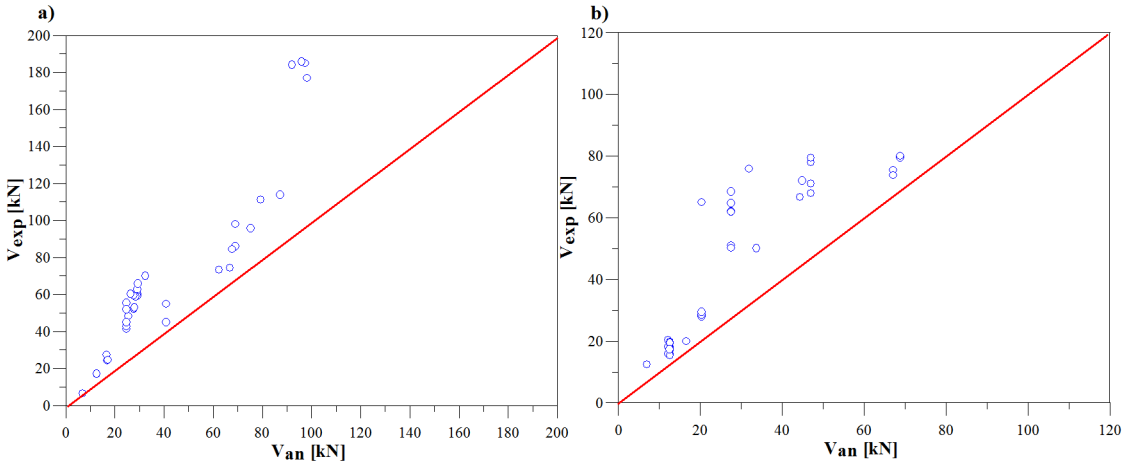

Figure 3.8: Test results vs predictions of Smith and Teng model [53].a)CFRP wet lay-up system (69 valid tests); b)CFRP prepeg system (39 valid tests).

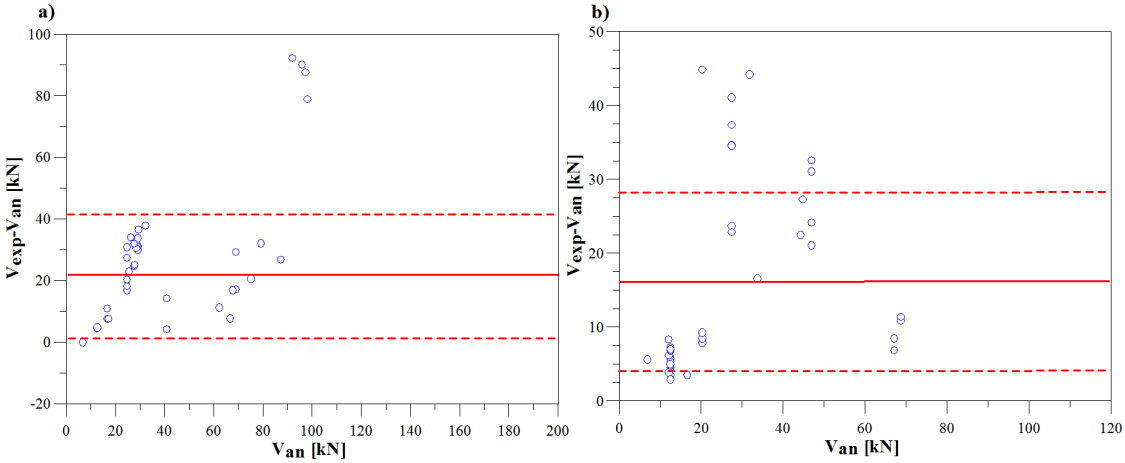

Figure 3.9: Difference between test results and analytical vs predictions of Smith and Teng model [53]. a)CFRP wet lay-up system μ=21,3kN, σ=21,6kN (69 valid tests); b)CFRP prepeg system μ=16,2kN, σ=12,9kN (39 valid tests).

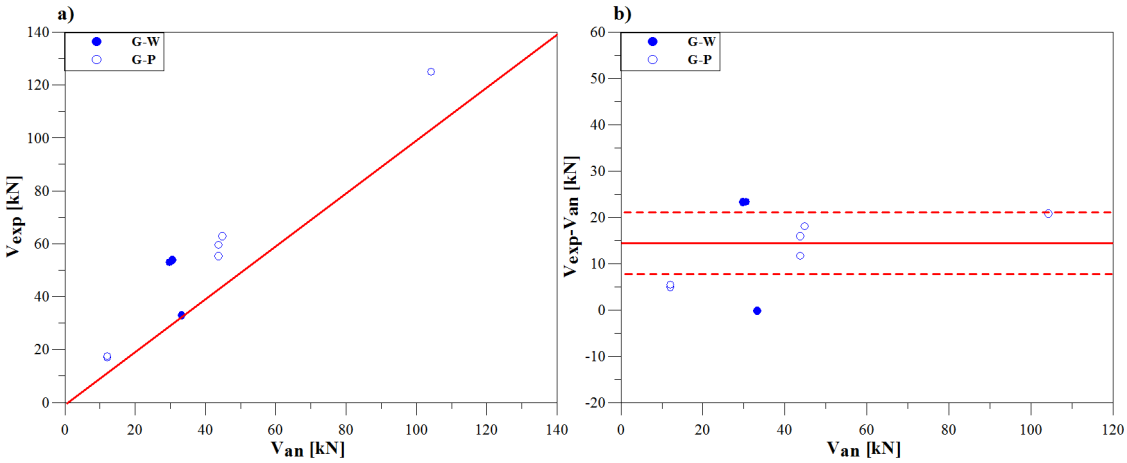

Figure 3.10: a)Test results vs predictions of Smith and Teng model [53], GFRP wet lay-up system (3 valid tests) and GFRP prepeg system (6 valid tests);b)Difference between test results and analytical vs predictions of Smith and Teng model [53] μ=13,7kN, σ=8,2kN.

3.5 Colotti et al. model

This model was based on the lesser load needed to fail the beam. Four different failure modes were considered: bond failure, shear failure, concrete crushing, flexural plate rupture mode. This model determines the ultimate load for each failure mode and then defines the failure mode that occurs and its load.

For many tests, the model predicts a different failure mode of debonding and reduces the number of valid tests. It is possible to take into account all loads predicted without difference between the four failure modes, as represented in Fig.3.11.

To compare these two hypothesis it was examined only the data of Smith and Teng [53] and Colotti et al. [18] database without distinction neither material nor applying system.

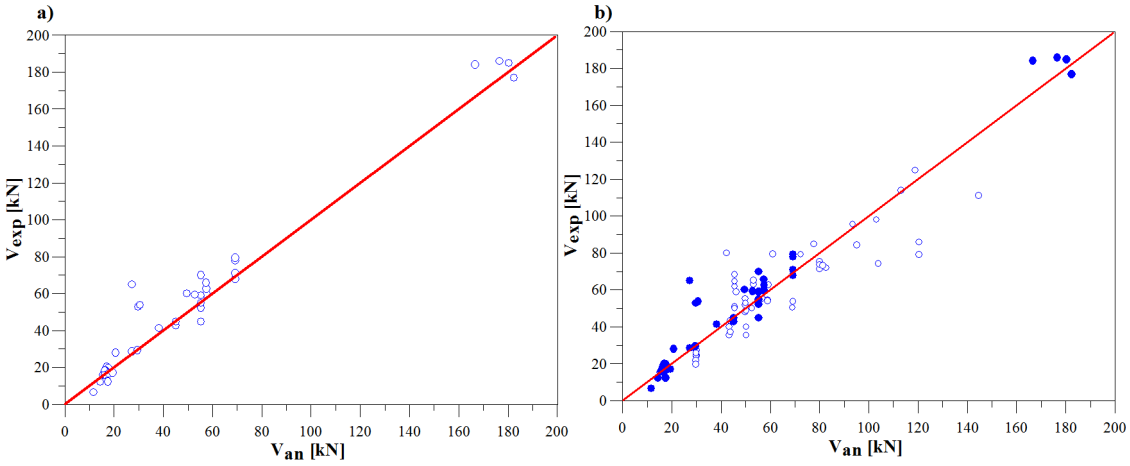

Figure 3.11: Comparison between test results vs predictions of Colotti et al. model [18]. a)only debonding failure mode; b) all failure modes

Failure modes considering	No. of valid tests	Average of difference	Bias	COV
Debonding	55	25,17%	1,66	37,21%
All	104	17,04%	1,46	37,98%

Table 3.5: Test-to-predicted debonding strength ratio for only debonding failure mode and for all failure modes.

The aim of this comparison was to demonstrate the good load prediction although it corresponds a different failure mode. Comparing the data position respect

the red line, the debonding failure mode data are above that while there are some data of the other failure mode that stay under the red line. If compares the average of difference, of bias and the COV, it was demonstrated that considering all data, improved the first two values without a significant variation of COV value (Tab.3.5). It means that the Colotti et al. model [18] gives a good prediction of the failure load; but it is better consider only debonding failure mode because all data stay above the red line and the model is safer.

Taking into account all data that it was collected, the Colotti et al. model [18] predicts 95 debonding failure mode, 62 flexural failure mode, 7 concrete crushing failure mode. Only the 58% of predictions corresponds at the real failure mode. The number of debonding failure load predictions is lower than predictions done with Smith and Teng model [53].

	Average of difference	Bias	COV	No. of valid tests
C-W	17,5%	0,90	23,6%	55
C-P	10,2%	1,09	39,8%	25
G-W	28,9%	1,52	24,3%	3
G-P	1,9%	0,99	9,8%	3

Table 3.6: Comparison between experimental and analytical results calculated with Colotti et al. model [18].

As seen in Tab.3.6, Colotti et al. model [18] improves the prediction for all groups. In this case, there is a difference of goodness between C-W and C-P reinforced beams. The beams reinforced with prepeg carbon plate present a coefficient of variation equal to $39,8\%$ which is too high to be acceptable, although the bias is very close to unity being $1,09$. C-W group presents very good prediction with a bias equal to $0,90$ and COV of $23,6\%$. Considering, glass prefabricated plate, the dispersion is nearly zero being COV equal to $9,8\%$ and it is characterized by a value of bias of $0,99\%$. Worst is the predictions for glass wet lay-up applied sheets where the coefficient of variation is $24,3\%$ and the bias is $1,52$. To test the goodness of model for glass applied material should be better take into account more data.

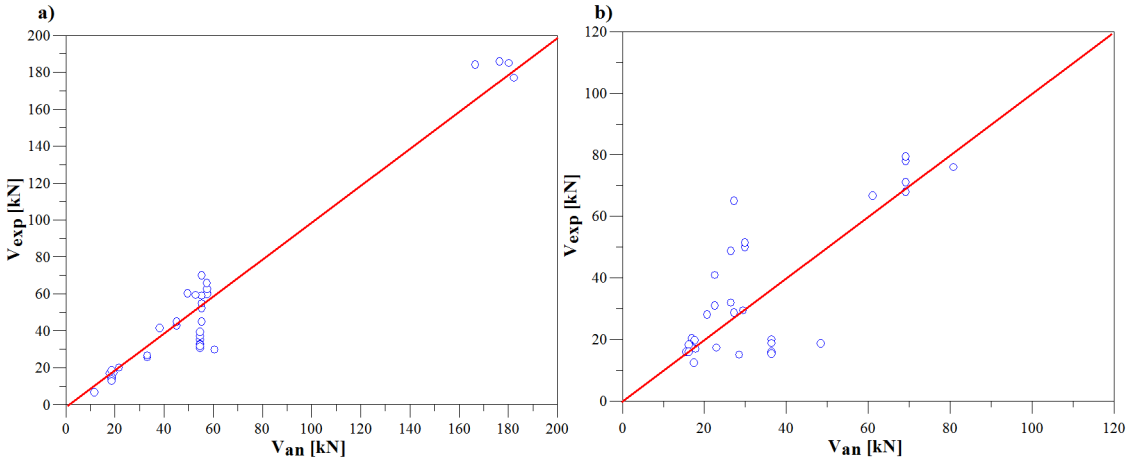

Figure 3.12: Test results vs predictions of Colotti et al. model [18]. a)CFRP wet lay-up system (55 valid tests); b)CFRP prepeg system (34 valid tests).

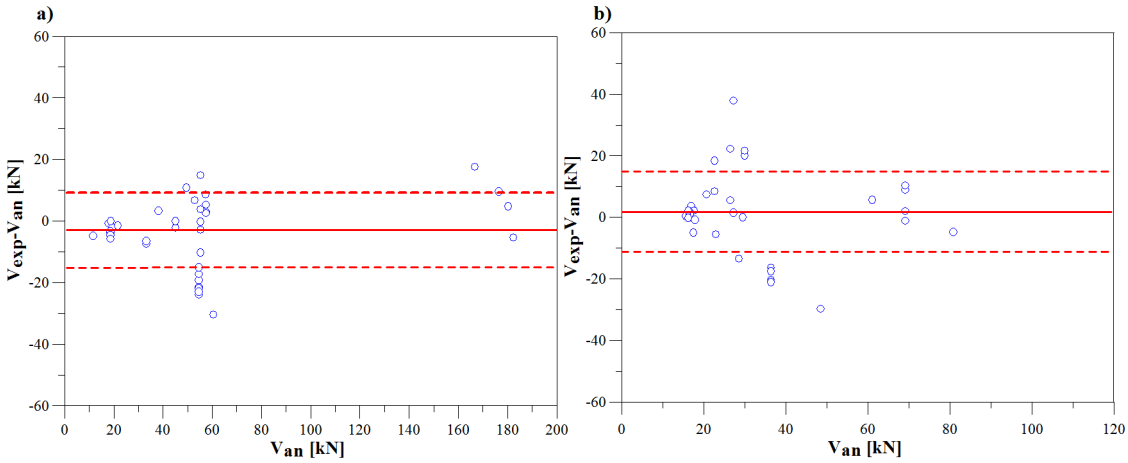

Figure 3.13: Difference between test results and analytical vs predictions of Colotti et al. model [18]. a)CFRP wet lay-up system μ=-3,0kN, σ=11,5kN (55 valid tests); b)CFRP prepeg system μ=1,6kN, σ=13,4kN (34 valid tests).

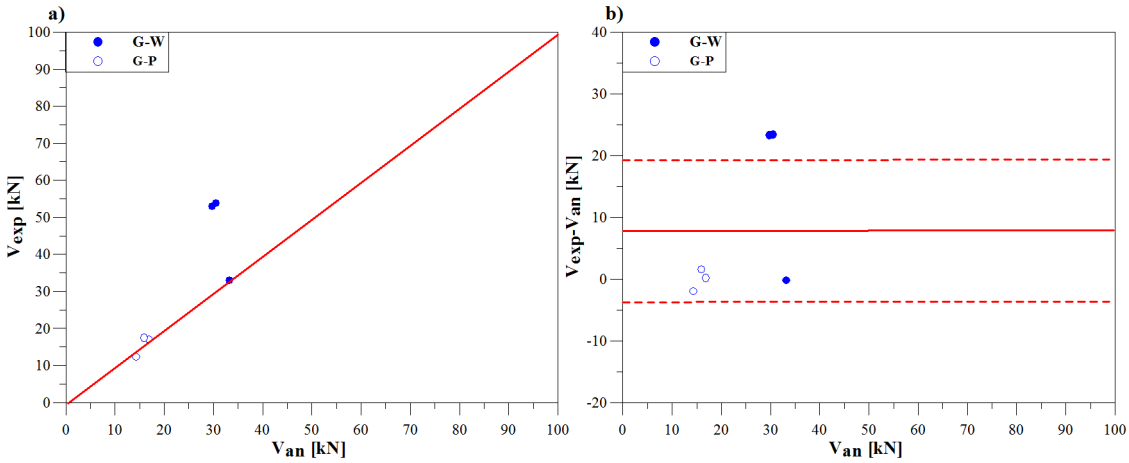

Figure 3.14: a)Test results vs predictions of Colotti et al. model [18], GFRP wet lay-up system (3 valid tests) and GFRP prepeg system (3 valid tests);b)Difference between test results and analytical vs predictions of Colotti et al. model [18] μ=7,7kN, σ=11,1kN.

The average of difference between experimental load and analytical load is equal to $-3,0kN$ and $-1,6kN$ for C-W and C-P, respectively, and the standard deviation is equal to $11,5kN$ and $13,4kN$ (Fig.3.13). These means that Colotti et al. model [18] predicts well the failure load with a low dispersion but the point are set under and over the line $V_{exp} = V_{an}$ and it is possible that the experimental load is higher or lower than analytical load.

In Tab.3.13 and Tab.3.14b are reported the difference between the experimental and analytical loads vs the analytical loads. The C-W group presents a average of this difference equal to $-3,0kN$ with a standard deviation of $11,5kN$, these means that there are underestimated and overestimated values. The prepeg carbon plates presented a value of μ closer to zero being $-1,6kN$ and a standard deviation equal to $13,4kN$. The glass reinforcements are characterized by the highest average between experimental and analytical load value, being $7,7kN$ with standard deviation similar to C-W data being $11,1kN$.

3.6 Comparison between Smith and Teng model and Colotti et al. model

The results (average of difference, bias and COV) of both of models presented a significantly different if were applied to the authors' database or were applied to all

data. This is due to the calibration, that the authors did using own database. More data it was used, higher is the uncertainty of the model.

	Average of difference	Bias	COV	No. of valid tests
Smith and Teng	35,8%	1,65	25,5%	56
Colotti et al.	3,0%	0,99	13,7%	63

Table 3.7: Comparison between Smith and Teng model [53] and Colotti et al. model [18] on own database.

Considering Table3.15, the best model was proposed by Colotti et al. [18]. The average of bias represents nearly the perfection of predictions. The coefficient of variation demonstrates a good precision of analytical result.

The Smith and Teng model [53] presents a worse bias with an excess of the experimental failure load on the analytical load. This results to be the purpose of the authors that wanted to create a good model to applying at beam design.

Taking into account all data collected, the goodness of the two model depends on the applying methodology. Comparing the predictions of two models for C-W data, Tab.3.8, Colotti et al. model [18] gave a value of bias, equal to $0,90$ better than Smith and Teng model [53] being $1,66$; the dispersion of data is lower with Colotti et al. model [18] where the COV is equal to $23,6\%$ while in Smith and Teng predictions is equal to $27,0\%$. Smith and Teng model [53], with 69 valid tests, admits more data than Colotti et al. model [18] which has 55 valid data.

	Average of difference	Bias	COV	No. of valid tests
Smith and Teng	35,7%	1,66	27,0%	69
Colotti et al.	17,5%	0,90	23,6%	55

Table 3.8: Comparison between Smith and Teng model [53] and Colotti et al. model [18] applied to C-W data.

To evaluate the critical shear load to cause debonding in C-P plated beams is better Smith and Teng model [53]. The data that used this model are 39, while the values of Colotti et al. model [18] are based on 34 valid tests. The COV is $26,8\%$ in the Smith and Teng model [53] and $39,8\%$ in the Colotti et al. model [18].

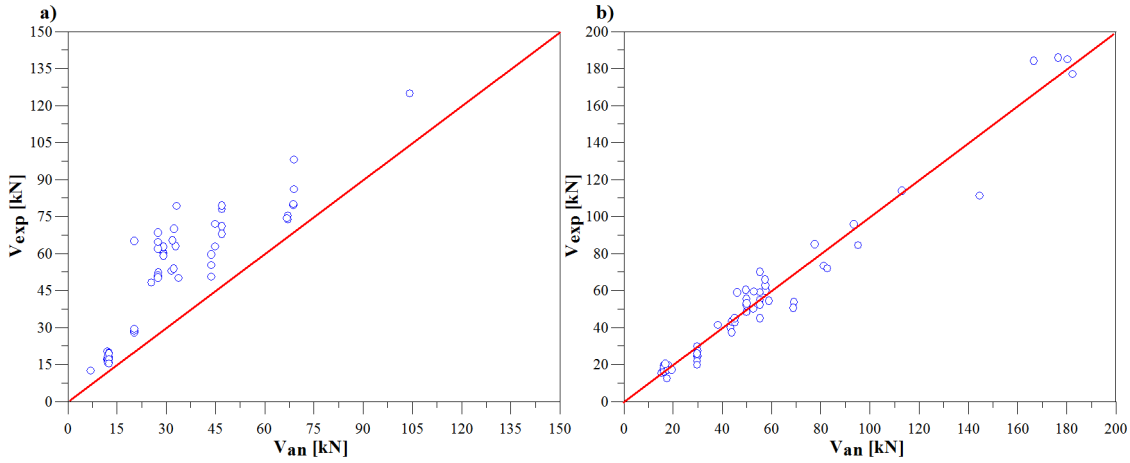

Figure 3.15: Test results vs predictions of a)Smith and Teng model [53] on own database (56 valid tests); b)Colotti et al. model [18] on own database (63 valid tests).

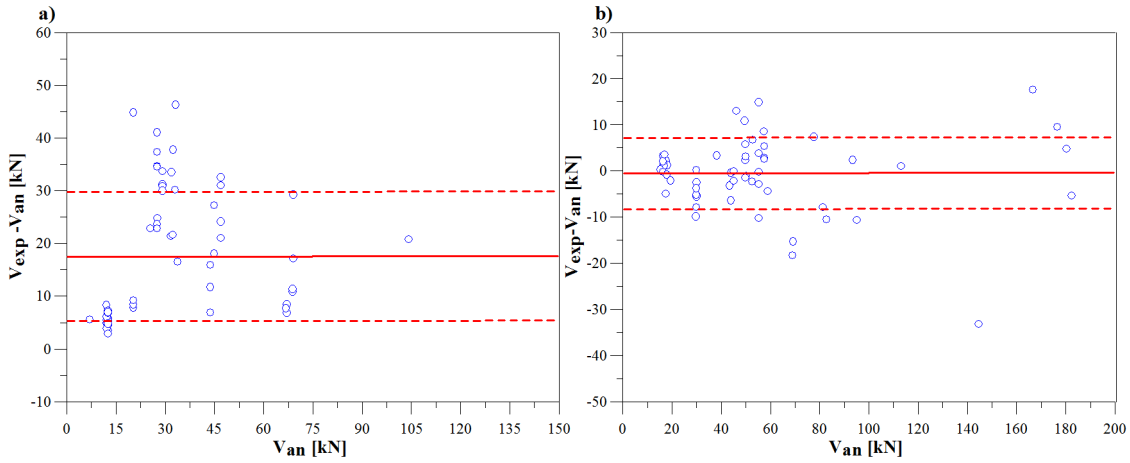

Figure 3.16: a) Difference between test results and analytical vs predictions of Smith and Teng model [53] μ=18,5, σ=12,4 (56 valid tests); b)Difference between test results and analytical vs predictions of Colotti et al. model [18] μ=-0,6, σ=7,7 (63 valid tests);.

To evaluate the critical shear load to cause debonding in C-P plated beams is better Smith and Teng model [53]. The data that used this model are 39, while the values of Colotti et al. model [18] are based on 34 valid tests. The COV is $26,8\%$ in the Smith and Teng model [53] and $39,8\%$ in the Colotti et al. model [18].

	Average of difference	Bias	COV	No. of valid tests
Smith and Teng	34,7%	1,62	26,8%	39
Colotti et al.	10,2%	1,09	39,8%	34

Table 3.9: Comparison between Smith and Teng model [53] and Colotti et al. model [18] applied to C-P data.

Comparing the graphical 3.15 and 3.16, it was seen that Smith and Teng model [53] presents all values above the red line. This means that the model underestimate the bond strength and it is the safest prediction model. The model proposed by Colotti et al. [18] gives a bias of $1,09$, $0,90$, $0,99$, $1,52$ for C-P data, C-W data, G-P data and G-W data, respectively. As explained in the previous section, Smith and Teng model [53] is based on a calibration of factors using their database of experimental data. There isn't any mechanical approach to resolve the problem of debonding. It should be possible that using more data, the author can improve the model. Colotti et al. [18] based their approach on strut and tie theory and the prediction of failure load is more exhaustive. Smith and Teng put a limitation in their model due to the impossibility to predict the end debonding failure load for all kind of beam. With Colotti et al. model [18] it is possible to know the mode of failure (concrete crushing, FRP rupture, end debonding, etc.).

3.7 Teng and Yao model

The authors took into account the beam's properties with and without soffit plate. It was considered the strengthened beam due to FRP laminates. The increase of flexural capacity reduces the shear debonding strength, it means that there will be a limit for the strengthen of beams. To calculate the contribution of the concrete to shear debonding strength, V_c, it can be used definitions from different codes. Three different codes were token into account: the English code (BS8110), the Australian code (AS600) and the American code (ACI318), as reported in Tab.3.10, Tab.3.11 and Tab.3.12. In the previous chapter it was explained the difference between the three equations.

For C-W material, using different code, could change the goodness of model. Comparing the values of COV , there is a maximum of $38,9\%$ and a minimum of

	Average of difference	Bias	COV	No. of tests
C-W	41,5%	1,96	36,4%	59
C-P	39,6%	1,84	34,8%	94
G-W	10,5%	1,10	44,7%	7
G-P	15,0%	1,31	34,0%	7

Table 3.10: Comparison between experimental and analytical results calculated with Teng and Yao model [61], using AS600 code definition for the contribution of the concrete to shear debonding strength.

	Average of difference	Bias	COV	No. of tests
C-W	21,1%	1,45	34,1%	59
C-P	19,5%	1,41	37,9%	90
G-W	33,3%	0,87	38,4%	7
G-P	5,2%	1,06	33,7%	7

Table 3.11: Comparison between experimental and analytical results calculated with Teng and Yao model [61], using ACI318 code definition for the contribution of the concrete to shear debonding strength.

$34,1\%$ with BS8110 and ACI318 definition, respectively. The bias has a maximum of $1,96$ with AS600 definition and a minimum of $1,45$ with ACI318. It means that the formulas for the contribution of the concrete can't use indifferently. Each code uses a different equation and the model depends on that. Considering these three codes, the American code gives the best value of COV of $34,1\%$ and the best bias value too, equal to $1,45$.

Using different type of material could change the goodness of results also. For C-P reinforcing material, it results that the maximum value of COV was obtained using ACI318 code and it is equal to $37,9\%$. Using BS8110 formula, it was obtained a value of $36,0\%$; while, with AS600, the COV is equal to $34,8\%$. Moreover, the maximum value of bias, $1,84$, was obtained considering the AS600 definition of shear debonding strength of concrete. Using ACI318 equation, this model gave a bias of $1,41$ close to $1,44$ which is the bias with BS8110 code definition.

This comparison demonstrated that there isn't a unique code that improves that model, but each equation could gave a better prediction values. Considering both bias and COV values, use an appropriate equation of V_c, could improve the goodness of model.

Considering the difference between the experimental load and the analytical

	Average of difference	Bias	COV	No. of valid tests
C-W	26,6%	1,57	38,9%	59
C-P	22,7%	1,44	36,0%	90
G-W	21,6%	0,94	37,4%	7
G-P	1,8%	1,03	22,1%	7

Table 3.12: Comparison between experimental and analytical results calculated with Teng and Yao model [61], using BS8110 code definition for the contribution of the concrete to shear debonding strength.

load, as seen in Fig.3.18 Fig.3.21 Fig.3.24, the average value changes with codes while standard deviation is the same for each kind of material applied (wet lay-up or prepeg). The data of beams reinforced with carbon prepeg plates, the value of μ has a maximum of $17,6kN$ with AS600 code and a minimum equal to $8,7kN$ with ACI318 code, while the British code standard deviation is equal to $11,6kN$. Standard deviation shows a little variation between the three different definition: the Australian code and the American code are characterized by the same value of σ being $14,6kN$, while with BS8110 standard deviation is equal to $14,8kN$. Taking into account beams reinforced with glass sheets, (Fig.3.19b Fig.3.22b Fig.3.25b) there is a variation of both average and standard deviation. Using the Australian code the average of $V_{exp} - V_{an}$ is equal to $-2,4kN$ with standard deviation equal to $19,4kN$. The American code is characterized by μ of $-13,9kN$ and σ equal to $22,1kN$. Finally the British code equation gives an average of $-7,9kN$ and a standard deviation of $18,1kN$.

Comparing carbon and glass sheets prediction values, it was seen that Teng and Yao model [61] overestimates the strength capacity of reinforce for glass material, while underestimates the failure load for beams reinforced with carbon sheets. As seen in Smith and Teng model [53], there isn't a mechanical approach in Teng and Yao model [61]. This means that the equations were calibrated on their experimental tests. They tested only one beam reinforced with GFRP, this could be the reason of higher variation between μ and σ values in GFRP sheets than in CFRP.

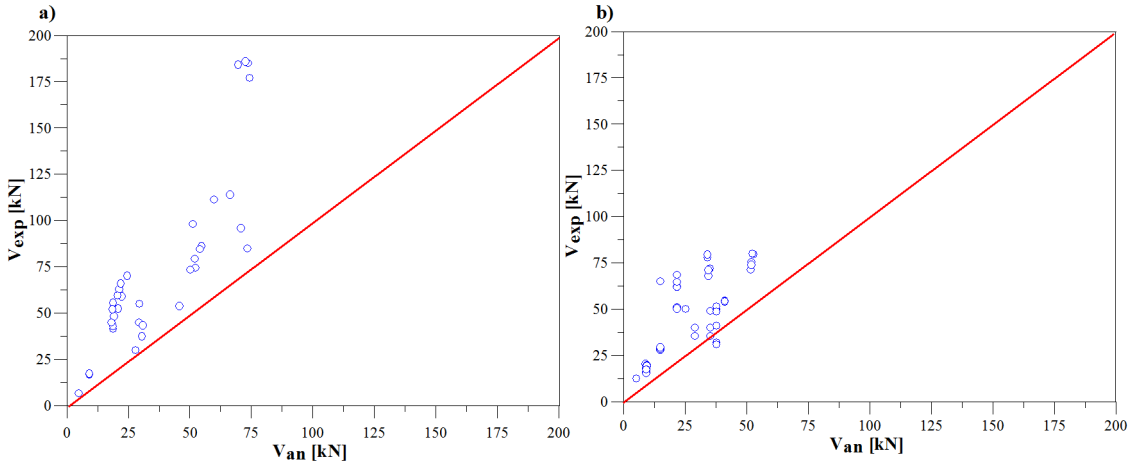

Figure 3.17: Test results vs predictions of Teng and Yao model [61] using AS600 code. a)CFRP wet lay-up system (90 valid tests); b)CFRP prepeg system (59 valid tests).

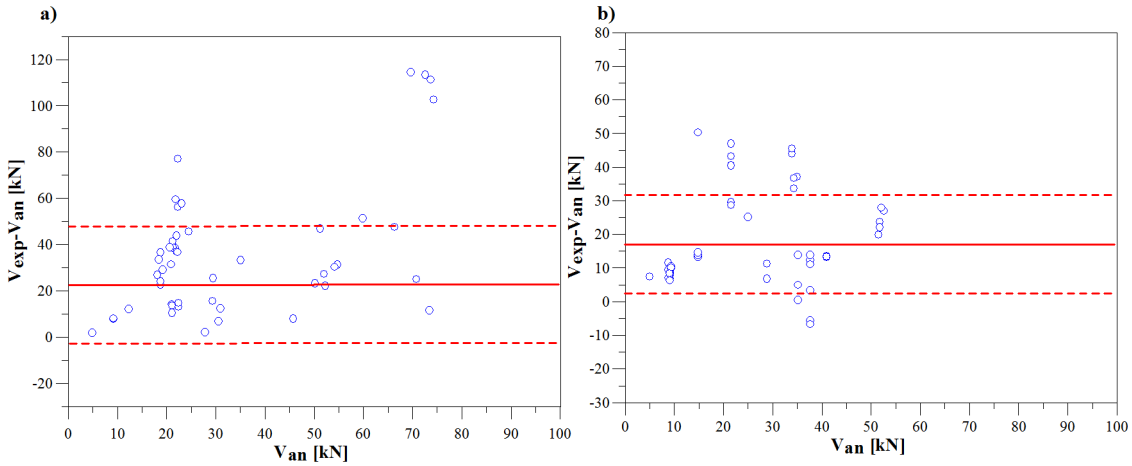

Figure 3.18: Difference between test results and analytical vs predictions of Teng and Yao model [61] using AS600 code. a)CFRP wet lay-up system μ=23,3kN σ=25,2kN (90 valid tests); b)CFRP prepeg system μ=17,6kN, σ=14,6kN (59 valid tests).

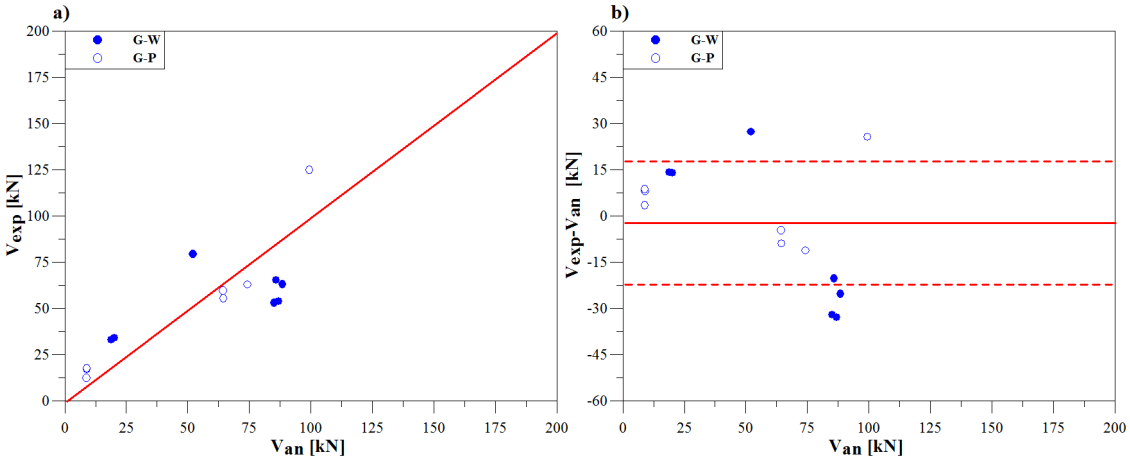

Figure 3.19: a)Test results vs predictions of Teng and Yao model [61] using AS600 code, GFRP wet lay-up system (7 valid tests) and GFRP prepeg system (7 valid tests);b)Difference between test results and analytical vs predictions of Teng and Yao model [61] using AS600 code μ=-2,4kN, σ=19,4kN.

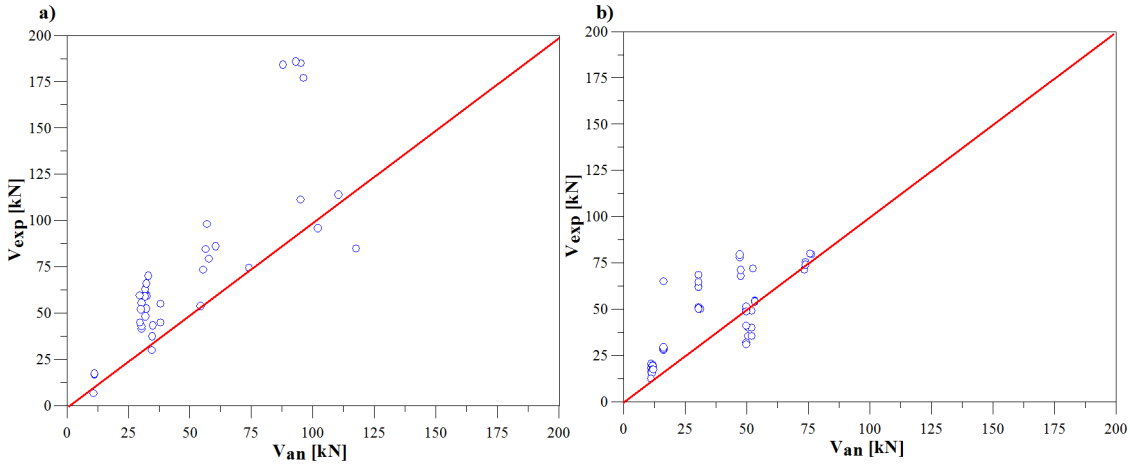

Figure 3.20: Test results vs predictions of Teng and Yao model [61] using ACI318 code. a)CFRP wet lay-up system (90 valid tests); b)CFRP prepeg system (59 valid tests).

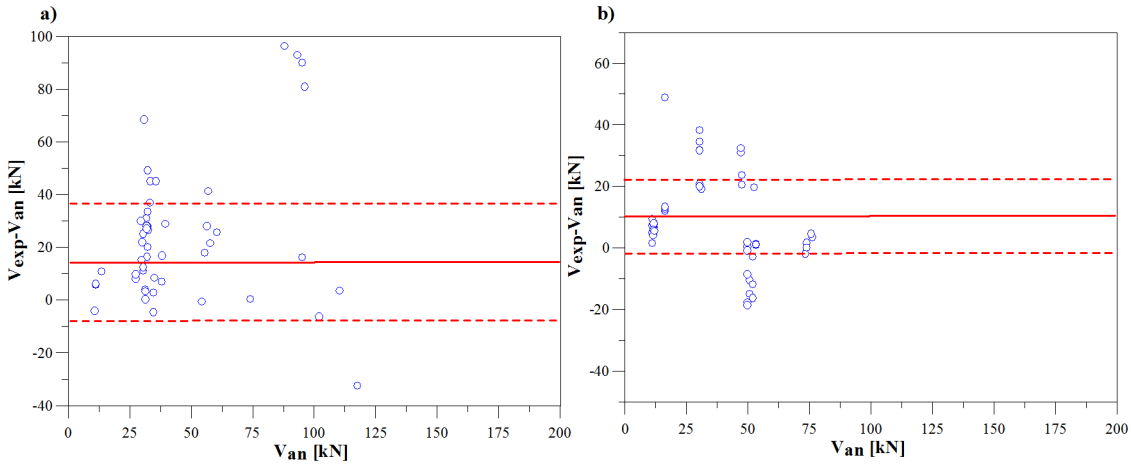

Figure 3.21: Difference between test results and analytical vs predictions of Teng and Yao model [61] using ACI318 code. a)CFRP wet lay-up system μ=14,0kN σ=23,2kN (90 valid tests); b)CFRP prepeg system μ=8,7kN, σ=14,6kN (59 valid tests).

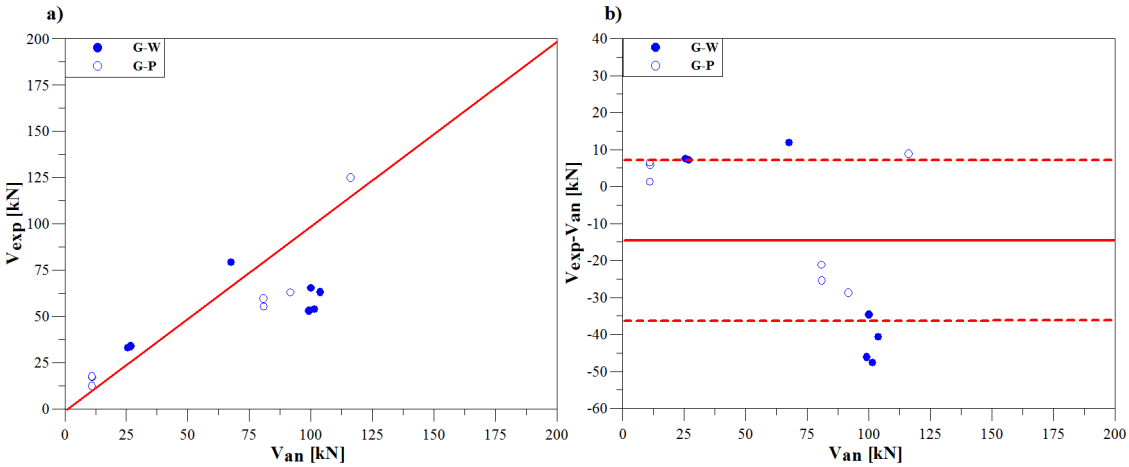

Figure 3.22: a)Test results vs predictions of Teng and Yao [61] model using ACI318 code, GFRP wet lay-up system (7 valid tests) and GFRP prepeg system (7 valid tests);b)Difference between test results and analytical vs predictions of Teng and Yao model [61] using ACI318 code μ=-13,9kN, σ=22,1kN.

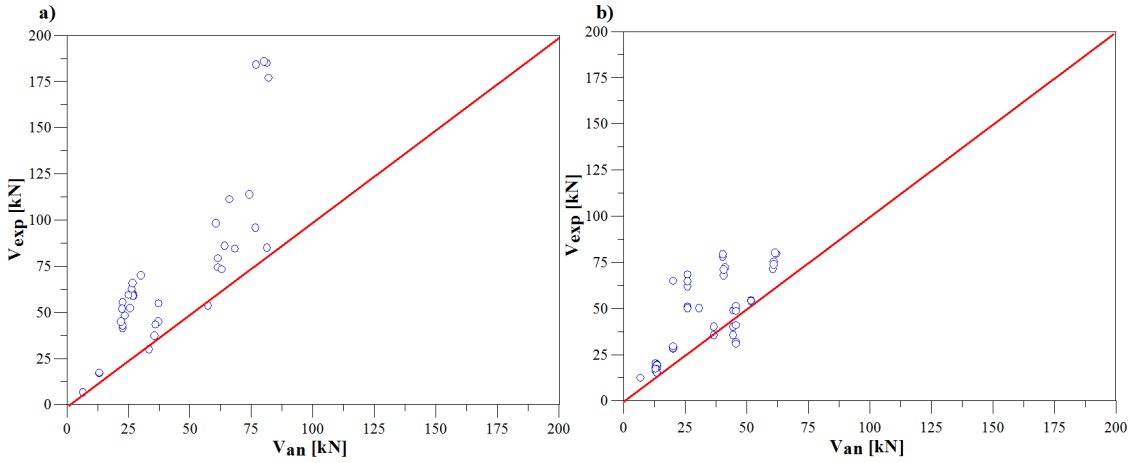

Figure 3.23: Test results vs predictions of Teng and Yao model [61] using BS8110 code. a)CFRP wet lay-up system (90 valid tests); b)CFRP prepeg system (59 valid tests).

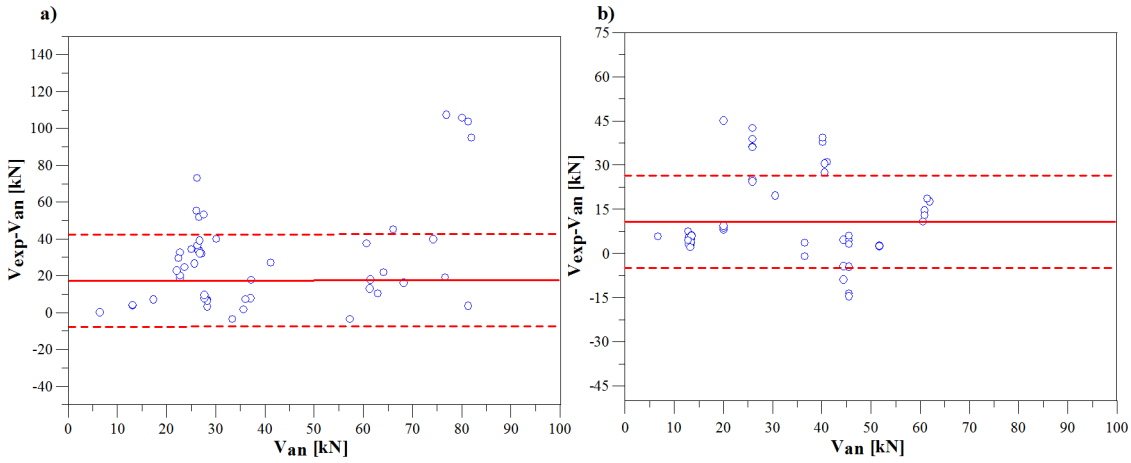

Figure 3.24: Difference between test results and analytical vs predictions of Teng and Yao model [61] using BS8110 code. a)CFRP wet lay-up system μ=17,0kN σ=25,0kN (90 valid tests); b)CFRP prepeg system μ=11,6kN, σ=14,8kN (59 valid tests).

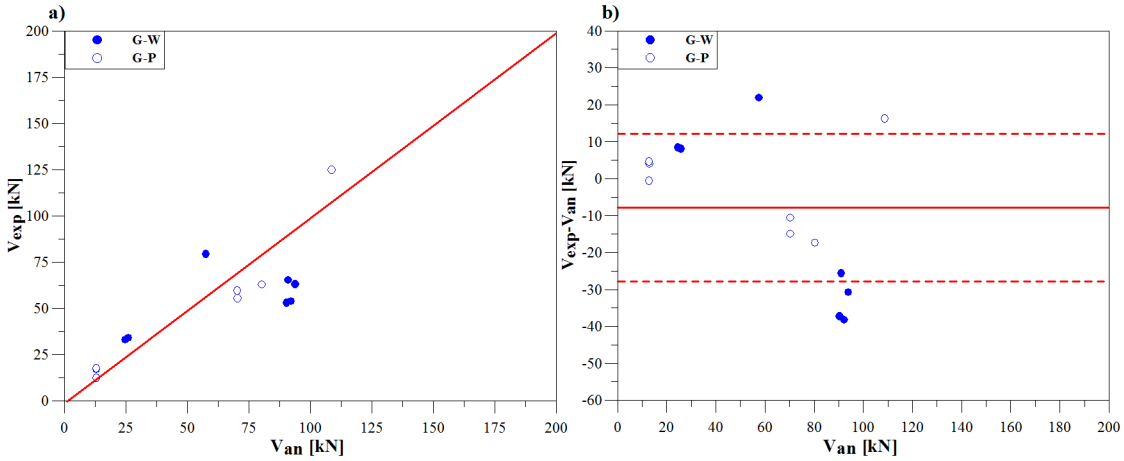

Figure 3.25: a)Test results vs predictions of Teng and Yao model [61] using BS8110 code, GFRP wet lay-up system (7 valid tests) and GFRP prepeg system (7 valid tests);b)Difference between test results and analytical vs predictions of Teng and Yao model [61] using BS8110 code μ=-7,9kN, σ=18,1kN.

3.8 Casas and Pascual model

This model can be included in interfacial stress based models, as it explained in the previous chapter. The authors took into account resin's characteristic of modulus of elasticity E_a and the its thickness t_a. Not in all beam tests it was founded this values, for two reasons: many models consider that the debonding failure occurs in the concrete cover, near the longitudinal steel reinforcement, and exclude the importance of the resin; the difficulty to evaluate the resin's characteristics when the FRP is applied *in situ*.

	total number of beam test	number of beam test with resin's characteristics
C-W	59	19
C-P	90	38
G-W	7	5
G-P	7	7

Table 3.13: Number of test valid for Casas and Pascual model [13].

The ratio between the shear modulus of resin G_a and the thickness t_a contributes to calculate the effective bond length L_e and consequently the maximum shear stress value T_u.

Considering all tests with resin's characteristic, this model gives a good results as follows:

	Average of difference	Bias	COV	No. of valid tests
C-W	52,6%	2,21	20,1%	19
C-P	54,1%	2,27	23,4%	38
G-W	17,2%	1,26	21,6%	5
G-P	33,7%	1,57	19,9%	7

Table 3.14: Comparison between experimental and analytical results calculated with Casas and Pascual model [13].

The model gives a good results of COV for both C-W and C-P material. The coefficient of variation is equal to $23,4\%$ for C-P material and $20,1\%$ for C-W material. The bias values obtained by Casas and Pascual model [13] are higher than values of other models ; $2,27$ is the value for C-P material and for C-W material the present model gives a value of bias equal to $2,21$. Although the bias value could be higher than the value derived from the other models, the COV results very good.

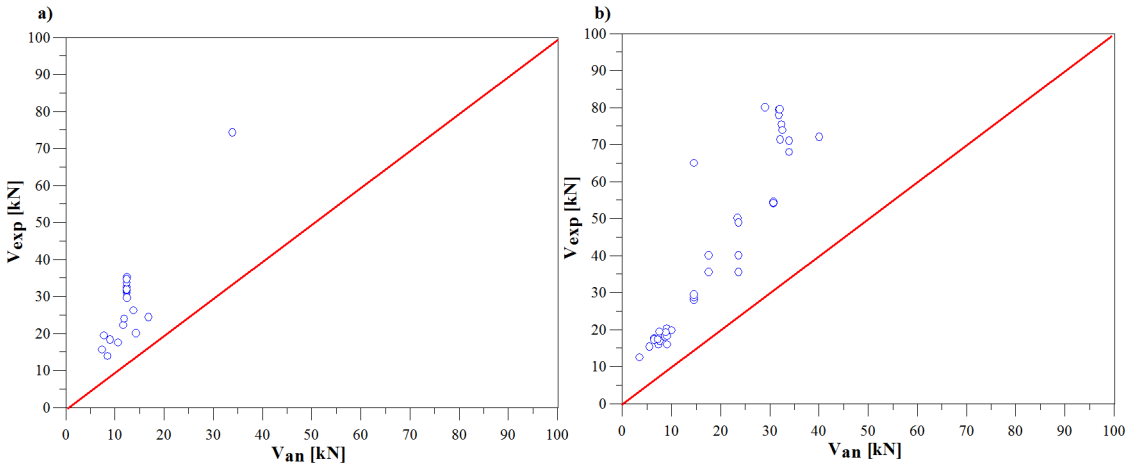

Figure 3.26: Test results vs predictions of Casas and Pascual model [13]. a)CFRP wet lay-up system (19 valid tests); b)CFRP prepeg system (38 valid tests).

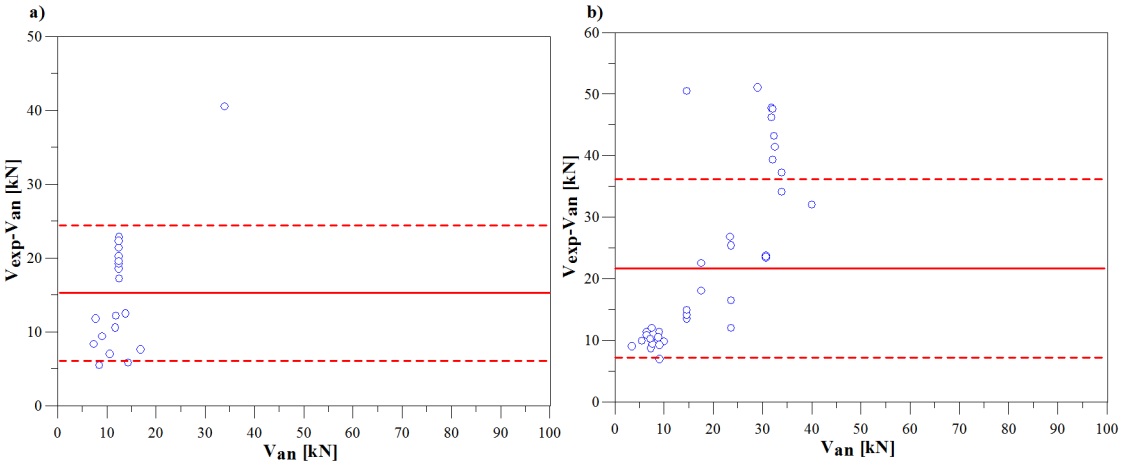

Figure 3.27: Difference between test results and analytical vs predictions of Casas and Pascual model [13]. a)CFRP wet lay-up system μ=15,4kN σ=9,0kN (19 valid tests); b)CFRP prepeg system μ=22,5kN, σ=14,3kN (38 valid tests).

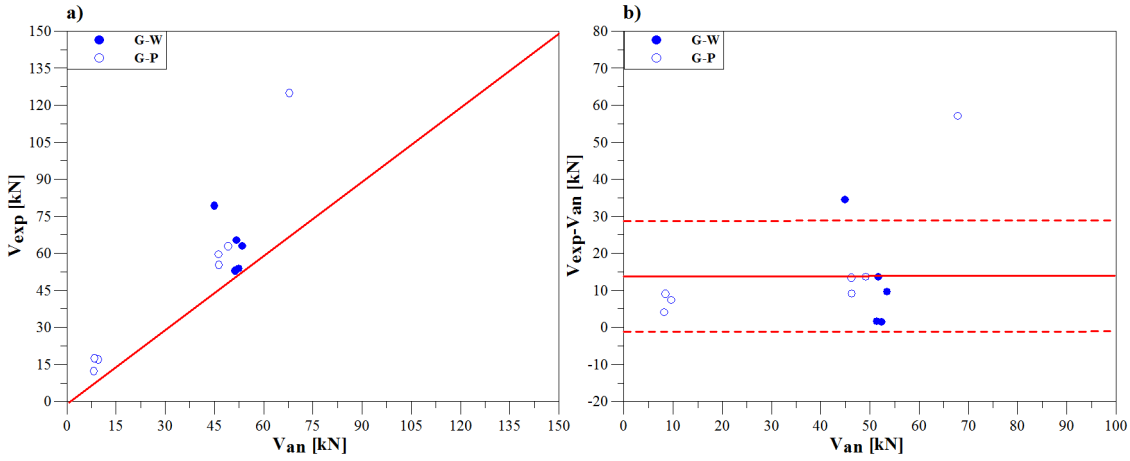

Figure 3.28: a)Test results vs predictions of Casas and Pascual model [13], GFRP wet lay-up system (5 valid tests) and GFRP prepeg system (7 valid tests);b)Difference between test results and analytical vs predictions of Casas and Pascual model [13] μ=14,6kN, σ=15,2kN.

As seen in Fig.3.27 and Fig.3.28b, Casas and Pascual model [13] underestimated the failure load due to end debonding. The low dispersion of prediction values is demonstrated by value of standard deviation too. Beams reinforced by wet lay-up CFRP are characterized by an average value of $15,4$ while standard deviation is equal to $9,0kN$; C-P group presents values higher than C-W being $22,5kN$ and $14,3kN$ the average and standard deviation, respectively. This model underestimated GFRP failure load too, with an μ and σ equal to $14,6kN$ and $15,2kN$, respectively.

3.9 Ziraba et al. models

These models are based on two different criterion. The first model used the Mohr-Coulomb failure criterion and the shear force to cause plate end interfacial debonding $V_{db,end}$ depends on two constants; These include some characteristics of strengthened beam, like FRP geometry, second moment of area of the cracked plated section $I_{trc,frp}$ and FRP alone I_{frp}, and modulus of elasticity E_a, shear modulus G_a, width b_a and thickness t_a of the adhesive layer. To calculate the shear modulus from modulus of elasticity, the Poisson coefficient is taken as 0,38 as proposed in Casas and Pascual paper [13].

The second model sums the shear capacity of concrete and the shear capacity of shear reinforcement. The characteristic of reinforce was included in the equation by a factor derived empirically, k, which included the geometry of FRP, $I_{trc,frp}$, I_{frp}

and resin characteristic, as explained in the first model.

As seen for Casas and Pascual model [13], Ziraba et al. models [70] required resin characteristics, due to the valid test data are: 38 for C-P reinforced beams, 19 for C-W, 7 for G-P and 5 for G-W.

The first model of Ziraba et al. [70] predicted better the C-W data than C-P reinforced beams (Tab.3.15). The bias is equal to $1,63$ for C-W material with a COV of $31,1\%$. Considering C-P reinforcing beams the value of bias is equal to $2,09$ but the coefficient of variation, $62,5\%$ is too high to consider the model. In the beams reinforced with GFRP, the model gives a value of bias of $1,15$ for G-P material and a value of $0,71$ for G-W. The variation of value is similar being COV equal to $45,8\%$and $41,5\%$ for G-P and G-W, respectively.

Using the second model, it was obtained the best prediction for C-W (Tab.3.16). The value of bias is equal to $1,17$ and the COV to $17,7\%$; for this kind of reinforced beams, this model is better than Casas and Pascual model [13] which present higher values of bias $(2,21)$ and similar value of COV $(20,1\%)$. The C-P prediction presents a good value of bias, equal to $1,26$ but it was characterized by a great dispersion with a COV equal to $40,9\%$. The prediction of failure loads for beams reinforced with GFRP was improved with this second model. The bias of G-P material is equal to $1,17$ while in G-W beams is $0,94$. The COV calculated is equal to $26,5\%$ and $20,6\%$ in G-P and G-W, respectively.

	Average of difference	Bias	COV	No. of valid tests
C-W	32,3%	1,63	31,1%	19
C-P	32,1%	2,09	62,5%	38
G-W	58,7%	0,71	41,4%	5
G-P	5,5%	1,15	45,8%	7

Table 3.15: Comparison between experimental and analytical results calculated with Ziraba et al. model I [70].

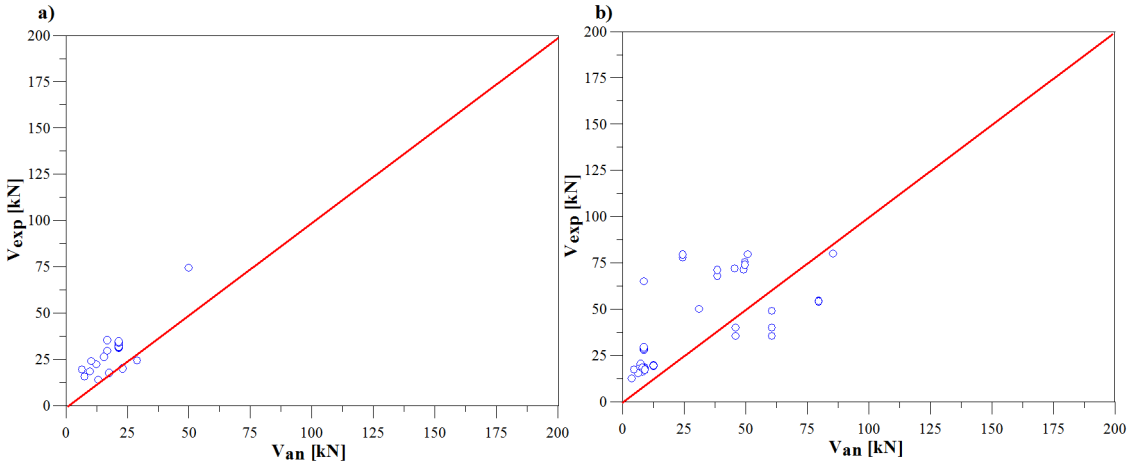

Figure 3.29: Test results vs predictions of Ziraba et al. model I [70]. a)CFRP wet lay-up system (19 valid tests); b)CFRP prepeg system (38 valid tests).

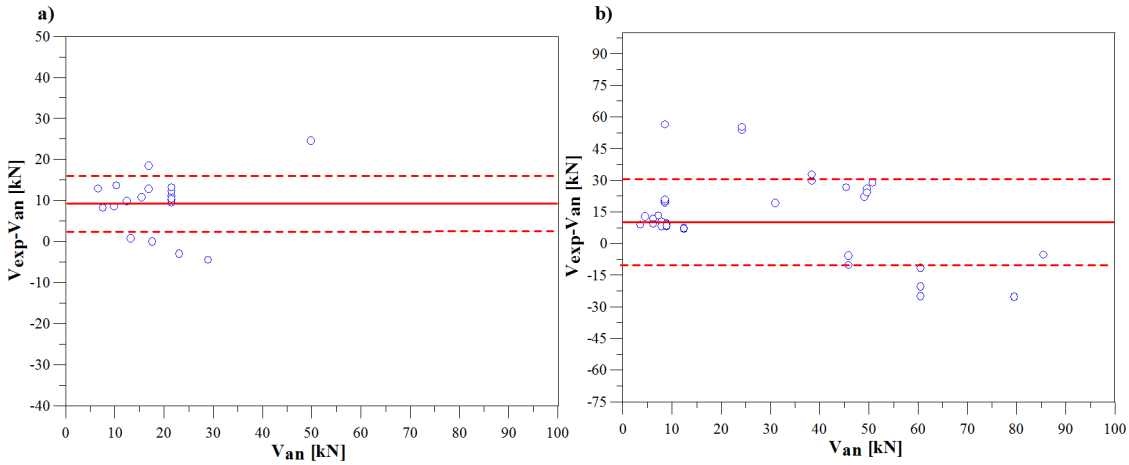

Figure 3.30: Difference between test results and analytical vs predictions of Ziraba et al. model I [70]. a)CFRP wet lay-up system μ=9,5kN σ=6,8kN (19 valid tests); b)CFRP prepeg system μ=11,2kN, σ=20,4kN (38 valid tests).

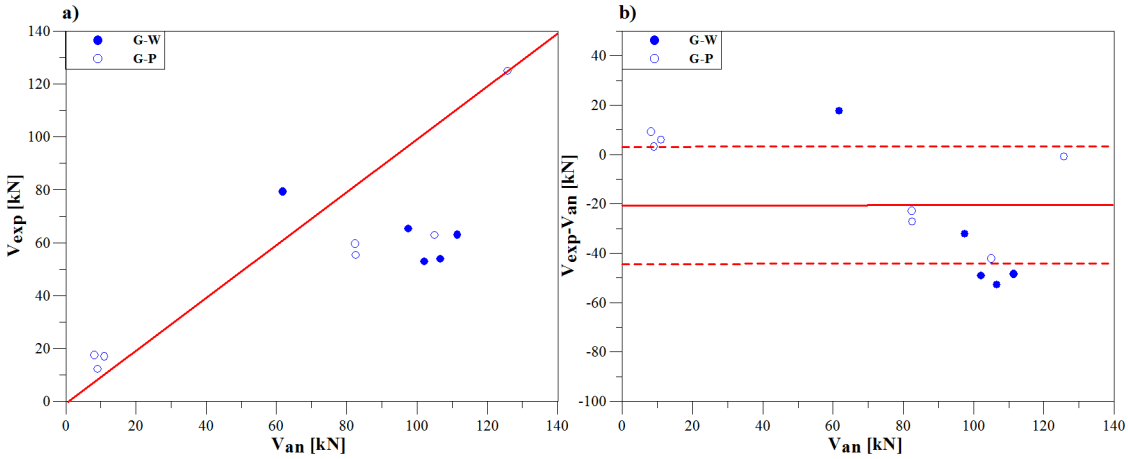

Figure 3.31: a)Test results vs predictions of Ziraba et al. model I [70], GFRP wet lay-up system (5 valid tests) and GFRP prepeg system (7 valid tests);b)Difference between test results and analytical vs predictions of Ziraba et al. model I [70] μ=-19,8kN, σ=24,6kN.

The first Ziraba et al. model [70], underestimated the value of failure load for beams reinforced with CFRP sheets, while underestimated the load of end debonding for beams reinforced with GFRP sheets. This means that it is not possible to have an unique behavior of predicted value. As seen in Fig.3.30, C-W data vs analytical gave an average of $9,5kN$ and a standard deviation of $6,8kN$; C-P beams reinforced are characterized by higher values being $11,2kN$ and $20,4kN$ the average of $V_{exp} - V_{an}$ and standard deviation, respectively. The glass reinforced beams (Fig.3.31b) have a negative value of average equal to $-19,8kN$ and a high dispersion of data being standard deviation equal to $24,6kN$.

	Average of difference	Bias	COV	No. of valid tests
C-W	11,9%	1,17	17,7%	19
C-P	6,0%	1,26	40,9%	38
G-W	10,0%	0,94	20,3%	5
G-P	8,8%	1,17	26,5%	7

Table 3.16: Comparison between experimental and analytical results calculated with Ziraba et al. model II [70].

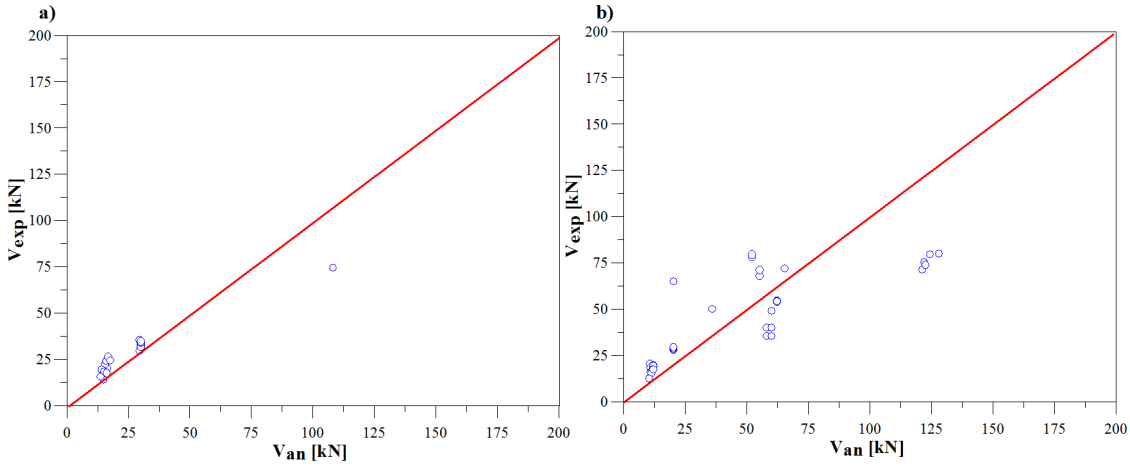

Figure 3.32: Test results vs predictions of Ziraba et al. model II [70]. a)CFRP wet lay-up system (19 valid tests); b)CFRP prepeg system (38 valid tests).

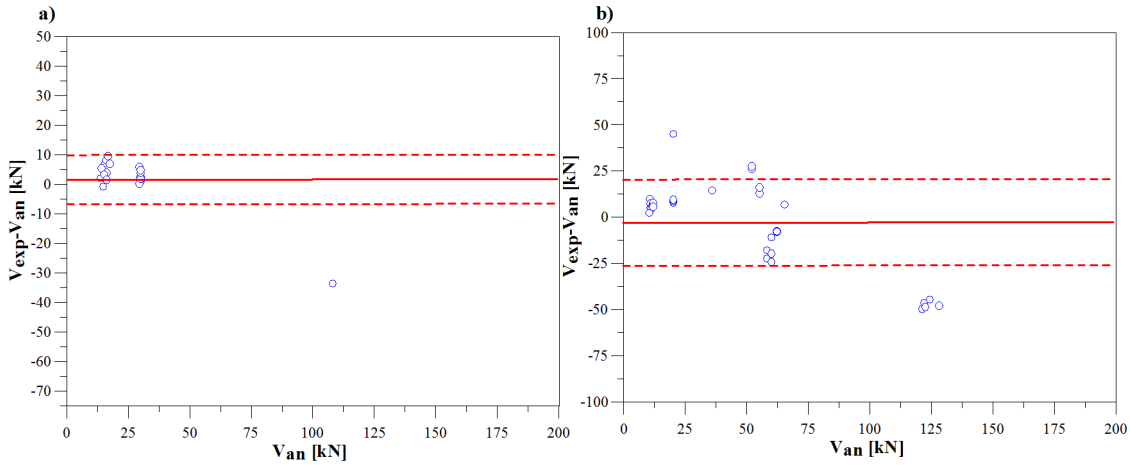

Figure 3.33: Difference between test results and analytical vs predictions of Ziraba et al. model II [70]. a)CFRP wet lay-up system μ=1,8kN σ=8,8kN (19 valid tests); b)CFRP prepeg system μ=-2,3kN, σ=21,9kN (38 valid tests).

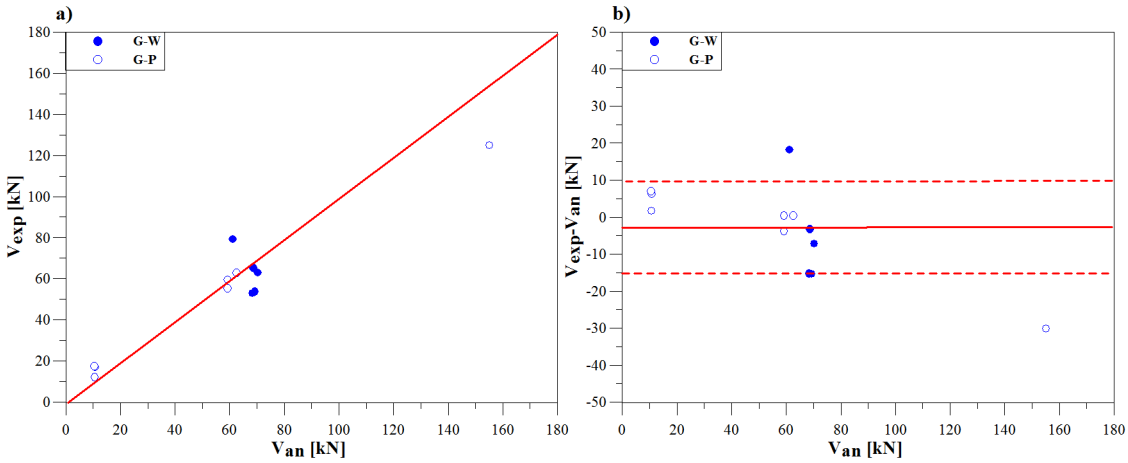

Figure 3.34: a)Test results vs predictions of Ziraba et al. model II [70], GFRP wet lay-up system (5 valid tests) and GFRP prepeg system (7 valid tests);b)Difference between test results and analytical vs predictions of Ziraba et al. model II [70] μ=-3,4kN, σ=12,0kN.

The second Ziraba et al. model [70] improves the quality of prediction. C-W data (Fig.3.33) present an average of $V_{exp} - V_{an}$ very close to zero, being $1,8kN$ and standard deviation of $8,8kN$ lower than C-W results in the first model. C-P group presents a negative value of μ equal to $-2,3kN$ and σ higher than in first model being $21,9kN$. Better results the prediction of glass reinforcement with an average of $-3,4kN$ and standard deviation of $12,0kN$. the second Ziraba et al. model [70] underestimates G-W data, which are set in safe side, as seen in Fig3.34b.

3.10 Other models

There are other four model base on the concept of a concrete "tooth" between two adjacent cracks as explained in the previous chapter. These models present a good values of bias, but a excessive dispersion of data. The authors based all their models on the geometry of FRP material, the strength of concrete and longitudinal steel reinforcement characteristic.

Raoof and Zhang model [42] gives a good values of bias for all kind of material. The best prediction, for C-W, presents a bias of $1,41$ and a COV of $61,2\%$. Worse are the results for C-P data which has a bias and COV being $1,68$ and $70,1\%$, respectively. Also in tests on reinforced beams with GFRP the predictions are not good. The G-P data present a bias of $1,30$ and a COV of $76,9\%$, while wet lay up GFRP the value of bias is closer to the unity being $0,93$ and the COV is equal to $48,60\%$. The model gives high dispersion of failure predictions for all kind of material.

	Average of difference	Bias	COV	No. of valid tests
C-W	27,3%	1,41	61,2%	90
C-P	12,7%	1,68	70,1%	59
G-W	38,2%	0,93	48,6%	7
G-P	111,2%	1,30	76,9%	7

Table 3.17: Comparison between experimental and analytical results calculated with Raoof and Zhang model [42].

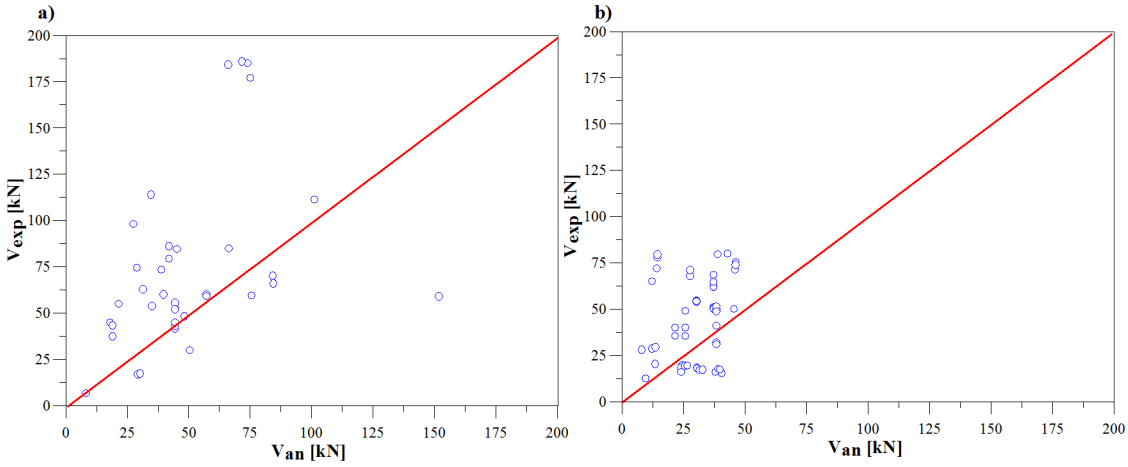

Figure 3.35: Test results vs predictions of Raoof and Zhang model [42]. a)CFRP wet lay-up system (90 valid tests); b)CFRP prepeg system (59 valid tests).

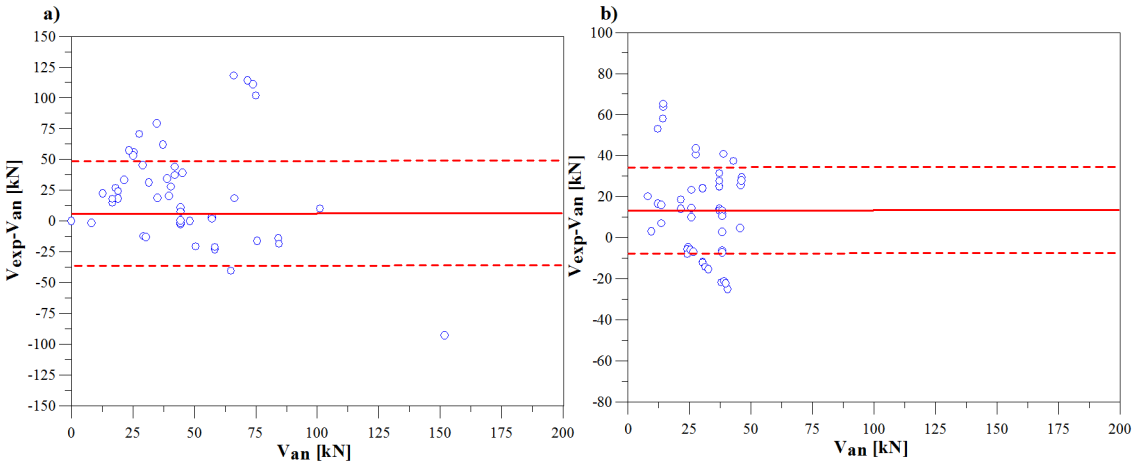

Figure 3.36: Difference between test results and analytical vs predictions of Raoof and Zhang model [42]. a)CFRP wet lay-up system μ=6,8kN σ=41,2kN (90 valid tests); b)CFRP prepeg system μ=13,0kN, σ=21,2kN (59 valid tests).

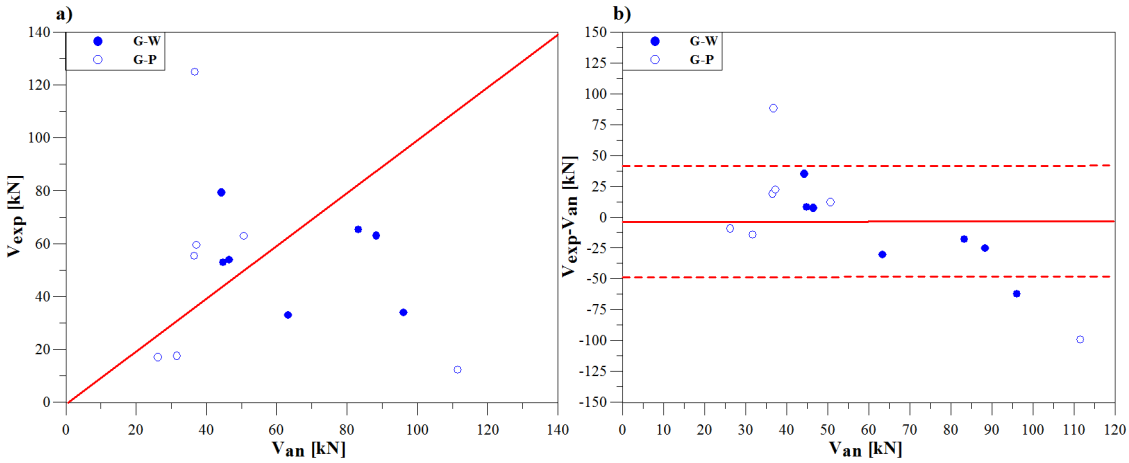

Figure 3.37: a)Test results vs predictions of Raoof and Zhang model [42], GFRP wet lay-up system (7 valid tests) and GFRP prepeg system (7 valid tests);b)Difference between test results and analytical vs predictions of Raoof and Zhang model [42] μ=-4,6kN, σ=42,9kN.

Considering the difference between experimental and analytical load, as shown in Fig.3.36 and Fig.3.37b, there is an high dispersion of data with overestimated and underestimated failure loads. The average in C-W group is equal to $6,8kN$, with a standard deviation of $41,2kN$. The beams reinforced with prepeg carbon plates presented a lower dispersion being σ equal to $21,2kN$ but the average is farer from zero, being $13,0kN$. Glass sheets present a negative average which is equal to $-4,6kN$ and standard deviation is as high as C-W reinforced beams, $42,9kN$.

Wang and Ling model [52] gives similar values of bias of Raoof and Zhang model [42] but the dispersion increases. Expect for G-W data, all groups have a COV over 60%; beams reinforced with wet lay up sheets present a better prediction than beams reinforced with prefabricated plate. The C-P group presents a bias of $1,62$ with a COV being $76,4\%$ while in C-W data the bias value improves being $1,43\%$ with a COV of $61,0\%$. The beams reinforced with prepeg GFRP the bias is equal to $1,31$ and the coefficient of variation is $79,26\%$. Finally, the model predicts for G-W data a values of $0,94$ and $46,98\%$ for bias and COV, respectively.

Taking into account Fig.3.39 and Fig.3.40b, the values of average and standard deviation are similar to the Raoof and Zhang model [42] results. The average of wet lay-up carbon sheets is equal to $6,9kN$ with a standard deviation of $40,1kN$. The prepeg carbon plates are characterized by a lower standard deviation and higher average, being $20,4kN$ and $12kN$, respectively. Glass reinforcement presents an av-

	Average of difference	Bias	COV	No. of valid tests
C-W	26,1%	1,43	61,0%	90
C-P	7,7%	1,62	76,4%	59
G-W	35,4%	0,94	47,0%	7
G-P	111,6%	1,31	79,3%	7

Table 3.18: Comparison between experimental and analytical results calculated with Wang and Ling model [52].

erage of difference between experimental and analytical failure load equal to $-4,2kN$ and a high dispersion equal to $42,5kN$.

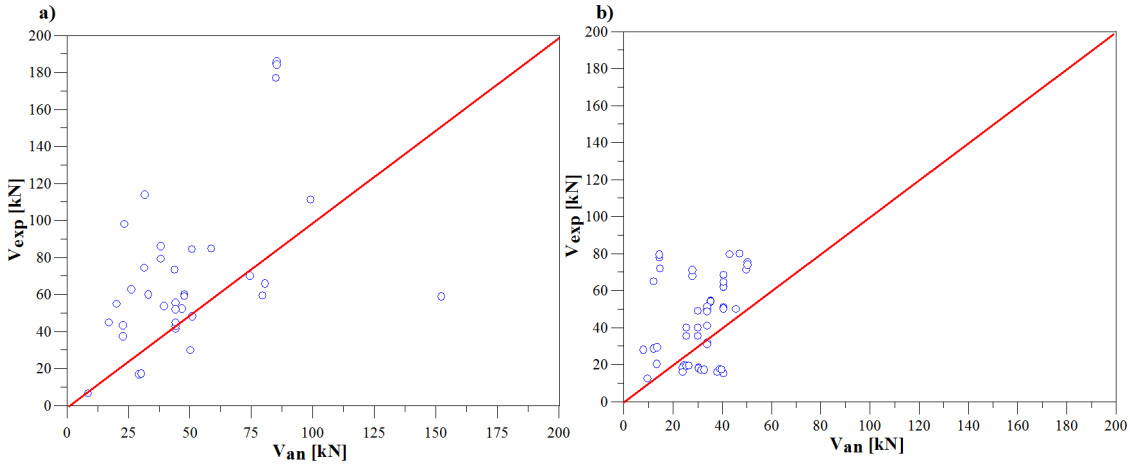

Figure 3.38: Test results vs predictions of Wang and Ling model [52]. a)CFRP wet lay-up system (90 valid tests); b)CFRP prepeg system (59 valid tests).

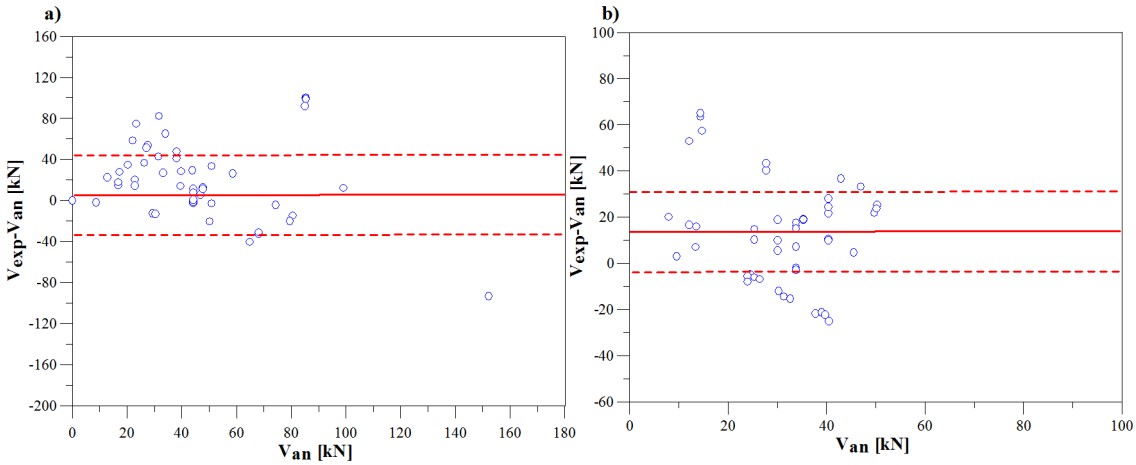

Figure 3.39: Difference between test results and analytical vs predictions of Wang and Ling model [52]. a)CFRP wet lay-up system μ=6,9kN σ=40,1kN (90 valid tests); b)CFRP prepeg system μ=12,0kN, σ=20,4kN (59 valid tests).

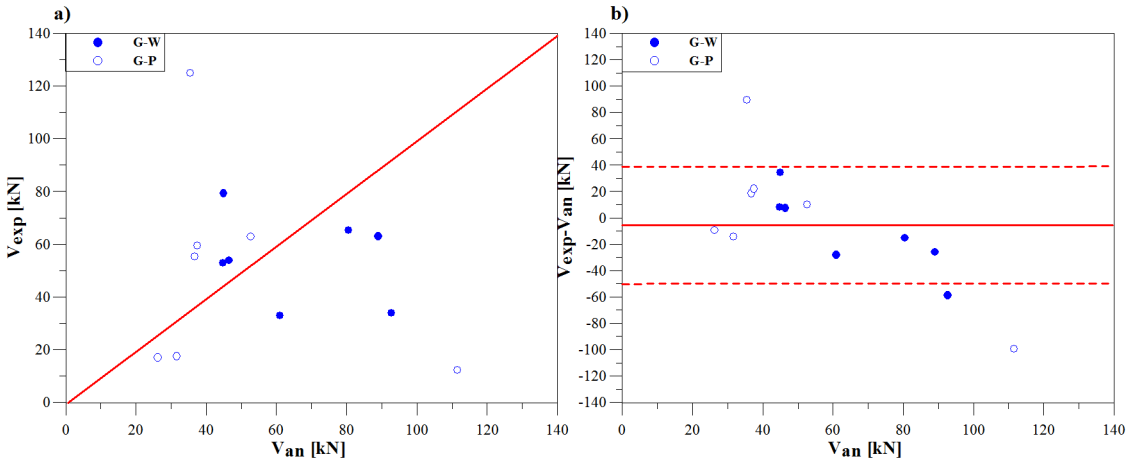

Figure 3.40: a)Test results vs predictions of Wang and Ling model [52], GFRP wet lay-up system (7 valid tests) and GFRP prepeg system (7 valid tests);b)Difference between test results and analytical vs predictions of Wang and Ling model [52] μ=-4,2kN, σ=42,5kN.

Raoof and Hassanen [43] redacted two model based on the same criterion and it doesn't solve a problem of high dispersion. In the first model, C-P, C-W and G-P groups present a COV over 60%, with a maximum of $89,7\%$ for beams reinforced with C-P material and a minimum of $65,7\%$ for G-P group; C-W presents a value of COV similar to G-P being $66,2\%$. The best value of COV was given for G-W material and it is equal to $48,7\%$. The values of bias present a maximum of $2,10$ for prepeg carbon plate and a minimum for wet lay up glass sheets being $0,78$; the C-W presents bias of $1,55$, while G-P bias is the closest to unity with a value of $1,01$.

The second model doesn't improved the bias of prediction of failure load and grows the dispersion of data. The maximum value of bias is present in C-P data with a $3,11$ and a COV of $103,8\%$. In C-W group the predictions are characterized by a bias of $2,27$ and a COV of $84,1\%$. The glass sheets reinforcement present intermediate values of COV with $61,8\%$ and $47,5\%$ for G-P and G-W, respectively, and bias of $1,45$ and $40,82$ for G-P and G-W, respectively.

	Average of difference	Bias	COV	No. of valid tests
C-W	7,7%	1,55	66,2%	90
C-P	27,1%	2,10	89,7%	59
G-W	72,5%	0,78	48,7%	7
G-P	74,5%	1,01	65,7%	7

Table 3.19: Comparison between experimental and analytical results calculated with Raoof and Hassanen model I [43].

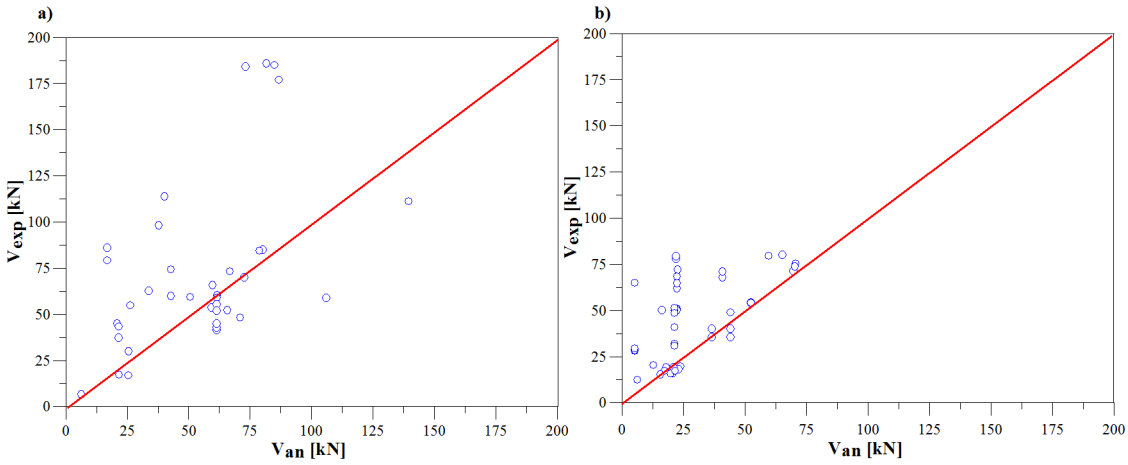

Figure 3.41: Test results vs predictions of Raoof and Hassanen model I [43]. a)CFRP wet lay-up system (90 valid tests); b)CFRP prepeg system (59 valid tests).

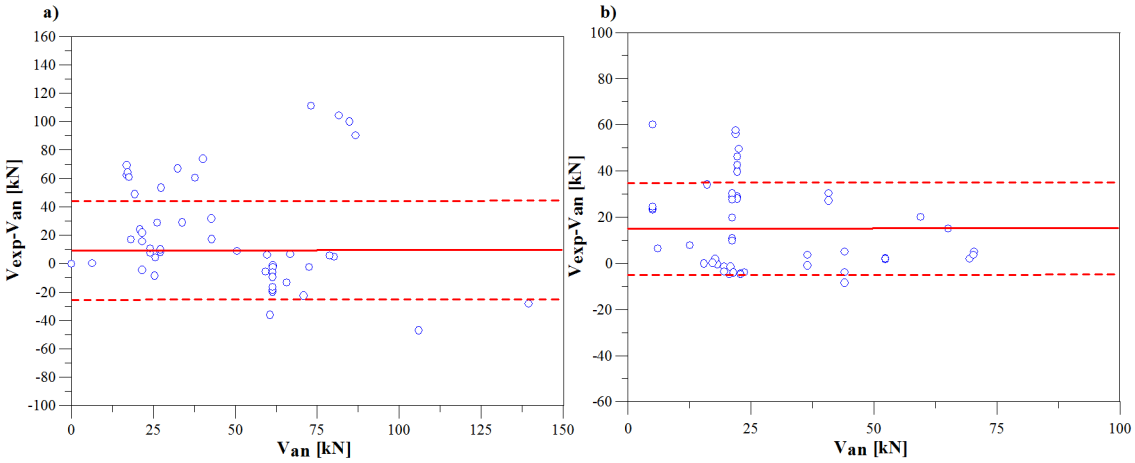

Figure 3.42: Difference between test results and analytical vs predictions of Raoof and Hassanen model I [43]. a)CFRP wet lay-up system μ=10,2kN σ=34,9kN (90 valid tests); b)CFRP prepeg system μ=16,3kN, σ=18,8kN (59 valid tests).

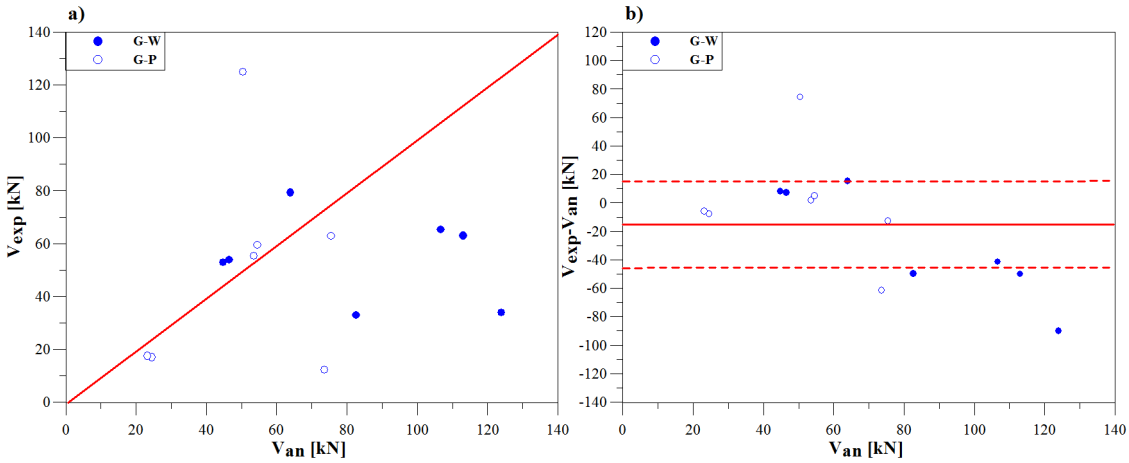

Figure 3.43: a)Test results vs predictions of Raoof and Hassanen model I [43], GFRP wet lay-up system (7 valid tests) and GFRP prepeg system (7 valid tests);b)Difference between test results and analytical vs predictions of Raoof and Hassanen model I [43] μ=-14,6kN, σ=39,3kN.

In Fig.3.42 and 3.43b are shown the difference between the experimental failure load and the analytical load for each beam. The beams reinforced with prepeg carbon plates present an average equal to $16,3kN$ and a standard deviation of $18,8kN$. Higher is σ value in C-W group being $34,9kN$, while the average is equal to $10,2kN$. Glass reinforced beams are characterized by high value of standard deviation and negative average, being $39,3kN$ and $-14,6kN$, respectively.

	Average of difference	Bias	COV	No. of valid tests
C-W	22,0%	2,27	84,1%	90
C-P	49,7%	3,11	103,8%	59
G-W	57,1%	0,82	47,5%	7
G-P	16,0%	1,45	61,8%	7

Table 3.20: Comparison between experimental and analytical results calculated with Raoof and Hassanen model II [43].

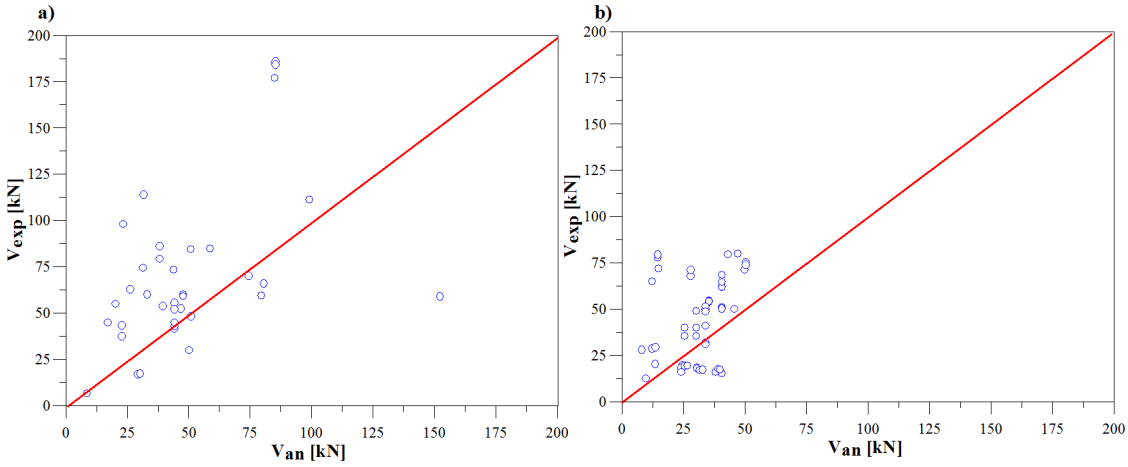

Figure 3.44: Test results vs predictions of Raoof and Hassanen model II [43]. a)CFRP wet lay-up system (90 valid tests); b)CFRP prepeg system (59 valid tests).

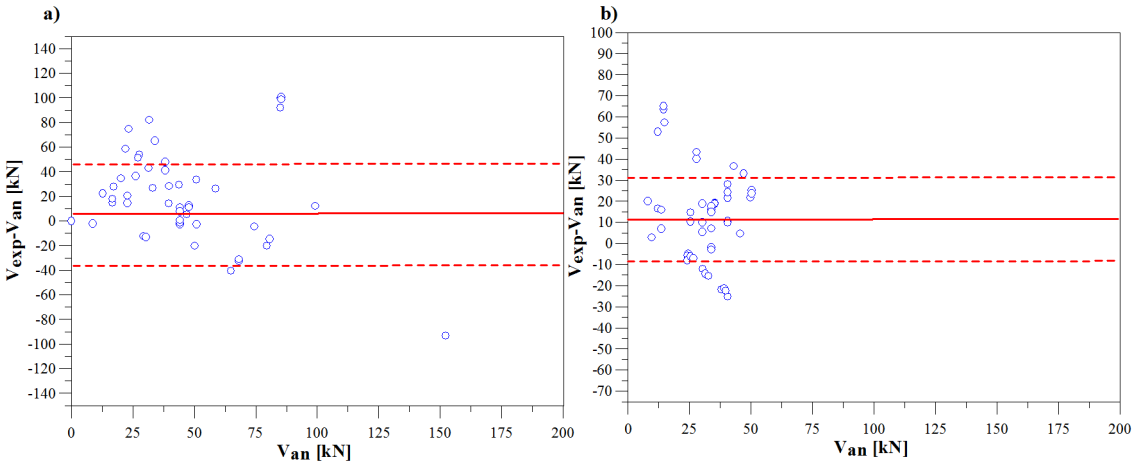

Figure 3.45: Difference between test results and analytical vs predictions of Raoof and Hassanen model II [43]. a)CFRP wet lay-up system μ=6,9kN σ=40,1kN (90 valid tests); b)CFRP prepeg system μ=12,0kN, σ=20,4kN (59 valid tests).

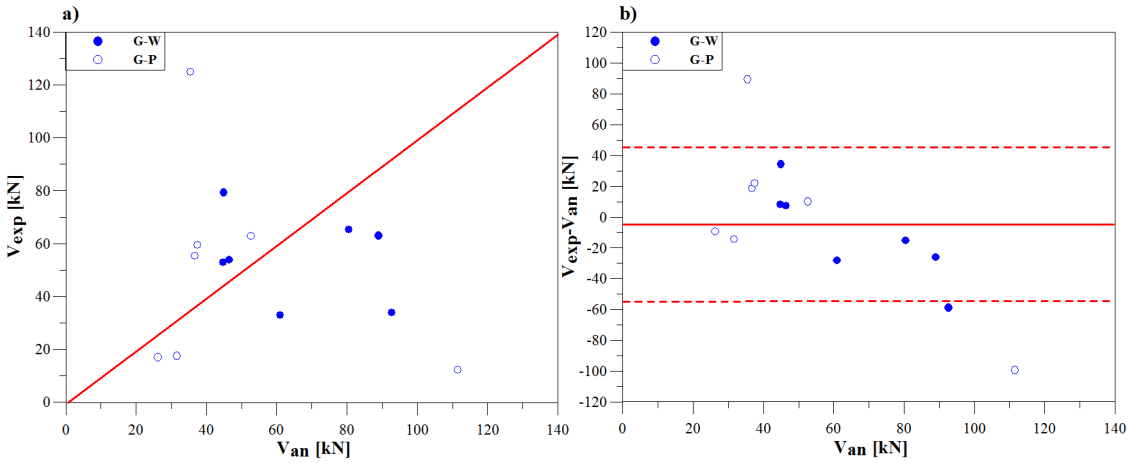

Figure 3.46: a)Test results vs predictions of Raoof and Hassanen model II [43], GFRP wet lay-up system (7 valid tests) and GFRP prepeg system (7 valid tests);b)Difference between test results and analytical vs predictions of Raoof and Hassanen model II [43] μ=-4,2kN, σ=42,5kN.

In Fig. 3.45 and 3.46b, it can see the improvement due to the application of second model in average results, being $6,87kN$, $12,0kN$ and $-4,19kN$ for C-W, C-P and GFRP group, respectively; but standard deviation results higher than in the first Raoof and Hassanen model [43]; C-W data are characterized by a σ equal to $40,1kN$, similar to GFRP standard deviation being $42,5kN$. In C-P data, the values of standard deviation results to be $20,4kN$.

3.11 Selection of end debonding model.

To compare better the different models, the same beam tests will be token into account. As discussed in the previous sections, not all models accept the same experimental data. The first step is compare the different model using all their valid tests. The comparison in Tab.3.21 and Tab.3.22 was done considering only carbon sheets divided in C-W and C-P group. There aren't enough G-W and G-P data to do a realistic comparison between the models. The most important factor to compare the goodness of data is the COV; it is important that each model is characterized by a low dispersion of data.

	Average of difference	Bias	COV	No. of valid tests
Smith and Teng (2002)	35,7%	1,66	27,0%	69
Colotti et al. (2004)	17,5%	0,90	23,6%	55
Teng and Yao, AS600 (2007)	41,5%	1,96	36,4%	90
Teng and Yao, ACI318 (2007)	21,1%	1,45	34,1%	90
Teng and Yao, BS8110 (2007)	26,6%	1,57	38,9%	90
Casas and Pascual (2007)	52,6%	2,21	20,1%	19
Ziraba et al. II (1995)	11,9%	1,17	17,7%	19
Jansze (1997)	77,8%	0,68	44,0%	77
Ahmed and van Gemert (1999)	69,2%	0,67	47,0%	77
Ziraba et al. I (1995)	32,3%	1,63	31,1%	19
Raoof and Zhang (1997)	27,3%	1,41	61,2%	90
Wang and Ling (1998)	26,1%	1,43	61,0%	90
Raoof and Hassanen I (2000)	7,7%	1,55	66,2%	90
Raoof and Hassanen II (2000)	22,0%	2,27	84,1%	90

Table 3.21: Comparison between different models, applying to beams reinforced with wet lay-up carbon sheets.

Considering C-W values (Tab.3.21), Teng and Yao model [61] presents the highest values of COV, being $36,4\%$, $34,1\%$, $38,9\%$, using AS600, ACI318, BS8110 equation definition, respectively, as explained in previous sections. This model is based on the greatest database with 90 valid tests. Ziraba et al. model [70] presents the lowest value of coefficient of variation being $17,7\%$ with bias of $1,17$. Casas and Pascual model [13] is characterized by a bias of $2,21$ and a COV of $20,1\%$. These two models need resin characteristics and are based on a database of 19 carbon wet lay-up beams reinforced. Colotti et al. model [18] is the unique model that gives a bias less than one, being $0,90$, with a COV equal to $23,6\%$. Finally, Smith and Teng model [53] gives a bias equal to $1,66$ and a COV of $27,0\%$.

	Average of difference	Bias	COV	No. of valid tests
Smith and Teng (2002)	34,7%	1,62	26,8%	39
Colotti et al. (2007)	10,2%	1,09	39,8%	34
Teng and Yao, AS600 (2007)	39,6%	1,84	34,8%	59
Teng and Yao, ACI318 (2007)	19,5%	1,41	37,9%	59
Teng and Yao, BS8110 (2007)	22,4%	1,44	36,0%	59
Casas and Pascual (2007)	54,1%	2,27	23,4%	38
Ziraba et al. II (1995)	6,9%	1,26	40,9%	38
Jansze (1997)	82,1%	0,64	43,1%	50
Ahmed and van Gemert (1999)	51,3%	0,82	68,3%	50
Ziraba et al. I (1995)	32,1%	2,09	62,5%	38
Raoof and Zhang (1997)	12,7%	1,68	70,1%	59
Wang and Ling (1998)	7,7%	1,62	76,4%	59
Raoof and Hassanen I (2000)	27,1%	2,10	89,7%	59
Raoof and Hassanen II (2000)	49,7%	3,11	103,8%	59

Table 3.22: Comparison between different models, applying to beams reinforced with prepeg carbon sheets.

The goodness of model changes applying these to C-P data, as reported in Tab.3.22. Generally, the number of data is less than C-W group. Ziraba et al. model [70], which with C-W data gave the best value of COV, presents an high value of coefficient of variation being $40,9\%$ and a bias of $1,26$. Casas and Pascual model [13] is characterized by the best value of COV equal to $23,4\%$; the bias is high, being $2,27$. Colotti et al. model [18] gives a value of bias of 1,09, the closest to unity, the COV is equal to $39,8\%$. The second best value of COV is predicted by Smith and Teng model [53] being $26,8\%$ with a bias of $1,62$. Teng and Yao models [61] are characterized by high values of COV equal to $34,8\%$, $37,9\%$, $36,0\%$ for AS600, ACI318, BS8110 equation definition applying, respectively.

The models compared start from different approaches. Smith and Teng model [53] and Teng and Yao model [61] are based on calibration of value of experimental tests, there isn't a mechanical justification. Colotti et al. model [18] is based on strut and tie theory and permits to predict the mode of failure. Casas and Pascual [13] model and Ziraba et al. model [70] are based on the interface interaction, they based their model on resin behavior.

The goodness of the first two model depends on the quantity of beams tested taking into account during the calibration, it could changed considering a beam with different geometry of beam, different resin or FRP material. Colotti et al. model [18]

is the most complete model because permits to predict the real failure mode, while the other models consider only debonding failure mode. In the beams reinforced with carbon sheets applying with wet lay-up could be difficult evaluated the real value of resin thickness. For these reason many authors didn't indicated the t_a value. Consequently, their models don't take into account the interface between concrete and resin behavior. They admit that the end debonding failure takes place in cover concrete. Ziraba et al. [70] model and Casas and Pascual model [13] consider an interfacial debonding. To use these model is important the value of Young's modulus of the resin and its thickness; could be difficult calculate t_a value when the sheet is applied *in situ*, where the uncertainty is higher than in prepeg plates.

The second step is compare the different models taking into account the same data. Considering beam tests which are related the resin characteristic, the first model examined is Colotti et al. model [18]. As explained in previous sections, this model predicts the load which causes the end debonding fail but, also, calculates the loads for each mode of failure. it has done two hypothesis: firstly are token into account only the beams where the model predicts an end debonding failure, then for all beams has been calculated the load of end debonding failure mode ignoring other failure modes.

As reported in Fig.3.47 and Fig.3.48, not all data, using Colotti et al. model [18], fail for end debonding. On 19 C-W data, only 9 analytical results predict the real failure mode, while on 38 C-P data, 19 beams fail for end debonding.

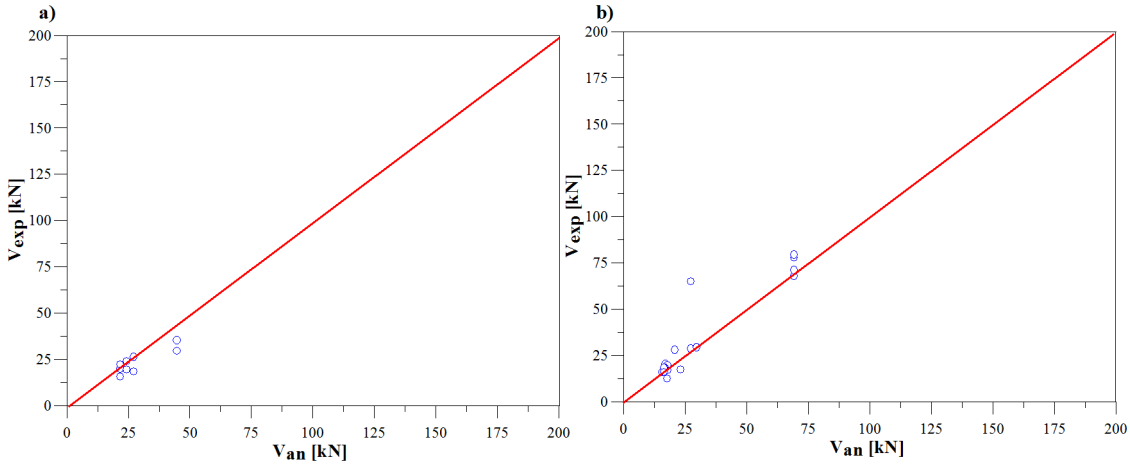

Figure 3.47: Test results vs predictions of Colotti et al. model [18] taking into account the beams which fail for end debonding of Casas and Pascual model [13] valid tests. a)CFRP wet lay-up system (9 valid tests); b)CFRP prepeg system (19 valid tests).

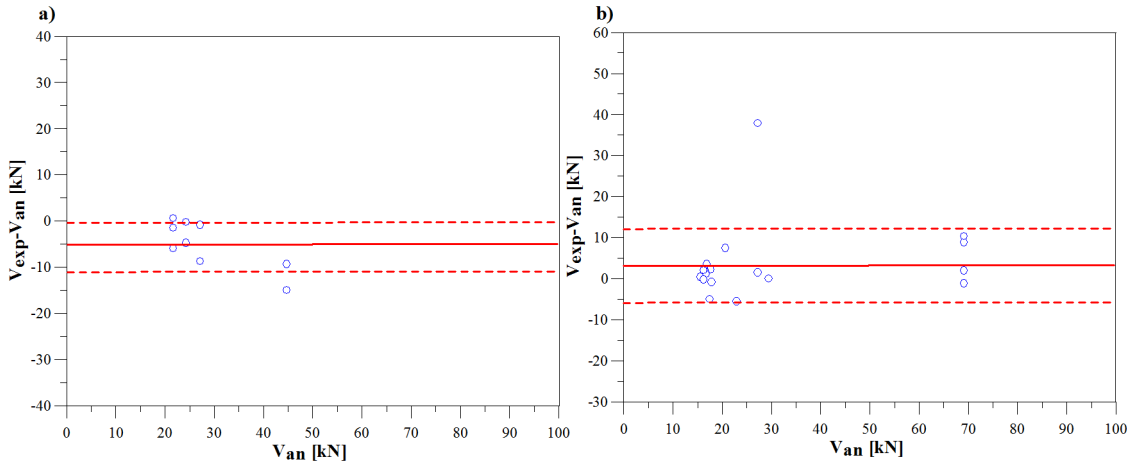

Figure 3.48: Difference between test results and analytical vs predictions of Colotti et al. model [18] taking into account the beams which fail for end debonding of Casas and Pascual model [13] valid tests. a)CFRP wet lay-up system μ=-5,0kN σ=4,9kN (9 valid tests); b)CFRP prepeg system μ=3,6kN, σ=9,0kN (19 valid tests).

This model gives good results for both of C-W and C-P data (Tab.3.23). The COV for beams reinforced with carbon sheets applied *in situ* is equal to $15,7\%$ being the bias $0,84$. The dispersion of C-P prediction values is higher being $29,6\%$ with a bias equal to $1,12$. Considering the difference between experimental load and analytical failure load (Fig.3.48), the average is lower than in Casas and Pascual model [13]. In C-W group the model overestimated the experimental failure load being the average equal to $-5kN$ and standard deviation is equal to $4,9kN$. The beams reinforced with prepeg carbon plates (Fig.3.48) presents an average equal to $3,6kN$ and a value of standard deviation higher than C-W group being $14,3kN$.

	Average of difference	Bias	COV	No. of valid tests
C-W data				
Colotti et al. (2004)	21,5%	0,84	15,7%	9
Casas and Pascual (2007)	52,6%	2,21	20,1%	19
C-P data				
Colotti et al. (2004)	5,7%	1,12	29,7%	19
Casas and Pascual (2007)	54,1%	2,27	23,4%	38

Table 3.23: Comparison between Casas and Pascual model [13] and Colotti et al. model [18], taking into account the beams which fail for end debonding of Casas and Pascual model [13] valid tests.

In Fig.3.49 and Fig.3.50 the number of data are the same considered in Casas and Pascual model [13]. In this comparison are ignored the failure modes corresponding to FRP rupture, concrete crushing and shear failure mode.

	Average of difference	Bias	COV	No. of valid tests
C-W data				
Colotti et al. (2004)	36,9%	0,76	18,9%	19
Casas and Pascual (2007)	52,6%	2,21	20,1%	19
C-P data				
Colotti et al. (2004)	64,1%	0,82	50,8%	38
Casas and Pascual (2007)	54,1%	2,27	23,4%	38

Table 3.24: Comparison between Casas and Pascual model [13] and Colotti et al. model [18] taking into account the end debonding failure mode for Casas and Pascual model [13] valid tests.

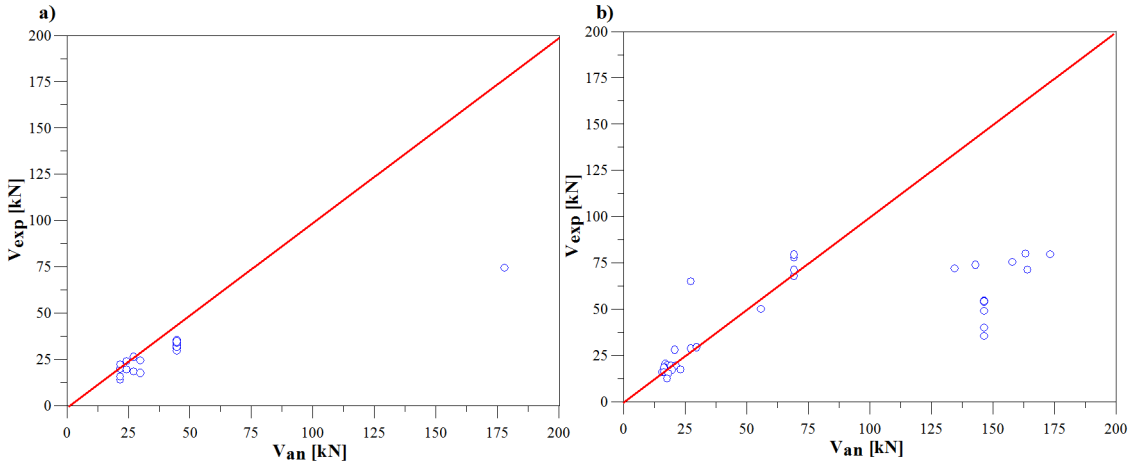

Figure 3.49: Test results vs predictions of Colotti et al. model [18] taking into account the end debonding failure mode of Casas and Pascual model [13] valid tests. a)CFRP wet lay-up system (19 valid tests); b)CFRP prepeg system (38 valid tests).

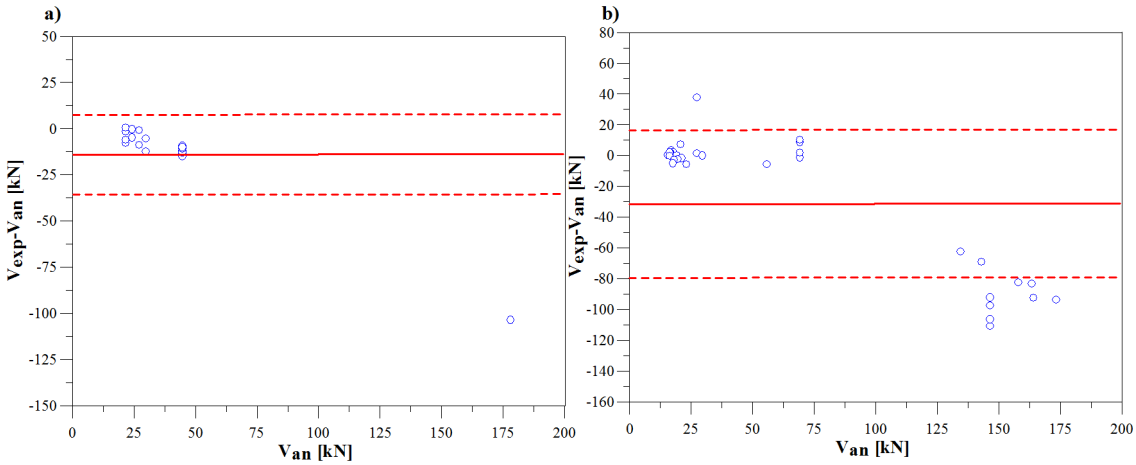

Figure 3.50: Difference between test results and analytical vs predictions of Colotti et al. model [18] taking into account the end debonding failure mode of Casas and Pascual model [13] valid tests. a)CFRP wet lay-up system μ=-12,9kN σ=21,8kN (19 valid tests); b)CFRP prepeg system μ=-32,4kN, σ=46,9kN (38 valid tests).

Colotti et al. model [18], considering the end debonding failure mode for all beams, improves the prediction for C-W data. The COV is lower than in Casas and Pascual analytical data, being $18,9\%$. Although, $18,9\%$ is higher than the COV is the previous comparison, now, are taking into account all valid tests; the bias is equal to $0,76$. In C-P values the coefficient of variation is too high to consider this model, being $50,8\%$; the bias is equal to $0,82$. Considering only the end debonding failure mode, the model isn't able to predict correctly the load of fail.

The average of difference between experimental and analytical failure load presents, in C-W group, a negative value of $-12,9kN$ with a standard deviation equal to $21,8kN$. The C-P reinforced beams are characterized by an average equal to $-32,4kN$ and a standard deviation of $46,9kN$.

The same comparison was done with Teng and Yao model [61], applying this to the data valid in Casas and Pascual model [13]. It was considered the predictions given by Teng and Yao model [61] using AS600 equation. As commented in the previous sections, this gave the best prediction for C-P data, although the C-W predictions could be improved using other equations.

	Average of difference	Bias	COV	No. of valid tests
C-W data				
Teng and Yao (2007)	20,1%	1,27	11,0%	19
Casas and Pascual (2007)	52,6%	2,21	20,1%	19
C-P data				
Teng and Yao (2007)	42,4%	1,86	29,9%	38
Casas and Pascual (2007)	54,1%	2,27	23,4%	38

Table 3.25: Comparison between Casas and Pascual model [13] and Teng and Yao model [61] taking into account beam tests with information on resin's characteristics.

As seen in Fig.3.51a, the analytical values predicted by Teng and Yao model [61] are very good with a low dispersion being the COV equal to $11,0\%$ and a value of bias, equal to $1,27$, lower than Casas and Pascual [13]. The prediction of end debonding load for beams reinforced with prepeg carbon plates is not as good as Casas and Pascual model [13]. C-P group is characterized by coefficient of variation equal to $29,9\%$ and a bias of $1,86$. All predicted values are set on safe side, because the model underestimated the end debonding failure load. The average of difference between experimental and analytical load is equal to $5,4kN$ and $17,0kN$ for C-W and C-P data, respectively; while the standard deviation is equal to $2,7kN$ and $12kN$ for C-W and C-P data, respectively.

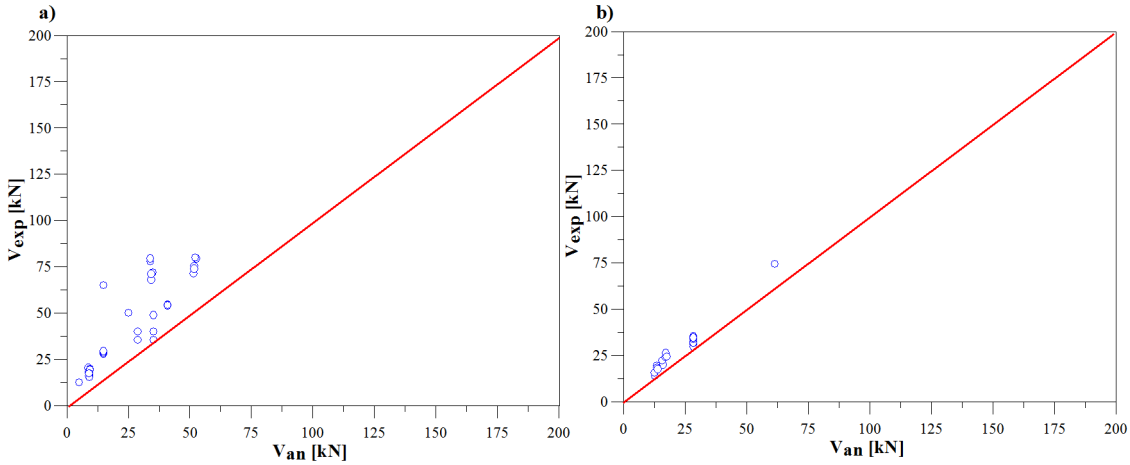

Figure 3.51: Test results vs predictions of Teng and Yao model [61] taking into account data with resin characteristics. a)CFRP wet lay-up system (19 valid tests); b)CFRP prepeg system (38 valid tests).

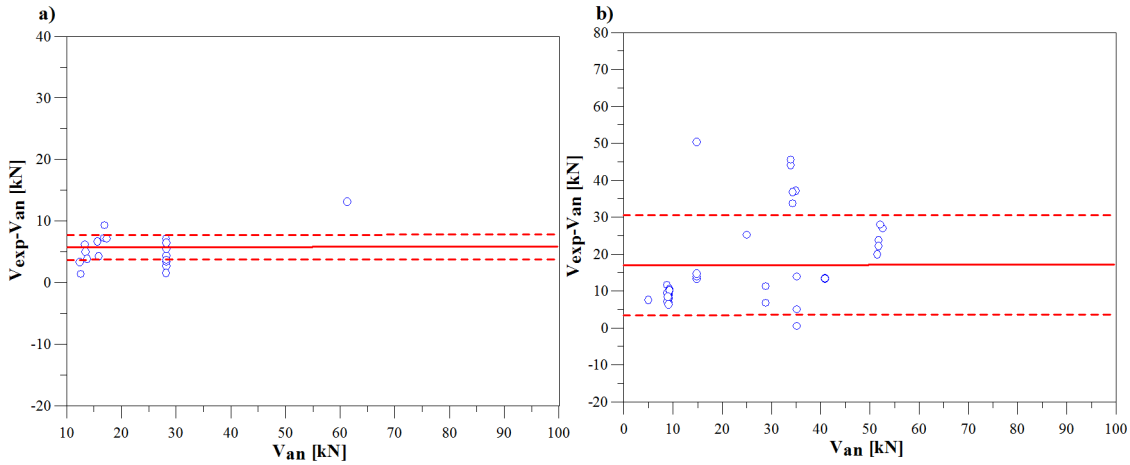

Figure 3.52: Difference between test results and analytical vs predictions of Teng and Yao model [61] taking into account data with resin characteristics. a)CFRP wet lay-up system μ=5,4kN σ=2,7kN (19 valid tests); b)CFRP prepeg system μ=17,0kN, σ=12,3kN (38 valid tests).

Finally, applying Smith and Teng model [53] to Casas and Pascual's data, it was compare the goodness of this model. The values of COV are equal to $12,0\%$ and $24,5\%$ for C-W and C-P data, respectively. The value of bias for beams reinforced with wet lay-up carbon sheets is equal to 1,34. Considering beams reinforced with prepeg carbon plates, the bias is equal to $1,50$. Considering the difference between the experimental loads and the analytical predictions, as shown in Fig.3.52, all data present a positive prediction ($V_{exp} \geq V_{an}$) because the model underestimated the beam strength, and all test were set in the safe side.The average of $V_{exp} - V_{an}$ is equal to $5,9kN$ and $11,8kN$ for C-W and C-P data, respectively; C-P group is characterized by standard deviation of $2,0kN$, while C-W's standard deviation is equal to $10,3kN$.

	Average of difference	Bias	COV	No. of valid tests
C-W data				
Smith and Teng (2002)	24,0%	1,34	12,0%	15
Casas and Pascual (2007)	52,6%	2,21	20,1%	19
C-P data				
Smith and Teng (2002)	30,7%	1,50	24,5%	29
Casas and Pascual (2007)	54,1%	2,27	23,4%	38

Table 3.26: Comparison between Smith and Teng model [53] and Casas and Pascual model [13]taking into account beam tests with information on resin's characteristics.

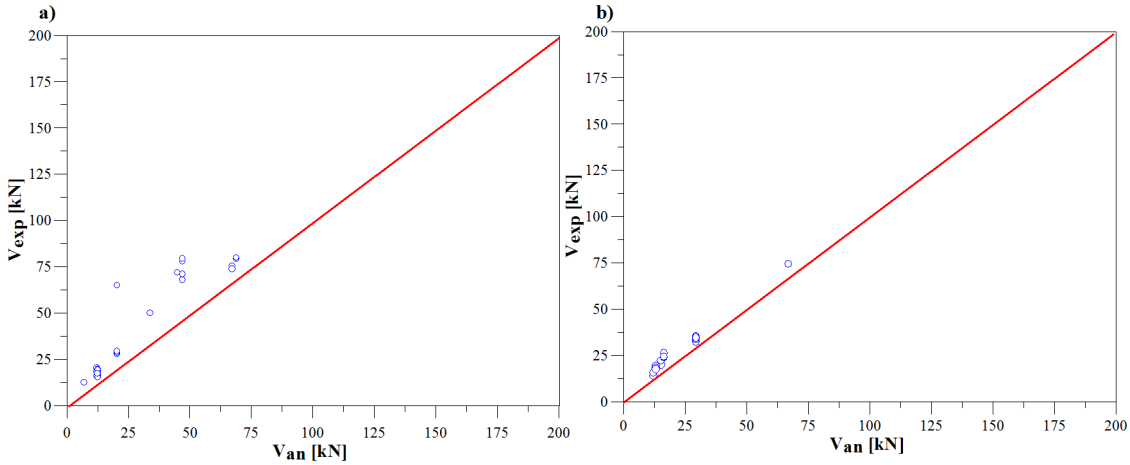

Figure 3.53: Test results vs predictions of Smith and Teng model [53] taking into account data with resin characteristics. a)CFRP wet lay-up system (15 valid tests); b)CFRP prepeg system (29 valid tests).

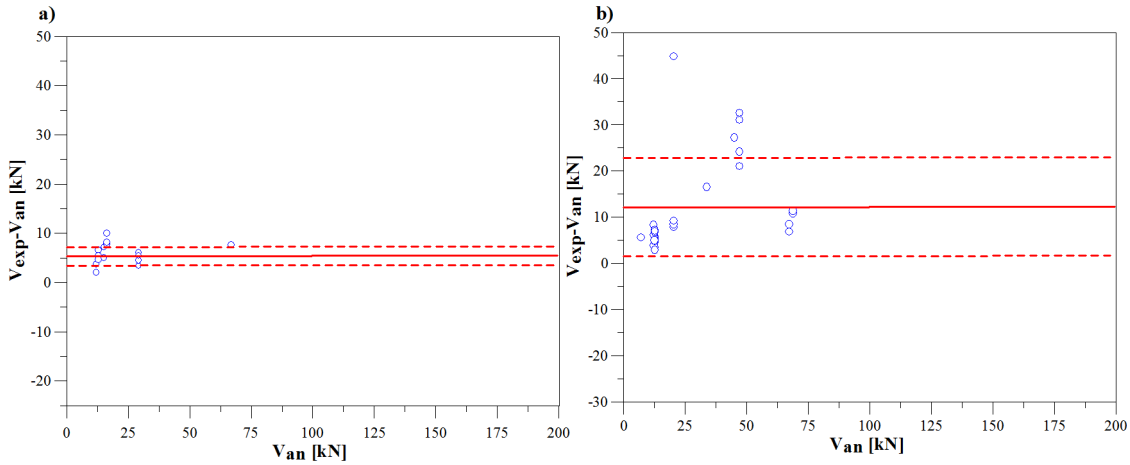

Figure 3.54: Difference between test results and analytical vs predictions of Smith and Teng model [53] taking into account data with resin characteristics. a)CFRP wet lay-up system μ=5,9kN σ=2,0kN (15 valid tests); b)CFRP prepeg system μ=11,8kN, σ=10,3kN (29 valid tests).

Applying the selected models to data with resin characteristics, it was demonstrated that the prediction of end debonding failure load with Casas and Pascual model [13] could be improved using other model. Casas and Pascual model [13] gives the best results to calculated the end debonding failure load in beams reinforced with prepeg carbon plates (Tab.3.27). The aim is to choose a model which can give a good prediction for both C-W and C-P reinforced beams, and this model results the unique characterized by good values for both groups. Moreover, with Ziraba et al. model [70], it is based on the behavior on interface between the resin and the concrete.

The great difference between the C-W and C-P analytical results depends on single data, because the models don't change their equation with applied system. These means that a good model has to give a good predictions for both wet lay-up and prepeg carbon sheets.

	Average of difference	Bias	COV	No. of valid tests
C-W data				
Casas and Pascual (2007)	52,6%	2,21	20,1%	19
Colotti et al. I (2004)	21,5%	0,84	15,7%	9
Colotti et al. II (2004)	36,9%	0,76	18,9%	19
Teng and Yao (2007)	20,1%	1,27	11,0%	19
Smith and Teng (2007)	24,0%	1,34	12,0%	15
C-P data				
Casas and Pascual (2007)	54,1%	2,27	23,4%	38
Colotti et al. I (2004)	5,7%	1,12	29,7%	19
Colotti et al. II (2004)	64,1%	0,82	50,8%	38
Teng and Yao (2007)	42,4%	1,86	29,9%	38
Smith and Teng (2002)	30,7%	1,50	24,5%	29

Table 3.27: Comparison between Casas and Pascual model [13] and other models taking into account beam tests with information on resin's characteristics. Colotti et al. I [18]: take into account only the beams which fail for end debonding; Colotti et al. II [18]: take into account for all beams the end debonding failure mode.

Chapter 4

Analysis of shear tests data

It was collected 176 prisms FRP bonded tested by 11 authors from 1996 to 2007. They were divided in five groups like it was done for beam tests: C-W, C-P, G-W, G-P(C=CFRP, G=GFRP, A=AFRP, P=pultruded,W=wet lay-up plate). There are 6 C-P data, 131 C-W data, 2 G-P data, 31 G-W data, 6 A-W data.

All the nineteen models explained in the second chapter were applied to the data tests. All models are independent of material type, except for Izumo model [62] that can be applied to either carbon fiber sheets or aramid fiber sheets; It is not valid for glass fiber sheets. The models will be divided in 3 groups: models considering effective bond length, models not considering effective bond length, model independent of bond length.

The first group includes 9 models; they were developed by Chen and Teng [16], Maeda et al. [62], Khalifa et al. [33], Neubauer and Rostasy [62], Niedemermeier [62], Lu et al. [34], Sato et al. [62], ISO [62] and Yang et al. [62]. The prediction of bond strength is based on the effective bond length L_e.

Each model gives a different expression to define L_e value, and they should be very different. L_e depends on the modulus of elasticity of FRP, its thickness, and sometimes, on the concrete strength. Yang et al. considered the effective bond length as a constant equal to $100mm$.

For example, considering a data test with: $E_{frp} = 110GPa$, $t_{frp} = 0,495mm$ and $f'_c = 17MPa$; the effective bond length should be equal from a maximum of $117mm$ [34] to a minimum of $45mm$ [62].

If L_e is longer than the measured bond length, all models consider the last one to define the bond strength.

To compare the models it was used the same values of previous chapter: average of difference, average of bias (experimental to predicted bond strength ratio) and COV. Each model was called with a number put in the same order how it was

	Mod 1	Mod 2	Mod 3	Mod 4	Mod 5	Mod 6	Mod 7	Mod 8	Mod 9
C-P	3,8% 1,30 53,6%	25,1% 0,92 37,1%	40,5% 0,76 25,8%	25,2% 0,91 40,0%	8,4% 1,00 28,8%	7,7% 1,25 41,9%	323,5% 0,35 72,6%	12,9% 1,07 49,8%	17,0% 0,95 32,1%
C-W	12,8% 1,26 33,5%	6,5% 1,17 32,7%	23,5% 1,44 27,3%	12,1% 0,96 30,2%	26,7% 1,13 40,8%	11,5% 1,24 33,7%	74,1% 0,80 58,3%	11,1% 1,22 29,9%	18,8% 1,33 27,4%
G-P	13,1% 0,88 3,0%	20,1% 0,84 8,8%	9,0% 1,11 8,8%	40,0% 0,72 4,9%	9,0% 0,92 4,9%	14,3% 0,88 3,9%	4,7% 0,96 2,8%	0,8% 1,00 8,8%	5,8% 0,95 8,8%
G-W	25,4% 1,50 36,3%	28,4% 1,63 43,6%	31,5% 1,68 39,8%	7,0% 1,21 37,9%	20,6% 1,48 43,6%	27,5% 1,55 37,9%	58,2% 0,85 96%	25,9% 1,53 38,9%	35,7% 1,77 39,3%
A-W	35,0% 1,59 17,8%	31,7% 1,52 18,4%	18,9% 1,30 22,7%	13,15% 1,19 17,8%	32,4% 1,53 17,8%	38,1% 1,67 17,0%	17,7% 1,23 148,5%	22,1% 1,32 17,1%	24,0% 1,40 24,1%

Table 4.1: Experimental to predicted bond strength ratios (average of difference, bias and COV). Models considering effective bond length: Chen and Teng [16], Maeda et al. [62], Khalifa et al. [33], Neubauer and Rostasy [62], Niedemeier [62], Lu et al. [34], Sato [62], Iso [62], Yang et al. [62]; C-P=6 tests, C-W=131 tests, G-P=2 tests, G-W=31 tests, A-W=6 tests.

explained in the second chapter (Mod 1 = Chen and Teng [16], Mod 2 = Maeda et al. [62] ,etc.).

The data of C-P, C-P and A-W are not enough to verify the goodness of the models. The other two groups, C-W and G-W, present different models that have a good experimental to analytic bond strength ratio and are different for each groups.

For C-W data, the predictions done with Khalifa et al. model [33], present a COV equal to 27,3%, and bias equal to 1,44. To improve this value it is possible to use Neubauer and Rostasy model [62] being 0,96 the value of bias, but in this case, the COV is greater and was found to be 30,2%.

Yang et al. model [62] presents the same COV values of Khalifa model [33] and bias equal to 1,33. The Maeda et al. model [62] is characterized by a bias of 1,17 with COV being 32,7%.

Another good prediction can be done with Iso model [62] that presents a COV equal to 27,4% and a bias equal to 1,33.

There is not a good prediction for G-W data. Chen and Teng model [16] presents the best values, the COV and the bias were found to be 36,3% and 1,5, respectively.

The highest COV value was found with Sato model [62] where is $95,7\%$ with bias being $0,85$. Using Neubauer and Rostasy model [62], COV and bias are $37,9\%$ and $1,21$, respectively.

Second group includes models that not consider effective bond length. It is not possible to use these models on all test data, it is important to know the bond length. For example, using too large anchorage, Tanaka model [62] should predict a negative value of P_u; if the bond length is equal to $45cm$, P_u is null, the maximum bond strength is founded for $L = 169mm$. If $L \to \infty$, many models predicts infinite bond strength.

This group includes: Tanaka model [62], Hiroyuki and Wu model [62], Brosens and van Germet model [62], Izumo model [62], Adhikary and Mutsuyoshi model [62]. To compare these models, it was followed the previous numeration.

	Mod 10	Mod 11	Mod 12	Mod 13	Mod 14
C-P	$71,7\%$ $4,48$ $57,0\%$	$67,4\%$ $3,13$ $14,2\%$	$29,1\%$ $2,44$ $77,0\%$	$66,6\%$ $0,33$ $81,2\%$	$32,4\%$ $1,37$ $80,0\%$
C-W	$50,8\%$ $2,37$ $52,2\%$	$50,6\%$ $2,42$ $48,6\%$	$13,0\%$ $1,71$ $60,3\%$	$14,4\%$ $0,86$ $68,0\%$	$48,0\%$ $1,06$ $60,9\%$
G-P	$11,5\%$ 1,14 $8,76\%$	$26,9\%$ 1,38 $8,76\%$	$19,1\%$ 1,25 $8,76\%$		$32,8\%$ 0,76 $8,76\%$
G-W	$69,0\%$ 3,43 $27,3\%$	$72,4\%$ 3,77 $21,9\%$	$57,3\%$ 2,60 $30,4\%$		$25,1\%$ 1,49 $32,2\%$
A-W	$58,8\%$ $2,67$ $29,8\%$	$41,6\%$ $1,88$ $29,8\%$	$89,7\%$ $0,59$ $33,0\%$	$60,8\%$ $0,39$ 29,3%	$249,0\%$ $0,32$ 34,0%

Table 4.2: Experimental to predicted bond strength ratios (average of difference, bias and COV). Models not considering effective bond length: Tanaka [62], Hiroyuki and Wu [62], Brosens and van Germet [62], Izumo [62], Adhikary and Mutsuyoshi [62]; C-P=6 tests, C-W=131 tests, G-P=2 tests, G-W=31 tests, A-W=6 tests.

These models predict better GFRP bond strength than CFRP. Tanaka model [62], used on G-W data, gives a COV equal to $27,34\%$ and bias is $3,43$. With Hiroyuki and Wu model [62] the same values of bias and COV were found to be $21,88\%$ and $3,77$, respectively. In the other two models, the COV and bias are $30,4\%$ and $2,6$, respectively, using Brosens and van Germet model [62] and $32,2\%$

and $1,49$, respectively, using Adhikary and Mutsuyoshi model [62] and there is an improvement bias value.

The prediction of C-W data is not good because the COV value is ever too high, $48,6\% - 68,5\%$. Izumo model [62] that used different expression for carbon sheets and aramid sheet has a COV of $81,2\%$ and $68,5\%$ for C-P data and C-W data, respectively. Adhikary and Mutsuyoshi model [62] gives the best bias value that is $1,06$. A value of $1,71$ is given by Brosens and van Germet model [62].

The last group includes Taljsten model [57], Yuan and Wu model [67] and Dai et al. model [19]. They are independent on bond length. The variables are the modulus of elasticity and the geometry of FRP and concrete strength. In Taljsten model [57], Yuan and Wu model [67] the prediction depends on specimen geometry also.

	Mod 15	Mod 16	Mod 17
C-P	$29,4\%$ $0,87$ $34,1\%$	$30,6\%$ $0,86$ $34,9\%$	$60,1\%$ $0,68$ $30,3\%$
C-W	$27,1\%$ $1,48$ $26,5\%$	$26,6\%$ $1,47$ $26,8\%$	$39,6\%$ $1,99$ $45,3\%$
G-P	$14,0\%$ $1,17$ $8,7\%$	$13,7\%$ $1,17$ $8,8\%$	$53,8\%$ $2,17$ $2,8\%$
G-W	$33,3\%$ $1,76$ $43,0\%$	$32,6\%$ $1,75$ $43,4\%$	$34,5\%$ $2,19$ $68,2\%$
A-W	$36,4\%$ $1,62$ $16,2\%$	$36,2\%$ $1,61$ $16,4\%$	$69,3\%$ $3,27$ $6,2\%$

Table 4.3: Experimental to predicted bond strength ratios (average of difference, bias and COV). Models independent of bond length: Taljsten [57], Yuan and Wu [67], Dai et al. [19]; C-P=6 tests, C-W=131 tests, G-P=2 tests, G-W=31 tests, A-W=6 tests.

Analyzing C-W data, Yuan and Wu model [67] gives a COV of $26,9\%$ and a bias equal to $1,47$. Taljsten model [57] and Yuan and Wu model [67] give similar results. And both are good to predict shear debonding in C-W data.

Taking into account G-W data, the predictions of Taljsten model [57] and Yuan and Wu model [67] are not as good as C-W data predictions but are better than

Dai et al. model [19]. COV and bias were found to be 43% and $1,75$, respectively, using Taljsten model [57] and Yuan and Wu [67] model.

The comparison of graphical is presented in the order of the previous classification. The graphical data points include all data collected. Chen and Teng model [16] gives a bias of $1,26$ and $1,50$ for C-W data and G-W data respectively which implies that the predicted bond strengths are in the safe range; it means that the data point ($P_{u,an}$; $P_{u,exp}$) are above the red line ($P_{u,an} = P_{u,exp}$). But the percent unsafe design are $30,5\%$, $16,3\%$ for C-W and G-W data, respectively.

The safest prediction models, for C-W data, are Tanaka model [62] and Hiroyuki and Wu model [62] with percent unsafe design of $2,29\%$. All models included in the third group, Taljsten model [57], Yuan and Wu model [67], Dai et al. model [19], have a good percent unsafe design, $10,6\%$, $11,4\%$ and $8,4\%$, respectively. The Khalifa et al. model [33] has $18,3\%$ of prediction data under the red line and is the safest model in the second group.

The third group, where the models were independent of bond length, presents a good values of unsafe predictions, $10,7\%$, $11,4\%$, $8,4\%$, for Taljsten model [57], Yuan and Wu model [67], Dai et al. model [19], respectively. Neubauer and Rostasy [62], Sato [62] and Izumo [62] proposed the three unsafest models with a percent unsafe prediction of $70,2\%$, $78,6\%$ and $62,6\%$, respectively. All these models overestimate the bond strength and generally have largely scattered results.

Yang et al. [62], Tanaka [62], Hiroyuki and Wu [62], Brosens and van Gemert [62] proposed models that gave all safe predictions. The models included in the third group have a good percentage of unsafe predictions; It was found to be $6,4\%$, $9,7\%$, $9,7\%$ for Taljsten model [57], Yuan and Wu model [67] and Dai et al. model [19], respectively. The worst percent unsafe predictions was given by Sato model [62] being equal to $71,0\%$.

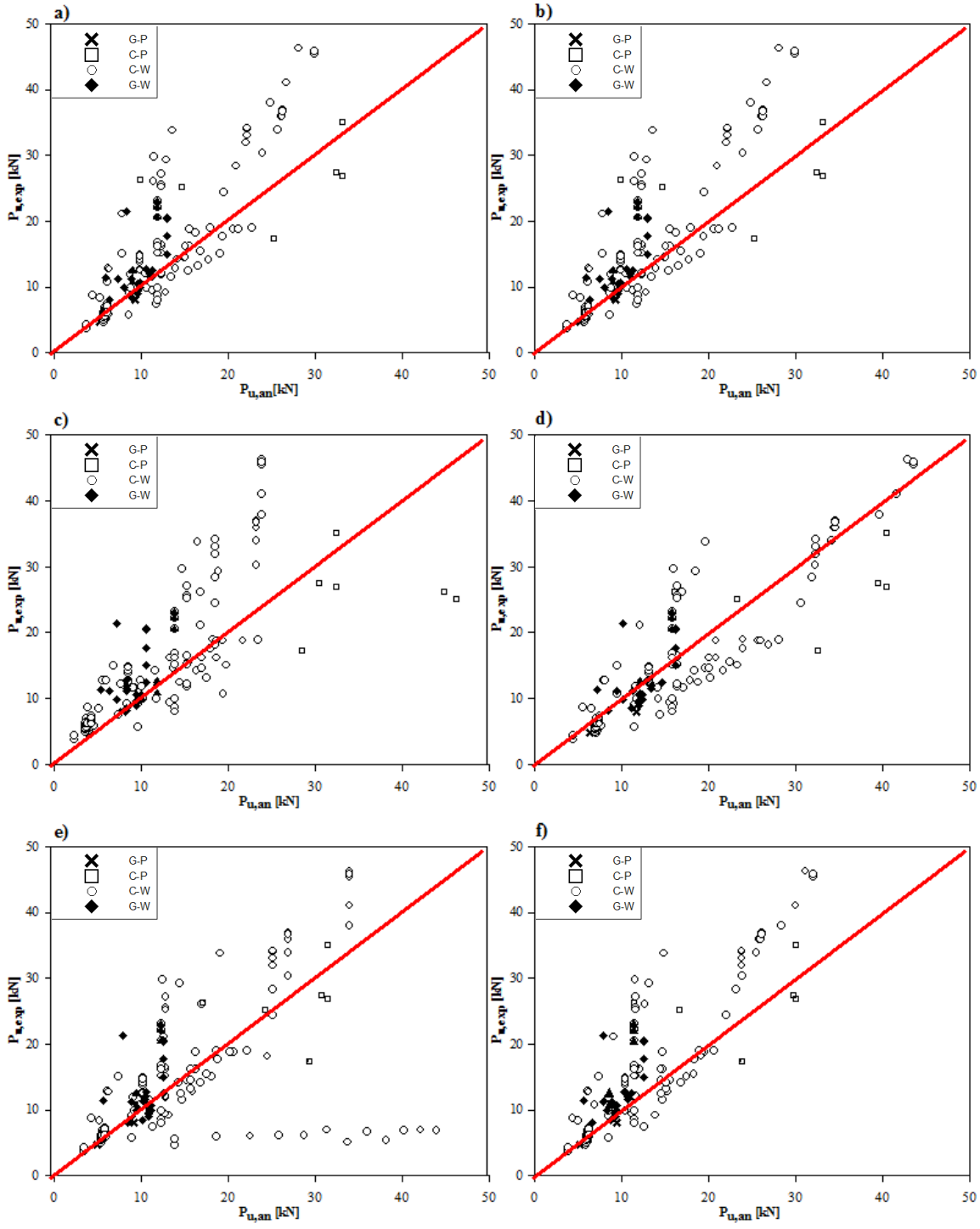

Figure 4.1: Test bond strength vs predicted bond strength using: a)Chen and Teng model [16]; b) Maeda et al. model [62]; c) Khalifa et al. model [33]; d) Neubauer and Rostasy model [62]; e) Niedermeier model [62]; f) Lu et al. model [34].

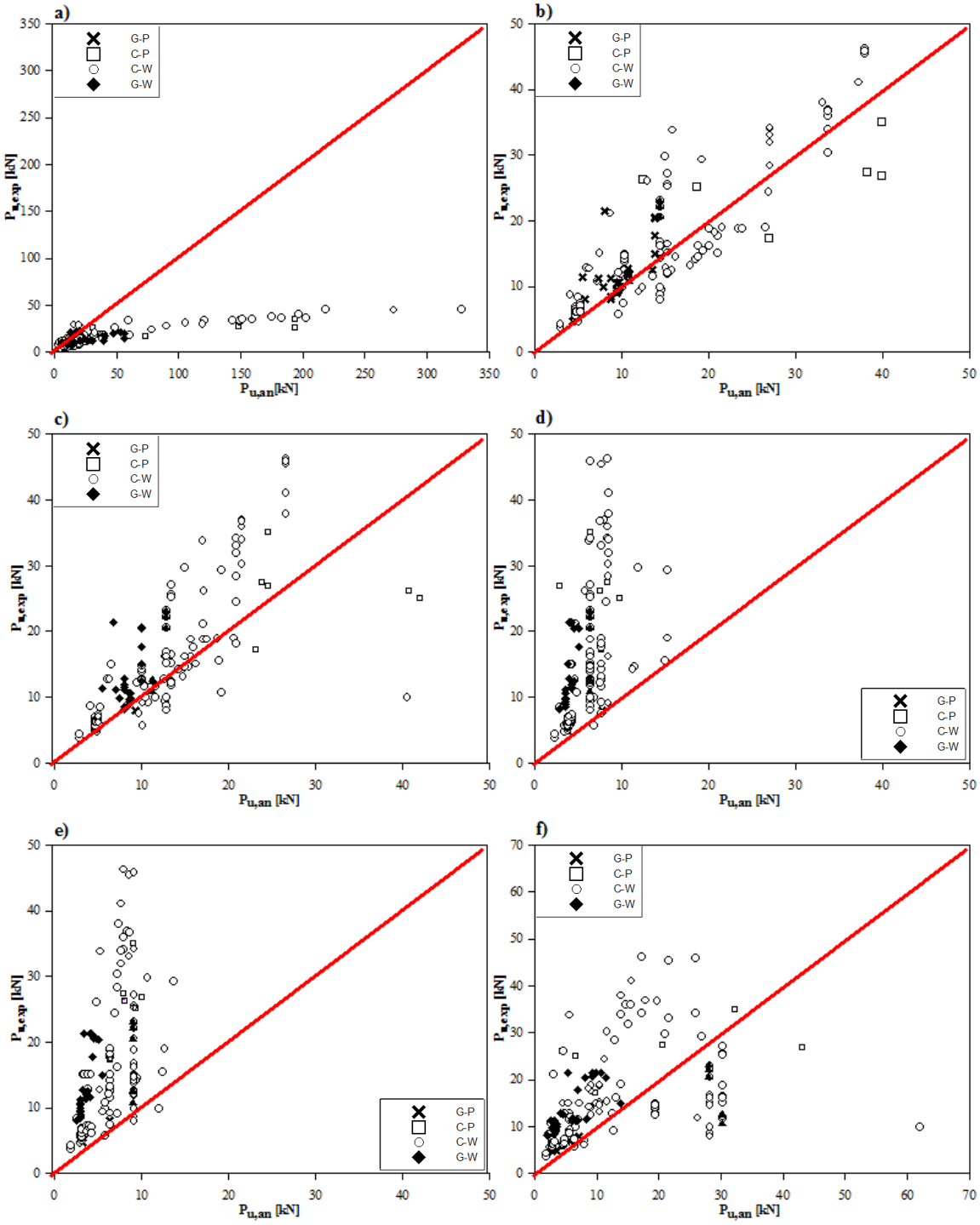

Figure 4.2: Test bond strength vs predicted bond strength using: a)Sato model [62]; b) ISO model [62]; c) Yang et al. model [62]; d) Tanaka model [62]; e) Hiroyuki and Wu model [62]; f) Brosens and van Germet model [62].

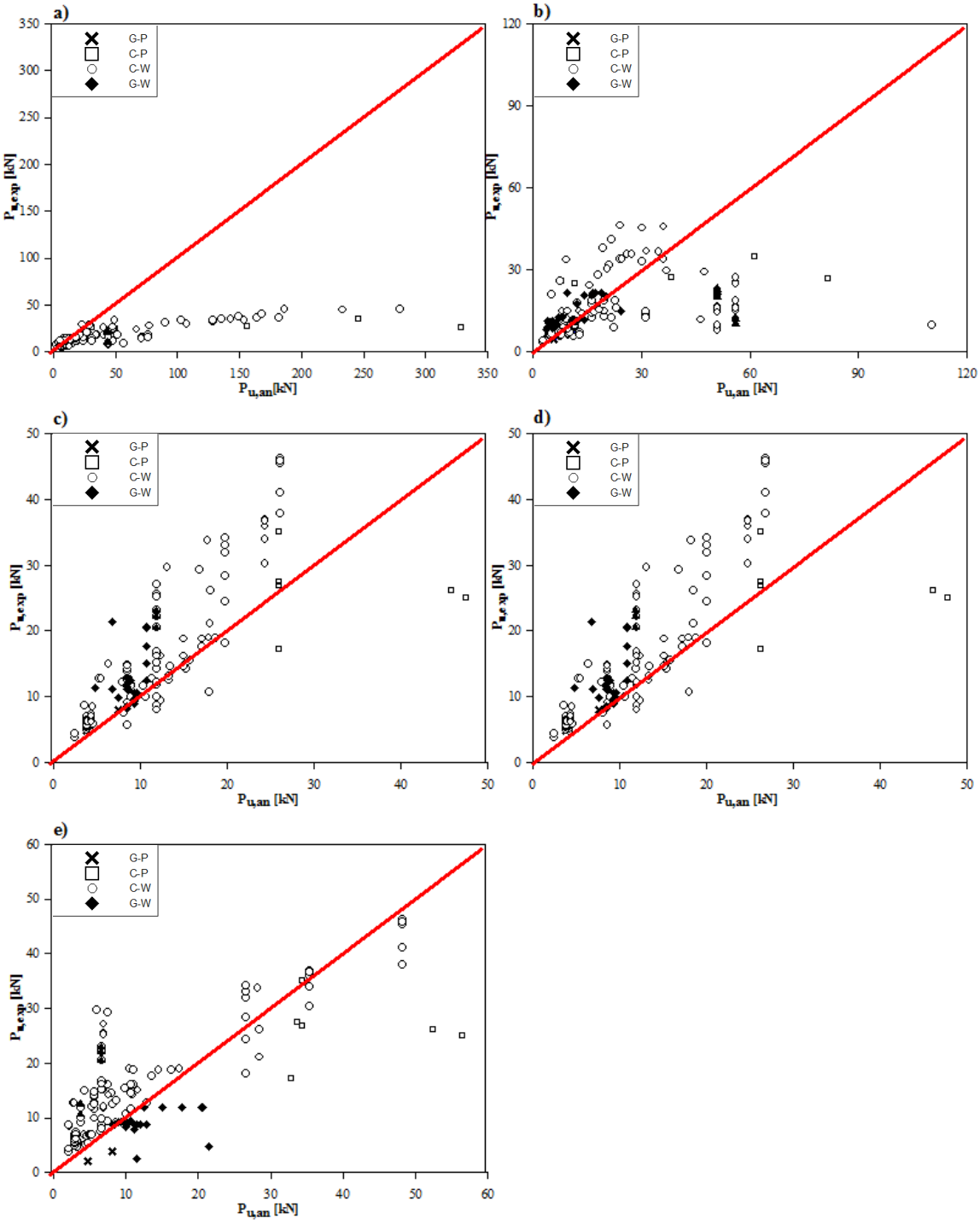

Figure 4.3: Test bond strength vs predicted bond strength using: a)Izumo model [62]; b) Adhikary and Mutsuyoshi model [62]; c) Taljsten model [57]; d) Yuan and Wu model [67]; e) Dai et al. model [67].

	C-W	C-P	G-W	G-P	A-W
No. of tests	131	6	31	2	6
Model 1	30, 5%	50, 0%	16, 1%	100, 0%	0, 0%
Model 2	35, 9%	50, 0%	9, 7%	100, 0%	0, 0%
Model 3	18, 3%	83, 3%	12, 9%	0, 0%	16, 7%
Model 4	70, 2%	66, 7%	54, 8%	100, 0%	16, 7%
Model 5	31, 3%	50, 0%	35, 5%	100, 0%	0, 0%
Model 6	35, 9%	50, 0%	6, 4%	100, 0%	0, 0%
Model 7	78, 6%	100, 0%	71, 0%	100, 0%	0, 0%
Model 8	26, 7%	66, 7%	12, 9%	50, 0%	0, 0%
Model 9	17, 6%	50, 0%	0, 0%	50, 0%	16, 7%
Model 10	2, 3%	0, 0%	0, 0%	0, 0%	0, 0%
Model 11	2, 3%	0, 0%	0, 0%	0, 0%	0, 0%
Model 12	24, 4%	16, 7%	0, 0%	0, 0%	100, 0%
Model 13	62, 6%	100, 0%	-	-	100, 0%
Model 14	48, 1%	66, 7%	16, 1%	100, 0%	100, 0%
Model 15	10, 7%	50, 0%	6, 4%	0, 0%	0, 0%
Model 16	11, 4%	50, 0%	9, 7%	0, 0%	0, 0%
Model 17	8, 4%	83, 3%	9, 7%	0, 0%	0, 0%

Table 4.4: Percent unsafe design.

Chen and Teng [16] modified their expression to propose a model that can be used for ultimate strength design. The modified model gives a bias of $1,70$ and $2,03$ for C-W and G-W data, respectively, which implies that the predicted bond strengths are in the safe range. But it is also interesting to note that the percent unsafe design was only $3,05\%$ and $0,0\%$ for C-W and G-W data, respectively, making it the safest prediction model. This model was designed to calculate bond strength on the basis of ultimate strength design. Hence, high average strength is obtained.

	Chen and Teng	Chen and Teng modified
C-P	3,8% 1,30 53,6% 50,0%	29,0% 1,76 53,6% 16,7%
C-W	12,8% 1,26 33,5% 30,5%	35,7% 1,70 33,5% 3,0%
G-P	13,1% 0,88 3,0% 100,0%	16,6% 1,20 3,0% 0,0%
G-W	25,4% 1,50 36,3% 16,1%	45,0% 2,03 36,3% 0,0%
A-W	35,0% 1,59 17,8% 0,0%	52,0% 2,16 17,8% 0,0%

Table 4.5: Experimental to predicted bond strength ratios (average of difference, bias, COV and percent unsafe predictions); C-P=6 tests, C-W=131 tests, G-P=2 tests, G-W=31 tests, A-W=6 tests.

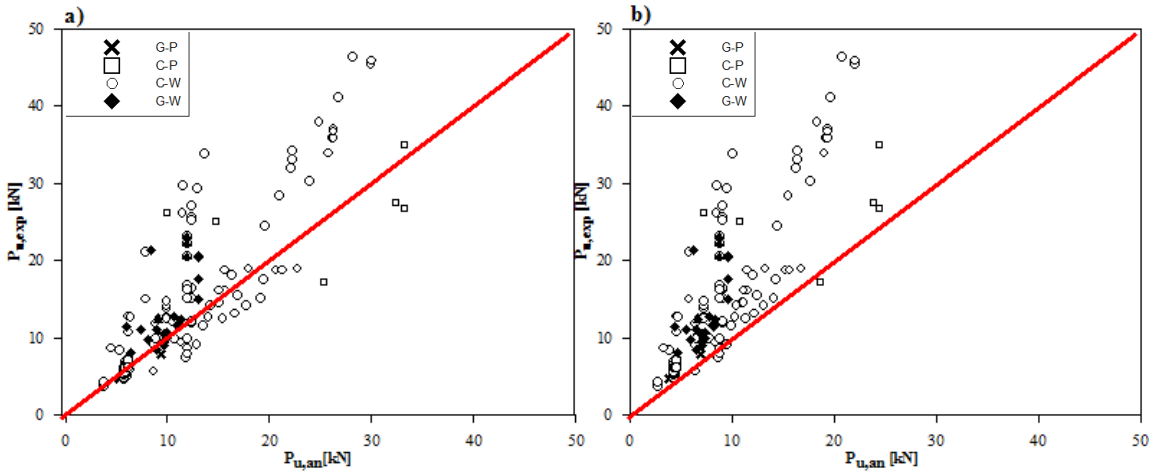

Figure 4.4: Test bond strength vs predicted bond strength using: a)Chen and Teng model [16]; b) Chen and Teng model modified [16].

4.1 Applying the models to flexural test data

The specimens treated in this chapter consist in a concrete prisms bonded with FRP sheets and tested under direct shear. In the previous chapter, beams were tested under four-point bending. It means that the beams were subjected to flexural solicitation. Debonding happens for shear force between beam surface and FRP plate. For this reason it is possible to think to apply these models to the beam specimens.

Considering a generic section in constant moment zone, FRP plate is characterized by a tensile stress. This force is constant between the two applied loads and decreases between an applied load and the end of the plate. It is possible to take into account a part of FRP plate in moment variation zone and this length is the bond length. It was imagined to apply the shear load where starts the constant moment zone. Debonding occurs in the same mode but FRP plate is considered stressing in different way.

The first step is to calculate the moment at load applying section. Then it is possible to define the neutral axis and the stress in the FRP plate as follows:

$$c = \frac{(A'_s + A_s)n_s + A_{frp}n_{frp}}{4b} + \sqrt{\left(\frac{(A'_s + A_s)n_s + A_{frp}n_{frp}}{2b}\right)^2 + \frac{A'_s d' + A_s d + A_{frp}d_{frp}}{b}}$$

$$\varepsilon_{frp} = \frac{M/E_c(d_{frp} - c)}{A_{frp}(d_{frp} - c)d_f n_{frp} + A_s(d - c)dn_s - c^3\frac{b}{3} - (c - d')d'n_s A'_s}$$

The experimental shear force at the plate to cause debonding is equal to

$$P_{u,exp} = \varepsilon_{frp}E_{frp}b_{frp}t_{frp}$$

It was used the database described in the previous chapter. The data were divided in four groups: C-W, C-P, G-W, G-P. There are 59 C-P data, 90 C-W data, 7 G-P data, 7 G-W data.

The first group is composed by the first 9 models; they are developed by Chen and Teng [16], Maeda et al. [62], Khalifa et al. [33], Neubauer and Rostasy [62], Niedemermeier [62], Lu et al. [34], Sato et al. [62], ISO [62] and Yang et al. [62]. The prediction of bond strength is based on the effective bond length L_e.

If L_e is longer than the measured bond length, all models consider the last one to define the bond strength.

The data of G-P and G-W (7 and 7, respectively) are not enough to verify the goodness of the models, the comparison will be done with CFRP data only.

	Mod 1	Mod 2	Mod 3	Mod 4	Mod 5	Mod 6	Mod 7	Mod 8	Mod 9
C-P	22,8%	5,8%	5,6%	7,4%	16,4%	21,2%	312,2%	16,8%	12,0%
	1,42	1,17	1,19	1,03	1,32	1,39	0,33	0,93	1,27
	30,4%	33,8%	35,7%	31,5%	31,5%	30,3%	61,8%	29,8%	36,0%
C-W	7,5%	10,6%	11,0%	26,3%	1,7%	6,8%	404,4%	37,4%	2,0%
	1,21	1,02	1,07	0,89	1,15	1,19	0,30	0,84	1,13
	30,0%	32,6%	38,8%	30,7%	30,7%	28,7%	49,4%	33,0%	35,1%
G-P	0,1%	22,9%	21,2%	35,1%	5,2%	0,5%	197,6%	39,0%	15,4%
	1,14	0,87	0,90	0,84	1,08	1,12	0,39	0,76	0,95
	31,6%	27,9%	33,4%	32,0%	32,0%	29,9%	37,0%	23,7%	33,3%
G-W	2,7%	56,4%	45,5%	42,3%	10,7%	7,0%	85,6%	51,7%	54,2%
	1,02	0,67	0,72	0,73	0,94	0,97	0,61	0,68	0,69
	23,8%	24,7%	22,3%	23,1%	23,1%	23,7%	45,2%	18,6%	27,1%

Table 4.6: Experimental to predicted bond strength ratios (average of difference, bias and COV). Models considering effective bond lenght: Chen and Teng [16], Maeda et al. [62], Khalifa et al. [33], Neubauer and Rostasy [62], Niedemermeier [62], Lu et al. [34], Sato et al. [62], ISO [62] and Yang et al. [62]; C-P=59 tests, C-W=90 tests, G-P=7 tests, G-W=7 tests.

Taking into account C-P data, Sato model [62] and ISO model [62] overestimate the bond strength and bias are 0,33 and 0,95 respectively. The other models propose a bias bigger than one. The biggest is equal to 1,42 proposed by Chen and Teng model [16] which is characterized by COV of 30,4% ; while Lu et al. model [34] is characterized by a bias of 1,39 with COV of 30,3%. Neubauer and Rostasy model [62] proposes the same Lu et al. (2005) COV value but the average experimental to predicted ratio is lower and is equal to 1,03.

Sato model [62] gives the highest coefficient of variation, that is found to be 61,8%. Lu et al. model [34] does a good prediction of shear load failure with a bias of $1{,}_3\,9$ and COV of 30,3%. In this first group the best estimation was given by Iso (2003) with a bias and COV equal to 0,93 and 29,8%, respectively.

Applying Chen and Teng model [16] to C-W data, it gives a lower dispersion with COV equal to 30,0% and a bias of 1,21. The worst prediction is given by Sato model [62] being COV and bias equal to 49,4% and 0,30, respectively. Lu et al. model [34] is characterized by the best prediction, the COV and bias values are found to be 28,7% and 1,19. Like in C-P group, Neubauer and Rostasy model [62] and Niedermeier model [62] give the same coefficient of dispersion equal to 30,75% but the bias values are different being 0,89 and 1,15 for Neubauer and Rostasy model [62] and Niedermeier model [62], respectively. Other two model have a bias

less than the unity, they are Sato model [62] and Iso model [62] with a bias equal to $0,30$ and $0,84$, respectively; the COV in Iso model [62] was found to be $33,0\%$. The bias closer to unity was given by Maeda et al. [62] being $1,02$ with a coefficient of variation of $32,6\%$.

Second group includes models that not consider effective bond length. This group includes: Tanaka model [62], Hiroyuki and Wu model [62], Brosens and van Germet model [62], Izumo model [62], Adhikary and Mutsuyoshi model [62].

This model was calibrated on prism tests were the bond length is not very large. The beam test, considering like a particular concrete prisms, have a bond length which can arrive until $1,5-2m$. Tanaka model [62] gives negative values of shear load failure. Brosens and van Germet model [62] proposed $P_{u,an}$ values too high to be credible. The same thing happens with Adhikary and Mutsuyoshi model [62]. In this case there is a great dispersion of data too, with a COV of $67,4\%$ and $68,0\%$ for C-P and C-W specimens, respectively. Bias is $0,29$ and $0,49$ for C-P data using Adhikary and Mutsuyoshi model [62] and Brosens and van Germet model [62], respectively; and is $0,27$ and $0,46$ for C-W plated beams.

	Mod 10	Mod 11	Mod 12	Mod 13	Mod 14
C-P	$151,6\%$ $0,76$ $1106,95\%$	$42,3\%$ $2,09$ $49,5\%$	$173,8\%$ $0,49$ $64,6\%$	$1022,1\%$ $0,11$ $47,7\%$	$376,4\%$ $0,29$ $67,4\%$
C-W	$160,3\%$ $10,2$ $249,8\%$	$30,5\%$ $1,83$ $47,9\%$	$205,0\%$ $0,46$ $59,5\%$	$1190,4\%$ $0,11$ $54,5\%$	$432,8\%$ $0,27$ $69,5\%$
G-P	$199,5\%$ $0,30$ $334,9\%$	$8,3\%$ $1,19$ $33,9\%$	$310,6\%$ $0,29$ $42,6\%$		$617,9\%$ $0,17$ $42,1\%$
G-W	$1,9\%$ $5,05$ $197,1\%$	$26,3\%$ $0,84$ $27,2\%$	$218,1\%$ $0,33$ $23,0\%$		$442,4\%$ $0,19$ $22,2\%$

Table 4.7: Experimental to predicted bond strength ratios (average of difference, average of experimental to predicted bond strenght ratio and COV). Models not considering effective bond length: Tanaka [62], Hiroyuki and Wu [62], Brosens and van Germet [62], Izumo [62], Adhikary and Mutsuyoshi [62]; C-P=59 tests, C-W=90 tests, G-P=7 tests, G-W=7 tests.

Izumo model [62] overestimates the bond strength of CFRP data. The bias is equal to $0,11$ for both C-P and C-W beam reinforced, with different COV being $47,7\%$ and $54,5\%$,for C-P and C-W data, respectively. Hiroyuki and Wu [62] pre-

	Mod 15	Mod 16	Mod 17
C-P	11,8%	11,5%	16,4%
	1,23	1,23	1,36
	30,6%	30,9%	39,4%
C-W	5,2%	5,5%	0,8%
	1,08	1,08	1,24
	33,2%	33,5%	36,4%
G-P	14,2%	14,5%	21,7%
	0,94	0,94	1,37
	27,5%	27,5%	25,5%
G-W	31,5%	31,5%	41,3%
	0,79	0,79	1,72
	20,5%	20,5%	9,6%

Table 4.8: Experimental to predicted bond strength ratios (average of difference, bias and COV). Models independent of bond length: Taljsten [57], Yuan and Wu [67], Dai et al. [19]; C-P=59 tests, C-W=90 tests, G-P=7 tests, G-W=7 tests.

sented a model which underestimates strength load with the highest bias being 2,09 and 1,83 for C-P and C-W data, respectively. COV is equal to 49,5% for C-P specimens and 47,9% for C-W specimens. Brosens and Van Germet model [62] presents too high dispersion of data, for both C-W and C-P reinforced beams, with COV being 64,6% and 59,5% for C-P and C-W data, respectively; while the bias is equal to 0,49 and 0,46 for beams reinforced with wet lay-up and prepeg carbon sheets, respectively.

The last group includes Taljsten model [57], Yuan and Wu model [67] and Dai et al. model [19]. They are independent on bond length. The variables are the modulus of elasticity and the geometry of FRP and concrete strength. In Taljsten model [57], Yuan and Wu model [67] the prediction depends on specimen geometry also.

Predicted bond strength are overestimated by all three models. Taljsten [57] proposes a bias of 1,23 for C-P plated beams and 1,08 for C-W plated beams and COV equal to 30,6% and 33,2% for C-P and C-W data, respectively. Yuan and Wu model [67] gives similar values obtained by the previous model, with a COV of 30,9% and 33,5% for C-P and C-W specimens, respectively, and the same bias being 1,23 for C-P data and 1,08 for C-W data. Using Dai et al. model [19], COV and bias are found to be 39,4% and 1,36, respectively, for C-P data, 36,4% and 1,24, respectively, for C-W data.

Finally, Sharma et al. model [51] gave not good values of prediction. Taking

into account beams reinforced with wet lay-up carbon sheets, bias is equal to $0,46$ with a COV of $81,4\%$; while C-P group is characterized by a bias and COV equal to $0,68$ and $68,6\%$, respectively.

The comparison of graphical is presented in the order of the previous classification. The graphical data points include all data collected. Each group is represented by a different color.

Chen and Teng model [16] gives a good percent unsafe prediction value of $15,2\%$ for C-P data and $28,9\%$ for C-W data. Another good model is proposed by Lu et al. [34] which presents only $23,7\%$ and $31,1\%$ of values of C-P data and C-W data, respectively, under the red line. To improve C-P percent unsafe data should be used Hiroyuki and Wu model [62] which presents a values of $1,7\%$ unsafe C-P data and $21,1\%$ unsafe data.

Izumo model [62] and Sato model [62] overestimated bond strength and all their predicted bond strength values are unsafe. Adhikary and Mutsuyoshi [62] defines $98,3\%$ unsafe C-P data and $99,0\%$ unsafe C-W data. A similar percentage is given by Brosens and Germert model [62] with $96,6\%$ of unsafe C-P data and $94,4\%$ of unsafe C-W data.

Taljsten [57], Yuan and Wu [67], Maeda et al. [62], Khalifa et al. [33] propose similar percent unsafe values of $33,9\%$, $35,6\%$, $47,5\%$, $42,4\%$, respectively, for C-P data and $47,8\%$, $47,9\%$, $50,0\%$, $47,8\%$, respectively, for C-W data.

	C-W	C-P	G-W	G-P
No. of tests	90	59	7	7
Model 1	28,8%	15,2%	71,4%	42,9%
Model 2	50,0%	47,5%	85,7%	85,7%
Model 3	47,8%	42,4%	85,7%	85,7%
Model 4	61,1%	50,9%	85,7%	71,4%
Model 5	36,7%	32,2%	85,7%	42,9%
Model 6	31,1%	23,7%	85,7%	42,9%
Model 7	100,0%	100,0%	100,0%	100,0%
Model 8	63,3%	64,4%	100,0%	85,7%
Model 9	45,6%	35,6%	85,7%	85,7%
Model 10	55,6%	67,8%	57,1%	57,1%
Model 11	21,1%	1,7%	71,4%	42,9%
Model 12	94,4%	96,6%	100,0%	100,0%
Model 13	100,0%	100,0%	-	-
Model 14	98,9%	98,3%	100,0%	100,0%
Model 15	47,8%	33,9%	85,7%	71,4%
Model 16	47,8%	35,6%	85,7%	71,4%
Model 17	26,7%	27,1%	0,0%	14,3%
Model 18	90,0%	78,0%	100,0%	100,0%

Table 4.9: Percent unsafe design.

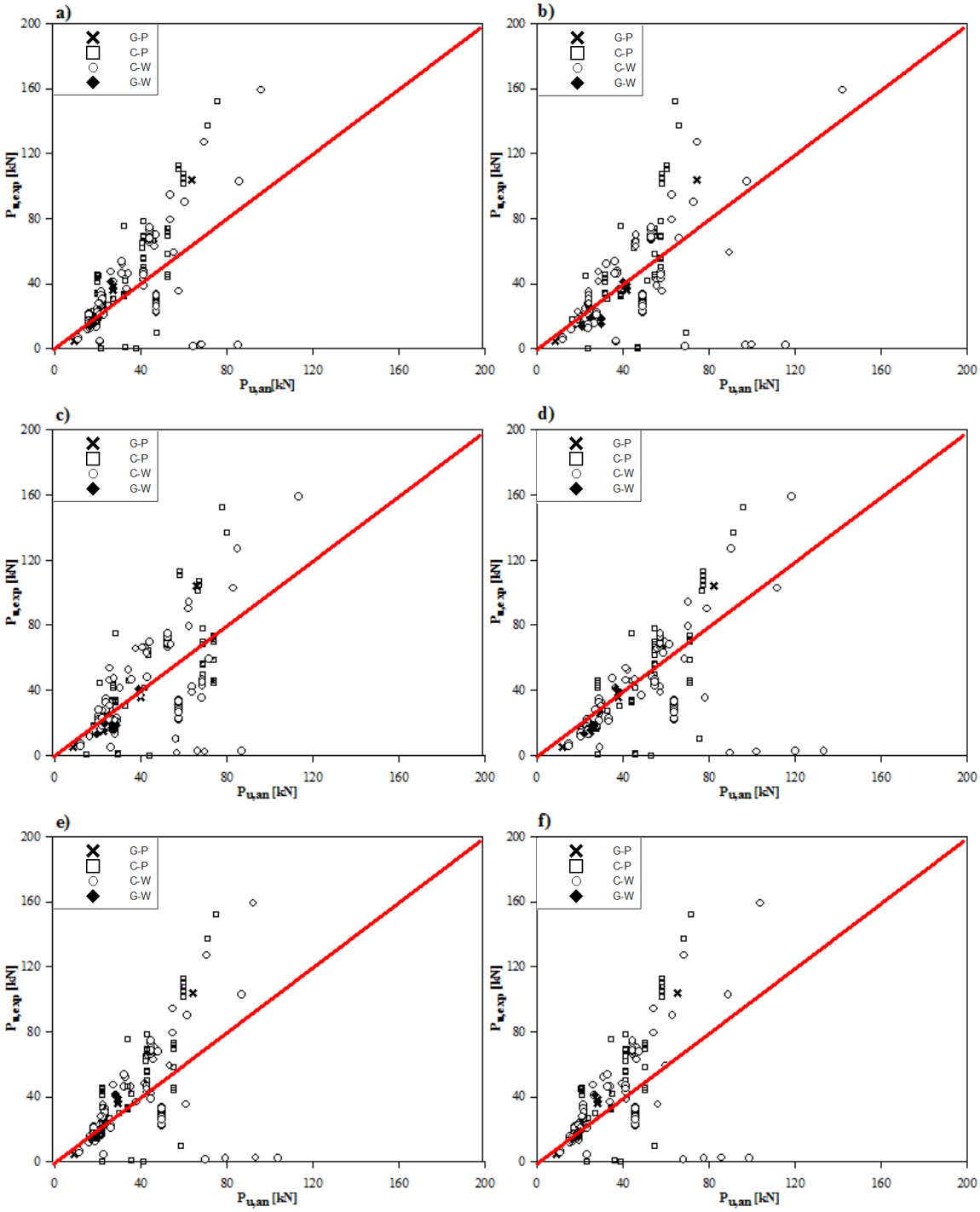

Figure 4.5: Test bond strength vs predicted bond strength using: a)Chen and Teng model [16]; b) Maeda et al. model [62]; c) Khalifa et al. model [33]; d) Neubauer and Rostasy model [62]; e) Niedermeier model [62]; f) Lu et al. model [34].

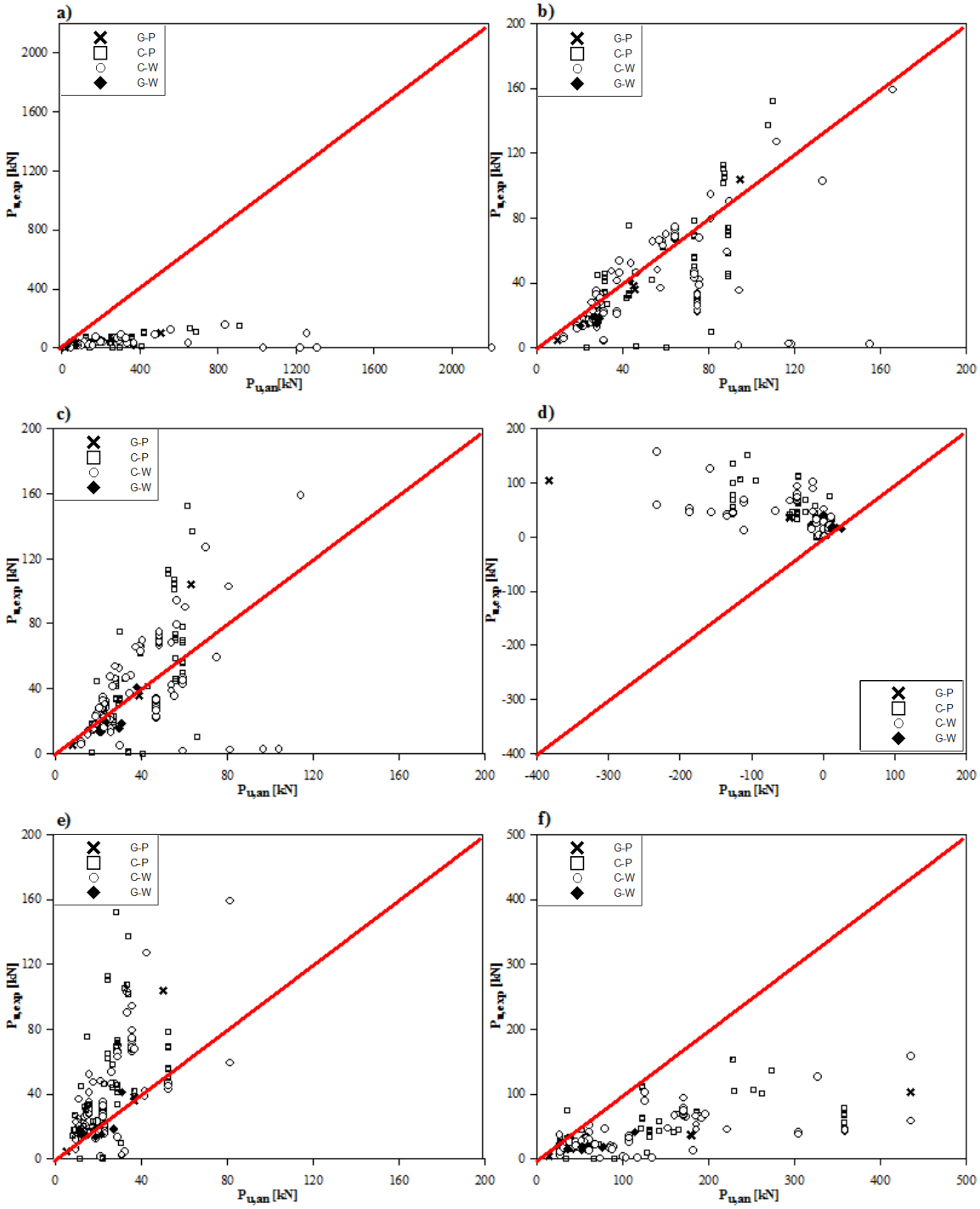

Figure 4.6: Test bond strength vs predicted bond strength using: a)Sato model [62]; b) ISO model [62]; c) Yang et al. model [62]; d) Tanaka model [62]; e) Hiroyuki and Wu model [62]; f) Brosens and van Germet model [62].

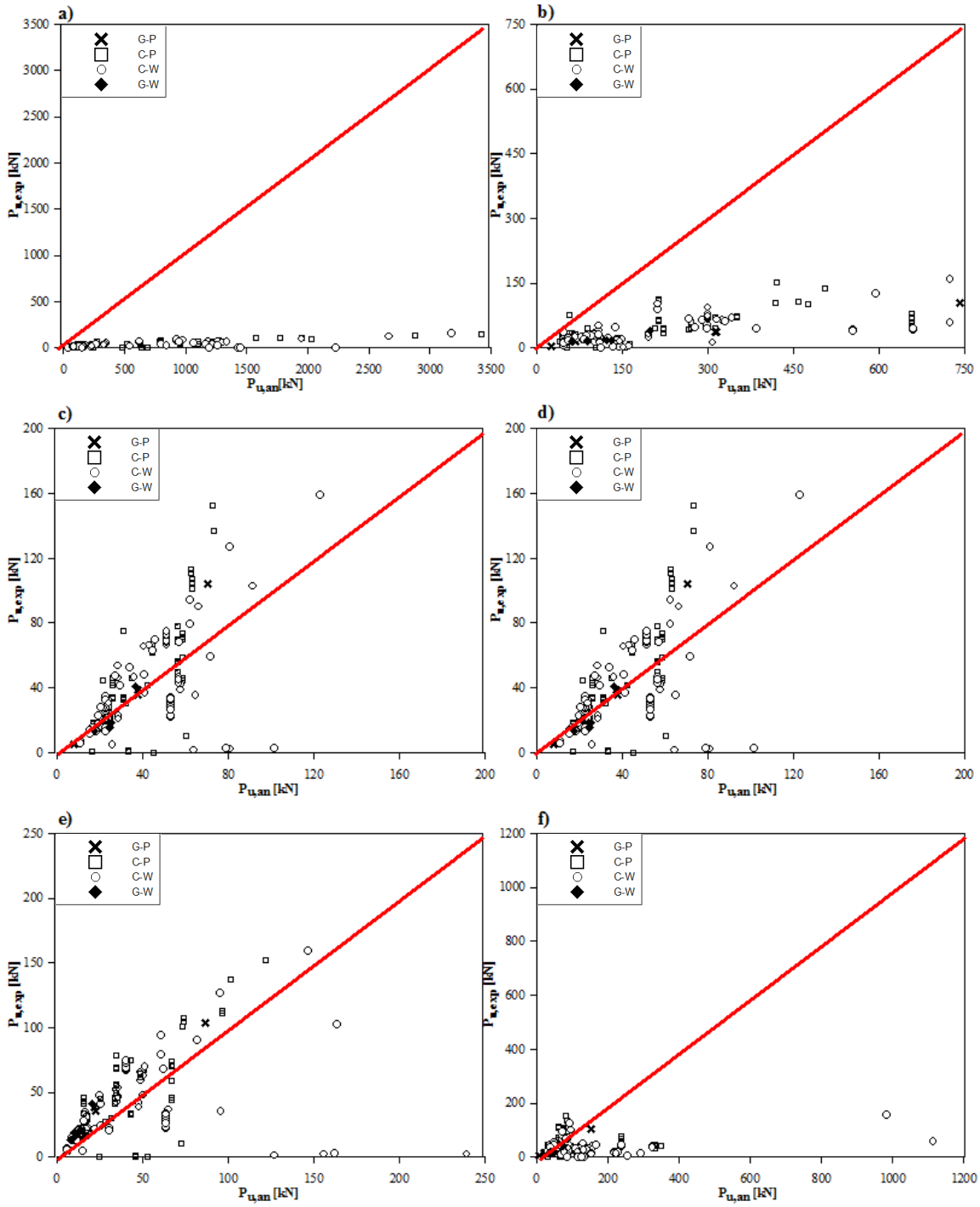

Figure 4.7: Test bond strength vs predicted bond strength using: a)Izumo model [62]; b) Adhikary and Mutsuyoshi model [62]; c) Taljsten model [57]; d) Yuan and Wu model [67]; e) Dai et al. model [19]; f) Sharma et al. model [51].

	Chen and Teng	Chen and Teng modified
C-P	22,83% 1,42 30,4% 15,2%	43,1% 1,92 30,4% 0,0%
C-W	7,5% 1,21 30,0% 28,9%	31,8% 1,65 30,0% 15,6%
G-P	0,1% 1,14 31,6% 42,9%	26,3% 1,55 31,6% 14,3%
G-W	2,7% 1,02 23,7% 71,4%	24,2% 1,38 23,7% 0,0%

Table 4.10: Experimental to predicted bond strength ratios (average of difference, average of experimental to predicted bond strenght ratio, COV and percent unsafe predictions); C-P=59 tests, C-W=90 tests, G-P=7 tests, G-W=7 tests.

Chen and Teng [16] modified their expression to propose a model that can be used for ultimate strength design. The modified model gave a bias 1,92 and 1,65 for C-P and C-W data, respectively, which implies that the predicted bond strengths are moved in the safe range. But it is also interesting to note that the percent unsafe design was only 0,00% and 15,6% for C-P and C-W data, respectively, making it the safest prediction model. This model was designed to calculate bond strength on the basis of ultimate strength design. Hence, high average strength is obtained.

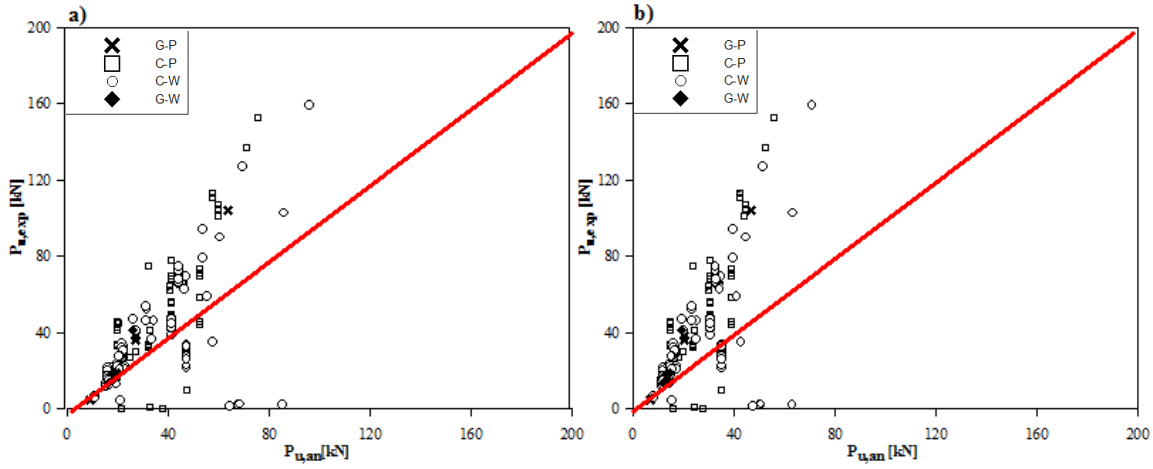

Figure 4.8: Test bond strength vs predicted bond strength using: a)Chen and Teng model [16]; b) Chen and Teng model modified [16].

Chapter 5

Intermediate crack-induced debonding

5.1 Experimental data

An extensive literature survey was conducted by Teng et al. [59] to collect available beam test data. All these test data have been grouped into three sets, the first set for failure by intermediate flexural crack induced debonding in beams (Tables 5.1-5.2-5.3) (8 results), the second set for failure by intermediate flexural-shear crack-induced debonding in beams (Tables 5.4-5.5-5.6) (15 results), and the third set for failure by intermediate flexural crack-induced debonding in cantilever slabs (Tables 5.7-5.8-5.9) (6 results).

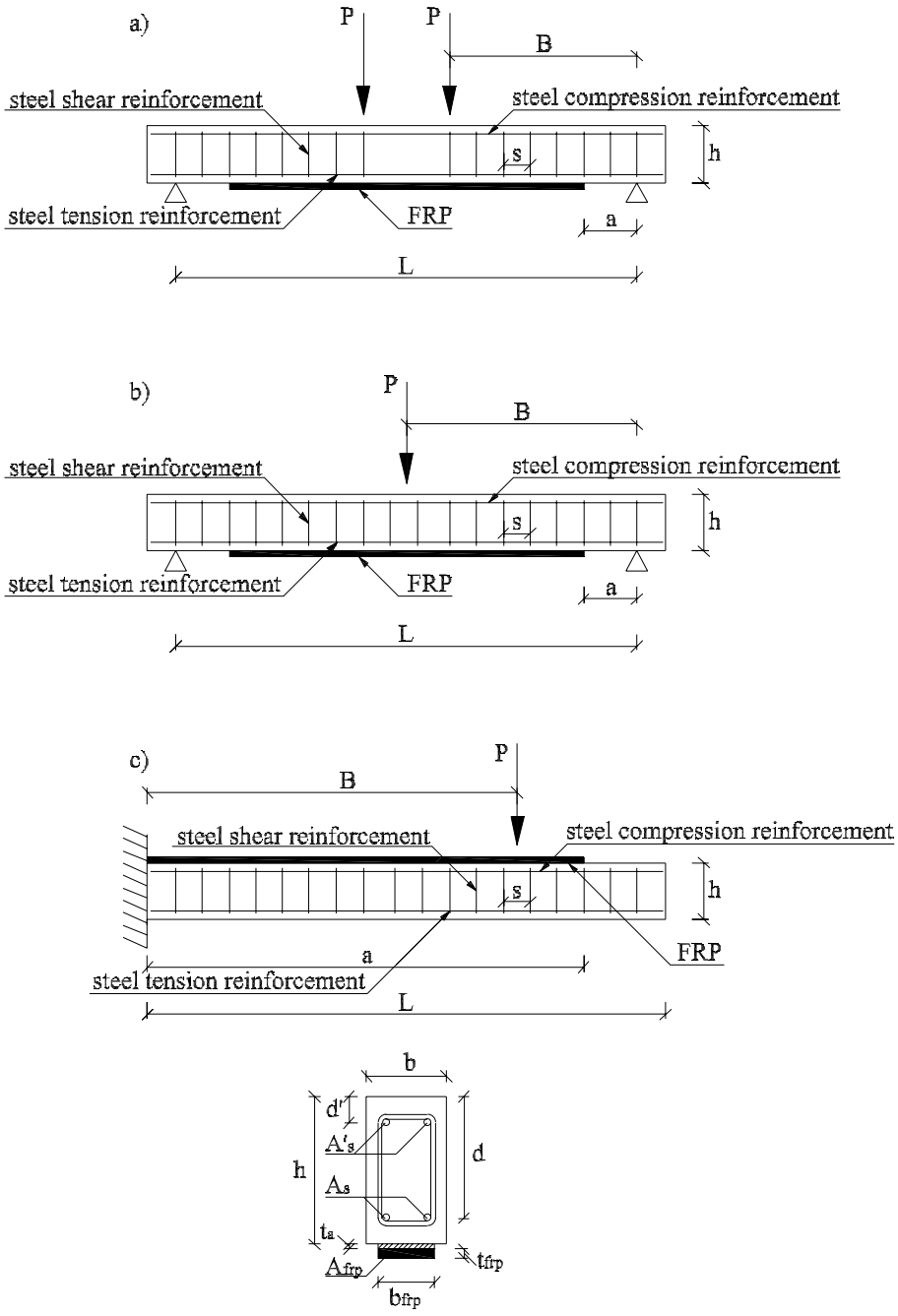

Figure 5.1: Beam test: a)Four point bending test; b)Three point bending test; c)One point bending test.

Table 5.1 and Table 5.4 give the RC beam details where b, h, d, d', f'_c and a denote the width of RC beam, overall depth of RC beam, distance from beam compression face to centroid of steel tension reinforcement, distance from beam compression face to centroid of steel compression reinforcement, concrete cylinder compressive strength and distance from the support to the nearer end of the soffit plate for simply supported beams (tests C4u,1.0 and C5u,1.0 were carried out on cantilever beams subject to a single point load near the free end and, therefore, a denotes the distance from the plate end to the applied load). Table 5.2 and Table 5.5 give the reinforcement properties where E_s and E'_s denote the moduli of elasticity of the steel tension reinforcement and steel compression reinforcement, respectively, while f_y and f'_y denote the corresponding yield strengths, and A_s and A'_s the corresponding cross-sectional areas. Unless otherwise given, the modulus of elasticity of the steel is assumed to be 200GPa. Table 5.3 and Table 5.6 define the adhesive layer, and FRP geometric and material properties where t_a, E_{frp}, f_{frp}, t_{frp}, b_{frp} and a denote the thickness of adhesive layer, modulus of elasticity of FRP, tensile strength of FRP in the main fibre direction, FRP thickness, FRP width.

Some assumptions had to be made about the adhesive thickness: for all wet lay-up plate tests a value of 0.42mm was used based on the authors' own measurements of sample plates of the same kind while a value of 2mm, which is similar to the average adhesive thickness of beams bonded with pultruded plates in a large test database created by Smith and Teng [53], was assumed for tests on beams with pultruded plates conducted by Triantafillou and Plevris [64] . The determination of wet lay-up plate thicknesses is fully explained in Smith and Teng database [53]. Table 5.1 and Table 5.4 also give the details of the loading configuration and the failure load where B, L represent the distance from the support to the nearer applied load, the span of the beam. Details of the failure load are given in Table 5.3 and Table 5.6 where V_{exp} represents the experimental shear force at the plate end at debonding failure.

Table 5.7 and Table 5.8 give the test data for the RC cantilever slabs reported by Yao et al. [66]. The notation used in Table 5.7 and Table 5.8 are the same as to these used in Table 5.1 and Table 5.6.

The beams listed in Tables 5.1-5.2-5.3 and Tables 5.4-5.5-5.6 were strengthened with unstressed and unanchored plates, without any initial loading prior to plating. Tests C4u,1.0 and C5u,1.0 of Garden et al. (1998) were carried out on cantilever beams subject to a single point load near the free end, while all the other test beams of Tables 5.1-5.2-5.3 and Tables 5.4-5.5-5.6 were simply supported subject to three or four point bending. All the cantilever slabs tested by Yao et al. [66] were also strengthened without pre-stressing or end anchoring of the plate at their free end and without initial loading. These slabs were all subjected to a point load near the free end. In all tests included in the present study, a thin layer of concrete

Reference	Beam specimen	b (mm)	h (mm)	d (mm)	d' (mm)	f'_c (MPa)	a (mm)	B (mm)	L (mm)
I)	E	205	455	400	55	35,0	155	1983	4575
II)	C4u,1.0	100	100	84	16	51,2	45	587	587
	C5u,1.0	100	100	84	16	51,2	45	772	772
III)	A1	150	300	250	-	51,7	-	1065	2130
	A2	150	300	250	-	51,7	-	1065	2130
	A7	150	300	250	-	51,7	-	1065	2130
	C1	150	300	250	-	51,7	-	1065	2130
IV)	B2	270	400	341	54	22,6	101	1300	3650

Table 5.1: Teng et al. Database [59]: Intermediate flexural crack-induced debonding in beams. E, B2 were tested under four point bending; C4u,1.0, C5u,1.0 were tested under cantilever beam test; A1, A2, A7, C1 were tested under three point bending. I)Saadatmanesh et al. [46]; II)Gardern et al. [27]; III)Tumialan et al.; IV)Bonacci et al.[8]

remained attached to the FRP upon debonding indicating that the failure occurred in the concrete adjacent to the concrete-to-adhesive interface with the exception of all Tumialan et al. (1999) tests who noted that cover separation occurred at an intermediate crack. At a small distance away from the crack, separation then occurred between the FRP plate and the RC beam that then propagated to the nearer end of the plate.

All beams and slabs were rectangular in cross-section, conventionally reinforced and strengthened with a glass or carbon FRP plate. As the flexural reinforcement was constant over the span for all the test specimens, one of the two sections under the two loads for four point bending tests, the mid-span section for three point bending tests and the section at the support for the cantilever members were taken as the critical sections for predicting the debonding strength in this study.

5.2 Wu and Niu model

By using the concept of fracture mechanics, closed-form analytical equations can be derived for the stress transfer and ultimate load-carrying capacity of the FRP-bonded blocks. It is found that the effective transfer length of FRP sheets may be dependent on the interfacial bond stress-slip relationship, but the ultimate load-carrying capacity is mainly governed by interfacial fracture energy consumed for the debonding failure (or the area beneath the bond stress-slip curve), which was also confirmed in the case of FRP-strengthened beams. Provided that the bond length

Beam specimen	E_s (GPa)	f_y (MPa)	A_s (mm^2)	E'_s (GPa)	f'_y (MPa)	A'_s (mm^2)
E	-	-	-	200	456	253
C4u,1.0	215	350	85	215	350	57
C5u,1.0	215	350	85	215	350	57
A1	207	427	792	-	-	-
A2	207	427	792	-	-	-
A7	207	427	792	-	-	-
C1	207	427	792	-	-	-
B2	201	484	900	199	507	142

Table 5.2: Teng et al. Database [59]: Intermediate flexural crack-induced debonding in beams. E, B2 were tested under four point bending; C4u,1.0, C5u,1.0 were tested under cantilever beam test; A1, A2, A7, C1 were tested under three point bending.

Beam specimen	t_a	Type	E_{frp} (GPa)	f_{frp} (MPa)	t_{frp} (mm)	b_{frp} (mm)	V_{exp} (kN)
E	1,5	G-P	37,23	400	6	152	32,5
C4u,1.0	2,0	C-P	111,0	1414	0,82	67	15,43
C5u,1.0	2,0	C-P	111,0	1414	0,82	67	11,33
A1	-	C-W	230,0	3400	0,165	150	72,8
A2	-	C-W	230,0	3400	0,33	150	84,9
A7	-	C-W	230,0	3400	0,33	75	86,1
C1	-	C-W	230,0	3400	0,165	150	77,2
B2	-	C-W	230,0	3400	0,165	250	148

Table 5.3: Teng et al. Database [59]: Intermediate flexural crack-induced debonding in beams. E, B2 were tested under four point bending; C4u,1.0, C5u,1.0 were tested under cantilever beam test; A1, A2, A7, C1 were tested under three point bending.

Reference	Beam specimen	b (mm)	h (mm)	d (mm)	d' (mm)	f'_c (MPa)	a (mm)	B (mm)	L (mm)
V)	4	76	127	111	-	44,7	75	458	1220
	5	76	127	111	-	44,7	75	458	1220
	6	76	127	111	-	44,7	75	458	1220
	7	76	127	111	-	44,7	75	458	1220
	8	76	127	111	-	44,7	75	458	1220
II)	B3u,1.0	100	100	84	16	43,2	20	340	900
	B4u,1.0	100	100	84	16	43,2	20	340	900
	B5u,1.0	100	100	84	16	43,2	20	400	900
	B1u,4.5	145	230	205	25	37,6	40	1525	4400
VI)	B3	200	150	120	30	49,2	85	750	2100
	B4	200	150	120	30	49,2	85	750	2100
	B5	200	150	120	30	49,2	85	750	2100
	B6	200	150	120	30	49,2	85	750	2100
	B7	200	150	120	30	49,2	85	750	2100
	B8	200	150	120	30	49,2	85	750	2100

Table 5.4: Teng et al. Database [59]: Intermediate flexural crack-induced debonding in beams. All beams were tested under four point bending. II)Gardern et al. [27]; V)Triantafillou et al. [64]; VI)Rahimi et al. [40]

Beam specimen	E_s (GPa)	f_y (MPa)	A_s (mm^2)	E'_s (GPa)	f'_y (MPa)	A'_s (mm^2)
4	200	517	33	-	-	-
5	200	517	33	-	-	-
6	200	517	33	-	-	-
7	200	517	33	-	-	-
8	200	517	33	-	-	-
B3u,1.0	215	350	85	215	350	57
B4u,1.0	215	350	85	215	350	57
B5u,1.0	215	350	85	215	350	57
B1u,4.5	220	556	226	220	556	101
B3	210	460	157	210	460	157
B4	210	460	157	210	460	157
B5	210	460	157	210	460	157
B6	210	460	157	210	460	157
B7	210	460	157	210	460	157
B8	210	460	157	210	460	157

Table 5.5: Teng et al. Database [59]: Intermediate flexural crack-induced debonding in beams. All beams were tested under four point bending.

L is larger than the effective transfer length, the maximum transferable load, P_{max}, in pull-push or pull-pull shear tests can be expressed in a same form irrespective of interfacial constitutive relationship:

$$P_{max} = b_{frp}\sqrt{2G_f E_{frp} t_{frp}} \tag{5.1}$$

where E_{frp}, t_{frp} and b_{frp} are modulus, thickness and width of the FRP, respectively; G_f is the interfacial fracture energy consumed for debonding failure.

Generally, debonding failure occurs in RC beams or one way slabs accompanied with many distributed cracks. The crack spacing and crack width can be further reduced with the presence of FRP. It is found that mean crack spacing ranges from 50mm to 175mm for tension RC members, which may depend on concrete cover, concrete properties, steel and FRP reinforcement, and the loading conditions (preload, tension or bending). Due to the existence of multiple cracks, some interaction between concrete cracking and debonding propagation may complicate the stress transfer mechanisms, which may be far different from the simple bond test. As shown in Fig.5.2, the FRP between cracks is subjected to tension forces at the ends, which is far different from the FRP end or simple bond test only subjected to

Beam specimen	t_a	Type	E_{frp} (GPa)	f_{frp} (MPa)	t_{frp} (mm)	b_{frp} (mm)	V_{exp} (kN)
4	2,0	C-P	186,0	1450	0,65	63,2	14,8
5	2,0	C-P	186,0	1450	0,65	63,2	15,3
6	2,0	C-P	186,0	1450	0,90	63,3	14,0
7	2,0	C-P	186,0	1450	0,90	63,3	12,8
8	2,0	C-P	186,0	1450	1,90	63,9	18,7
B3u,1.0	2,0	C-P	111,0	1414	0,82	67,0	17,0
B4u,1.0	2,0	C-P	111,0	1414	0,82	67,0	17,0
B5u,1.0	2,0	C-P	111,0	1414	0,82	67,0	17,0
B1u,4.5	2,0	C-P	115,0	1284	1,28	90,0	30,0
B3	2,0	C-P	127,0	1532	0,40	150,0	27,6
B4	2,0	C-P	127,0	1532	0,40	150,0	26,3
B5	2,0	C-P	127,0	1532	1,20	150,0	34,9
B6	2,0	C-P	127,0	1532	1,20	150,0	34,8
B7	2,0	G-P	36,0	1074	1,80	150,0	29,6
B8	2,0	G-P	36,0	1074	1,80	150,0	30,8

Table 5.6: Teng et al. Database [59]: Intermediate flexural crack-induced debonding in beams. All beams were tested under four point bending.

Reference	Beam specimen	b (mm)	h (mm)	d (mm)	d' (mm)	f'_c (MPa)	a (mm)	B (mm)	L (mm)
VII)	CP1	301,5	150,5	117,4	-	27,0	100	1000	1100
	CP2	303,6	151,5	111,3	-	37,7	100	1000	1100
	CP3	302,7	150,0	108,2	-	12,6	100	1000	1100
	CP5	304,0	149,0	117,4	-	25,6	100	1000	1100
	CS1	303,0	150,8	115,3	-	21,4	100	1000	1100
	GS1	302,0	151,2	117,9	-	22,6	100	1000	1100

Table 5.7: Teng et al. Database [59]: Intermediate flexural crack-induced debonding in cantilever slabs. All beams were tested under cantilever beam test. VII)Yao et al. [66]

Beam specimen	E_s (GPa)	f_y (MPa)	A_s (mm^2)	E'_s (GPa)	f'_y (MPa)	A'_s (mm^2)
CP1	208	343	314	-	-	-
CP1	208	343	314	-	-	-
CP1	208	343	157	-	-	-
CP1	210	355	157	-	-	-
CP1	208	343	157	-	-	-
CP1	208	343	157	-	-	-

Table 5.8: Teng et al. Database [59]: Intermediate flexural crack-induced debonding in cantilever slabs. All beams were tested under cantilever beam test.

Beam specimen	t_a	Type	E_{frp} (GPa)	f_{frp} (MPa)	t_{frp} (mm)	b_{frp} (mm)	V_{exp} (kN)
CP1	1,0	C-P	165,0	2800	1,2	50,0	19,95
CP2	1,0	C-P	165,0	2800	1,2	50,0	17,58
CP3	1,0	C-P	165,0	2800	1,2	50,0	13,31
CP4	1,0	C-P	165,0	2800	1,2	50,0	10,00
CS1	0,52	C-W	271,0	3720	0,165	50,0	8,51
GS1	0,27	G-W	20,5	269	1,27	89,7	10,00

Table 5.9: Teng et al. Database [59]: Intermediate flexural crack-induced debonding in cantilever slabs. All beams were tested under cantilever beam test.

the tension force at one end. This must be taken into consideration when formulating the predictive model. It should be noticed that the models obtained from simple bond tests may not be directly applicable to the strengthened beam with cracks due to different boundary conditions.

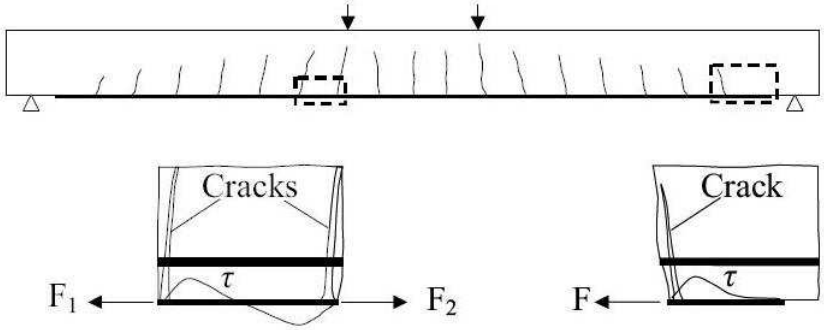

Figure 5.2: Different loading conditions applying on FRP composites in strengthened RC beams (from Wu and Niu [68]).

At the ultimate limit state, cracks are assumed to smear over the whole beam and thus the debonding mechanism can be assumed to be similar to that of unique localized crack pattern. With this consideration, final debonding failure is assumed to be reached once the difference in magnitude between the FRP tensile forces over an equivalent transfer length L_e' (an increased effective transfer length caused by distributed cracks), measured from the maximum moment exceeds the maximum transferable force determined by Eq.5.1. This can be clearly shown in Fig.5.2, where f_1 and f_2 are the FRP tensile forces and L_e is the equivalent transfer length. If no cracking occurs at the section of f_1, this corresponds to the case of a unique localized crack (in this case, f_1 should be very small as compared to f_2, which can be determined by the section analysis).

Seen from Fig.5.2, interfacial fracture energy, G_f is defined as the area beneath the bond stress-slip curve:

$$G_f = \int_0^\infty \tau d\delta \approx 0,644 f_c'^{0,19}$$

And the effective bond length, L_e, required to develop the maximum transferable FRP tensile stress as determined by Eq.5.1, can be approximately computed as:

$$L_e = \frac{0,649\sqrt{E_{frp}t_{frp}}}{f_c'^{0,095}}$$

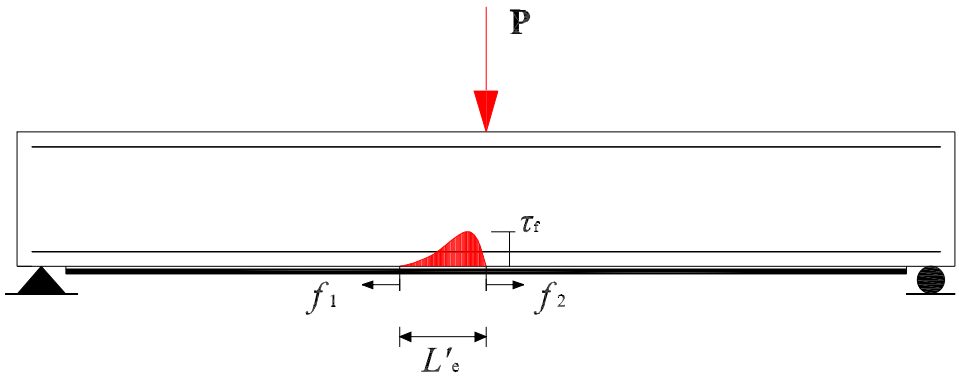

Figure 5.3: Schematic bond-slip relationship.

Then the equivalent transfer length, L'_e can be determined as follows:

$$L'_e = 2L_e = \frac{1,3\sqrt{E_{frp}t_{frp}}}{f_c'^{0,095}}$$

The debonding failure may be predicted by the comparison of the difference between the FRP tensile forces with a spacing of L'_e measured from the maximum moment near the support toward the support and the maximum transferable load in the FRP determined by Eq.5.1, as shown in Fig.5.2. This can be easily implemented by a iterative method: (i) first assumed a load; (ii) compute f_1 and f_2 for the given load using the section analysis; (iii) compare (f_1-f_2) with the maximum transferable FRP tensile force and determine if the debonding failure occurs or not; (iv) if not debonding failure, repeat from step (i) until any failure occurs, debonding failure, FRP rupture or concrete crushing.

To validate the above proposed methodology for predicting the debonding failure load, test data consisting of 180 beams/one-way slabs having a wide range of geometric sizes, reinforcement ratios, material properties (different FRP types), and load configuration are collected for comparison. These specimens were strengthened with unstressed and unanchored FRP, without initial loading prior to the application of the FRP, and failed in debonding caused by intermediate flexural cracks. The Wu and Niu database [68] included: Beber et al. (1999), Benjamin (2005), Bonacci and Maleej (2000), Chan et al. (2001), Chan and Li (2000), Delaney (2006), Gao et

al. (2004), Garden et al. (1998), Kishi et al. (1998), Kishi et al. (2003), Kotynia (2005), Kurihashi et al. (1999), Kurihashi et al. (2000), Leung (2004), Maalej and Leong (2005), Maeda et al. (2001), Matthys (2000), M'Bazaa et al. (1996), Mikami et al. (1999), Niu et al. (2006), Rahimi and Hutchinson (2001), saadatmanesh and Ehsani (1991), Seim et al. (2001), Spadea et al. (2001), Takahashi and Sato (2003), Takeo et al. (1999), Tumialan et al. (1999), Wu et al. (1999), Wu et al. (2000), Yao et al. (2005), Zarniç et al. (1999), Zhang et al. (2005).

5.3 Results of tests

In tests collected for this kind of failure mode, there aren't information about resin elastic modulus. Only in 26 tests were reported the values of thickness of resin (3 beams with G-W reinforced, 1 with G-P, 2 with C-W and 20 beams reinforced with C-P) in any cases there isn't the value of E_a. It is possible to put an arbitrary value taking an average of Young modulus of resin between E_a values present in the other database. Taking into account the 96 beams reinforced with C-W or C-P material the average of E_a is equal to $7389MPa$. Due to few tests for C-W, it is considering CFRP without distinction of applying mode. Casa and Pascual model [13] gives good result for this failure mode. The authors' data was used too. Using their model, the prediction of the load of failure is better than in end debonding analysis. The model gives a bias of $1,80$ and a COV of $22,8\%$.

The model overestimated the real failure load with an average of the difference between the experimental load and the analytical load $V_{exp} - V_{an}$ of $7,9kN$ and a standard variation equal to $3,7kN$.

To compare the goodness of the two models, the Wu and Niu model [68] was applying on the same tests. In this case, the resin characteristic doesn't influence the predictions of failure loads and this could improve the results. The bias is closer to unit than bias calculated with Casas and Pascual model [13] being $0,6$ and it is affected by higher variation equal to $30,8\%$.

Wu and Niu model [68] prediction underestimate the real failure load with an average of the difference $V_{exp} - V_{an}$ equal to $-13kN$ and a standard deviation of $7,0kN$. This model considers the possibility that the beam fails for concrete crushing or for FRP rupture. In 5 of 22 tests taking into account, the model, has predicted a different failure mode (3 FRP rupture and 2 concrete crushing), it was a reduction of number of valid tests.

As explained, the data collected don't present information about the resin's Young's modulus; it was put a value of $7389MPa$ which is the average of values proposed in end debonding database, taking into account C-W and C-P data. This is an arbitrary value, but changing it, the goodness of Casas and Pascual model

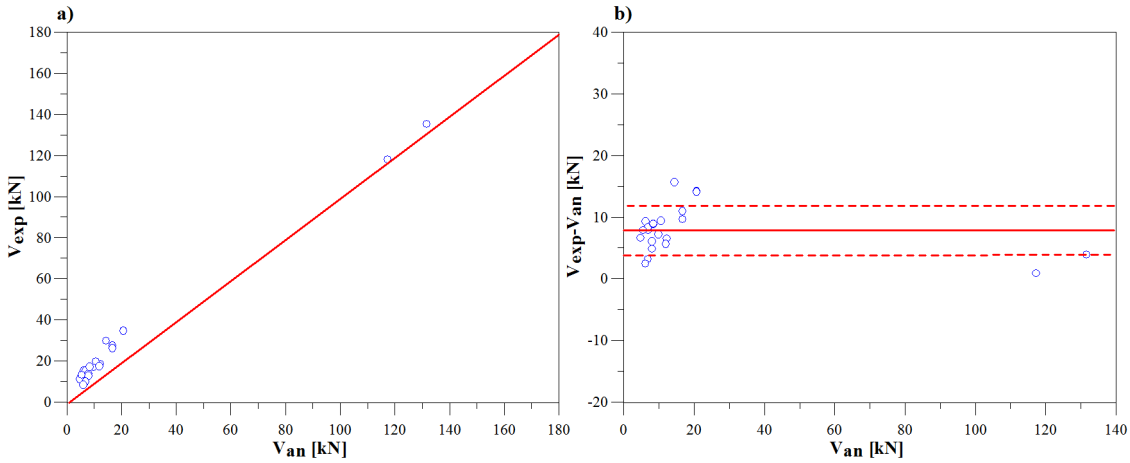

Figure 5.4: a)Test results vs predictions of Casas and Pascual model [13], CFRP (22 valid tests) (;b)Difference between test results and analytical vs predictions of Casas and Pascual model [13] μ=7,9kN, σ=3,7kN.

	Bias	COV	No. of valid tests
E_a=3000MPa	1,67 (7,8%)	21,3% (7,0%)	22
E_a=7389MPa	1,80 (0,0%)	22,8% (0,0%)	22
E_a=12000MPa	1,84 (2,2%)	23,4% (2,6%)	22

Table 5.10: Casas and Pascual model [13] results changing the Young's modulus of the resin. In parenthesis are reported the difference with the used values.

[13] doesn't change significantly. It was considered two values of Young's modulus E_a equal to $3000MPa$ and $12000MPa$; Casas and Pascual model [13] gives the following results:

As shown in Tab.5.10, between the maximum and the minimum values of COV and bias there are a difference of $9,8\%$ and $10,1\%$, respectively.

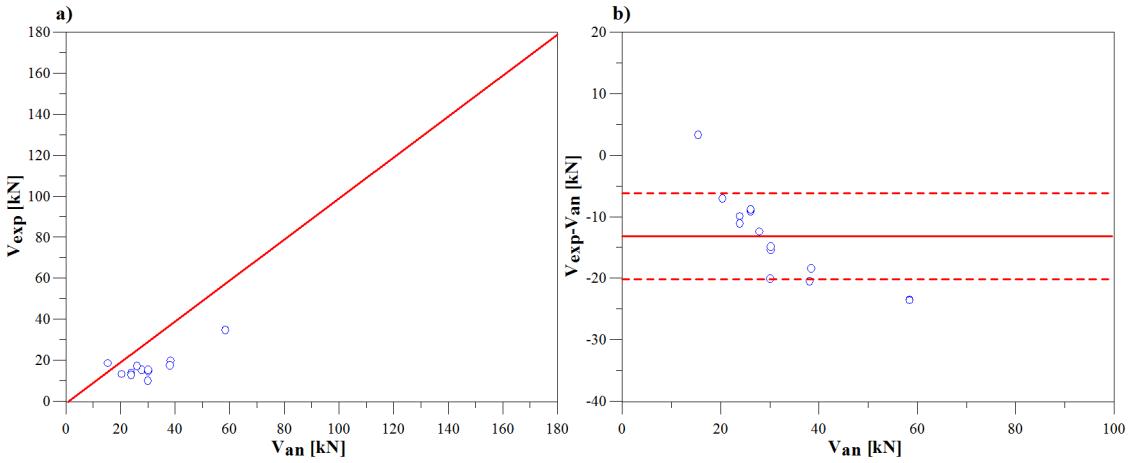

Figure 5.5: a)Test results vs predictions of Wu and Niu model [68], CFRP (22 valid tests) (;b)Difference between test results and analytical vs predictions of Wu and Niu model [68] μ=-13,3kN, σ=7,0kN.

	Bias	COV	No. of valid tests
Casas and Pascual (2007)	1,80	22,83%	22
Wu and Niu (2007)	0,60	30,77%	17

Table 5.11: Comparison between Casas and Pascual model [13] and Wu and Niu model [68] to predict the I-C induced debonding.

Chapter 6

Calibration

6.1 Eurocode specifications

Regarding the verification of concrete bridges in front of ULS, two traffic load models defined in Eurocode 1.3 [10], are referenced. The first model consists on concentrated and distributed loads which includes all effects of cars and lorries. This model is used for global and local verifications. LM1, as seen in Fig.6.1 consists of two partial systems per notational lane:

- One complete double-axle concentrated load (tandem system: TS), each axle having the following weight: $\alpha_Q Q_k$, where α are adjustment factors. Each axle of the tandem comprises two identical wheels, the load per wheel being equal to $0,5\alpha_Q Q_k$. The contact surface of aech wheel is taken as a square of side $0,40m$;
- an UDL system which has the following weight per square meter: $\alpha_q q_k$, where α_q are adjustment factors. these loads is applied only in the unfavourable parts of the influence area, longitudinally and transversally.

On notional lane i, the load magnitudes, depending on the traffic and on classes of road, are referred to as $\alpha_{Qi} Q_{ik}$ and $\alpha_{qi} q_{ik}$; on the remaining areas, as $\alpha_{qr} q_{rk}$

Load model 2 (LM2) is reduced to a single axle load $\beta_Q Q_{ak}$ (with Q_{ak} equal to $400kN$, dynamic amplification included) applied on a specific tyre contact surface. This model covers the dynamic effects of the normal traffic on short bridges.

However, under some circumstances, only one wheel of $200\beta_Q$ (kN) may be taken into account. The value of β_Q is equal to the value of α_{Q1}. The contact surface of the wheel is taken into account as a rectangle of sides $0,35$ and $0,60m$ (Fig.6.1).

Regarding actions on footways, three models of vertical loads, mutually exclusive, should be taken into account:

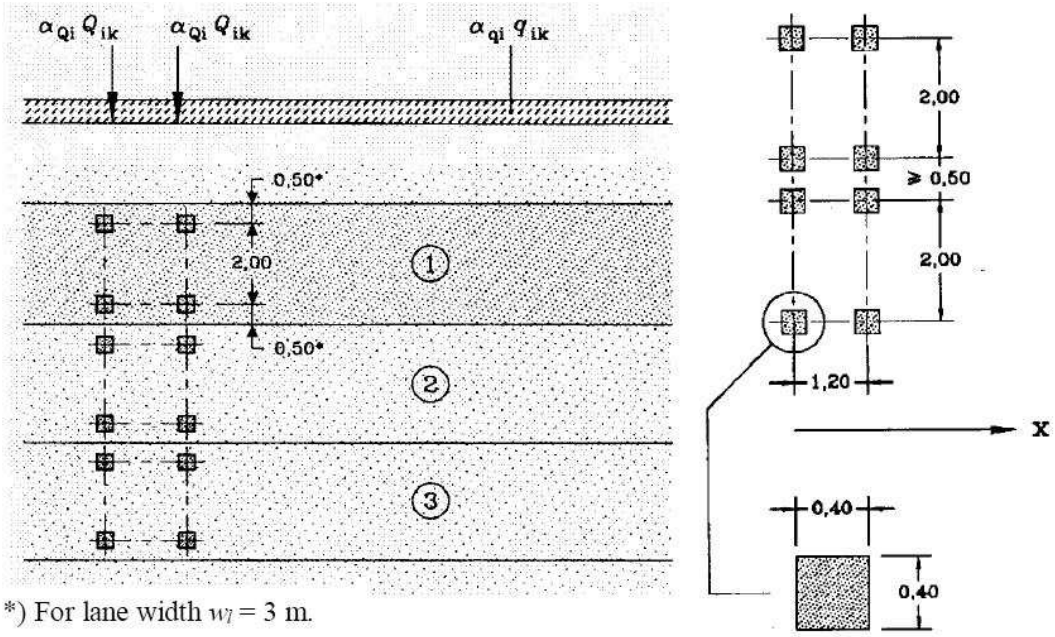

Figure 6.1: Load model 1

- a uniformly distributed load q_{fk};
- a concentrated load Q_{fwk};
- loads representing service vehicles Q_{serv}.

The uniformly distributed load and the concentrated load should be used for road and railway bridges as well as footbridges, where relevant.

The value of uniformly distributed load is

$$q_{fk} = 5kN/m^2$$

If the span is longer than 10m, the value of q_{fk} is (Fig.6.1)

$$2,5kN/m^2 \leq q_{fk} = 2,0 - \frac{120}{L_{sj} + 30} \leq 5,0kN/m^2$$

where L_{sj} is the length of the bridge span.

	Tandem system Q_{ik}[kN]	UDL system q_{ik} [kN/m^2]
Lane number 1	300	9
Lane number 2	200	2,5
Lane number 3	100	2,5
Lane number ≥ 4	0	2,5
Remaining area	0	2,5

Table 6.1: Load model 1.

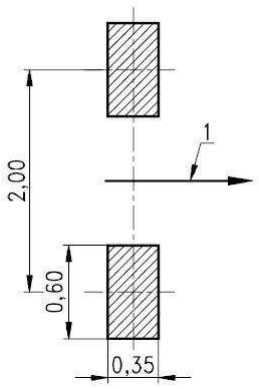

Figure 6.2: Load model 2. 1 represents the bridge longitudinal axis direction.

In road bridge with footway, should be considered a value of 5kN/m^2, as seen in Fig.6.1.

The concentrated load Q_{fwk} is equal to 10 kN and is applied on a surface of side 0,1m. This model should be taken into account in local verification. The loads representing service vehicles Q_{serv} are used only if is requested.

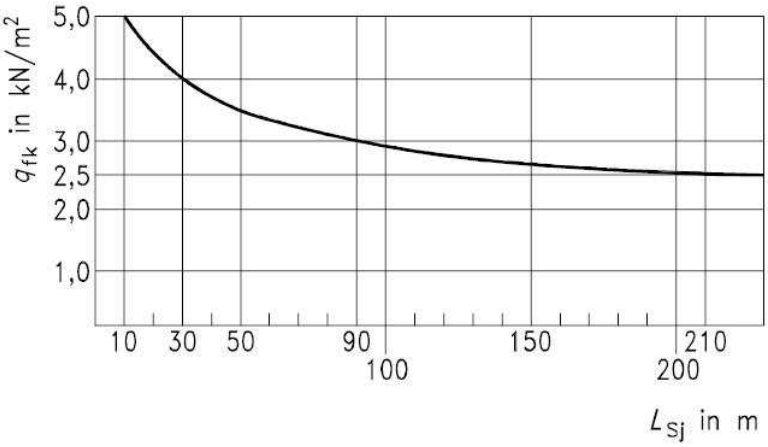

Figure 6.3: Uniformly distributed load q_{fk}.

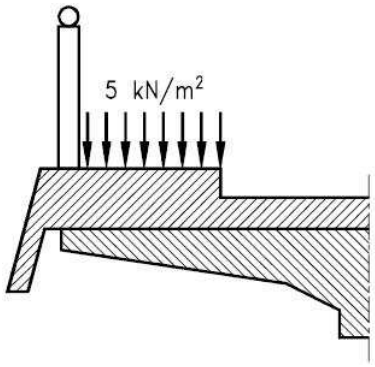

Figure 6.4: Uniformly distributed load q_{fk}.

6.2 Procedure of calibration

An iterative procedure was used to calibrate the resistance factors. Resistance factors were calibrated to meet a target reliability index of 3,5 which corresponds at a time of return of 50 years and a failure probabilities of approximately 1 in 4298.

6.2.1 Uncertainty of load

The first step in calibration is to calculate the dead load and the live load as explained in previous section. The statistical distribution parameters for each of these load components were calculated based on bias factors and COV provided in the Euro Codes. For the dead loads, the bias is equal to 1,05 and the COV is assumed 8%. In this case a normal distribution was used:

$$\overline{D} = \text{bias} \cdot G_{ki}$$
$$\sigma_D = \text{COV} \cdot \overline{D}$$

A Gumbel distribution was used to represent the variability of the live loads. In the previous section, the characteristic value of live loads with a time of return of 50 years was calculated. To determine the mean value, it was used the next formula:

$$\mu_{1000} = \mu_{50} + \frac{\sqrt{6}}{\pi}\sigma \ln(n)$$

where μ_{1000} is the mean value for time of return of 1000 years and it is equal to the characteristic value with time of return of 50 years; σ is the standard deviation and is the same for both 50 years and 1000 years, and μ_{50} is the mean value for time of return of 50 years.

Using Gumbel distribution equation, it was calculated a variable live load value:

$$y = \frac{\ln\left[-\ln\left(f_y\right)\right]}{-\alpha} + u$$

where $\alpha = \sigma/1,282$ and $u = \mu_{50} - \frac{0,5772}{\alpha}$.

The COV is equal to 20%.

Then, when Monte Carlo simulation will be applied, it will be taken values including in these defined ranges.

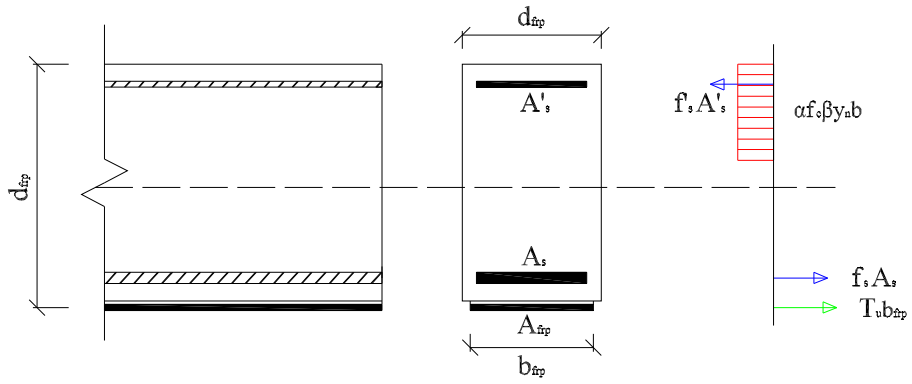

Figure 6.5: Equilibrium in the cross section, ultimate moment resistance.

6.2.2 Uncertainty of ultimate moment resistance and Monte Carlo simulation

To determine the amount of FRP needed to strengthened the bridge, it was calculated the ultimate moment resistance and compared it with the loads applying to the bridge with a Monte Carlo simulation to obtained the probability of failure requested.

The resistance of cross sectional shape was calculated using sectional analysis, wherein following the conventional approach, plane sections were assumed to remain plane under bending, resulting in a linear strain distribution through the depth of the member. It was assumed that the girder would reach its ultimate capacity when either the concrete or FRP reached a limiting strain value; due to the geometry of the sections the FRP strain was the controlling value. It is noted that at this point the steel had usually been strained beyond yield. The neutral axis of the girder was found by enforcing equilibrium and continuity in the presence of the limiting strains.

The ultimate moment resistance took the form, Fig.6.5:

$$M_u = A_s f_s \left(d - \frac{\alpha y_n}{2}\right) + A_{frp} f_{frp} \left(d_{frp} - \frac{\alpha y_n}{2}\right) + A'_s f'_s \left(\frac{\alpha y_n}{2} - d''\right)$$

As it was done with load components, it was taken into account the uncertainty of M_u. As reported in Tab.6.2 the values of bias and COV were calculated in the previous chapter applying Casas et al. model at the database collected, and they depend on the type of material (C-W or C-P).

failure mode	material	Bias	COV
end debonding	C-W	2,21	20,10%
	C-P	2,27	23,38%
IC induced debonding	CFRP	1,80	22,83%

Table 6.2: Values of bias and COV used in the calibration for the three different cases.

To considerate the variability of ultimate moment resistance, it was used a normal distribution:

$$\overline{M_u} = \text{bias} \cdot M_u$$
$$\sigma_{M_u} = \text{COV} \cdot \overline{M_u}$$

Now, it is possible calculate the probability of failure, using a Monte Carlo simulation. Considering the failure equation:

$$Z = M_{u_i} - M_{D_j} - M_{L_k}$$

where M_{u_i}, M_{D_j}, M_{L_k} are casual values of ultimate moment resistance, dead load moment, live load moment, respectively. If $Z < 0$ the structure fails, when $Z > 0$ the structure is safe. The probability of failure is defined as the ratio between the number of fail and the total number of combination considered.

$$P_f = Pr\left[M_u < M_{applied}\right] = \frac{\text{n. of Z} < 0}{\text{n. total of Z}} \tag{6.1}$$

In this case, safety is measured using the reliability index, β, that is obtained by:

$$\beta = \Phi^{-1}\left(-P_f\right)$$

where $\Phi^{-1}\left(\right)$ is the inverse of the cumulative Normal distribution function.
To obtain the value of 3,5 for β, t_{frp} is varied.

6.2.3 Calculation of resistance

The design resistant moment, following the American code procedure, is equal to the nominal moment multiplied by a reduction factor, it takes the form (Fig.6.5):

$$M_{u,d} = \phi \left(A_s f_{s,d} \left(d - \frac{\alpha y_n}{2} \right) + A'_s f'_{s,d} \left(\frac{\alpha y_n}{2} - d'' \right) + T_{u,frp} b_{frp} \left(d_{frp} - \frac{\alpha y_n}{2} \right) \right)$$

where A_s is the area of tension steel, A'_s is the area of compression steel, d is the depth from the compression face to the tension steel, d'' is the depth from the compression face to the compression steel, α is a parameter of stress block, y_n is the depth of the neutral axis, $T_{u,frp}$ is the force per unit of width in the FRP calculated with Casas and Pascual formula [13], b_{frp} is the width of FRP and d_{frp} is the total depth of the section. f_s is the tensile strength of the tension steel and f'_s is the tensile strength of the compression steel.

The nominal moment required is equal to the sum of dead load and live load multiplied by the load safety factors, as follows:

$$M_{nom.req.} = \gamma_{Gi} \cdot M_{G_{ki}} + \gamma_{Qi} \cdot M_{Q_{ki}}$$

where $M_{G_{ki}}$ and $M_{Q_{ki}}$ are the values of the moment applying the characteristic dead load and the characteristic live load, respectively.

The safety condition, following the American code procedure, is:

$$\phi M_u \geq M_{nom.req.} \tag{6.2}$$

ϕ is the resistance factor applied to the total resistance.

With the Mont Carlo simulation it was obtained the thickness of FRP sheet, to satisfy the safety equation (Eq.6.2.3), the resistant factor is varied.

6.3 Description of the bridges take in exam

A set of bridges covering over the most common structural schemes found in Spanish roadway net, was first defined. It included both, continuous and simply supported bridges. Their span lengths were also chosen to represent the most characteristic situations, and their cross sectional shapes were determined as a function of these lengths, according to common bridge engineering practice.

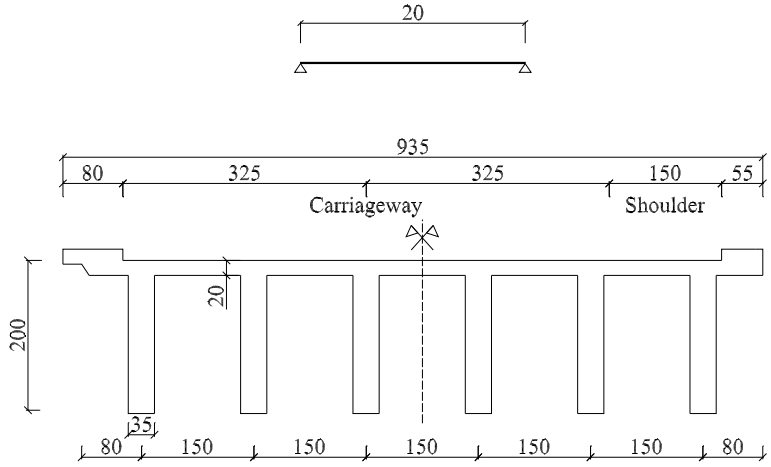

Figure 6.6: B20RC bridge.

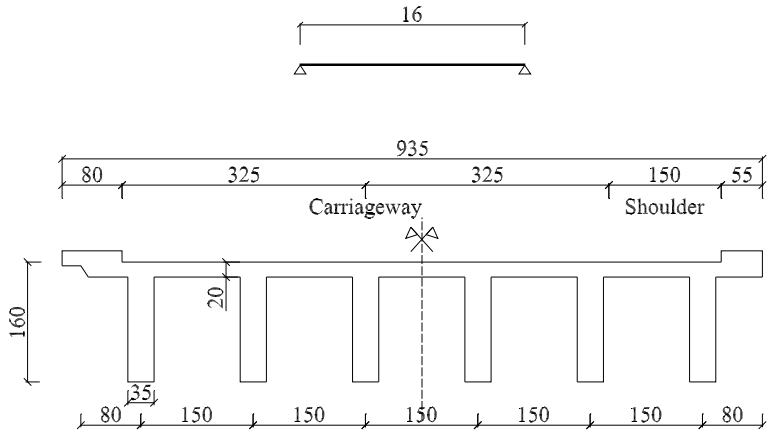

Figure 6.7: B16RC bridge.

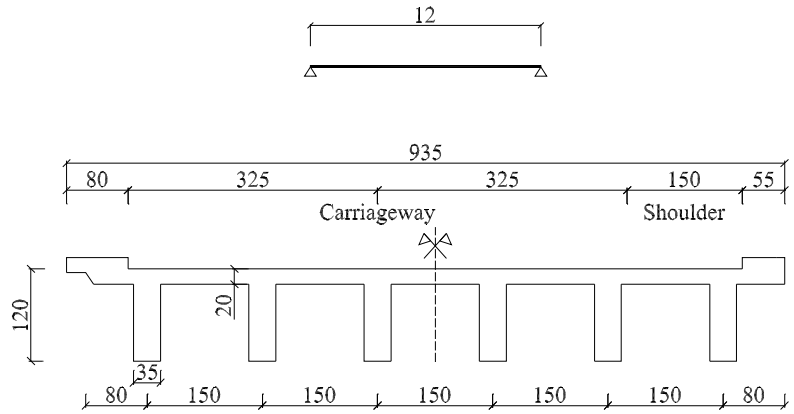

Figure 6.8: B12RC bridge.

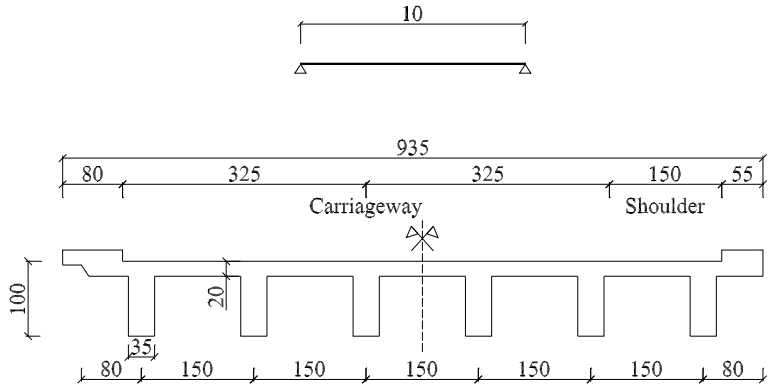

Figure 6.9: B10RC bridge.

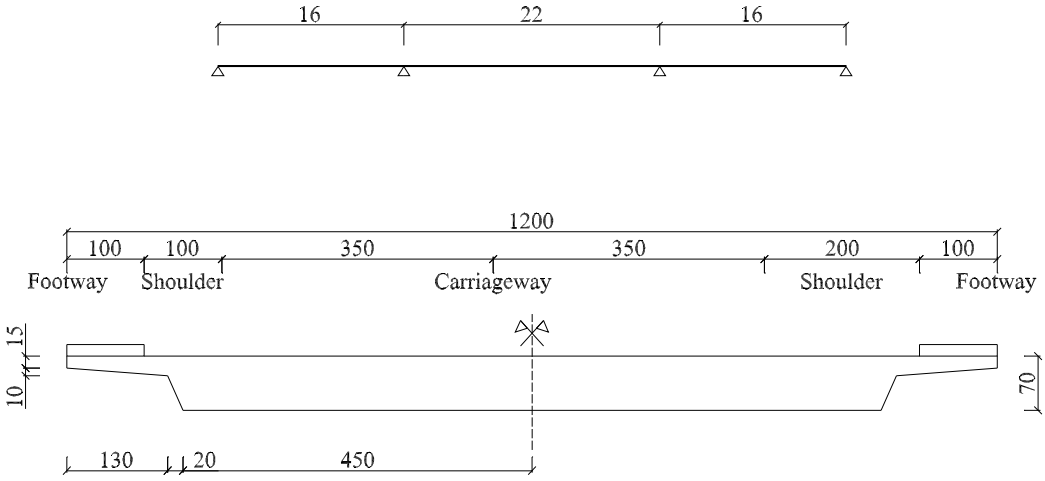

Figure 6.10: S1622PT bridge.

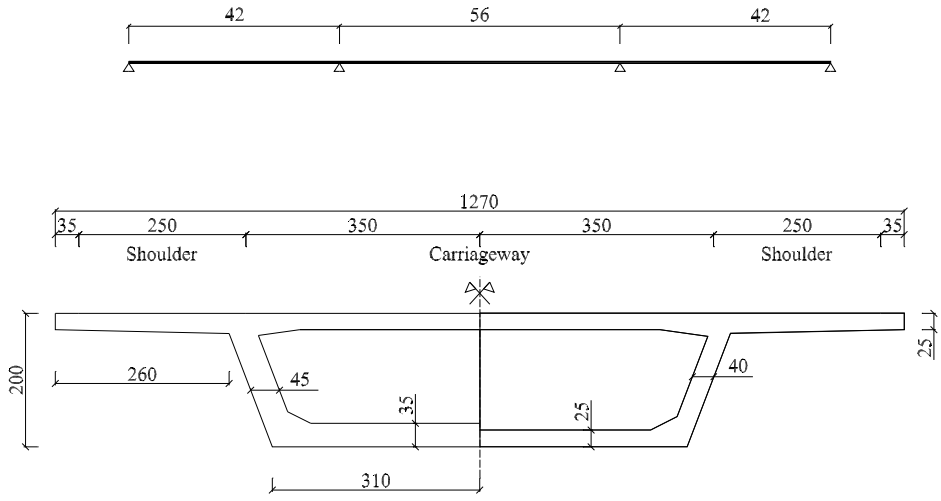

Figure 6.11: C4256PT bridge.

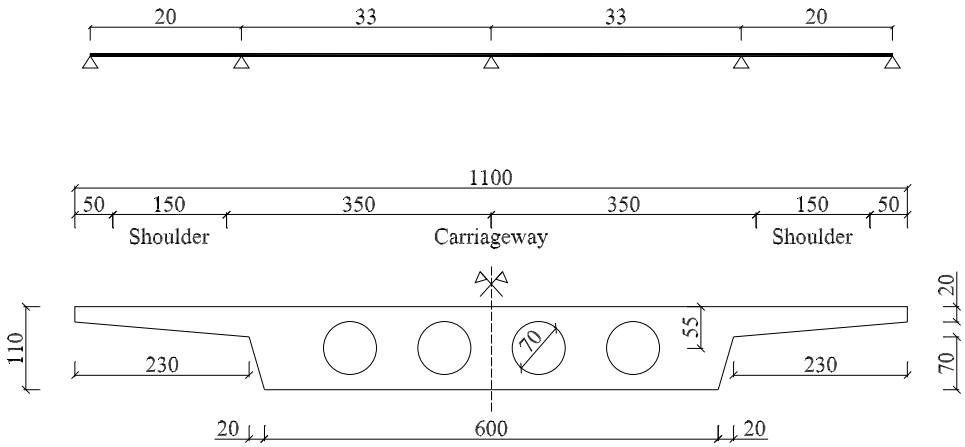

Figure 6.12: S2033PT bridge.

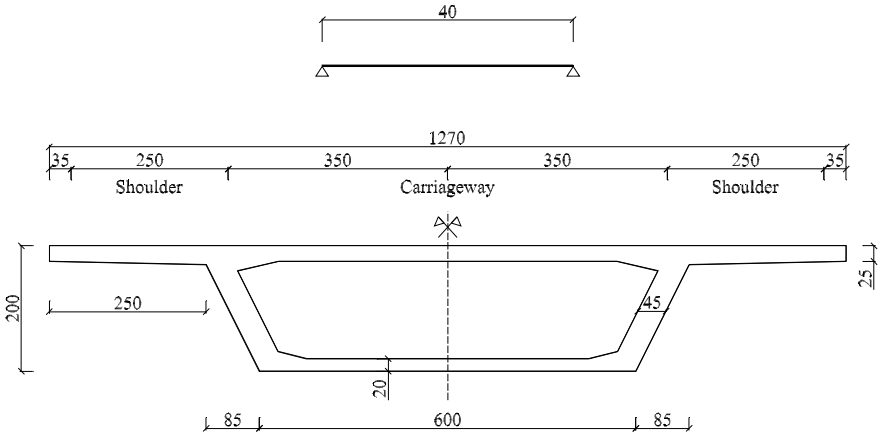

Figure 6.13: G40PT bridge.

Bridge	DL (kNm)	LL (kNm)	P_∞ (kN)	Ap (cm^2)	Ar (cm^2)
B10RC	2340	2993	-	-	436
B12RC	3369	3711	-	-	436
B16RC	5990	5264	-	-	544
B20RC	9360	6975	-	-	544
S1622PT	4526	6197	16313	134,4	549
S2033PT	9532	10138	23861	201,6	603
C4256PT	22563	23719	29684	268,8	935
G40PT	34830	21900	32962	208,0	935

Table 6.3: Bridge characteristics.

To simplify the references to the bridges, the special notation will be used. The first character, indicates the shape of the cross-section of the bridge. There will be four possibilities: B, which means beam, S, which means slab, G which means box-girder, and C, which means box-girder built by the balanced cantilever method.

The four following characters, in continuous bridges, indicate the lengths of the two first spans. In simply supported bridges, only two digits are needed for showing the length of the span of the referred bridge.

Last two characters indicate the reinforced concrete bridge (RC) and postensioned concrete bridge (PT).

In continuous bridges the section of the main span has been studied. In the simply bridges the section at midspan has been analyzed.

The columns in Tab.6.3 refer to: DL, dead loads; LL, live loads; P_∞, prestressing force after all loses; Ap, area of prestressing steel; Ar, area of reinforcing steel.

The concrete used is different for RC and PT bridges; reinforced concrete bridges are characterized by a concrete strength, f_{ck}, of 20MPa; while in postensioned concrete bridges, the concrete is stronger being 35MPa the characteristic compressive strength. The same steel reinforcement was used in both typologies of bridges, RC and PT, with yielding stress equal to 216MPa. To prestress the concrete, an harmonic steel with nominal yielding stress, f_{py}, equal to 1500MPa and elastic modulus of 190GPa, was used.

To apply the CFRP material, will be used the same resin in all cases; the elastic modulus is equal to 2305MPa (G_a=835, ν=0,38) and the thickness is equal to 0,52mm. The carbon sheets have a strength of 1892MPa and Young's modulus equal to 105GPa.

6.4 Results

The first step of calibration is calculate for each bridge the CFRP area to obtain a reliability index β equal to 3,5. Are considered 262116 trials to calculate the probability of failure.

Where it is possible, it is preferred to choose a larger FRP sheet, than a thicker carbon reinforcement. As explained previous, applying Casas and Pascual model [13], increasing the thickness of polymer material, decreases the ultimate deformation and, consequently, the ultimate resistance moment. In reinforced concrete bridges the FRP is applied on all beams with a width equal to the beam's width (350mm). In the box-girders bridges, the FRP will be applied under the connection between the top and bottom of the section, were are set the prestressing cable. In slab bridges, the FRP could be applying on all bottom surface.

In many cases, the index of reliabity without FRP is higher than 3,5 yet. But is more interesting to consider a variable percentage of corrosion in both reinforcing steel and prestressing steel. An index of corrosion, i_{corr}, bigger than zero, represents the real condition of some structure when need a reinforcement, many years after their construction.

The resistance factors for each level of relative steel loss are summarized in Tab.6.4, Tab.6.5 and Tab.6.6; in the first two tables is represented the phenomenon of end debonding, while in the third table is calculated the resistant factor for IC induced debonding phenomenon.

It not possible to consider for all bridges the same percentage of steel corrosion; it depends on the typology of bridge, the kind of material used to reinforce and the mode of failure studied. In prestressed concrete the corrosion affected both the reinforcing and prestressing steel. It was demonstrated that the value of ϕ is independent from the variation of i_{corr}.

Comparing Tab.6.4 with Tab.6.5, the percentages of corrosion are lower in the section reinforced with C-P material, these means that applying *in situ* the reinforcement improves the strengthened of the structure. To obtain the same value of reliability factors, it has to applying more FRP or reduce the amount of steel loss.

As represented in Tab.6.4, the amounts of relative steel loss is higher in prestressing concrete bridges than in reinforced concrete bridges; this is due to the different purpose in initial design: the calibration is done in ULS while the design of prestressing bridge is done to satisfy the SLS of decompression. In RC bridges the maximum value of i_{corr} is $0,20$ while in PT bridges the percentage of steel loss has a minimum of $0,30$ for S1622PT bridge until a maximum of $0,55$ for C4256PT and S2033PT bridges. The area of FRP increases with reduction of steel and in order to not increase the thickness of FRP, it was preferred to increase its width. G40PT and C4256PT are characterized by the bigger FRP area needed to have a

Bridge	i_{corr}	b_{frp} (mm)	t_{frp} (mm)	ϕ
B12RC	0,10	2100	0,02	0,990
	0,15	2100	0,51	0,991
	0,20	2100	1,69	1,000
B16RC	0,15	2100	0,21	0,970
	0,20	2100	1,51	0,970
	0,25	2100	4,0	0,970
B20RC	0,00	2100	0,36	0,946
	0,10	2100	4,74	0,947
S1622PT	0,30	2000	0,95	0,948
	0,35	3000	3,97	0,949
	0,40	5000	4,23	0,949
S2033PT	0,40	2000	0,21	0,920
	0,45	2500	5,01	0,921
	0,50	4000	6,61	0,923
	0,55	6000	6,54	0,919
G40PT	0,40	1000	1,64	0,915
	0,45	5000	5,05	0,914
	0,50	6000	8,46	0,905
C4256PT	0,45	1000	0,22	0,956
	0,50	3000	3,15	0,955
	0,55	6000	3,89	0,954

Table 6.4: Summary of resistance factors for different amounts of relative steel loss. Applying wet lay-up carbon sheets, taking into account end debonding phenomenon; reliability factor, β, equal to 3,5.

Bridge	i_{corr}	b_{frp} (mm)	t_{frp} (mm)	ϕ
B10RC	0,00	2100	0,26	0,801
	0,10	2100	3,03	0,800
	0,15	2100	5,43	0,801
B16RC	0,00	2100	5,83	0,743
S1622PT	0,10	2000	0,20	0,740
	0,15	2000	5,63	0,743
	0,20	5000	3,13	0,737
	0,25	6000	4,77	0,741
S2033PT	0,20	2000	1,12	0,685
	0,25	3500	4,74	0,680
	0,30	5000	6,61	0,677
	0,35	6000	8,56	0,678
G40PT	0,15	4000	2,73	0,628
	0,20	6000	5,78	0,626
C4256PT	0,30	1000	2,65	0,740
	0,35	3000	4,82	0,739
	0,40	5000	6,86	0,739
	0,45	6100	10,4	0,739

Table 6.5: Summary of resistance factors for different amounts of relative steel loss. Applying prepeg carbon plates, taking into account end debonding phenomenon; reliability factor, β, equal to 3,5.

Bridge	i_{corr}	b_{frp} (mm)	t_{frp} (mm)	ϕ
B10RC	0,00	2100	0,19	0,654
	0,10	2100	3,80	0,654
S1622PT	0,00	9000	4,27	0,572
S2033PT	0,00	3000	0,15	0,559
	0,10	6000	3,95	0,554
	0,15	6000	7,21	0,557
G40PT	0,00	6000	5,88	0,513
C4256PT	0,15	2000	1,81	0,605
	0,20	4000	3,65	0,604
	0,25	6000	5,62	0,604

Table 6.6: Summary of resistance factors for different amounts of relative steel loss. Applying carbon sheets, taking into account IC induced debonding; reliability factor, β, equal to 3,5.

reliability index equal to $3,5$; these two bridges are characterized by the highest applied moments due to their span of 40m and 56m.

In Tab.6.4 are reported different value of safety factors with a maximum of $1,00$ and a minimum equal to $0,914$. To determine a safety factor, it was decided to divide the two typologies of bridge to define different value of ϕ for each other. In both of case was token into account the maximum value founded. For reinforced concrete bridges, ϕ is equal to 1, while for postensioned concrete bridges, ϕ is equal to $0,95$. Considering an unique group could be more conservative for reinforced concrete bridge typology. Moreover, the percentage of steel corrosion is significantly different between RC bridges (0%-25%) and PT bridges (30%-55%). The choice of the highest values for ϕ is due to the high value of bias determined for the model used. In this case, bridges reinforced with C-W sheets, the bias is equal to $2,21$ this means that there is a "safety factor" in the moment resistant formula, yet. Due to the bias, it makes possible to consider a lower value of ϕ.

In Tab.6.5 are represented the calibration done for the bridges reinforced applying prepeg carbon plates. Only B10RC and B16RC can be reinforced with C-P plates, but are still sufficient to divided the calibration of ϕ in two group. For RC bridges it was proposed the value of $0,8$ for the safety factor, while a value of $0,7$ was proposed for PT bridge typologies.

To prevent the end-debonding failure mode, it was determined four different values. There is a significant difference between C-W and C-P reinforced and it is correct maintain the two groups. If it wants simplify the design recommendation it could be eliminated the difference between reinforced and postensioned concrete bridges, considering an unique group with all bridges, it will be obtain a values more conservative for reinforced concrete bridge typology, being ϕ equal to $0,95$ and $0,7$ for bridges strengthened with C-W and C-P sheets, respectively.

In Tab.6.6 are reported the values of ϕ to prevent the intermediate crack induced debonding. Only B10RC bridge can be reinforced with CFRP sheets in reinforced concrete bridge group. For this reason it was proposed an unique safety factor value for postensioned bridges, equal to $0,6$. If it wants include the reinforced concrete bridge, it could be proposed a value of $0,65$. In according to the codes, the phenomenon of IC induced debonding is more restricted of end debonding failure mode.

In Tab.6.7 are reported the values of safety factors proposed by this work.

The Atadero et al. [4, 5] works, confirms the goodness of this calibration. They took into account some girder bridges (only reinforced concrete bridge typology) with a maximum span of 22,9m considering different level of corrosion (from 5% to 30%) and three target reliabilities (β equal to 2,5, 3,0 and 3,5). To define the maximum tensile force in the FRP, Atadero et al. used Wu and Niu model [68] without any distinction between wet lay-up and prepeg applying system. The value

Mode of failure	Type of FRP	ϕ_{RC}	ϕ_{PT}
End debonding	C-W	1,00	0,95
	C-P	0,80	0,70
I-C induced debonding	CFRP	0,60	0,60

Table 6.7: Summary of proposed safety factors; reliability factor, β, equal to 3,5. ϕ_{RC} safety factor for reinforced concrete bridge, ϕ_{PT} safety factor for postensioned concrete bridge.

who proposed for $\beta = 3,5$ is equal to 0,85-0,90 very similar to the new *phi* values proposed in this work. The authors proposed different safety factors for different reliability values but did not considered different typologies of bridges and considered only simply supported bridges.

Chapter 7

Conclusions

In the first part of this work, they were created three different experimental database for prims tests, beam failed for end debonding and beam failed for IC-induced debonding. The first database includes 11 testing programs, consisting on 176 tests; the database for beams failed for end debonding includes 34 testing programs, consisting on 161 data applied on beam tests; 187 beams failed for intermediate crack induced debonding (38 experimental works) compose the last database. Also it was examined the most important models to tested their goodness.

Nineteen models applied on prism tests and then on beam tests, thirteen models applied on end debonding database and two models applied to intermediate crack induced debonding database.

Many authors proposed their models calibrated on different database and therefore it is not possible to do a correct comparison between the models. The work of comparison was divided in three parts, one for prism tests, the second one for the beam tests representing the end debonding failure mode and, the last one concerning the IC induced debonding failure mode.

Were found nineteen models based on the prism tests. These can be divided in three groups: the models considering effective bond length, models not considering the effective bond length and models independent of effective bond length. Basing the comparison on the values of bias (the ratio of the mean to the nominal value) and coefficient of variation (COV), it was demonstrated that the models proposed are not very good, and applying then to the beam tests the results made worse.

To predict the failure load in the RC beams reinforced with FRP, thirteen models were found divided into three groups: shear capacity based models, concrete tooth based models, interfacial stress based models. Not all models are based on mechanical criteria. The shear capacity based models were calibrated on a particular database and could give a incorrect prediction for RC beams outsides these

databases. In many case the authors did not want to predict correctly the load of failure, but put all data in the safe side with an analytical load lower than the experimental. Colotti et al. proposed a model [18] based on mechanical criterion that predicts different modes of failure for the RC beam strengthened. The model which gave the best values of bias (the ratio of the mean to the nominal value) and coefficient of variation (COV) is the Casas and Pascual model [13] considering the interaction between FRP, the resin and the concrete. Not many authors based their models on the interfacial behavior and a restricted number of beam tests presents information on the resin's characteristics. In Tab.7.1 and Tab.7.2 are reported the models applied to beams tested to study the end debonding failure mode.

One of the advantage of Casas and Pascual model [13] is that it can be used to predict the intermediate crack-induced debonding too. To test the goodness of the model for this mode of failure, beam tests failed for intermediate crack-induced debonding were collected. Casas and Pascual model [13] was compared with Wu and Niu model [68] and the first one results better to predict the phenomenon (Tab.7.3). The reduce number of data did not allow to divide the data in carbon wet lay-up and carbon prepeg sheets and it was considered an unique group.

	Average of difference	Bias	COV	No. of valid tests
Smith and Teng (2002)	35,7%	1,66	27,0%	69
Colotti et al. (2004)	17,5%	0,90	23,6%	55
Teng and Yao, AS600 (2007)	41,5%	1,96	36,4%	90
Teng and Yao, ACI318 (2007)	21,1%	1,45	34,1%	90
Teng and Yao, BS8110 (2007)	26,6%	1,57	38,9%	90
Casas and Pascual (2007)	52,6%	2,21	20,1%	19
Ziraba et al. II (1995)	11,9%	1,17	17,7%	19
Jansze (1997)	77,8%	0,68	44,0%	77
Ahmed and van Gemert (1999)	69,2%	0,67	47,0%	77
Ziraba et al. I (1995)	32,3%	1,63	31,1%	19
Raoof and Zhang (1997)	27,3%	1,41	61,2%	90
Wang and Ling (1998)	26,1%	1,43	61,0%	90
Raoof and Hassanen I (2000)	7,7%	1,55	66,2%	90
Raoof and Hassanen II (2000)	22,0%	2,27	84,1%	90

Table 7.1: Comparison between different models, applying to beams reinforced with wet lay-up carbon sheets.

It was noted that there is not an unique idea on the problem of debonding and the authors proposed their models based on different criteria. Some of these

	Average of difference	Bias	COV	No. of valid tests
Smith and Teng (2002)	34,7%	1,62	26,8%	39
Colotti et al. (2007)	10,2%	1,09	39,8%	34
Teng and Yao, AS600 (2007)	39,6%	1,84	34,8%	59
Teng and Yao, ACI318 (2007)	19,5%	1,41	37,9%	59
Teng and Yao, BS8110 (2007)	22,4%	1,44	36,0%	59
Casas and Pascual (2007)	54,1%	2,27	23,4%	38
Ziraba et al. II (1995)	6,9%	1,26	40,9%	38
Jansze (1997)	82,1%	0,64	43,1%	50
Ahmed and van Gemert (1999)	51,3%	0,82	68,3%	50
Ziraba et al. I (1995)	32,1%	2,09	62,5%	38
Raoof and Zhang (1997)	12,7%	1,68	70,1%	59
Wang and Ling (1998)	7,7%	1,62	76,4%	59
Raoof and Hassanen I (2000)	27,1%	2,10	89,7%	59
Raoof and Hassanen II (2000)	49,7%	3,11	103,8%	59

Table 7.2: Comparison between different models, applying to beams reinforced with prepeg carbon sheets.

models are characterized by a mechanical approach and they are valid for all kind of beam; other authors proposed models based on an empirical calibration using different database. This implies a limitation of validity. Applying those models to the greater database previously created, it was noted the goodness of mechanical criteria approach and the limitation of models calibrated on little database. The choice to divided the composite material into two groups (wet lay-up and prepeg plates) has permitted to demonstrate that many models give a good prediction for wet lay-up applied sheets and not good for prepeg plates. It was very hard to find authors who take into account this difference of behavior depending on the applying system.

Casas and Pascual [13] model results the unique model which predicts the failure load for both end debonding and intermediate crack induced debonding failure mode with adequate value of bias and COV which are the parameter taking into account to compare the models. Comparing with other models on the same number of data, it was demonstrated that is the unique model which gave a good prediction for C-W and C-P group of beam tested to study the end debonding failure mode. The absence in the majority of technical papers of the information about the resin characteristic has provoked some difficulties. Many authors presume that the debonding failure doesn't affect the FRP-concrete interface. It results fundamental taking into account

	Bias	COV	No. of valid tests
Casas and Pascual (2007)	1,80	22,83%	22
Wu and Niu (2007)	0,60	30,77%	17

Table 7.3: Comparison between Casas and Pascual model [13] and Wu and Niu model [68] to predict the I-C induced debonding.

the quality of resin for example with its elastic modulus and its thickness.

The calibration was done following the Monte Carlo procedure on eight different bridges (four reinforced concrete bridges and four postensioned concrete bridges) and five values of safety factors were founded. In order to determine an appropriate range of geometries to represent the existing strucutres, they were selected bridges having spans ranging from 10m to 56m, continuous and simply supported structures, four different cross sectional shape (girder, slab, box-girder, box-girder built by the balanced cantilever method).

The intermediate crack induced debonding requests the lowest value of safety factor and it was not possible to strengthen all bridges. Doing hypothesis on the corrosion of reinforcing and postensioned steel demonstrated the goodness of procedure and the different range, for reinforced concrete bridges and postensioned concrete bridges. The proposed safety factors were divided into two groups which represented the reinforced concrete bridges and the postensioned concrete bridges: Due to the different aim in their design (RC bridges are designed for ULS, while postensioned bridges are designed for SLS), it was preferred to maintain two different groups. The values proposed in this work, reported in Tab.7.4, are characterized to be higher for C-W sheets than for C-P sheets; it depends on the values of bias and COV obtained applied the model to the collected database.

Mode of failure	Type of FRP	ϕ_{RC}	ϕ_{PT}
End debonding	C-W	1,00	0,95
	C-P	0,80	0,70
I-C induced debonding	CFRP	0,60	0,60

Table 7.4: Summary of proposed safety factors; reliability factor, β, equal to 3,5. ϕ_{RC} safety factor for reinforced concrete bridge, ϕ_{PT} safety factor for postensioned concrete bridge.

The comparison between the code limitations and the experimental tests, demonstrated large discrepancies in these limitations and many value were on the unsafe side. These means that there is not a common way to evaluate the debonding phe-

nomena and many of those do not result correct. A similar comparison was done by Aram et al. [2] who affirmed that a discrepancy of up to 250% was found between predicted debonding failure loads using various codes and guidelines.

This calibration follows a new model, and it is based on statistical study, while the actual codes limitation are based on empirical solutions or on constant values that do not take into account the geometry and strength characteristic of strengthened beams.

7.1 Further investigations

Given the time constraints restricting the amount of work within its scope, further initiatives for research were not able to be pursued. The following are recommendations for future work to be completed in this area:

- Create a bigger database with more information on the characteristics of resin. There are many experiments that can not be modeled with Casas and Pascual model [13] because in the literature there is not information on the properties of the resin.
- Future testing programs to test beams to obtain higher values of failure load to cover the spectrum load which characterizes the bridges.
- Improve Casas and Pascual model [13]. In this model it is not considered, for example, the contribution of tensile steel or the cover concrete thickness.
- Calibration of safety factors for the European format of safety. In this case, it has to be studied the tensile stress level in FRP and compare this with the analytical values. The Monte Carlo simulation will be done on the value of T_{frp} to calibrate the value of γ_{frp}.
- Calibrate the values for the other typologies of composite material (glass and aramid fiber-reinforced polymer)

Bibliography

[1] ACI440.2R-08. *Guide for the design and construction of externally bonded FRP systems for strengthening concrete structures.* American Concrete Institute 2008.

[2] Aram MR, Czaderski C and Motavalli M. *Debonding failure modes of flexural FRP-strengthened RC beams.* Composite Part B: Eng 2008;39:826-841.

[3] Arya C, Clarke JL, Kay EA and O'Regan PD. *T55: Design guidance for strengthening concrete structures using fibre composite materials: a review.* Eng and Struct 2002;24:889-900.

[4] Atadero RA and Karbhari VM. *Calibration of resistance factors for reliability based design of externally-bonded FRP composites.* Composite Part B: Eng 2008;39:665-679.

[5] Atadero RA and Karbhari VM. *Sources of uncertainty and design values for field-manufactured FRP.* Comp Struct 2009;89:83-93.

[6] Benjeddou O, Ouezdou MB and Bedday A. *Damaged RC beams repaired by bonding of CFRP laminates.* Constr and Build Mat 2007;21:1301-1310.

[7] Bizindavyi L and Neale KW. *Transfer lengths and bond strengths for composties bonded to concrete.* J Comp Construct 1999;3(4):153-160.

[8] Bonacci JF and Maalej M. *Externally bonded fiber-reinforced polymer for rehabilitation of corrosion damaged concrete beams.* ACI Struct J 2000;97(5):703-711.

[9] Breña SF and Macri BM. *Effect of carbon-fiber-reinforced polymer laminate configuration on the behavior of strengthened reinforced concrete beams.* J Comp Construct 2004;8(3):229-240.

[10] BS EN1991-2. *Actions on structures-Part2: Traffic loads on bridges.* European Commitee for Strandardization (CEN) 1991.

[11] BS EN1992. *Design of concrete structures*. European Commitee for Strandardization (CEN) 1992.

[12] Camata G, Spacone E, Al-Mahaidi and Saouma V. *Analysis of test specimens for cohesive near-bond failure of fiber-reiforced polymer-plated concrete*. J Comp Construct 2004;8(6):528-538.

[13] Casas JR and Pascual J. *Debonding of FRP in bending: Simplified model and experimental validation*. Constr and Build Mat 2007;21:1940-1949.

[14] Chajes MJ, Thomson Jr TA, Januska TF and Finch Jr WW. *Flexural strengthening of concrete beams using externally bonded composite materials*. Constr and Build Mat 1994;8(3):191-201.

[15] Chajes MJ, Finch Jr WW, Januska TF and Thomson Jr TA. *Bond and force transfer of composite material plates bonded to concrete*. ACI Struct J 1996;93(2):208-217.

[16] Chen JF and Teng JG. *Anchorage strength models for FRP and steel plates bonded to concrete*. J Struct Eng 2001;127(7):784-791.

[17] CNR-DT 200/2004. *Guide for the design and construction of externally bonded FRP systems for strengthening concrete structures*. Nation Research council 2004.

[18] Colotti V, Spadea G and Swamy RN. *Structural model to predict the failure behavior of plated reinforced concrete beams*. J Comp Construct 2004;8(2):104-122.

[19] Dai J, Ueda T and Sato Y. *Development of nonlinear bond stress-slip model of fiber reinforced plastics sheet-concrete interfaces with a simple method*. J Comp Construct 2001;9(1):52-62.

[20] De Lorenzis L, Miller B, Nanni A. *Bond of fiber-reinforced polymer laminates to concrete*. ACI Mat J 2001;98(3):256-264.

[21] El-Mihilmy MT and Tedesco JW. *Analysis of reinforced concrete beams strengthened with FRP laminates*. J Struct Eng 2000;126(6):684-691.

[22] Esfahani MR, Kianoush MR and Tajari AR. *Flexural behavior of reinforced concrete beams strengthened by CFRP sheets*. Eng Struct 2007;29:2428-2444.

[23] Fanning P and Kelly O. *Smeared crack models of RC beams with externally bonded CFRP plates*. Computational Mechanics 2000;26:325-332.

[24] Fanning P and Kelly O. *Ultimate response of RC beams strengthened with CFRP plates.* J Comp Construct 2001;5(2):122-127.

[25] Federation Internationale du Béton (fib). *Externally bonded FRP reinforcement for RC structures.* Fib bulletin 14, Lusanne, Switzerland 2001.

[26] Gao B, Kim JK and Leung CKY. *Experimental study on RC beams with FRP strips bonded with rubber modified resins.* Comp Science and Technology 2004;64:2557-2564.

[27] Garden HN, Quantrill RJ, Hollaway LC, Thorne AM and Parke GAR. *An experimental study of the anchorage length of carbon fibre composite plates used to strengthen reinforced concrete beams.* Constr and Build Mat 1998;12:203-219.

[28] Grace NF and Singh SB. *Durability evaluation of carbon fiber-reinforced polymer strengthened concrete beams: Experimental study and design.* ACI Struct J 2005;102(1):40-48.

[29] Harmon TG, Kim YJ, Kardos J, Johnson T and Stark A. *Bond of surface-mounted fiber-reinforced polymer reinforcement for concrete structures.* ACI Struct J 2003;100(5):557-564.

[30] Hollaway LC and Teng JG. *Strengthening and rehabilitation of civil infrastructures using fiber-reinforced polymer (FRP) composites.* Woodhead Publishing Limited 2008.

[31] JSCE. *Recommendations for upgrading of concrete structures with use of continuous fiber sheets.* Japan Society of Civil Engineers, Japan 2001.

[32] Karbhari VM, Niu H and Sikorsky C *Review and comparison of fracture mechanics-based bond strength models for FRP-strengthened structures.* J Reinforced Plastics and Composites 2006;25:1757-1794

[33] Khalifa A, Gold WJ, Nanni A and Aziz A. *Constribution of externally bonded FRP to shear capacity of RC flexural members.* J Comp Constr 1998;2(4):195-202.

[34] Lu XZ, Teng JG, Ye LP and Jiang JJ. *Bond-slip models for FRP sheets/plates bonded to concrete.* Eng Struct 2005;27(6):920-937.

[35] Nakaba K, Kanakubo T, Furuta T and Yoshizawa H. *Bond behavior between fiber-reinforced polymer laminates and concrete.* ACI Struct J 2001;98(3):359-367.

[36] Nguyen DM, Chan TK and Cheong HK. *Brittle failure and bond development length of CFRP-concrete beams.* J Comp Construct 2001;5(1):12-17.

[37] Niu HD, Vasquez A and Karbhari VM. *Effect of material configuration on strengthening of concrete slabs by CFRP composites.* Comp Part B: Eng 2006;37(2-3):226-226.

[38] Oehlers DJ. *Reinforced concrete beams with plates glued to their soffits.* J Struct Eng 1992;118(8):2023-2039.

[39] Pham HB and Al-Mahaidi R. *Prediction models for debonding failure loads of carbon fiber reinforced polymer retrofitted reinforced concrete beams.* J Comp Construct 2006;10(1):48-59.

[40] Rahimi H and Hutchinson A. *Concrete beams strengthened with externally bonded FRP plates.* J Comp Construct 2001;5(1):44-56.

[41] Ramos G, Casas JR and Alarcón A. *Normalized test for prediction of debonding failure in concrete elements strengthened with CFRP.* J Comp Construct 2006;10(6):509-519.

[42] Raoof M and Zhang S. *An insight into the structural behaviour of reinfirced concrete beams with externally bonded plates.* Proc Inst Civil Eng, Struct and Build 1997;122(November):477-492.

[43] Raoof M and Hassanen MAH. *Peeling failure of reinforced concrete beams with fibre-reinforced plastic or steel plates glued to their soffits.* Proc Inst Civil Eng, Struct and Build 2000;140(3):291-305.

[44] Ritchie PA, Thomas DA, Lu LW and Conelly GM. *External reinforcement of concrete beams using fiber reinforced plastics.* ACI Struct J 1991;88(4):490-499.

[45] Ross CA, Jerome DM, Tedesco JW, Hughes ML. *Strengthening of reinforced concrete beams with externally bonded composite laminates.* ACI Struct J 1999;96(2):212-220.

[46] Saadatmanesh H and Ehsani MR. *RC beams strenghtened with GFRP plates. I: Experimental study.* J Struct Eng 1991;117(11):3417-3433.

[47] Sas G. *FRP shear strengtneing of RC beams and walls.* Licentiate thesis, Luleå University of Technology, Sweden 2008.

[48] Seim W, Hörmann M, Karbhari V and Seible F. *External FRP poststrengthening of scaled concrete slab.* J Comp Construct 2001;5(2):67-75.

[49] Seracino R, Saifulnaz MRR and Oehlers DJ. *Generic Debonding resistance of EB and NSM plate-to-concrete joints*. J Comp Construct 2007;11(1):62-70.

[50] Sharif A, Al-Sulaimani GJ, Basunbul A, Baluch MH and Ghaleb BN. *Strengthening of initially loaded reinforced concrete beams using FRP plates*. ACI Struct J 1994;91(2):160-168.

[51] Sharma SK, Mohamed Ali MS, Goldar D and Sikdar PK. *Plate-concrete interfacial bond strength of FRP and metallic plated concrete specimens*. Composite Part B: Eng 2006;37:54-63.

[52] Smith ST and Teng JG. *FRP-strengthened RC beams. I: review of debonding stength models*. Eng Struct 2002;24:385-395.

[53] Smith ST and Teng JG. *FRP-strengthened RC beams. II: assessment of debonding stength models*. Eng Struct 2002;24:397-417.

[54] Spadea G, Bencardino F and Swamy RN. *Structural behavior of composite RC beams with externally bonded CFRP*. J Comp Construct 1998;2(3):132-137.

[55] Täljsten B. *Strengthening of concrete prisms using the plate bonding technique*. Int J Fract 1996;82:253-266.

[56] Täljsten B. *Strengthening of beams by plate bonding*. J Mat Civil Eng 1997;9(4):206-212.

[57] Täljsten B. *Defining anchor lengths of steel and CFRP plates bonded to concrete*. Int J Adhesion and Adhesives 1997;17:319-327.

[58] Teng JG, Smith ST and Lam L. *FRP strengthening RC structures*. John Wiley & Sons 2002.

[59] Teng JG, Smith ST, Yao J and Chen JF. *Intermediate crack-induced debonding in RC beams and slabs*. Constr and Build Mat 2003;17:447-462.

[60] Teng JG and Yao J. *Plate end debonding in FRP-plated RC beams I: Experiments*. Eng Struct 2007;29:2457-2471.

[61] Teng JG and Yao J. *Plate end debonding in FRP-plated RC beams II: Strength model*. Eng Struct 2007;29:2472-2486.

[62] Toutanji H, Saxena P, Zhao L and Ooi T. *Prediction of interfacial bond failure of FRP-concrete surface*. J Comp Construct 2007;11(4):427-436.

[63] TR55. *Design guidance for strengthening concrete structures using fobre composite materials*. Technical report no.55 of the Concrete Society,UK 2004;2nd edition.

[64] Triantafillou TC and Plevris. *Strengthening of RC beams with epoxy-bonded fibre-composite materials*. Mat and Struct 1992;25:201-211.

[65] Yao J, Teng JG and Chen JF. *Experimental study on FRP-to-concrete bonded joints*. Comp Part B: Eng 2005;36:99-113.

[66] Yao J, Teng JG and Lam L. *Debonding in RC cantilever slabs strengthened with FRP strips*. Proc Int Conf on Advanced Polymer Composite for Structural Applications in Construction, Southampton University, UK, 2002;125-133.

[67] Yuan H, Teng JG, Seracino R, Wu Z and Yao J. *Full-range behavior of FRP-to-concrete bonded joints*. Eng Struct 2004;26(5):553-565.

[68] Wu Z and Niu H. *Prediction of crack-induced debonding failure in R/C structures flexurally strengthened with externally bonded FRP compisites*. Doboku Gakkai Ronbunshuu E 2007;63(4):620-639.

[69] Zhang S, Raoof M and Wood LA. *Prediction of peeling failure of reinforced concrete beams with externally bonded steel plates*. Proc Inst Civil Eng: Struct and Build 1995;110(August):257-268.

[70] Ziraba YN, Baluch, Basunbul IA, Azad AK, Al-Sulaimanu GJ and Sharif AM. *Combined experimental-numerical approach to characterization of steel-glue-concrete interface*. Mat and Struct 1995;28(9):518-525.

Appendix A

Code limitations

To prevent plate end debonding at the last crack, the anchorage force existing at the last crack should be checked with a design limitation. There are numerous codes, guidelines and other reference that present this type of design limitation. All references include E_{frp}, t_{frp}, b_{frp} and f_{ctm}. *Fib* [25] proposes the most expanded equation for $T_{f,max}$ which includes various parameters such as FRP properties concrete tensile strength, concrete surface condition, internal shear reinforcement and geometry. It is worth noting that the ACI440 code [1] limits the shear load at the plate end. ISIS (2001), as reported in Aram et al. paper [2], defines a different type of anchorage length with a uniform bond strength along this anchorage length and the assumption is that midspan debonding can be avoided by using this anchorage length.

In order to prevent midspan debonding of the plate, the codes and guidelines give two different approaches. Generally, a design limitation is placed on the bond shear stress or the FRP tensile strain (or stress). *Fib* [25] gives two different approaches based on the calculation of the maximum possible increase in tensile FRP stress that can lead to the calculation of a maximum interfacial bond stress. A general diagram of the maximum possible increase in FRP tensile stress is shown in Fig.A.1 (approach 2 of *Fib* [25]). The strain (stress) limitations of *Fib*2, JSCE [31], depend on the stiffness of the FRP ($E_{frp}t_{frp}$) and on the concrete properties but ACI440 [1] uses $E_{frp}t_{frp}$ and the rupture strain of the FRP ($\varepsilon_{frp,u}$). The Italian guideline, CNR-DT 200/2004 [17], uses the same model for end debonding limitation, multiplying by a constant. Others recommend a constant value for it. Furthermore, the bond shear stress limitation of *Fib* [25] and SIA (2003), reported in Aram et al. paper [2], is related to the tensile and shear strength of the concrete, respectively.

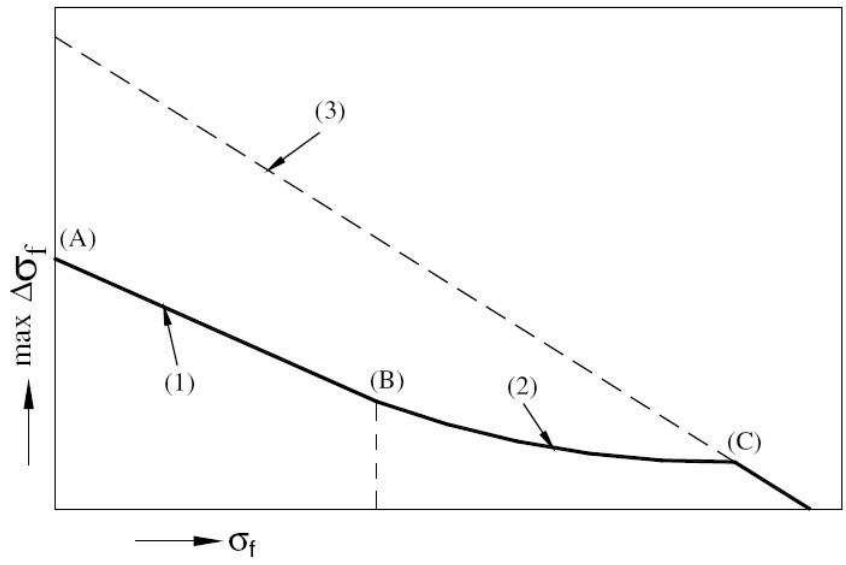

Figure A.1: Diagram of the maximum possible increase in FRP tensile stress (from Aram et al. [2]).

A.1 CNR recommendations

The CNR guide [17] classified the debonding failure modes for flexural strengthening in four categories: laminate/sheet end debonding, intermediate debonding caused by flexural cracks, debonding caused by diagonal shear cracks, debonding caused by diagonal shear cracks, debonding caused by irregularities roughness of concrete surface.

The ultimate value of the force transferred to the FRP system prior to debonding depends on the length, l_b, of the bonded area. The optimal bonded length, l_e, is defined as the length that, if exceeded, there would be no increase in the force transferred between concrete and FRP. The optimal bonded length, l_e, may be estimated as follows:

$$l_e = \sqrt{\frac{E_{frp} \cdot t_{frp}}{2 \cdot f_{ctm}}}$$

where E_{frp} and t_{frp} are Young modulus of elasticity and thickness of FRP, respectively, and f_{ctm} is the average tensile strength of the concrete.

The specific fracture energy (characteristic value, 5th percentile), Γ_{Fk}, of the FRP-concrete interface may be expressed as follows:

$$\Gamma_{Fk} = 0,03 \cdot k_b \cdot \sqrt{f_{ck} \cdot f_{ctm}} \quad \text{(forces in N, lengths in mm)}$$

where f_{ck} is the characteristic strength of concrete; k_b is a geometric coefficient depending on both width of the strengthened beam, b, and width, b_{frp}, of the FRP system; and k_b can be written as follows:

$$k_b = \sqrt{\frac{2 - \frac{b_{frp}}{b}}{1 + \frac{b_{frp}}{400}}} \geq 1 \quad \text{(lengths in mm)}$$

where $b_{frp}/b \geq 0,33$ (if $b_{frp}/b < 0,33$, the value for k_b corresponding to $b_{frp}/b = 0,33$ is adopted).

For laminate/sheet end debonding assuming that the provided bond length is equal to or larger than the optimal bonded length, the ultimate design strength, f_{fdd} can be calculated as follows:

$$f_{fdd} = \frac{1}{\gamma_{f,d} \cdot \sqrt{\gamma_c}} \cdot \sqrt{\frac{2 \cdot E_{frp} \cdot \Gamma_{Fk}}{t_{frp}}}$$

where $\gamma_{f,d}$ is the partial factor equal to $1,5$ and γ_c is the partial factor for concrete.

For bond lengths, l_b, shorter than the optimal bonded length, l_e, the ultimate design strength shall be reduced according to the following equation:

$$f_{fdd,rid} = f_{fdd} \cdot \frac{l_b}{l_e} \cdot \left(2 - \frac{l_b}{l_e}\right)$$

To prevent failure from intermediate debonding mechanism, a simplified procedure may be used. The maximum strength calculated in the FRP system shall be less than $f_{fdd,s}$:

$$f_{fdd,2} = k_{cr} \cdot f_{fdd} = \frac{k_{cr}}{\gamma_{f,d} \cdot \sqrt{\gamma_c}} \cdot \sqrt{\frac{2 \cdot E_f \cdot \Gamma_{Fk}}{t_f}}$$

where k_{cr} can be taken equal to 3,0.

The corresponding value of the design strain, ε_{fdd}, in the FRP system can be calculated as follows:

$$\varepsilon_{fdd} = \frac{f_{fdd,2}}{E_f}$$

A.2 ACI440-08

The flexural strength of a section depends on the controlling failure mode. ACI440-08 [1] divided in five groups the failure modes: crushing of the concrete in compression before yielding of the reinforcing steel, yielding of the steel in tension followed by rupture of the FRP laminate, yielding of the steel in tension followed by concrete crushing, shear/tension delamination of the concrete cover (cover delamination) and debonding of the FRP from the concrete substrate (FRP debonding).

To prevent such an intermediate crack-induced debonding failure mode, the effective strain in FRP reinforcement should be limited to the strain in FRP reinforcement should be limited to the strain level at which debonding may occur, ε_{fd}, as follows:

$$\varepsilon_{fd} = 0,41\sqrt{\frac{f'_c}{nE_{frp}t_{frp}}} \leq 0,9\varepsilon_{fu}$$

where f'_c is the compressive strength of concrete, n is the number of plies of FRP reinforcement, E_{frp} and t_{frp} are the Young modulus of elasticity and the thickness of FRP, respectively.

This equation takes a modified form of debonding strain equation proposed by Teng et al. [59] that was based on committee evaluation of a significant database for flexural beam tests exhibiting FRP debonding failure. The proposed equation was calibrated using average measured values of FRP strains at debonding and the database for flexural tests experiencing intermediate crack-induced debonding to determine the best fit coefficient of 0,41. Reliability of FRP contribution to flexural strength is addressed by incorporating an additional strength factor for FRP ψ_{frp} in addition to the strength reduction factor ϕ per ACI318-05 for structural concrete.

ACI440-08 [1], to reinforce the beam to prevent the phenomenon of end peeling, defines a limit of shear force. When the factored shear force at the termination point its grater than 2/3 the concrete shear strength (V_u>0,67V_c), the FRP laminates should be anchored with transverse reinforcement to prevent the concrete cover layer from splitting.

The bond capacity of FRP is developed over a critical length l_{df}. To develop the effective FRP stress at a section, the available anchorage length of FRP should exceed the value of:

$$l_{df} = \sqrt{\frac{nE_{frp}t_{frp}}{\sqrt{f'_c}}}$$

This equation was proposed by Teng et al. [58, 59].

A.3 TR550

End plate separation failure will be avoided by addressing two criteria: limiting the longitudinal shear stress between the FRP and the substrate or anchoring the FRP by extending it beyond the point at which it is theoretically no longer required.

With regards to the first criterion, field experience of installing FRP systems suggests that, provided that the longitudinal shear stress at the ultimate limit state does not exceed 0,8N/mm^2, premature peeling failure will be avoided. Rupture of FRP may occur at the service loads due to the sustained stresses that exist in the material. Therefore it is recommended that the maximum stress in the FRP at the service load, as a proportion of the design strength should not exceed the values given in Tab.A.1:

Material	Maximum stress (%)
Carbon FRP	65
Aramid FRP	40
Glass FRP	55

Table A.1: Maximum stress under service load to avoid stress rupture as a proportion of design strength (TR55 code [63]).

As explained in Arya et al. paper [3], the designer will need to check for end-plate separation failure. Anchoring the FRP by extending it beyond the point at which it is theoretically no longer required, and limiting the longitudinal shear stress between the FRP and the substrate to 0.8 N/mm2, can prevent this. The theoretical cut-off point can be determined if the maximum force in the FRP bonded to concrete, $T_{frp,max}$, is known. The actual cut-off point is then obtained by extending the FRP an anchorage length, $l_{t,max}$, past this point. The quantities $T_{frp,max}$ and $l_{t,max}$ can be estimated using the following expressions

$$T_{frp,max} = 0,5k_b b_{frp}\sqrt{E_{frp}t_{frp}f_{ctm}}$$

$$l_{b,max} = 0,7\sqrt{(E_{frp}t_{frp}/f_{ctm}}$$

where $k_b = 1,06\sqrt{\frac{2-\frac{b_{frp}}{b}}{1+\frac{b_{frp}}{400}}} \geq 1$, while b_{frp} is the plate width (in mm), b is the beam width (in mm), t_{frp} is the plate thickness (in mm), E_{frp} is the elastic modulus of the FRP, and f_{ctm} is the tensile strength of the concrete equal to $0,18(f_{cu})^{2/3}$.

The longitudinal shear stress should be checked at the plate ends, where the shear force acting on the strengthened member will be at its greatest. Additionally, the longitudinal shear stress should be checked at locations in the span where the steel reinforcement has yielded. At these locations, any steel reinforcement does not contribute towards the second moment of area of the transformed section, as its modulus of elasticity is zero.

A.4 FIB, bulletin 14

The first approach to prevent peeling-off is restricting the ultimate tensile strain $\varepsilon_{f,lim}$ at ULS to a certain value. The strain limitation approach has been incorporated in quite a few design guidelines and technical approvals, with $\varepsilon_{f,lim}$ ranging from $0,0065$ to $0,0085$. This text recommended, as example for the verification of the end anchorage, Neubauer and Rostasy model. It gives the maximum FRP force which can be anchored, $N_{fa,max}$, and the maximum anchorage length. $l_{b,max}$, equal to:

$$N_{fa,max} = \alpha c_1 k_c k_b b\sqrt{E_f t_f f_{ctm}} \ \ [N]$$

$$l_{b,max} = \sqrt{\frac{E_f t_f}{c_2 f_{ctm}}} \ \ [mm]$$

where α is a reduction factor, approximately equal to $0,9$, to account for the influence of inclined cracks on the bond strength (Neubauer and Rostasy 1999); k_c is a factor acconting for the state of compaction of concrete (k_c can generally be assumed to be equal to 1,0 but for FRP bonded to concrete faces with low compaction k_c=0,67) and k_b is a geometry factor:

$$k_b = 1,06\sqrt{\frac{2-\frac{b_{frp}}{b}}{1+\frac{b_{frp}}{400}}} \geq 1$$

with $b_f/b \geq 0,33$. Note that b, b_{frp} and t_f are measured in mm, and E_f, f_{ctm} are in MPa. c_1 and c_2, for CFRP strips, are equal to 0,64 and 2, respectively.

For bond lengths $l_b < l_{b,max}$, the ultimate bond force was calculated according to Holzenkämpfer [25] as follows:

$$N_{fa} = N_{fa,max} \frac{l_b}{l_{b,max}} \left(2 - \frac{l_b}{l_{b,max}}\right)$$

In the second approach, to verify that the growth in tensile stresses between two subsequent cracks does not exceed the maximum possible increase determined by the bond stresses, the achievable increase has to be estimated. This has to be done for the region where flexural cracks occur as for the anchorage zone. The maximum tensile force, which can be transferred from FRP to the concrete by means of bond stresses at the anchorage zone, can be calculated according to Niedermeier, as follows:

$$\sigma_{fad,max} = \frac{c_1}{\gamma_c} \sqrt{\frac{E_{frp}\sqrt{f_{ck} f_{ctm}}}{t_{frp}}} \ [MPa]$$

where c_1 equals 0,23. the maximum possible stress is closely related to an effective anchorage length $l_{b,max}$

$$l_{b,max} = c_2 \sqrt{\frac{E_{frp} t_{frp}}{\sqrt{f_{ck} f_{ctm}}}}$$

where c_2=1,44.

An increase in anchorage length above $l_{b,max}$ does not result in an increase in resisting tensile stresses. For anchorage lengths lower than $l_{b,max}$, the maximum tensile stress is described by:

$$\sigma_{fad} = \frac{l_b}{l_{b,max}} \left(2 - \frac{l_b}{l_{b,max}}\right) \sigma_{fad,max} \quad l_b \leq l_{b,max}$$

A.5 Other codes

Other two codes are taking into account to evaluate the existing limitations to prevent the debonding phenomenons. ISIS (2001) is the Canadian recommendation, while SIA166 (2003) is the Swiss code of FRP material, both reported in Aram et

al. paper [2]. The first one proposed a limitation on the anchorage length, for end debonding and midspan debonding, which depends on the tension characteristic of composite material, its geometry and the concrete strength;

$$l_f = f_{frp,u}\frac{b_{frp}t_{frp}}{\tau_{bu}b}$$

where $f_{frp,u}$ is the tensile strength of FRP, b_{frp} and t_{frp} are the width and thickness of FRP, respectively; b is the width of concrete section and τ_{bu} is the mean bond strength of the FRP to concrete and it is equal to:

$$\tau_{bu} = 0,307\sqrt{f_c}$$

The Swiss recommendation proposed both ultimate tension in FRP $T_{frp,max}$ and a critical anchorage length $l_{b,max}$. The two values depend on Young's modulus and geometry of FRP and the tensile strength of concrete.

$$T_{frp,max} = b_{frp}\sqrt{2G_{Fb}E_{frp}t_{frp}}$$

$$l_b \geq l_{b,max} = \frac{\pi}{2}\sqrt{\frac{2G_{Fb}E_{frp}t_{frp}}{\tau^2_{frp,0}}}$$

where E_{frp} is the modulus of elasticity of FRP, G_{Fb} is the fracture energy of concrete equal to $G_{Fb} = \frac{f_{ctH}}{8}$ while $\tau = \frac{4F_{ctH}}{3}$; where f_{ctH} is the surface tensile strength of concrete.

To prevent the midspan debonding, SIA166 proposes a strain limitation equal to TR55 code, being $\varepsilon_f \leq 0,8\%$.

Another guideline that proposed a limitation for midspan debonding is the Japanese code JSCE [31] which defines a limit for stress in FRP depending on the number of plies n_{frp} the thickness t_{frp} and Young's modulus E_{frp}:

$$\sigma_{frp} \leq \sqrt{\frac{2G_f E_{frp}}{n_{frp}t_{frp}}}$$

where $G_f \approx 0,5N/mm$.

Codes and guidelines	Debonding criteria
ACI440 (2008)	$V_{end} \leq 0,67V_c, \quad l_{df} = \sqrt{\frac{nE_{frp}t_{frp}}{\sqrt{f'_c}}}$
FIB (2001)	1) $T_{frp,max} = 0,64\alpha k_c k_b b_{frp}\sqrt{E_{frp}t_{frp}f_{ctm}}, \quad l_{b,max} = \sqrt{\frac{E_{frp}t_{frp}}{2f_{ctm}}}$ where $k_b = 1,06\sqrt{\frac{2-\frac{b_{frp}}{b}}{1+\frac{b_{frp}}{400}}} \geq 1$, $b_{frp}/b \geq 0,33$, generally k_c=1 but for FRP bonded to concrete face with low compaction k_c=0,67. Approximately α=0,9 but for beams with sufficient internal and external shear reinforcement α=1
	2) $T_{frp,max} = 0,23b_{frp}t_{frp}\frac{\sqrt{E_{frp}\sqrt{f_c f_{ctm}}}}{t_{frp}}, \quad l_{b,max} = 1,44\sqrt{\frac{E_{frp}t_{frp}}{\sqrt{f_c f_{ctm}}}}$
ISIS (2001)	$l_{frp} = f_{frp,u}\frac{b_{frp}t_{frp}}{\tau_{bu}b}, \quad \tau_b = 0,307\sqrt{f_c}$
SIA166 (2003)	$T_{frp,max} = b_{frp}\sqrt{2G_{Fb}E_{frp}t_{frp}}, \quad l_{b,max} = \frac{\pi}{2}\sqrt{\frac{2G_{Fb}E_{frp}t_{frp}}{\tau^2_{frp0}}}$ $G_{Fb} = \frac{f_{cH}}{8}, \quad \tau_{frp0} = \frac{4f_{cH}}{3}$
TR55 (2004)	$T_{frp,max} = 0,5k_b b_{frp}\sqrt{E_{frp}t_{frp}f_{ctm}}, \quad l_{b,max} = 0,7\sqrt{E_{frp}t_{frp}/f_{ctm}}$
CNR-DT200	$f_{fdd} = \frac{1}{\gamma_{f,d}\sqrt{\gamma_c}}\sqrt{\frac{2E_{frp}\Gamma_{Fk}}{t_{frp}}}, \quad l_e = \sqrt{\frac{E_{frp}t_{frp}}{2f_{ctm}}}$
(2004)	where $\Gamma_{Gk} = 0,03k_b\sqrt{f_{ck}f_{ctm}}, \quad k_b = 1,06\sqrt{\frac{2-\frac{b_{frp}}{b}}{1+\frac{b_{frp}}{400}}} \geq 1$

Table A.2: Design limitations to prevent plate end debonding.

Codes and guidelines	Debonding criteria
ACI440 (2008)	$\varepsilon_{fd} = 0,41\sqrt{\frac{f'_c}{nE_{frp}t_{frp}}} \leq 0,9\varepsilon_{fu}$,
FIB (2001)	The FRP strain limitation has a range from 0,65% to 0,85%
ISIS (2001)	Debonding can be avoided by using sufficient anchorage of Tab.A.2
SIA166 (2003)	$\varepsilon_{frp} \leq 0,8\%$
TR55 (2004)	$\varepsilon_{frp} \leq 0,8\%$
JSCE (2001)	$\sigma_{frp} \leq \sqrt{\frac{2G_{frp}E_{frp}}{n_{frp}t_{frp}}}$ $G_{frp} \approx 0,5N/mm$
CNR-DT200 (2004)	$f_{fdd,2} = 3\frac{1}{\gamma_{f,d}\sqrt{\gamma_c}}\sqrt{\frac{2E_{frp}\Gamma_{Fk}}{t_{frp}}}$, $l_e = \sqrt{\frac{E_{frp}t_{frp}}{2f_{ctm}}}$ where $\Gamma_{Gk} = 0,03k_b\sqrt{f_{ck}f_{ctm}}$, $k_b = 1,06\sqrt{\frac{2-\frac{b_{frp}}{b}}{1+\frac{b_{frp}}{400}}} \geq 1$

Table A.3: Design limitations to prevent midspan debonding.

A.6 Results

The main difference between the design limitation for plate end debonding and midspan debonding is the kind of comparison. In Tab.A.2, all codes proposed a limitations based on the stress level in the material. This one depends on both FRP material (geometry of plate and Young's modulus) and concrete (strength). The proposed anchorage length is based on the same characteristic of stress limitation. Considering midspan debonding (Tab.A.3, many codes propose a constant strain limitation which doesn't depend on the characteristic of beam or FRP. The Japanese code proposes a strain limitation, which depends on FRP characteristic only, while CNR-DT200 [17] proposes a simplified equation, multiplying the end debonding formula by k_c, taken equal to 3 if specific data are not available. Fib code proposes, both for end debonding and midspan debonding, various models, without an unique recommendation.

Comparing the experimental tests with the limitations proposed by different codes, it was demonstrated that not all models, actually used in design applications, present a good security. As shown in Tab.A.4, Tab.A.5, Tab.A.6, the percentage of unsafe tests could be significant. Taking into account the end debonding beam tests, all beams present an anchorage length longer than the length proposed in the code. The Swiss code presents the lowest recommended length, while the Canadian code is characterized by large anchorage length being the largest length proposed. Fib gives two different equation where the Fib2 citefib is more conservative, while Fib1 [25] proposes values similar to SIA166 results. CNR-DT200 [17] and TR55 [63] give the same values, being similar the equation used.

Regarding the stress limitations, each model presents a significant percentage of unsafe data. This means that some beams fail under a load lower than the code limitations. Should be better use real beams to do this comparison because, as explained in first chapter, not all beam are correctly designed (for example, underestimating or overestimating steel shear reinforcement). CNR recommendation citeCNR predicts only one unsafe test (beam reinforced with wet lay-up carbon plate) and it results the best prediction on this database. Fib proposes two different model, where the first one is characterized by too high quantity of unsafe data, being more than $50,0\%$ the percentage for each kind of material; the second one improves the number of unsafe tests. All these models improve their goodness applied to beams reinforced with CFRP, while it is more difficult give a correct stress limitation for GFRP plates. The ACI440-08 [1] code equation is characterized by good limitation for CFRP plate, resulting only 2 beams with wet lay-up carbon sheets in unsafe side.

Many models were calibrated on bond test results and then applied to beam tests; as seen in Tab.A.5, many models give good limitation of failure load, although are characterized by high number of unsafe tests in Tab.A.4. Fib2 [25] is characterized by $2,4\%$ of unsafe data for C-W data and no unsafe tests for both GFRP and AFRP sheets. Should be improve many model to prevent the end debonding failure in beams reinforced with prepeg carbon plates. TR55 code [63] gives a good value of ultimate stress being only 3 C-W beams and 3 C-P beams set in unsafe side. Only the Italian guide [17] proposes an equation that sets all data in safe side. FIB1 [25] is characterized by high value of unsafe tests, for all kind of material. It isn't possible to apply the ACI440-08 [1] equation to this tests because this equation was proposed only for beams. The number of SIA166 [2] unsafe tests is equal to 8 and 3 for C-W and C-P bond tests, respectively.

As seen in Fig.A.5 and Fig.A.6, in this tests are not respected the minimum anchorage length, but this appears independent from the goodness of stress limitation, although in some model the ultimate tension admitted had been reduced if the anchorage length was shorter than the minimum.

Codes and guidelines	kind of material	n.total tests	n.unsafe tests	n.unsafe tests(%)
FIB (2001) 1)	C-W	90	46	51,1
	C-P	59	28	47,4
	G-W	7	6	85,7
	G-P	7	5	71,4
FIB (2001) 2)	C-W	90	23	25,6
	C-P	59	4	6,8
	G-W	7	4	57,1
	G-P	7	2	28,6
ACI440-08 (2008)	C-W	90	2	2,2
	C-P	59	0	0,0
	G-W	7	2	28,6
	G-P	7	1	14,3
SIA166 (2003)	C-W	90	28	31,1
	C-P	59	9	15,2
	G-W	7	5	71,4
	G-P	7	2	28,6
TR55 (2004)	C-W	90	15	16,7
	C-P	59	2	3,4
	G-W	7	2	28,6
	G-P	7	2	28,6
CNR-DT200 (2004)	C-W	90	1	1,1
	C-P	59	0	0,0
	G-W	7	0	0,0
	G-P	7	0	0,0

Table A.4: Number of unsafe beams in end debonding tests.

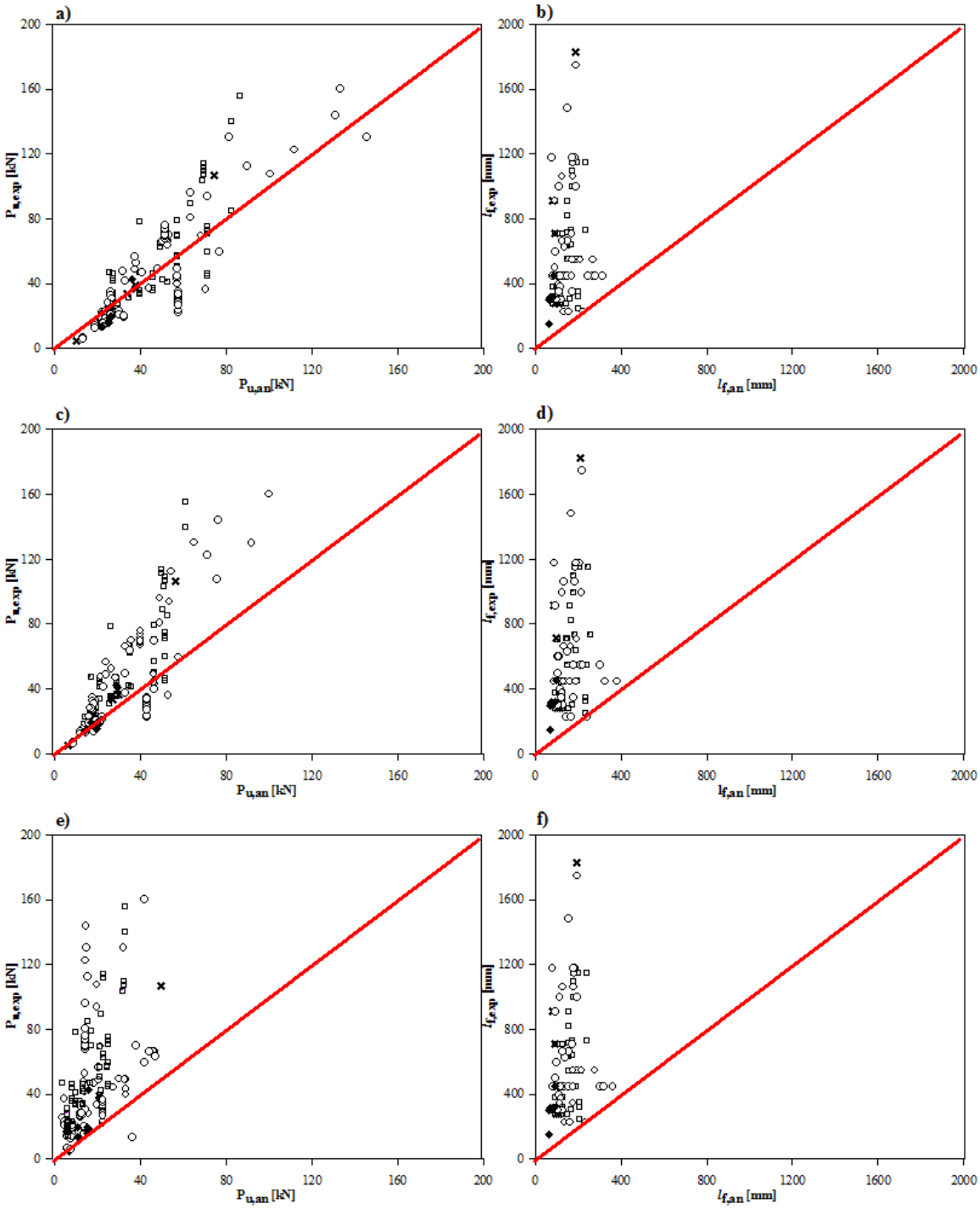

Figure A.2: Comparison between beam tests and code limitations (end debonding). a)Fib1 force , b)Fib1 anchorage length, c)Fib2 force, d)Fib2 anchorage length, e)ACI440-08 force, f)ACI440-08 anchorage length.

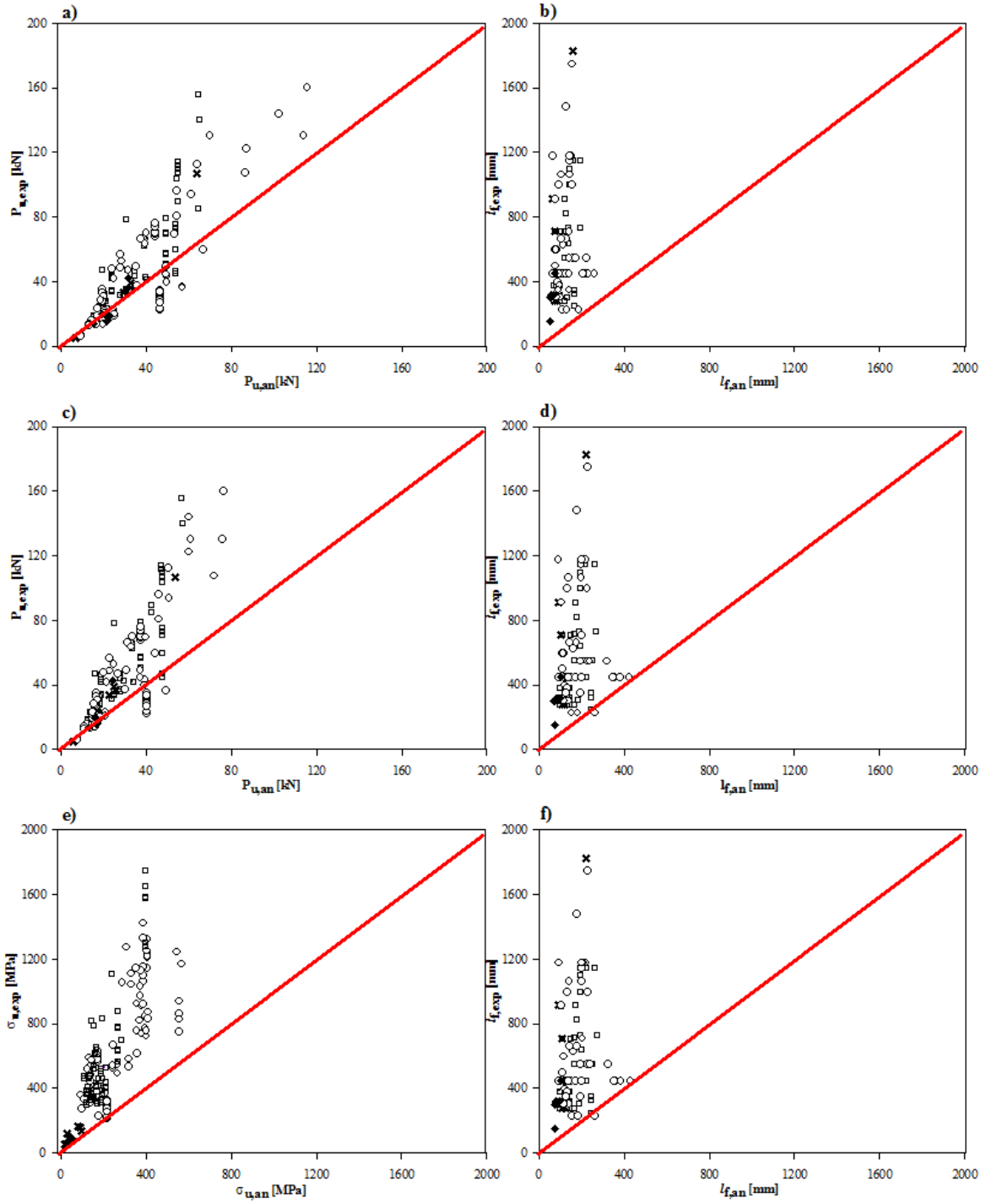

Figure A.3: Comparison between beam tests and code limitations (end debonding). a)SIA166 force , b)SIA166 anchorage length, c)TR55 force, d)TR55 anchorage length, e)CNR-DT200 force, f)CNR-DT200 anchorage length.

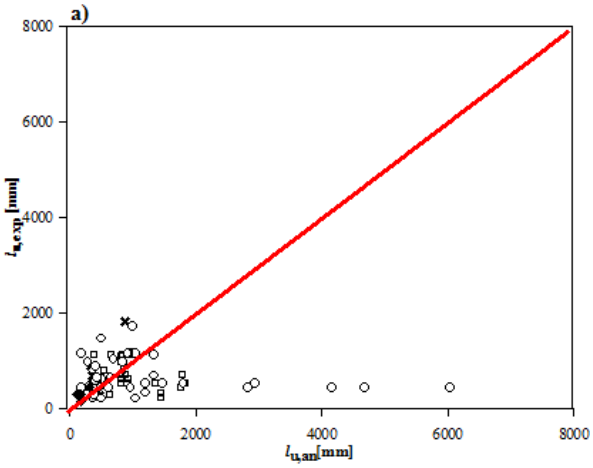

Figure A.4: Comparison between beam tests and code limitations (end debonding). a)ISIS length force.

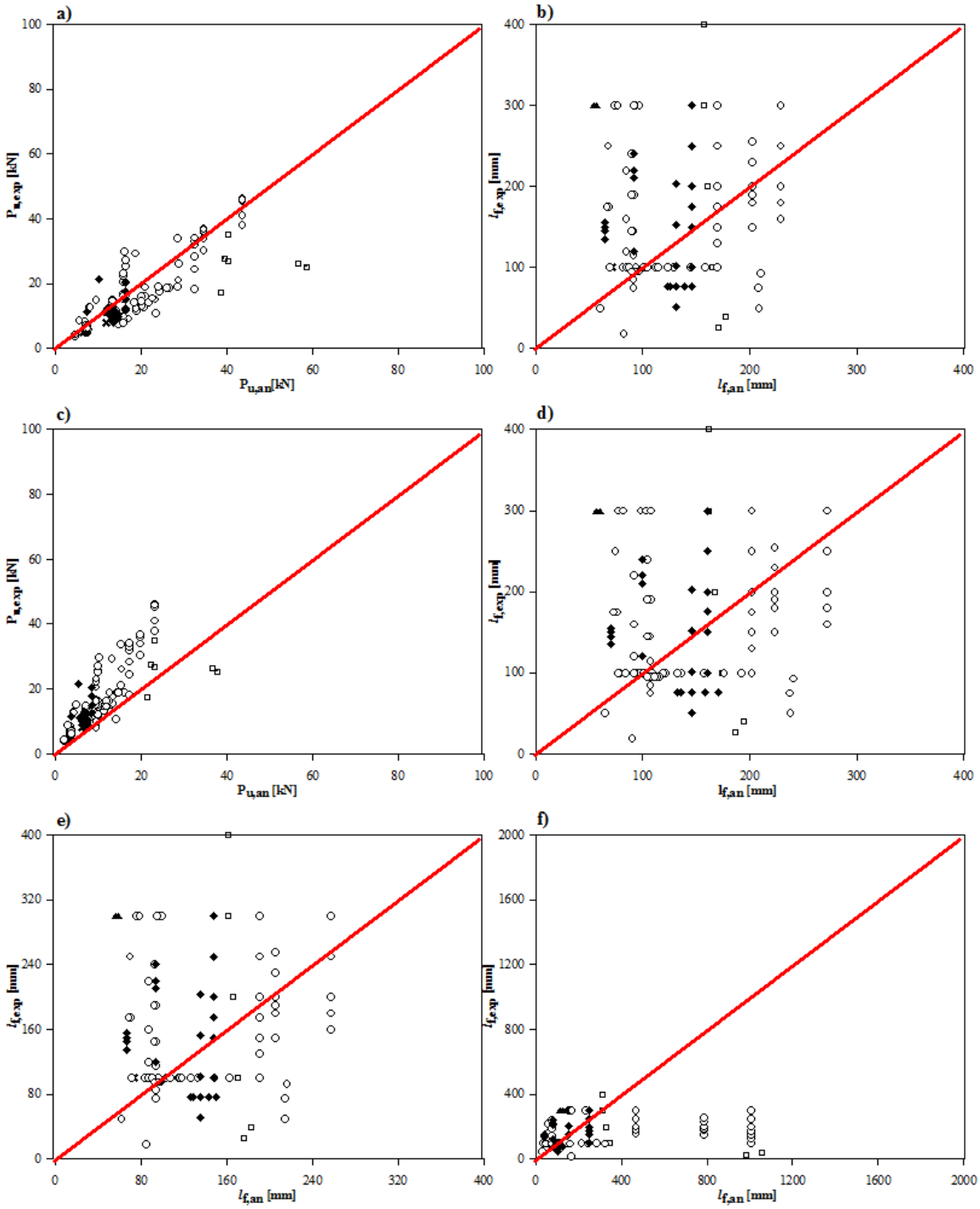

Figure A.5: Comparison between pull tests and code limitations (end debonding). a)Fib1 force , b)Fib1 anchorage length, c)Fib2 force, d)Fib2 anchorage length, e)ACI440-08 anchorage length, f)ISIS anchorage length.

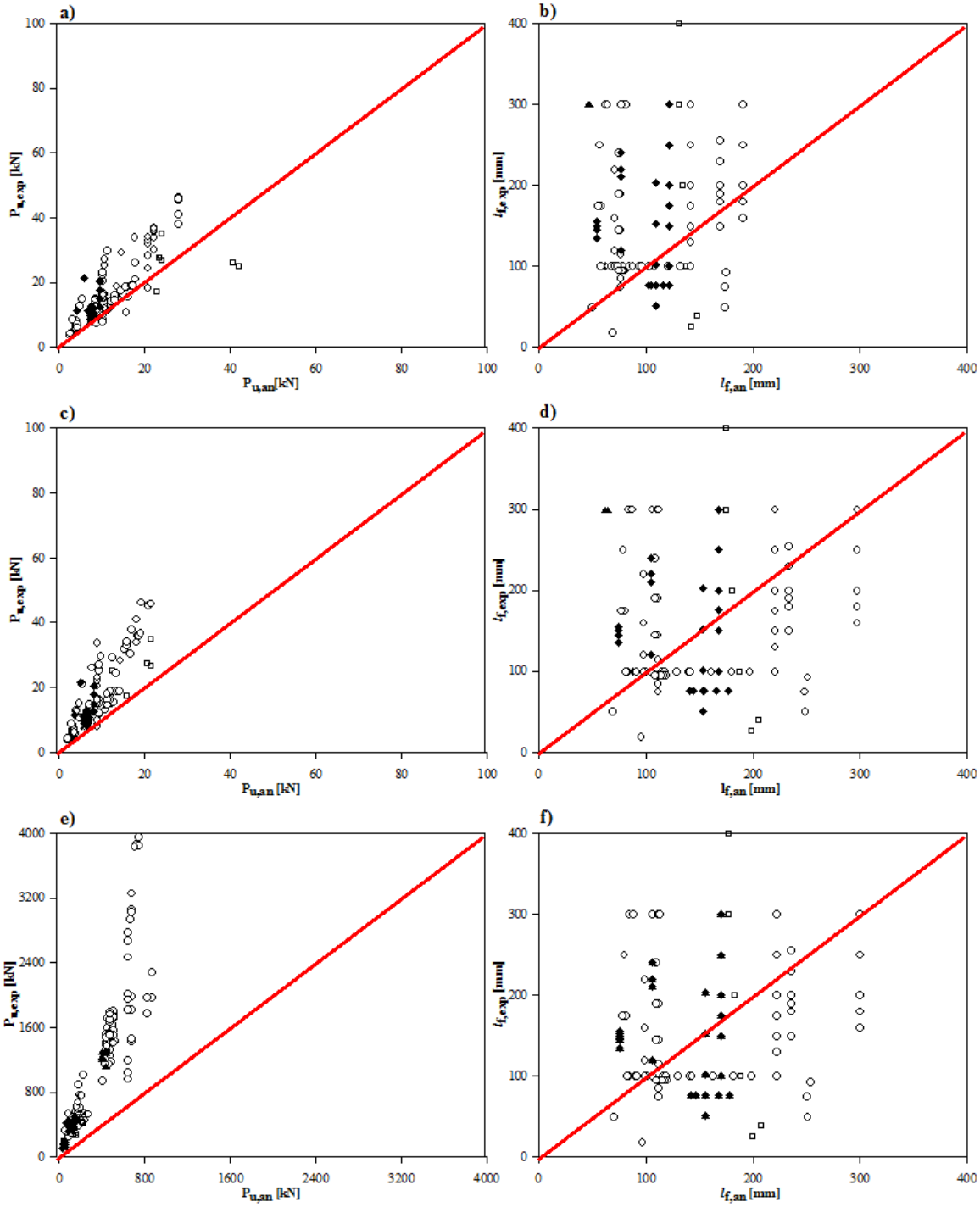

Figure A.6: Comparison between pull tests and code limitations (end debonding). a)SIA166 force , b)SIA166 anchorage length, c)TR55 force, d)TR55 anchorage length, e)CNR-DT200 force, f)CNR-DT200 anchorage length.

Codes and guidelines	kind of material	n.total tests	n. unsafe tests	n. unsafe tests (%)
FIB (2001) 1)	C-W	124	89	71,8
	C-P	6	6	100,0
	G-W	31	18	58,1
	G-P	2	0	0,0
	A-W	6	2	33,3
FIB (2001) 2)	C-W	124	3	2,4
	C-P	6	3	50,0
	G-W	31	0	0,0
	G-P	2	0	0,0
	A-W	6	0	0,0
ACI440-08 (2008)	C-W	124	-	-
	C-P	6	-	-
	G-W	31	-	-
	G-P	2	-	-
	A-W	6	-	-
SIA166 (2003)	C-W	124	8	6,4
	C-P	6	3	50,0
	G-W	31	0	0,0
	G-P	2	0	0,0
	A-W	6	0	0,0
TR55 (2004)	C-W	124	3	2,4
	C-P	6	3	50,0
	G-W	31	0	0,0
	G-P	2	0	0,0
	A-W	6	0	0,0
CNR-DT200 (2004)	C-W	124	0	0,0
	C-P	6	0	0,0
	G-W	31	0	0,0
	G-P	2	0	0,0
	A-W	6	0	0,0

Table A.5: Number of unsafe data in prism tests.

Codes and guidelines	kind of material	n.total tests	n.unsafe tests	n.unsafe tests (%)
FIB (2001) 3)	CFRP	147	147	100,0
	GFRP	8	8	100,0
	AFRP	32	32	100,0
ACI440-08 (2008)	CFRP	147	147	100,0
	GFRP	8	8	100,0
	AFRP	32	32	100,0
JSCE (2001)	CFRP	147	68	46,2
	GFRP	8	4	50,0
	AFRP	32	30	93,7
SIA166 (2003)	CFRP	147	147	100,0
	GFRP	8	8	100,0
	AFRP	32	32	100,0
CNR-DT200 (2004)	CFRP	147	127	86,4
	GFRP	8	6	75,0
	AFRP	32	32	100,0

Table A.6: Number of unsafe data in beams tested for I-C induced debonding.

The midspan induced debonding comparison, as seen in Fig.A.7 and Fig.A.8, presents an insufficient estimation of ultimate stress or strain in FRP. There are two kind of limitation: ACI440-08 [1], Fib [25], SIA166 [2] and TR55 [63] propose a value of deformation in FRP, while JSCE [31] and CNR-DT200 [17] guidelines give a strain limitation. ACI440 [1] equation depends on concrete strength and FRP characteristic, while the other codes present a constant value independent from beam characteristics. The Italian guideline [17] uses the same equation proposed for end debonding applying an factor equal to 3.

As shown in Fig.A.7 and Fig.A.8, there isn't any model which gives a good prediction of failure. The models based on a strain limitations, present all tests set on unsafe side. Only CNR-DT200 [17] and JSCE [31] present some valid limitation but the percentage of safe tests is insufficient to consider the goodness of these models. There is a good model which can help to predict the midspan debonding. JSCE guideline [31] uses an equation which depends on Young's modulus and thickness of FRP, while CNR-DT200 [17] adapts the equation used for another kind of fail. The constant values can't present a good solution because are independent from the characteristic of materials and their geometry.

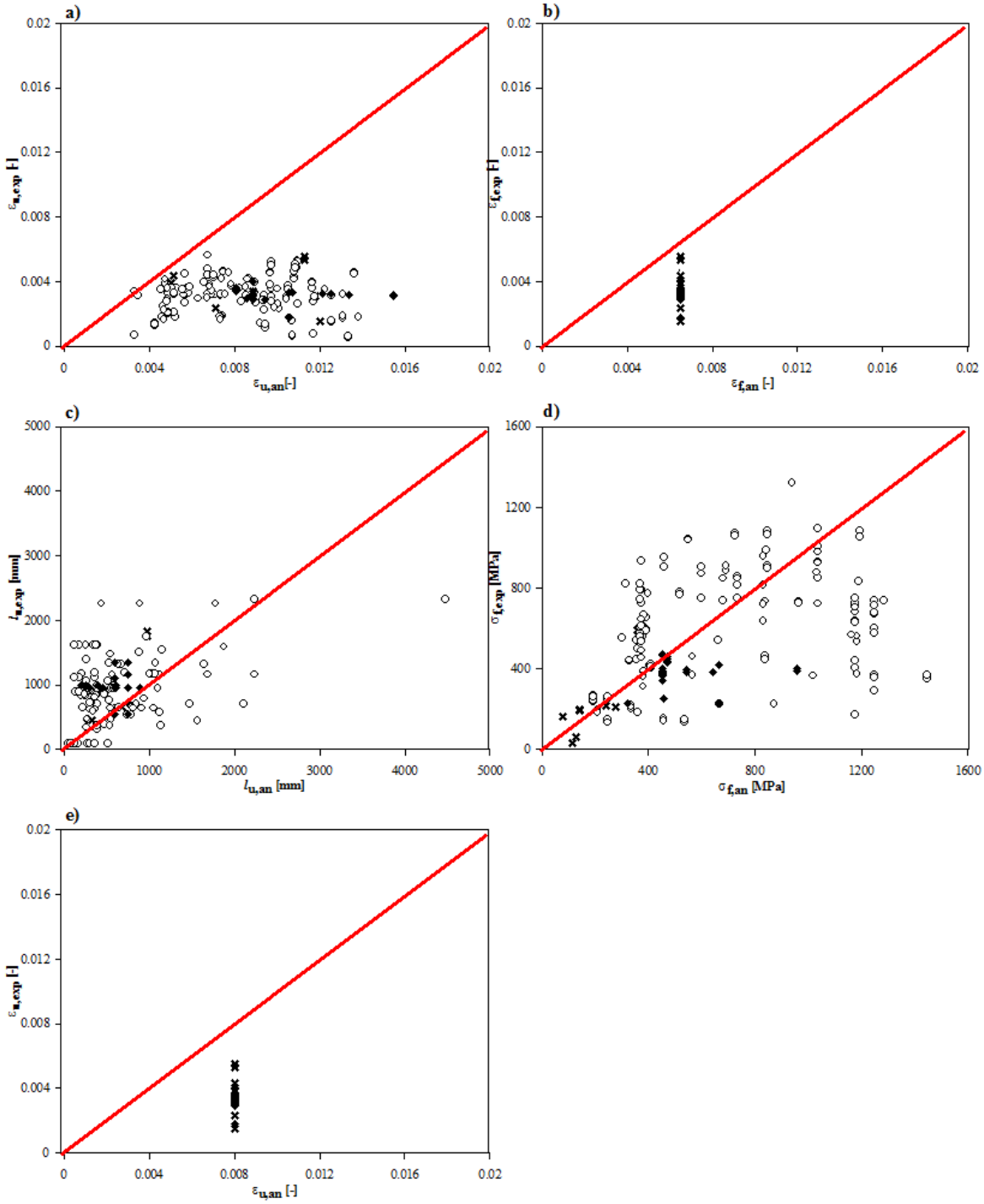

Figure A.7: Comparison between beam tests and code limitations (midspan debonding). a)ACI440-08 strain, b)Fib3 strain, d)ISIS anchorage length, e)JSCE stress, f)SIA166 strain.

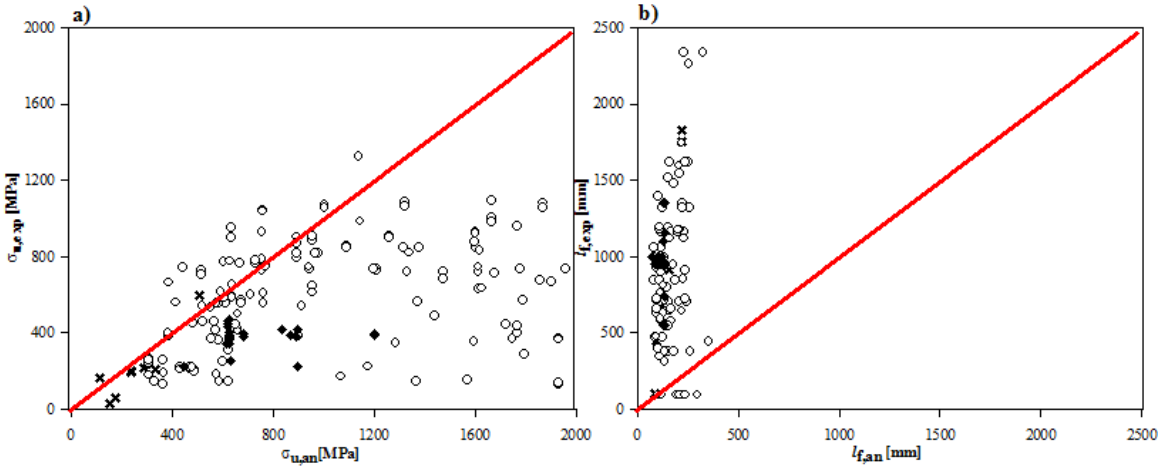

Figure A.8: Comparison between beam tests and code limitations (midspan debonding). a)CNR-DT200 stress, b)CNR-DT200 anchorage length.

Appendix B

Experimental Investigations

B.1 Flexural tests

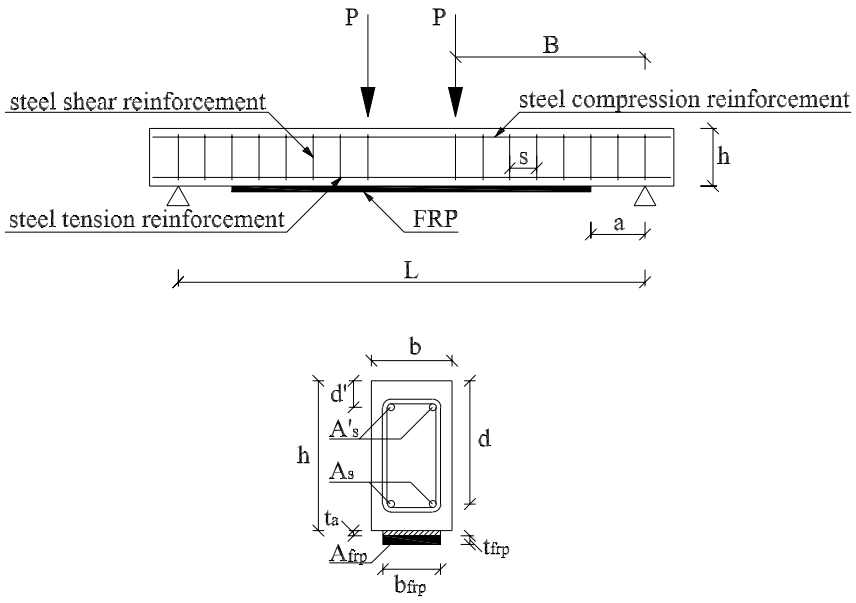

Figure B.1: Beam cross section and test setup.

Ritchie et al. (1991) [44] demonstrated the feasibility of reinforcing concrete beams externally using bonded plates of fiber reinforced plastic. The primary area of interest was the magnitude of increases of strength and stiffness of the beam provided by the bonded plates and the effect that the differing strength and elastic modulus of the plates had on these increases.

Sixteen beams were cast for the program. A standard ready-mix concrete was used, with a maximum aggregate size of 19mm, and a minimum compressive strength of 31MPa was specified. After eight beams were poured (Batch1 - Beams A,E,G,H,K,M,O,P), some water was added to the mix to improve workability (Batch2 - Beams B,C,D,F,I,J,L,N).

The steel reinforcement was chosen to approach the lower limit for an under-reinforced beam (minimum reinforced ratio A_{st}/bd is 0,0033, maximum ratio, 75 percent of balanced, is 0,0309, actual ratio used was 0,0067). This allowed the external reinforcement to be added without over-reinforcing the beam, which would lead to premature brittle failure of the concrete in compression. The dimensions of the beam were 152× 305× 2743mm. The span of the beam was limited by the length of the available FRP plates, since it was considered undesirable to try to splice the plates at this stage of the investigation.

The internal flexural reinforcement consisted of two no. 4 steel reinforcing bars (d=12,7mm) with 414MPa minimum yield stress. Tensile tests were performed on the reinforcing bars, and the values were used for theoretical predictions. Shear reinforcement consisted of D2.5 deformed steel bars every 102mm. The beam was overdesigned in shear (>100%) to avoid a brittle shear failure due to increased shear load on the strengthened beam. Although in many cases the load on the strengthened beams exceeded twice the design flexural ultimate strength, none of the beams failed in shear through the original cross section. Many, however, failed in local shear in the concrete, along the internal longitudinal steel.

The plates used in tests were as follows (beam designations in parentheses): A molded fiberglass standard pultruded fiberglass sheet (C,D,E,F); 0/90 deg molded fiber reinforced plastic (G); a molded fiberglass standard pultruded fiberglass channel $8\text{x}2^3/_{16}\text{x}^3/_8$ (H); 0/90 deg 65 percent glass/35 percent carbon fiber reinforced plastic (I); A spring-orientation glass fiber reinforced plastic (J,K); $0/\pm 60$ deg carbon fiber reinforced plastic (L); 0/90 deg carbon fiber reinforced plastic (M); unidirectional aramid fiber reinforced plastic (N); mild steel plate (O,P);

All the plates were subjected to longitudinal tensile tests to determine elastic modulus and ultimate strength.

Beam	Failure mode
A	Standard reinforced concrete beam failure steel yield, then concrete crushing.
B	Standard reinforced concrete beam failure steel yield, then concrete crushing.
C	Internal steel yield, shear failure through concrete and along reinforcing bar at plate end.
D	Internal steel yield, shear failure through concrete and along reinforcing bar at plate end.
G	Internal steel yield, shear failure through concrete and along reinforcing bar at plate end.
L	Internal steel yield, plate fracture in constant moment region.
M	Internal steel yield, shear failure through concrete and along reinforcing bar at plate end.
P	External and internal steel yield, large deflection, concrete crushing.

Table B.1: Failure mode for each beam(Ritchie et al. [44]).

Beam	Ultimate strength, (kNm)	Control beam strength (kNm)	Percent increase
A	33,3	33,	0,0
B	33,1	33,1	0,0
C	50,6	33,1	52,8
D	54,5	33,1	64,4
G	57,5	33,3	72,4
L	56,2	33,1	69,0
M	54,9	33,3	97,4
P	49,8	33,4	73,3

Table B.2: Failure mode for each beam(Ritchie et al. [44]).

The beams were tested in four-point bending over an 2438mm simple span with the load point 0,3m either side of the center. The beams were tested to ultimate load. Two beams without plates were tested as control specimens. Tab.B.1 and Tab.B.2 list the measured failure loads for each beams design tested, along with the failure mechanism.

The beams, however, failed, not in the maximum moment region, but at the end of the partial length plates. The strain in compression portion of the concrete never reached the crushing stage for any beam with an FRP plate bonded to it. Part of the reason for this is that the concrete was stronger than intended, ad it was able to withstand a higher compression force than originally anticipated.

Many plated beams failed through the concrete, with cracking initiating form the end of the plate, then proceeding at about 45 deg angle up to the internal longitudinal steel, then continuing horizontally through the concrete at the level of the reinforcing steel. The stress at the end of the plate decreased as failure initiated there, before failure could occur in the constant moment region. Attempts to reinforce the plate ends were only partially successful.

The internal steel yielded on most of the plated beams before failure. This could occur because the yield strain of the internal steel was much lower than the ultimate strain of the external plate.

It has been demonstrated that bonded plates of fiber reinforced plastic are indeed a feasible method of upgrading the strength and stiffness of a reinforced concrete beam. The light weight may be advantageous for installation, and the corrosion resistance should be useful under harsh environmental conditions.

The beams with externally bonded plates exhibited a desirable phenomenon in that the crack patterns shifted from several widely spaced and large width cracks to many more closed spaced narrower cracks. This could be advantageous in the serviceability of a structure, as it is always better to have a smaller, less noticeable cracks.

Saadatmanesh et al. (1991) [46] tested five rectangular beams (beams A through E). The cross section of rectangular beams was 455× 205mm. Each beam was 4,88m long and was supported on a clear span of 4,57m. To observe the effect of the original reinforcement ratio on the strength of upgraded beams, three different reinforcement ratio were used for the tension steel. Also, to investigate the effect of shear cracking and shear reinforcement, one beam (beam A) was underdesign for shear. The remaining beams were slightly overdesigned for shear to prevent premature shear failure so the flexural behavior could be observed throughout the loading up to failure.

All beams were strengthened with GFRP plate that were 152mm wide by 6mm thick and 4,26m long and bonded to their tension flanges. Ready-mixed concrete was used for all beams. The average compressive strength was 35MPa. The average

measured yield stress of the bars was 456MPa.

GFRP plate has an average modulus of elasticity of $37,23GPa$ and an average ultimate strength of $400MPa$.

Was used a two-component, rubber-toughened epoxy with a consistency similar to that of cement paste. According to the data supplied by the manufacturer, the lap shear strength of the epoxy with metal substrates ranged from 14 to 15MPa with a maximum elongation at failure of 40%.

It was difficult to maintain a perfectly uniform epoxy thickness throughout the length of the beam. However, on the average, the epoxy thickness was about 1,5mm.

All beams were simply supported on a clear span of 4,57m, and they were subjected to two concentrated loads symmetrically placed about the midspan. The loading points were 0,61m apart. The beams were incrementally loaded to failure.

The beam A was reinforced with three no.8 (d=25mm) tension bars and two no.4 (d=13mm) compression rebars. Even thought this beam was slightly underdesigned for shear, no major shear cracks or shear failure were observed throughout the loading. The failure was reached as a result of crushing of concrete in compression.

The beam B was reinforced with two no.8 (d=25mm) tension bars and two no.4 (d=13mm) compression rebars. The failure was caused by debonding of the composite plate and the beam just before reaching the crushing load of concrete. The debonding occurred suddenly and in a brittle manner; however, there was no major damage in the beam, and the beam could still carry load after debonding of the plate.

The composite plate for beam C was bonded while the beam was held cambered. The load was applied through two concentrated load points placed symmetrically about the midspan, 305mm apart. The beam was held in this position until the epoxy completely cured. The steel reinforcement in this beam consisted of two no.4 (d=13mm) tension rebars and two no.4 compression rebars.

The loading was applied until the beam failed as a result of sudden failure of concrete between the plate and longitudinal steel rebars. Plating significantly increased the yield and ultimate loads of the beam. Because the beam originally had a relatively small amount of reinforcement, the concrete in the beam could not be utilized efficiently.

Beam D had the same design parameters as those for beam C, except it had two no.8 (d=25mm) bars for tension reinforcement. This beam was also cambered in the same manner as beam C. This beam had been precracked prior to bonding of the composite plate. Cambering partially closed some of the cracks.

The beam failed as a result of the sudden failure of the concrete layer between the plate and rebars.

Beam E had no longitudinal steel, but shear reinforcement was provided at a spacing of 150mm. The beam was reinforced only with the composite plate exter-

nally bonded to the tension flange. Plating only slightly increased the load-carrying capacity of the beam.

The concrete did not reach its compressive strength because the beam failed at a load corresponded to a concrete strain well below the crushing strain.

The results of tests performed in this study indicate that significant increase in the flexural strength can be achieved by bonding GRFP plate to the tension face of reinforced concrete beams. Plating reduced crack size in the beams at all load levels. The successful application of this technique requires a careful preparation of concrete surface and the selection of a tough epoxy. Plating somewhat reduce the ductility of the beams. This reduction in ductility varies with the ductility of the original beam and must be considered in the design.

Triantafillou et al. (1992) [64] examined the influence of FRP plates on the failure mechanisms, the ductility and the stiffness of strengthened beams, and give the results of four-point bending experiments confirming their analysis.

Eight concrete beams were constructed and tested in four-point bending to study the effect of the FRP area fraction on the failure mechanism, ultimate moment capacity and stiffness of the strengthened member. Seven of the beams were strengthened with unidirectional CFRP plates with strength of 1450MPa and Young's modulus of 186GPa ; one beam was used as a control specimen.

Type I Portland cement with was used and the maximum size of the aggregate was 10mm. The average compressive strength was 35MPa and Young's modulus was 31,6GPa. Steel used had a yield strength equal to 517MPa.

Each beam had a cross-section of 76mm $\times$ 127mm and was 1350mm long. All beams were reinforced with two 4,6mm diameter bars; the effective depth was 111mm. The shear reinforcement consisted of 4,6mm diameter stirrups placed at 40mm spacing. The CFRP sheets were 1070mm long. The fibre-composite material consisted of high-modulus carbon fibres at a volume fraction of 65%, bonded together with an epoxy matrix. Each beam was bonded with a different CFRP thickness.

All the beams were loaded to failure, simply supported over a span of 1220m with equal point loads applied symmetrically with respect to the midspan at a distance of 305mm from each other.

Out of the eight beams tested, one failed by excessive yield of the steel reinforcement (this was the control specimen with ρ_{frp}=0), two by steel yield-FRP rupture and five by debonding due to peeling-off of the composite. Tab.B.3 lists the measured failure loads for each beams design tested, along with the failure mechanism.

The peeling-off debonding failure took place in the epoxy adhesive used to bond the CFRP to the concrete.

Strengthening of concrete beams with externally bonded composite sheets appears to be a feasible way of increasing the load-carrying capacity and stiffness

ρ_{frp}	Failure load (kN)	Failure mechanism
-	$8,59$	Under-reinforced RC beam
$0,0009$	$13,16$	Steel yield-FRP rupture
$0,0013$	$17,27$	Steel yield-FRP rupture
$0,0043$	$29,56$	Debonding (FRP peeling-off)
$0,0059$	$30,50$	Debonding (FRP peeling-off)
$0,0059$	$27,90$	Debonding (FRP peeling-off)
$0,0126$	$37,33$	Debonding (FRP peeling-off)

Table B.3: Measured failure loads for FRP-strengthened beams (Triantafillou et al. [64]).

characteristics of existing structures.

The testing program in Sharif et al.'s research (1994) [50] demonstrated the feasibility of strengthening structurally deteriorated concrete beams using externally bonded FRP plates.

A total of ten reinforced concrete beams 150× 150× 1250mm were cast, with the main steel reinforcement ratio selected to insure under-reinforced behavior under loading (the reinforcement ratio was 0,0098).

The internal reinforcement consisted of two 10mm diameter bars for the tension steel and two 6mm diameter bars spaced at 60mm center to center. The beams were overdesigned (>200 percent) in shear to avoid a brittle shear load in damaged beams after repair.

Ready mixed concrete was used for all beams. The average compressive strength was 37,7N/mm^2. The yield stress for the steel reinforcing bar was 450MPa.

The composite fiberglass reinforced plastic FRP material consisted of three layer of woven roving fiberglass embedded in a plastic matrix.

All beams were simply supported on a clear span of 1180mm and subjected to two concentrated loads. To define the preloading condition of the damage beams, one control beam was tested to failure for evaluating cracking, yielding and ultimate loadings. Another control beam was loaded to a 10mm central deflection, unloaded, then reloaded to failure. Similar behavior was noticed for both control beams up to failure.

Three FRP plate thicknesses were used: 3,2,1mm. The glue layer thickness was controlled using metallic spacers of 1mm in diameter.

As reported in Tab.B.4, the yielding and ultimate strength of the beams are increased relative to the control beam, and there is also a reduction of the ductile behavior for the repaired beams relative to the control beam. Beam P1 developed its flexural strength by rupturing the FRP plate and produced the highest ductility

Beam designation	Plate thickness	At yield		At ultimate		
		Load (kN)	Deflection (mm)	Load (kN)	Deflection (mm)	Ductility index
CB	-	35	5,1	53	17,6	3,5
P1	1	50	5,4	67	17,4	3,2
P2	2	53	6,0	68	14,1	2,4
P3	3	59	5,4	66	7,0	1,3

Table B.4: Experimental results(Sharif et al. [50]).

index of all the beams. The premature failure for Beam P2 and P3 was due to plate separation at the plate curtailment. The failure mechanism has been shown to be dependent on the plate thickness. For relatively thin plates, the shear and normal stresses at the end of the FRP plate are low, and for a sufficiently under-reinforced beam, the beam will fail by rupturing of the plate. As the plate thickness is increased, however, the shear and normal stresses developed at the end of the plate will increase and result in premature failure by virtue of plate separation accompanied by local shear failure in the concrete along the internal longitudinal steel. This can be referred to as concrete rip-off failure.

Based on the experimental investigation, the following conclusions can be made: the shear and normal stresses at the plate curtailment increase with increasing FRP plate thickness, leading to premature failure by plate separation and concrete rip-off; the beams developing their flexural capacities provided enough ductility despite the brittleness of FRP plates, indicating effectiveness of FRP plates for use a means of external fortification for underdesigned RC beams.

Four extensively instrumented beams were tested by Spadea et al. (1998) [54]. All beams had the same overall cross-sectional dimensions, and they also had the same internal longitudinal reinforcement and stirrup arrangement. All of the beams were tested under four-point loading.

All of the beams were 140× 300mm in cross section and 5000mm long. The beams were reinforced with 2-16mm diameter bars at the tension and compression faces, and they were provided with stirrups of 4mm diameter at 150mm center-to-center spacing. The basic concrete beam without external reinforcement was designed to have sufficient shear strength so as to fail in flexure. The CFRP sheets were all identical in size, 80mm wide × 1,2mm thick, and were bonded to the tension face of the beam over a length of 4700mm, slightly short of the effective span of 4800mm. The epoxy adhesive thickness was maintained constant at 2mm throughout the length and for all of the beams. All of the beams were tested over an effective span of 4800mm with the loads applied at 600mm on either side of the

Beam	Concrete strength (MPa)	Ultimate load (kN)	Mode of failure
A3	29,5	57,2	Tension steel yielding; concrete crushing.
A3.1	35,6	74,8	Sudden and total loss of load capacity; explosive debonding of CFRP plate.
A3.2	29,6	98,8	Debonding of supplemental anchorage.
A3.3	30,5	98,3	Gradual slip of CFRP strip.

Table B.5: Ultimate loads and failure modes (Spadea et al. [54]).

midspan.

The concrete in the beams was designed for a mean 28 day cube strength of about 30MPa. The internal steel reinforcing bars were hot-rolled, high-yield strength with an average measured yield strength of 435MPa.

In Tab.B.5 are reported the ultimate load and the mode of failure for each beams tested. Beam A3 was the control beam with no external reinforcement. This beam was designed to fail in flexure. The remaining three beams A3.1-A3.3 were strengthened with single CFRP sheets bonded to the tension faces. Beam A3.1 had no external anchorages, and contained only the externally bonded plate. Beam A3.2 was provided with external end anchorages for the plates, and in addition, had other anchorages along the span of the beam. Beam A3.3 also had the external end anchorages, but in addition, extra anchorages, different from those of beam A3.2, were provided along the spam of the beam.Control beam A3 was, able to undergo extensive rotation, and as before, the provision of the CFRP plate alone at the tension face results in considerable reduction in rotation capability. Strengthening structural beam with the bonded CFRP plate at the tension face only can result in a significant degradation of structural behavior, and that the provision of adequate anchorages at the ends of the plates and at critical sections along the span can restore a major part of the lost structural properties of the original unplated beam. All of the strengthened beams have similar stiffness, higher than that of the unplated beam, in evaluating structural behavior, the moment-curvature curve is more critical and provides better evidence of structural rigidity than the load-deflection behavior.

The control unplated beam A3 failed at an ultimate load of 57,2kN in conventional ductile flexure with yielding of the tension steel, followed by crushing of the concrete in the compression zone. Beam A3.1 carried an additional 17,6kN prior to failure, but failed suddenly in a brittle manner, with the load capacity dropping substantially at the instant of failure, with occurred by explosive debonding of the CFRP sheet. Analysis of the measured strains in the internal tension steel and the external CFRP plate showed that loss of composite action in this beam occurred at

about 64kN of the ultimate load. Clearly, providing the plate in the tension zone alone was inadequate to ensure composite action right up to failure, and the brittle failure with sudden total loss of load capacity is unacceptable.

The end anchorages and the additional anchorages in beam A3.2 andA3.3 were designed to prevent the sudden debonding and loss of composite action observed in beam A3.1.The effectiveness of these external anchorages was proved in that both beams A3.2 and A3.3 exhibited a much more ductile behavior than that of the beam A3.1. Although the process of debonding was much less destructive to the overall structural behavior of the beam.

Ross et al. (1999) [45] cast twenty-four rectangular, under-reinforced concrete beams in 200x200x3050mm steel forms for the experiments. A concrete mix consisting of Type I portland cement and maximum aggregate size of 10mm diameter was used. The average 28-day concrete compressive strength for all beams tested was 54,8MPa. The beams were divided into six groups of four, according to the percentage of flexural reinforcement ρ. All flexural steel consisted of Grade 60 standard reinforcement bars having a yield strength of 410MPa. All beams have a nominal steel depth d of 152mm.

The beam groups, designated as 1 through 6, represent six different reinforcement ratios. To preclude the possibility of a shear failure, the beams were also provided with shear reinforcement in the form of no.3 (d=9,5mm) stirrups spaced at 102mm on center.

The CFRP plates used in this study were a three-ply uniaxial laminate, measuring 2740× 203× 45mm. The material classification for the CFRP is an AS4/1919 graphite/epoxy composite that is 60 percent graphite fiber by volume, having a room temperature 0 deg tensile modulus of 138GPa. The composite plates were bonded to the tension face of the concrete beams using a two-part epoxy mixed at a 1:1 ratio and cured at room temperature. In each of six groups, three beams were fitted with CFRP plates (designated as B,C,D), and the remaining beam was left as a control (designated as A). It is important to note that the cross-sectional area of composite A_{frp} for each beam fitted with a CFRP plate is constat at 90,3mm^2.

The 24 beams were tested in third-point bending over 2,74m simple span in a 445kN test frame. The two load point were offset 457mm from the midspan of the beam. All beams were statically tested to failure at a load rate of approximately 22,25N/sec.

Two basic failure modes were exhibited by the beams strengthened with composite plates. For the heavily reinforced beams (Groups 4, 5 and 6), failure (Mode I) was by crushing of the concrete in the compression zone accompanied by horizontal cracking in the tension zone in the vicinity of the tension steel. For the light-to-moderately reinforced beams (Groups 1, 2 and 3), failure (Mode II) occurred by delamination between the CFRP plate and the adhesive.

Beam No.	Peak load (kN)	Enhancement ratio R_E	Composite ratio A_{frp}/A_s	Failure mode
1A	26,7	-	-	-
1B	80,1	3,00	0,64	II
1C	71,2	2,67	0,64	II
2A	46,7	-	-	-
2B	97,9	2,10	0,35	II
2C	71,2	1,52	0,35	II
2D	80,1	1,71	0,35	II
3A	62,3	-	-	-
3B	109,03	1,75	0,23	II
3C	108,14	1,74	0,23	II
3D	108,58	1,74	0,23	II
4A	71,2	-	-	-
4B	107,64	1,51	0,16	I
4C	104,58	1,47	0,16	I
4D	111,25	1,56	0,16	I
5A	115,7	-	-	-
5B	146,85	1,27	0,12	I
5C	146,85	1,27	0,12	I
5D	145,52	1,26	0,12	I
6A	133,5	-	-	-
6B	169,1	1,27	0,09	I
6C	153,1	1,15	0,09	I
6D	153,1	1,15	0,09	I

Table B.6: Beam test results (Ross et al. [45]).

In an effort to quantify the strengthening effect attributed to the CFRP plate, an enhancement ratio R_E has been calculated for the beams. The enhancement ratio is defined as the ratio of the peak load for the composite beam to the peak load of the control beam (Series A) in each group.

The results of the experimental program, in Tab.B.6, clearly indicate that significant strengthening of reinforced concrete beams can be realized by bonding a relatively small amount of FRP to the tension face of the beam. The degree of strength enhancement attained appears to be depend on several factors: the composite ratio A_{frp}/A_s; the percentage of conventional tensile steel reinforcement ρ; the bond achieved between the FRP and the concrete. For the light to moderately reinforced beams in which the composite ratio in high, the strengthening effect is

most evident.

The Nguyen et al.'s (2001) [36] experimental program was designed to investigate the brittle failure modes with particular emphasis on the ripping of concrete and to investigate the composite action between the plate and the concrete beam. The plate length, steel ratio, and concrete cover thickness were varied to study their effects on the failure mode and the ultimate load of strengthened beam.

A total of 10 beams, as reported in Tab.B.7, of 120× 150mm cross section and 1500mm length that were divided into three series (A, B and C), were cast. All beams were overdesigned in shear to avoid conventional shear failure. Nine beams were strengthened with CFRP plates attached to the soffit while one was used as a control beam. The R6 (d=6mm), R10 (d=10mm), T20 (d=20mm) steel bars had yield stresses of 400, 384, 466MPa, respectively. The CFRP plate of 80× 1,2mm cross section had an ultimate tensile strength of 3140MPa and an elastic modulus of 181GPa. The manufacturer reported an elastic modulus of 12,8GPa for the adhesive used for bonding the CFRP plates to the beam soffit.

The control beam, CB1, failed by crushing of concrete with corresponding yield of the steel bars, at an ultimate load of 42,3kN. Beams A950, A1100, and A1150 bonded with different plate lengths terminated before the supports exhibited an almost linear load-deflection behavior until failure without yielding of the reinforcing steel. The ultimate load for these beams ranged from 56 to 59kN, with an increase of 33-40% over the unplated reinforced concrete beam.

Beam A1500, which was bonded with the CFRP plate over its entire length, failed at a much higher ultimate load of 118kN; an increase of 167% over the unplated section. The ultimate load was slightly higher than the predicted flexural capacity indicating that full composite action could be obtained by extending the CFRP plate beyond the supports. The beam exhibited uniformly distributed cracks along the bending zone and failed in flexure by crushing of concrete in the compression zone and delamination of the CFRP plate between the supports.

Beam B1, which was underreinforced, exhibited large shear cracks that initiated at the end of the plate and extended nearly to the top of the beam at a load of 40kN. The beam was considered to have failed prematurely in shear at this load level. Upon continued application of load, the steel bars snapped at a load of 49kN. This beam exhibited the largest increase in capacity due to the low flexural capacity of the unplated section. In comparison, Beam B2, which was overreinforced, showed a ripping crack at a load of 120kN. The beam continued to carry additional load, and failed at a load of 130kN by ripping of concrete along the plate. The increase in flexural capacity was a 26% for this beam.

Beam C5, C10 and C20 which were designed with thinner concrete covers than the other beams, exhibited a combined failure mode of shear and ripping. The failure loads of this series of beams were higher than the failure load of beam A1100, which

Beam No.	Strength of unplated beam P_0 (kN)	Ultimate load P_u (kN)	Increase over unplated beam ΔP (%)	Mode of failure
CB1	42,1	42,3	-	Flexural
Series A				
A950	42,1	56,2	33	Ripping off
A1100	42,1	57,3	36	Ripping off
A1150	42,1	58,9	40	Ripping off
A1500	44,1	118,0	167	Flexural
Series B				
B1	14,6	49,2	236	Shear
B2	103,0	130,1	26	Ripping off
Series C				
C5	48,3	71,0	47	Hybrid
C10	46,3	68,0	47	Hybrid
C20	42,1	63,0	49	Hybrid

Table B.7: Test Results (Nguyen et al. [36]).

had a similar plate length of 1100mm but with a larger cover.

CFRP-strengthened beams showed considerable enhancement of strength. The higher increase was found on beams that failed either in flexural mode (increase of 167% for beam A1500) or when the original beam was severely underreinforced (increase of 236% for beam B1). The beams, which exhibited brittle ripping and hybrid failure modes, showed smaller increases with increases ranging from 26% to 49%. It is important to note that both the steel bars and CFRP plate were still in the elastic range during the onset of the ripping failures. Only two beams, control beam CB1 and beam A1500 exhibited plastic failure with concrete failing in compression and steel yielding.

The aim of the Rahimi et al.'s research (2001) [40] was to investigate the suitability of FRP for externally bonded reinforcement of concrete structures subjected to flexural loading. Aspects of adhesive bonding technology, composite materials, and numerical modeling were used and applied to plate bonding technology.

The concrete mix providing a compressive strength of about 50MPa after 28 days.

The beams were 200 × 150 × 2300mm, and they were typically 4-6 months old at the time of strengthening. Glass FRP, carbon FRP and mild steel external reinforcement were used. Two replicate beams of Type A (A8 and A9) were incrementally loaded to 20kN, then unloaded, to cause cracking in the concrete and yielding in the

tensile rebars. This preload represented 80% of the ultimate strength of unplated Type A beams, resulting in some permanent flexural deformation. These beams were externally strengthened with 0,8mm CFRP plates.

Prepeg tapes with unidirectional fiber reinforcement were chosen for their versatility and ease of shaping for experimental purposes.

The FRP plates were 1930mm long, similar to the clear distance between the support (1950mm), and 150mm wide, which covered the distance between the tensile rebars (140mm). The thickness of the CFRP laminates was varied from 0,4mm (2 ply) to 1,2mm (6 ply). Due to the relatively low modulus of GFRP, the chosen thickness of these laminates was 1,8mm (12 ply).

For comparison, four beams (two each of Types B and C) were strengthened with 3mm thick mild steel plates of the same lengths and widths of the composite plates.

Sikadur 31 plate bonding adhesive, a two-part, room temperature curing epoxy adhesive was selected.

The beams were tested in four-point bending, being simply supported on a pivot bearing on one side and a roller bearing on the other, over a span of 2100mm. Identical bearing pads were placed at the loading points on top of the beams.

For the three types of unplated beams tested, the strength was limited to the maximum compressive fiber strain in the concrete, which was around 3500μ *varepsilon*. This was validated experimentally, showing concrete crushing at the ultimate load levels.

The effectiveness of bonded external reinforcement becomes apparent when comparing the performance of a 2-ply CFRP-plated type B beam with an unplated type C control beam. The amount of conventional reinforcement used in type C beams was 1,68%, compared with 0,65% in type A/B beams. Thus even with a relatively small amount of bonded external reinforcement added to type B beams, comparable performance is obtained with a beam containing a relatively high percentage of conventional reinforcement.

For a given load, the GFRP plates (12-ply and 1,8mm thick), used on the type B and C beams, strained by the same amount as a 0,5mm CFRP plate. The ultimate loading capacity of the type B GFRP-plated beams was 60kN, compared with 29kN for the control beams. It should be noted that the elastic modulus of the CFRP used was around 120GPa, compared with 36GPa for GFRP. The strain to failure of GFRP is higher than CFRP, although its ultimate strength is some-what lower.

No adhesion failures took place at the bonded interfaces. Plate detachment, when it occurred, resulted typically in a layer of adhesive and cement paste still being attached to the FRP surface.

As reported in Tab.B.8 and Tab.B.9, the failure of strengthening type A/B beams was characterized by either classical shear failure of the beams or concrete

cover failure/plate debonding at ultimate load levels. It should be remembered that the type A beams were relatively underreinforced in shear, but although some exhibited shear failure, their failure loads were above the theoretical values.

Bonded external reinforcement contributes to the shear load carrying capacity of strengthened beams. The shear load in a plate-bonded beam is probably carried by the full depth of concrete and not limited to the area of the tensile rebars. Moreover, aggregate interlocking will play an important contribution to shear stress transfer in a cracked beam. Type B beams had sufficient shear reinforcement to prevent premature shear failure; thus, there was no classical shear failure in these beams. Shear cracks appeared at relatively high load levels, but they did not extend to the compression face and no concrete crushing took place.

The failure pattern of the type B beams changed as the plate thickness increased from 0,4mm (2-ply CFRP) to 1,2mm (6-ply CFRP). There were fewer cracks in the 2-ply CFRP-plated beam, and these did not develop as far as the plate ends: also there was no concrete cover failure.

Beams No.	Type of external reinforcement and plate thickness	Cross-sect. area plate (mm^2)	Ultimate load (kN)	Midspan deflection (mm)	Type of failure
A1	None	-	26,2	48,3	CC
A2	None	-	26,2	60	CC
A3	None	-	26,6	49,7	CC
A4	CFRP laminate, 4-ply (0,8mm)	120	61,9	32	S/C/P
A5	CFRP laminate, 4-ply (0,8mm)	120	63,2	31,3	S/C/P
A6	CFRP laminate, 6-ply (1,2mm)	180	59,4	23,1	S/C/P
A7	CFRP laminate, 6-ply (1,2mm)	180	70,6	27,9	S/C/P
A8	CFRP laminate, 4-ply (0,8mm) beams preloaded to 20kN before plating	120	65,2	31,9	S/C/P
A9	CFRP laminate, 4-ply (0,8mm) beams preloaded to 20kN before plating	120	63,9	33	S/C/P
A10	CFRP laminate, 4-ply (0,8mm) beams preloaded to 20kN before plating	120	67,5	41,2	S/C/P
A11	CFRP laminate, 4-ply (0,8mm) beams preloaded to 20kN before plating	120	69,4	40	S/C/P

Table B.8: Load-deflection data for concrete test beams (Rahimi et al. [40]).

Beams No.	Type of external reinforcement and plate thickness	Cross-sect. area plate (mm^2)	Ultimate load (kN)	Midspan deflection (mm)	Type of failure
B1	None	-	29,2	54,6	CC
B2	None	-	28,4	40,4	CC
B3	CFRP laminate, 2-ply (0,4mm)	60	55,2	38,7	C/P
B4	CFRP laminate, 2-ply (0,4mm)	60	52,5	38,1	C/P
B5	CFRP laminate, 6-ply (1,2mm)	180	69,7	30,3	C/P
B6	CFRP laminate, 6-ply (1,2mm)	180	69,9	28,3	C/P
B7	GFRP laminate, 12-ply (1,8mm)	270	59,1	33,3	C/P
B8	GFRP laminate, 12-ply (1,8mm)	270	61,6	34,2	C/P
C1	None	-	58,5	34,9	CC/P
C2	None	-	56,3	24,7	CC/P
C3	CFRP laminate, 2-ply (0,4mm)	60	74,9	25,5	CC/P
C4	CFRP laminate, 2-ply (0,4mm)	60	77,2	30,8	CC/P
C5	CFRP laminate, 6-ply (1,2mm)	180	103,1	32,4	CC/P
C6	CFRP laminate, 6-ply (1,2mm)	180	101,4	31,4	CC/P
C7	GFRP laminate, 12-ply (1,8mm)	270	87,1	34,4	CC/P
C8	GFRP laminate, 12-ply (1,8mm)	270	86,7	31,3	CC/P

Table B.9: Load-deflection data for concrete test beams (Rahimi et al. [40]).

Fanning et al. studied (2001) [23, 24], the effect of different $B/(B-a)$ ratio (% of shear span plated) on the ultimate response of eight 3,0m RC beams is studied in an attempt to develop a relationship between the bonded length of a plate within the shear span and the load at which failure by plate peel-off occurs.

Ten three meter long beams, 155mm wide by 240mm deep, were selected for the test programme to negate any effects of scale in this sensitive region. Three 12mm diameter steel bars are included in the tension zone with two 12mm steel bars as compression steel. Ten shear links, formed from 6mm mild steel bars, are provided at 125mm centers in the shear spans. Two unplated beams formed a control set, (B1 and B2), and four different plate lengths were used in subsequent pairs of beams, (B3 to B10). Each of the beams was simply supported with a clear span of 2,8m and loaded symmetrically and monotonically, under displacement control, in four point bending, with point loads 0,3m either side of the mid-span location, to failure.

The Sika Carbodur System, comprising CFRP composite material plates and a two-part epoxy resin adhesive, provided the external reinforcement on the strengthened beams. The Carbodur S plates, with a longitudinal modulus of elasticity of 155GPa, a lower bound tensile strength of 2400MPa with an associated strain to failure of 1,4%, were used in these tests. These plates, consisting of unidirectional carbon fibres embedded in an epoxy matrix, were 1,2mm thick, 120mm wide and were manufactured by a pultrusion process.

Beams B3 and B4 had plates bonded along their full length. These plates were thus continuous under the support locations with the support locations anchoring the plates to prevent plate peel-off. Beams B5 and B6 had 2,03m long plates centered on the mid-span resulting in 65% of the shear spans being plated, and beams B7 and B8 had 1,876m plates, (resulting in 58% of the shear spans being plated), similarly arranged. The shortest applied were 1,7m long, and placed centrally on beams B9 and B10.

The unstrengthened beams, B1 and B2, failed at 68,3kN and 67,9kN respectively. These beams exhibit a large amount of ductility under loading and the mode of failure is characterized by initial yielding of the tensile reinforcement (at approximately 50 to 54kN) followed by total collapse once the neutral axis of strengthened beams rises above the compression steel.

The ultimate strength of beams B3 and B4 were 118 and 111kN respectively. The additional tensile stiffness provided by the strengthening plates keep the neutral axis of the beam lower in the section thereby allowing greater bending moments to be sustained. Although consistently stiffer and stronger, the strengthened beams are less ductile and the mode of failure was characteristic of a shear failure in the shear span of the beam.

Therefore provided sufficient anchorage is provided at the plate ends these test results demonstrate that the additional plates provide additional flexural capacity

such that the limiting strength condition becomes the shear capacity of the beam. The beam strength has been increased by approximately 70% of its original capacity although it is noted that the mode of failure is no longer ductile.

Beams B5 and B6, which were strengthened with 2,03m long plate lengths, reached loads of 100 and 103kN respectively. Beams B7 and B8, 1876m long plates, failed at loads of 97 and 64kN respectively. Finally beams B9 and B10 with 1,7m plates failed at 64 and 82kN. The mode of failure for each of these beams was due to plate peeling. Failure was sudden and catastrophic in all cases, and no indication of imminent failure was evident from the load versus deflection response.

The loss of strength between beams with anchored plates B3, B4 and B5, B6 is of the order of 10% for both beam tested. Beam B7 saw a further albeit small decrease in ultimate capacity, whereas the similarly plated B8 failed before reaching the ultimate load recorded for the control specimens. A further reduction in plate length to 1,7m shows a significant loss in beam strength with beam B9 failing at a lower ultimate load than control beams.

The test programme clearly demonstrates that the potential for CFRP composite materials in strengthening schemes is significant. The strength of the 3,0m reinforced concrete beams, in four point bending, were increased by up to 70% of their original value while the stiffness was increased by approximately 40%. Examination of the crack distributions under loading indicated that the size and distribution of cracks in the strengthened beams were also less significant than those recorded at equivalent load points in the control beams.

Beam No.	Plate configuration	% of shear span plated	Plate peel-off load (kN)	Ultimate load (kN)	Mode of failure
B1	No plate	0,0	-	68,3	Flexure
B2	No plate	0,0	-	67,9	Flexure
B3	Anchored plate	-	100	111	Shear
B4	Anchored plate	-	100	118	Shear
B5	2,03m	65	77,3	100	Plate peel-off
B6	2,03m	65	77,3	103	Plate peel-off
B7	1,876m	58	68,4	97	Plate peel-off
B8	1,876m	58	68,4	64	Plate peel-off
B9	1,7m	50	58,8	62	Plate peel-off
B10	1,7m	50	58,8	82	Plate peel-off

Table B.10: Summary of beam test results (Fanning et al. [23]).

It is also evident from the test data (Tab.B.10) that the mode of failure and the load at which failure occurs is dependent on the length of plate and whether or not the plate is anchored. The largest strength enhancement is achieved with anchored plates and the resulting full composite action between the existing beam and the strengthening plates allows classical reinforced concrete design calculations to be extended to reliably predict the ultimate load and mode of failure.

The effectiveness of the external plates in strengthening the reinforced concrete beams was found to reduce as plate lengths were shortened. In the case of strengthened systems having plates bonded over 65% of their shear spans, strength enhancements of 50% over the strength of the percentage of the shear span which was plated was reduced to 50% the strength enhancements, for one beam of a pair, was 22% with the second beam failing at a lower load than the unstrengthened system.

The primary goal of the Breña et al.'s research project (2004) [9] was to evaluated the effects of laminate configuration on the behavior of strengthened reinforced concrete members.

Thirteen small-scale specimens were fabricated and tested in the laboratory to evaluate the behavior of CFRP-strengthened beams. Two were used as control specimens and the remaining 11 were strengthened using different number of CFRP layer. All the beams had a 102mm square cross section and a 914mm total length. Shear reinforcement consisted of no. 6 gauge wire spaced at 51mm within the shear span. The shear reinforcement was designed to avoid shear failure of the strengthened specimens prior to reaching flexural strength. Two patterns (types I and II) of reinforcing steel were used in the specimens to examine the effect of area of existing reinforcement on the behavior of the beams. Type I consisted of one no. 3 bar (d=9,5mm) used as tension and compression reinforcement, and type II consisted of two no. 3 bar top and bottom. The longitudinal reinforcement had a nominal yield stress of 435MPa. The calculated reinforcement ratios (A_s/bd) for the beams with reinforcing type I and II were 0,0078 and 0,0156, respectively.

The specimens were cast in groups of six using three different batches of concrete. The concrete compressive strength was determined for each specimen by testing three 102mm diameter by 203mm high concrete cylinders at the time of testing.

The configuration of composites that have been used in practice to strengthen beams have been very diverse, including varying the number of layers of composites. The composite laminates were attached on the bottom face of specimens. Laminates with different numbers of layer and widths were formed and applied to the specimens using this configuration. Eight specimens were strengthened using a unidirectional fiber composite system applied by the wet-layup procedure (composite system MB). Only specimen A6-1 was strengthened using a unidirectional carbon fiber plate fabricated through pultrusion (composite system SK). The length of the laminates was 762mm for all specimens and the fibers were oriented parallel to the longitudinal

axis of the beams to provide the maximum efficiency of the composites for flexural strengthening.

The specimens were simply supported at the ends and were loaded using two concentrated loads with a 152mm spacing. The loading points were located symmetrically about the centerline of the beams. The clear span of the beams was equal to 813mm. The tests were conducted in a 1780kN Tinius Olsen universal testing machine by applying the loading monotonically to failure. A 220kN load cell was positioned between the machine cross head and the specimens to monitor the total load during testing.

The Tab.B.11 shows the general trends in the behavior of the strengthened specimens were similar for the different specimens. Specimens exhibited limited deformation and cracking before reaching the load corresponding to yielding of the reinforcement. All specimens failed after yielding of reinforcement and sustained different deformation depending on the total area of steel and CFRP composites that was used as tensile reinforcement. All the specimens failed in one of two modes associated with the interaction between the composites and the concrete surface.

Failure of specimens from all other groups involved a combination of debonding and concrete cover separation. The amount of concrete cover that was lost after failure varied for each specimen, ranging from only a wedge-shaped portion to a significant percentage of the concrete cover between the support and the first load point. In most cases the end region of the composites separated from the surface without pulling the concrete cover with laminate.

The effect of composite area in load-deflection behavior of the beams was evaluated by varying the number of layers of a 51mm wide laminate. Groups o specimens with equal reinforcement ratios (type I or II reinforcement patterns) but various number of composite layers (1-3 layers) were used. Therefore the comparisons presented here are restricted to specimens where the composites were positioned on the tension face of the specimens. Specimens A1-I, A2-I and A3-I represented the group with type I reinforcement while specimens A1-II, A2-II and A3-II formed the group with type II reinforcement. The yield load and the ultimate load increased in the specimens as the number of layer was increased. On the other hand, the yield displacement did not change significantly while the ultimate displacement decreased with increasing number of composite layers. Finally, there was an increase in the stiffness of the specimens prior to yielding with increasing number of layer of CFRP.

The effects of using different composite widths on the load-deflection behavior of specimens was evaluated by comparing beams with equal areas of steel reinforcement and equal ares of composite laminates. It can be observed that the main difference in the behavior was that specimens with larger composite widths has increased deformation capacities. Because the beams with wider laminates were capable of reaching higher deformation, the composites developed higher forces as the curva-

ture in the beams increased translating into a higher load. The larger deformation capacity may be attributable to the lower interface shear stresses associated with larger contact areas between the composites and the concrete surface characteristic of specimens with wider laminates. In contrast with specimens with varying ares of CFRP composites with the same width, the change in preyield and postyield stiffness of the specimens was negligible. Similar trends were observed in the comparisons for specimens A2-I and A5-I, or A2-II and A5-II where the composite widths changed from 51 to 102mm.

Specimen identification	Yield load		Capacity	
	Deflection (mm)	Load (kN)	Deflection (mm)	Load (kN)
Control I	4,04	16,0	13,21	21,6
Control II	4,78	26,3	12,45	36,0
A1-I	4,65	20,0	12,04	27,9
A1-II	5,72	31,0	9,80	40,2
A2-I	4,60	24,5	7,26	31,4
A2-II	5,26	36,2	8,92	44,5
A3-I	5,72	31,9	7,95	39,0
A3-II	5,23	39,4	7,29	48,0
A4-I	5,18	28,7	7,80	36,8
A4-II	5,87	41,0	9,27	52,5
A5-I	5,74	27,0	10,46	35,2
A5-II	5,69	37,9	10,49	48,9
A6-I	5,41	34,8	5,41	34,8

Table B.11: Summary of experimental parameters measured in tests (Breña et al. [9]).

The Pham et al.'s study (2006) [39] focuses on debonding failure in reinforced concrete beams with carbon fiber reinforced polymer composite bonded on the soffit using the wet lay-up method.

In the experimental program, a total of 18 RC beams were constructed. Two were control beams and sixteen were retrofitted with CFRP fabrics using a wet lay-up method.

The beams were divided into two main groups. The E group had ten beams retrofitted with a relatively thick layer of CFRP (six layer or more). The S group had six beams retrofitted with two layers of CFRP. Two identical beams were manufactured for each configuration and denoted as "a" and "b". All beams in experiment program were tested under four-point bending.

The CFRP fibers used were MBrace CF 130 fibers, which are also known as S&P C-sheet 240. They are supplied in undirectional tow sheets of 300mm width. The nominal thickness, based on the total thickness of fibers only in a unit width, was reported to be 0,176mm. Mbrace Primer was used to improve the bonding of the composite to the substrate. It is a two-part epoxy product with low viscosity and 100% solids content. It has the ability to penetrate the substrates and to bond to a saturated surface dry concrete surface. The resin used was MBrace Saturant, which is a two-part epoxy with 100% solids content used to both impregnate the fibers to form a composite and bond it to the primed surface.

Tab.B.12 reports the failure load and failure mode for each beams tested. Beam C1a failed by typical steel yielding followed by the secondary compression failure of concrete. Beam E1a failed by end debond. Flexural vertical cracks were observed first in the pure bending region of the beam. As load increased, shear cracks became visible in the shear span. At 39kN shear load level, a shear crack originating from the CFRP composite end was observed. The shear cracks widened progressively as the load increased. The portion of the end shear crack in the concrete cover layer became more inclined and finally joined the adjacent shear crack. At 59kN, this crack opened further and about 100mm of the composite was separated from the concrete. The crack propagated further into the shear span until the load reached a peak of 71kN.

Beam S2a failed by intermediate span debond. The tensile steel in this beam yielded at around 65kN. Flexural and flexure-shear cracks were clearly visible after that. A wide flexural shear crack was observed under the load point and delamination of the laminate from concrete was initiated at its tip as the shear load reached 78kN. This was followed by gradual delamination of the composite from the beam along the bond surface toward the beam end. The load continued to increase to a peak of 80,4kN, when the concrete cover near the tip of the flexure-shear crack broke from the beam leading to complete separation of the composite from that location to the steel clamp.

Beam S1a failed by a combination of intermediate span debond and end debond. At ultimate, concrete fracture occurred simultaneously from the unclamped end of the composite and from the tip of a wide flexure-shear crack near the middle of the shear span. Stress transferred and concrete cracking propagated toward the middle of the beam along the tension reinforcement level.

Designation	Failure modes	P_{exp} (kN)
Ca	Concrete crushing	54,4
Cb	Concrete crushing	53,9
E1a	End debond	70,7
E1b	End debond	74,6
E2a	End debond	51,4
E2b	End debond	53,4
E3a	End debond	66,0
E3b	End debond	65,2
E4a	End debond	79,0
E4b	End debond	61,2
E5a	End debond	63,3
E5b	End debond	63,2
S1a	Intermediate span and end debond	73,8
S1b	Intermediate span and end debond	74,5
S2a	Intermediate span debond	80,4
S2b	Intermediate span debond	74,5
S3a	Intermediate span debond	60,3
S3b	Intermediate span and end debond	60,2
E3b2	End debond	60,0

Table B.12: Experimental program results (Pham et al. [39]).

Benjeddou et al. (2007) [6] casted eight type of RC beams (120 × 150 × 2000mm). One beam form each type of concrete is considered as a control beam, without carbon fiber laminates. The remaining beams were damaged with a fixed damage and then repaired by bonding carbon fibers laminates in their tensile face by using an epoxy resin. Three sets of beams were tested in this study, two control beams, the beam RB1 (not damaged but reinforced directly), and four damaged and repaired bemas with different amounts of carbon fibers reinforcement by changing the damage degree, the width of laminate, and the concrete class. The length of all laminates used to repair the damaged beams is 1700 mm. Finally, all beams were tested under four point bending. The details of the experimental program were described in Tab.B.13.

Beam Reference	f_c (MPa)	D (%)	b_{frp} (GPa)	Failure load (kN)	Deflection at failure (mm)	Failure modes
CB1	21	-	-	21,41	12,86	Steel yielding
CB2	38	-	-	23,92	13,50	Steel yielding
RB1	21	0	100	40,11	9,02	Peeling off
RB2	21	80	100	37,66	8,65	Peeling off
RB3	21	90	100	32,10	9,87	Peeling off
RB4	21	100	100	30,75	19,50	Peeling off
RB5	21	90	50	30,10	13,50	Interfacial debonding
RB6	38	90	100	37,37	10,50	Peeling off

Table B.13: Materials and results (Benjeddou et al. [6]). D= damage degree

Two types of concrete have been caste: a C21 concrete having an average compressive strength of 21MPa and a C38 concrete having an average compressive strength of 38MPa. For all concrete test beams, standard deformed reinforcement steel bars with a characteristic strength of 400MPa and an elastic modulus of 200GPa, were used for the longitudinal reinforcement: two high yield steel bars of 10mm diameter were used in the tensile face and two high yield steel bars of 8mm diameter were used in the compressive face. Mild steel bars of 6mm diameter (stirrups) with a characteristic strength of 235MPa and an elastic modulus of 200GPa were used for the shear reinforcement.

Twenty-eight days after concrete hardening, six beams were damaged at different damage degree. Then, these beams were repaired using unidirectional carbon fibers laminates "SIKA CARBODUR LAMELLE". Five beams were repaired with S1210 having 100mm width and one beam was repaired with S1205 having 50mm width. The carbon fibers laminates were bonded by using the epoxy resin SIKADUR 30 COLLE with an elastic modulus of 12,8GPa. The thickness of the two types of

laminate is 1.2mm, the Elastic modulus is 165GPa and the the tensile strength is equal to 2800MPa. All beams were tested in four-point bending under displacement control. The beam supports consisted of a pin support and a roller support at the two ends. The outer loading span was 1800mm and the inner loading span was 600mm. The damaged beams were precracked also by this machine.

For all repaired beams, the authors observed two failure modes in the concrete structures: peeling off and interfacial debonding. The peeling off was observed for all reinforced beams with the laminate width of 100mm and the interfacial debonding was observed for all reinforced beams with the laminate width of 50mm. From these observations, the authors can conclude that the width laminate affects the failure modes of the repaired RC beams. For a larger width, the failure that took place by peeling off is explained by the fact that the contact between the laminate and the concrete is strong enough so that no debonding occurs, while for smaller width this contact does not allow good adherence.

Finally, the authors noted that the mechanical behavior of the repaired beams changed from elastoplastic to elastic behavior. The authors conclude that for any damage degree the repairing of RC beams by using CFRP laminates is effective and that the performance of the repaired beam is mainly attributed to the higher mechanical characteristics of the CFRP laminates. The increase of laminate width contributed to a small increase of a load capacity (from 140% for RB5 to 150% for RB3), but contributed also to a significant increase of rigidity (from 137% for RB5 to 189% for RB3). For any concrete class, the CFRP laminates added about a half of the load capacity.

Esfahani et al. (2007) [22] investigated the flexural behavior of reinforced concrete beams strengthened using CFRP sheets (E_{frp}= 237GPa, f_{frp}= 2845MPa). The effect of reinforcing bar ratio ρ on the flexural strength of the strengthened beams is examined. Twelve concrete beam specimens with dimensions of 150mm width, 200mm height, and 2000mm length were manufactured. The design compressive strength of 25MPa was used. Different sizes od reinforcing bars, 8, 10, 12, 16 and 20mm were used in specimens (f_y= 350, 365, 400, 406, 350MPa, respectively). For each bar size, three samples were tested under tension. The adhesive used for applying the CFRP sheet on the concrete surface was hand-mixed epoxy.

The dimensions of the specimens represent a model of approximately 1/2 scale of an actual RC beam designed and constructed. These specimens fall in the category of slender beams with a span to depth ratio of 10 which are expected to fail in flexure. The reinforcing bar ratios in the beams were approximately 30%, 60% and 80% of the tensile reinforcement balanced ratio, ρ_b. At the top of the beams, two 10mm diameter deformed bars were used in all specimens. Plain bars with 8mm diameter were used as transverse reinforcement. All specimens were provided with adequate transverse reinforcement to prevent shear failure. The dimensions and the

Beam Reference	b_{frp} (mm)	n. of layers	f'_c (MPa)	A_s (mm^2)	A'_s (mm^2)	d (mm)	d' (mm)
B1-12D-0L	0	0	25,2	226	157	166	25
B2-12D-1L15	150	1	25,2	226	157	166	25
B3-12D-2L15	150	2	25,2	226	157	166	25
B4-12D-3L15	150	3	25,2	226	157	166	25
B5-16D-0L	0	0	23,8	402	157	164	25
B6-16D-1L15	100	1	23,8	402	157	164	25
B7-16D-1L15	150	1	23,8	402	157	164	25
B8-16D-2L15	150	2	23,8	402	157	164	25
B9-20D-0L	0	0	24,1	628	157	162	25
B10-20D-1L10	100	1	24,1	628	157	162	25
B11-20D-1L15	150	1	24,1	628	157	162	25
B12-20D-2L15	150	2	24,1	628	157	162	25

Table B.14: Details of beam specimens (Esfahani et al. [22]).

details of reinforcement of specimens are shown and Table B.14. Nine specimens were strengthened using CFRP sheets. The number of layers and the width of CFRP sheets varied in different specimens. Three specimens were kept without strengthening as control specimens.

The displacement and ultimate strength, Pu, of the specimens are given in Table B.15.

Teng and Yao (2007) [60] presented an experimental study on plate end debonding failures in FRP-plated RC beams, which was conducted to develop a better understanding of the behavior and failure mechanisms for the subsequent development of a predictive model. The results of ten four-point bending tests and eleven three-point bending tests conducted on simply-supported FRP or steel plated RC beams are presented.

The experimental program consisted of ten tests on simply supported RC beams bonded with a soffit plate made of FRP or steel (one of the beams). All of the RC beams were designed to have the same nominal dimensions: 1700mm long, 150mm wide and 250mm deep, with a span of 1500mm. Moreover, the beams were each under-reinforced with the same high yield steel bars: two 10mm tension bars, two 10mm compression bars, and 10mm stirrups at 100mm centres. Beam CS-NS had only three stirrups, placed at the two ends and the mid-span of the beam, to hold the longitudinal reinforcement in position. To examine the effect of the thickness of concrete cover on the plate end debonding strength, nominal concrete covers of 10mm and 50mm to the tension bars were adopted for beams CS-C10 and CS-C50

Beam Reference	P_u (kN)	Displacement at failure (mm)	Failure modes
B1-12D-0L	49,46	23,34	1
B2-12D-1L15	61,45	10,20	2
B3-12D-2L15	70,94	9,14	3
B4-12D-3L15	74,44	11,60	3
B5-16D-0L	75,94	15,52	1
B6-16D-1L15	84,93	12,03	2
B7-16D-1L15	94,92	11,01	2
B8-16D-2L15	105,91	14,14	2
B9-20D-0L	96,42	16,24	1
B10-20D-1L10	106,32	16,54	2
B11-20D-1L15	108,91	19,14	4-a
B12-20D-2L15	113,41	19,35	4-b

Table B.15: Details of beam specimens (Esfahani et al. [22]). Type (1) Flexural failure by crushing of compressive concrete which could happen before or after yielding of tensile steel reinforcement; Type (2) Rupture of the FRP laminate after yielding of the steel in tension; Type (3) Cover delamination at the end of FRP (shear delamination of the concrete cover); Type (4) Debonding of the FRP from the concrete substrate: Type (4-a) inter-facial debonding induced by flexural crack: Type (4-b) interfacial debonding induced by flexural shear crack.

Beam Reference	f_{cu} (MPa)	f_y (MPa)	E_s (GPa)	f_{frp} (MPa)	E_{frp} (GPa)	Type of plate
CS	30,7	536	199	4114	256	C-W
CS-L1	36,4	536	199	4114	256	C-W
CS-L3	32,9	536	199	4114	256	C-W
CS-W50	39,5	536	199	4114	256	C-W
CS-W100	37,8	536	199	4114	256	C-W
CP	37,0	536	199	2800	165	C-P
SP	35,4	536	199	-	174	steel plate
GS	38,9	536	199	351	22,5	C-W
CS-C10	27,3	536	199	4114	256	C-W
CS-C50	38,8	524[a]	199[b]	4114	256	C-W

Table B.16: Details of beam specimens (Teng and Yao [60]). a. Shear reinforcement yield strength is equal to 536MPa; b. Shear reinforcement Elastic modulus is equal to 199MPa.

respectively, while a nominal cover of 30mm was adopted for all other beams.

The length of the soffit plate was the same for all beams, being nominally 850mm. The plate width varied from 50 to 148mm (Table 1). As the corners of the RC beams were slightly rounded by the casting mould, the nominal width of the soffit plates bonded onto beams CS, CS-L1, CS-L3, CP, SP, GS, CSC10 and CS-C50 was deliberately set to be less than the width of the RC beams to avoid the soffit plate curling up or not being properly bonded near the rounded corners of the beam. To examine the effect of the flexural rigidity of plated beam on debonding failure, soffit plates of different materials were used, including steel, CFRP and GFRP. The FRP plates included pultruded CFRP plates and CFRP/GFRP plates formed by the usual wet lay-up process.

The cube strength was averaged from the results of three 150mm cubes while the elastic modulus, Poisson's ratio and splitting tensile strength were averaged from the results of three cylinders of 100mm in diameter by 200mm in height. These data are given in Table B.16. Two different batches of high yield steel bars of 10mm in diameter were used in the test beams for both the longitudinal and the shear reinforcement, as the first batch was exhausted half-way through the experimental program. As a result, the second batch of high yield steel bars was used for the stirrups in beam CS-C50. The average yield strength, ultimate strength and elastic modulus from tensile tests of three coupons for each batch are listed in Table B.16. The tensile properties of the FRP materials are listed in Table B.16.

The specimens were tested under three-point bending test with the distance load from the support of 500mm. The plate end under investigation was positioned near

Beam Reference	P_u (kN)	Deflection at loading point (mm)	Failure mode
CS	81,5	4,61	CS
CS-L1	74,8	6,62	FF
CS-L3	78,5	3,35	CS
CS-W50	71,3	5,80	IC
CS-W100	80,8	6,42	CS
CP	76,0	2,54	CS
SP	68,3	2,38	CS
GS	82,0	9,04	IC
CS-C10	99,4	8,50	CS
CS-C50	82,9	8,36	FF

Table B.17: Summary of results of beam tests (Teng and Yao [60]). CS = cover separation, IC = intermediate crack debonding, and FF = flexural failure of unplated section of RC beam.

the support and is referred to here as the support plate end where the moment is almost zero. The beam segment near the midspan was clamped with the use of G-clamps.

Table B.17 summarizes the experimental results of the ten three-point bending tests. The failure process of all tests consists of the following three stages: (1) opening-up and extension of the old cracks induced in test A; (2) appearance and spreading of new cracks and (3) initiation and then propagation of a debonding crack leading to final debonding failure, or development of a major old crack leading to flexural failure of the debonded section or the unplated section of the beam.

Beam Reference	t_{frp} (mm)	b_{frp} (mm)	E_{frp} (GPa)	t_a (mm)	G_a (MPa)	f_c (MPa)	ε_{exp} (%)	T_{exp} (kN)
TFC	0,43	600	105	0,52	835	35	0,500	135,45
CFK	1,40	250	150	0,50	3900	35	0,225	118,12

Table B.18: Materials in segmental beams tests and results (Ramos et al. [41]). Where T_{exp} represents the tensile force in FRP plate.

Ramos et al.'s test (2006) [41] consists in two segmental beams previously tested up out failure by bending, which were repaired and strengthened. The beams had a total length of 7,20m, a box-type cross section, and consisted in seven prefabricated segments; five central segments with a length of 1,2m, and two end segments of 0,825m, with dry joint and multiple shear keys. The characteristic ultimate compressive strength of concrete was 40MPa.

First, the joints that were damaged in previous tests were repaired using a commercial repairing mortar with a compressive strength of 49MPa at 7 days. Then, the segments were prestressed by means of two $\phi 15$ external prestressing strands and the beam placed on two steel supports. The prestressing forces in each strand were 120 and 130kN, which correspond to a stress level in the steel after prestressing losses of 857 and 928MPa, respectively. The first beam was reinforced with three TFC (structural reinforcement system that consists of the adhesion of carbon fibers to a binding matrix) sheets of 200mm width, and the second beam was reinforced with five CFK (using unidirectional carbon fiber plates impregnated in an epoxy resin and partially prestressed) bands of 50mm width. Two centered load separated 2,40m were applied. In Tab.B.18 is reported the failure load for the two beams tested.

The failure mechanism was initiated by a localized diagonal crack in the area next to the joint of the segments. This crack propagated along the concrete fiber interface, causing the debonding of the fiber by a peeling process. The failure was by FRP debonding due to the opening of the central joints.

B.2 Shear tests

Chajes et al. (1996) [15, 14] presented the results to direct bond tests performed on joints consisting of composite materials plates bonded to concrete. The tests conducted focus on both bond strength and force transfer.

Test were performed using a single/lap shear test specimen and a constant bond length to evaluate the effect of surface preparation, type of adhesive, and concrete strength on average bond strength.

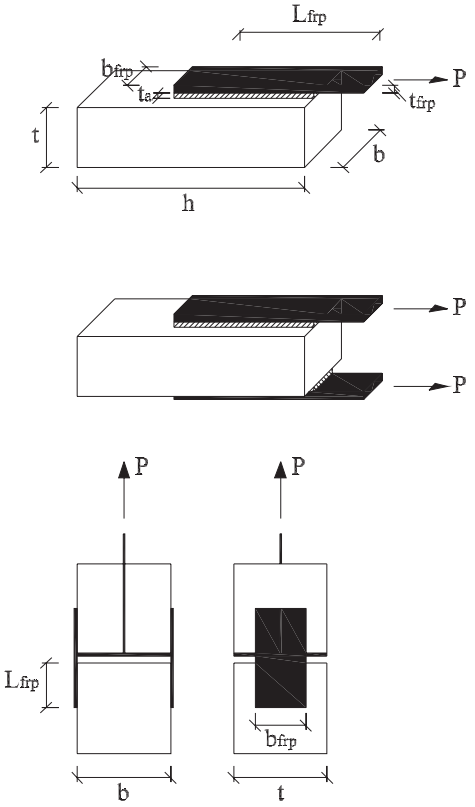

Figure B.2: Bond test specimens.

To study the strength of advanced composite material plates bonded to concrete, an adhesively bonded joint in single/lap shear was used. The test specimen consisted of a 25,4mm wide composite plate bonded to a concrete block (152,4 × 152,4 × 228,6mm) with a 76,2mm bond length. In the test setup, the concrete block was mounted to the bottom crosshead of a 133,5kN capacity testing machine with 9,5mm thick steel plates and four 12,7mm diameter steel all-thread at the corners of the plate. The top of the composite plate was clamped in a serrated grip that was free to rotate in all directions.

Each plate consisted of a 6-ply unidirectional laminate with an overall thickness of 1mm and an individual cured ply thickness of 0,17mm. The following material properties were found: E_1=108,38GPa, ε_{1ult} = 0,015, σ_{1ult}=1654MPa, ν=0,268,E_2=11,57GPa, ε_{2ult} = 0,003, σ_{2ult}=39MPa, ν=0,25, where 1 signifies the direction parallel to the fiber direction and 2 signifies the direction perpendicular to the fiber direction.

The blocks used measured 152,4 × 152,4 × 228,6mm and were fabricated using a concrete mix. It contained Type 1 portland cement, potable water, concrete sand, rice graven for the small aggregate, and pea gravel for the large aggregate. The concrete was internally vibrated, and the top was steel-trowelled.

Three sets of blocks, having compressive strengths ranging from 24,1 to 44,7MPa, were created.

To evaluated the effect of surface preparation on the bond strength, three different procedures were employed prior to adhering the composite plates. The surface preparations investigated were: no surface preparation; grinding with a stone wheel to give a smooth finish; mechanically abrading with a wire wheel to give a finish that would leave the aggregate slightly exposed.

The plate was then applied to the concrete block having a 76,2mm bond length and extending 152,4mm beyond the edge of the concrete block. The thickness of the adhesive layer was in the range of 1,58mm.

The load was increased monotonically to failure. For all the joints, the failures occurred as result of the concrete shearing directly beneath the bond surface. In all tests, failure was initiated due to shearing of the concrete just beneath the adhesive. A trend of increased bond strength with increased concrete strength can be seen.

The second set of tests, in which the bond length was varied, was performed to study the force transfer from the composite material plate into the concrete.

From the test results (Tab.B.19), the following conclusions can be drawn: surface preparation of the concrete can influence the ultimate bond strength. To achieve the best possible bond the concrete surface should be mechanically abraded or sand-blasted and a primer should be applied. The surface of the composite material plate should also be roughened through the use of bread blasting and then cleaned with an approved solvent; an "off-the-shelf" epoxy can be effectively used to bond composite material plates to concrete. Use of ductile adhesives leads to a less effective bond; the failure mode of the joints is governed by shearing of the concrete directly beneath the bond, the value of the ultimate bond strength will be proportional to $\sqrt{f'_c}$; there is a bond development length for a joint L_{jd} beyond which no further increase in failure load can be achieved.

n. specimen	f'_c (MPa)	L_{frp} (mm)	P_u (kN)	n. specimen	f'_c (MPa)	L_{frp} (mm)	P_u (kN)
C1	36,1	76,2	8,5	C9	24,0	76,2	11,2
C2	47,1	76,2	9,9	C10	28,9	76,2	9,9
C3	47,1	76,2	10,6	C11	43,7	76,2	9,3
C4	47,1	76,2	10,6	C12	36,4	76,2	11,2
C5	43,6	76,2	10,5	C13	36,4	50,8	8,1
C6	43,6	76,2	9,0	C14	36,4	101,6	12,8
C7	43,6	76,2	9,6	C15	36,4	152,4	11,9
C8	43,6	76,2	10,5	C16	36,4	203,2	11,6

Table B.19: Ultimate load for specimen. For C1-C14 specimens b=228,6mm and t=152,4mm; for specimens C15 and C16, b=t=152,4mm (Chajes et al. [15])

Bizindavyi et al. (1999) [7] presented a new simple experimental apparatus designed and constructed in their laboratory. With this test rig it is possible to investigate the shear conditions between the composite and concrete, and to make direct measurement of the bond measurements of the bond strengths.

For the experimental program, two batches of concrete blocks of dimensions 150×150×400mm were fabricated from a normal density concrete mix with a maximum aggregate size of 14mm. The mean compressive strength for all the batches was 42,5MPa with a standard deviation of 1,35MPa, and the mean tensile strength from the standard three-point flexure tests was 3,5MPa with a standard deviation of 0,24MPa. The Young's modulus of the concrete, estimated from the concrete compressive strength, was found to be E_c=33,5MPa

Two types of fiber-reinforced composite laminate were used: GFRP and CFRP. Unidirectional laminates of both GFRP and CFRP with one and two plies were prepared in specially designed steel moulds so as to give a uniform laminates thickness. These laminates were each cut into strips 25,4mm wide and were bonded to the concrete blocks. From the static tensile tests on the GFRP laminates, the values of mean strength and mean Young's modulus were found to be $472MPa$ with a standard deviation of 27,8MPa, and 29,2GPa with a standard deviation of 0,42GPa, respectively. From these tests, the values for Poisson's ratio ν_a and shear modulus G_a were found to be 0,4 and 1,18GPa, respectively, with a standard deviation of 0,073GPa for the latter. From tensile tests on the CFRP laminates, the tensile strength and tensile modulus were found to be 1014MPa with a standard deviation of 27,5MPa, and 75,7GPa with a standard deviation of 3,69GPa, respectively. The values of Poisson's ratio for epoxy resins used with similar CFRP systems reported in the literature vary from ν=0,38-0,4.

During the preparation of specimens, a relatively uniform thickness of 1-1,2mm of the adhesive layer was assured by using aluminium guides.

From the tests (Tab.B.20 and Tab.B.21), it was possible to develop the full tensile capacity of the bonded composite for both 1 and 2-ply GFRP and CFRP laminates. It was seen that, for 1-ply and 25mm wide GFRP.to-concrete joints, bond lengths of 160mm were sufficient to develop the full tensile capacity of the composite. For 2-ply and 25mm wide GFRP-to-concrete joints, bond length of 260mm were sufficient to develop the full tensile capacity of the composite. In the case of 1 and 2-ply 25mm wide CFRP-to-concrete joints, bond lengths of 80 and 220mm, respectively, were sufficient to develop the full capacity of composites.

Chen et al. (2001) [16] collected a single and double shear test data from the existing literature based on an extensive literature survey, reported in Tab.B.20 and Tab.B.21. These data show that most experimental joints failed on the concrete a few millimeters beneath the concrete/adhesive interface (van Germert 1997; Maeda et al. 1997). Interfacial failure, between either the adhesive and the concrete or the adhesive and the plate, is not found in this database. This is a consequence of the availability of strong adhesives that bond well to steel, FRP and concrete. For the same reason, adhesive failure is rare, as only such case is seen in database. A small number of specimens failed by FRP rupture and an equal number of specimens failed by FRP delamination. This database is primarily concerned with concrete failure beneath the plate-to-concrete interface. Neubauer and Rostásy (1997) showed that the same energy release rate model is applicable to both the concrete fracture failure mode and the FRP delamination failure mode. This is because, even in FRP delamination failure mode, concrete failure usually occurs in the first 20-50% of the bond length, which is the key failure process and predominates the fracture energy release rate. Cracking then extends into the FRP matrix, leading to FRP delamination.

A very important aspect of bond behavior is that there exits an effective bond length cannot increase the bond strength. This is a fundamental difference between the anchorage design of an externally bonded plate and an internal reinforcement for which a sufficiently long anchorage length can always be found, so that the full tensile strength of the reinforcement can be achieved. Thin stiff plates should be used to make the best use of the tensile strength of the bonded plate.

The Yao et al. (2005) [65] article presents an experimental study on the bond shear strength between FRP and concrete using a near-end supported (NES) single-shear pull test in which the concrete prism is supported at the end nearer the applied load. A total of 72 specimens in seven series were prepared to investigate the effects of the above factors on the bond strength (Tab.B.22). The variables considered in Series I include the bond length L_{frp}. Series II and III were designed to investigate the effects of the FRP-to-concrete width ratio. Concrete prisms of two different

n. of specimen	Adhesive E_a (MPa)	Concrete				
		Width b (mm)	Thickness t (mm)	Compressive strength f'_c (MPa)	Young's modulus E_a (MPa)	Tensile strength f_{ct} (MPa)
C1	5172	228,6	152,4	36,1	-	-
C2	5172	228,6	152,4	47,1	-	-
C3	5172	228,6	152,4	47,1	-	-
C4	5172	228,6	152,4	47,1	-	-
C5	2207	228,6	152,4	43,6	-	-
C6	234	228,6	152,4	43,6	-	-
C7	234	228,6	152,4	43,6	-	-
C8	1584	228,6	152,4	43,6	-	-
C9	1584	228,6	152,4	43,6	-	-
C10	1584	228,6	152,4	24,0	-	-
C11	1584	228,6	152,4	28,9	-	-
C12	1584	228,6	152,4	43,7	-	-
C13	1584	228,6	152,4	42,4	-	-
C14	1584	228,6	152,4	42,4	-	-
C15	1584	152,4	152,4	42,4	-	-
C16	1584	152,4	152,4	42,4	-	-
M1	5000	100	100	40,8	-	-
M1	5000	100	100	40,8	-	-
M1	5000	100	100	43,3	-	-
M1	5000	100	100	42,4	-	-
M1	5000	100	100	42,4	-	-
M1	5000	100	100	42,4	-	-
M1	5000	100	100	44,7	-	-
C100 50A	6700	200	200	-	35000	3,9
C200 50A	6700	200	200	-	35000	4,1
C300 50A	6700	200	200	-	35000	4,3
C400 50A	6700	200	200	-	35000	4,3

Table B.20: Single and Double shear test data collected from literature (Chen et al. [16]).Specimens C1-C16 are from Chajes et al.(1996). Specimens M1-M8 are from Bizindavy and Neale (1999). Specimens C100-C400 are from Taljsten (1997).

n. of specimen	Type	Plate					Measured failure load P_u (kN)
		Thickness t_{frp} (mm)	Width b_{frp} (mm)	Bond length L_{frp} (MPa)	Young's modulus E_{frp} (GPa)	Ultimate strength $f_{u,frp}$ (MPa)	
C1	GFRP	1,016	25,4	76,2	108,5	1655	8,5
C2	GFRP	1,016	25,4	76,2	108,5	1655	9,9
C3	GFRP	1,016	25,4	76,2	108,5	1655	10,6
C4	GFRP	1,016	25,4	76,2	108,5	1655	10,6
C5	GFRP	1,016	25,4	76,2	108,5	1655	10,5
C6	GFRP	1,016	25,4	76,2	108,5	1655	9,0
C7	GFRP	1,016	25,4	76,2	108,5	1655	9,6
C8	GFRP	1,016	25,4	76,2	108,5	1655	10,5
C9	GFRP	1,016	25,4	76,2	108,5	1655	11,2
C10	GFRP	1,016	25,4	76,2	108,5	1655	9,9
C11	GFRP	1,016	25,4	76,2	108,5	1655	9,3
C12	GFRP	1,016	25,4	76,2	108,5	1655	11,2
C13	GFRP	1,016	25,4	50,8	108,5	1655	8,1
C14	GFRP	1,016	25,4	101,6	108,5	1655	12,8
C15	GFRP	1,016	25,4	152,4	108,5	1655	11,9
C16	GFRP	1,016	25,4	203,2	108,5	1655	11,6
M1	CFS	0,11	50	75	230,0	3500	5,8
M2	CFS	0,11	50	150	230,0	3500	9,2
M3	CFS	0,11	50	300	230,0	3500	11,9
M4	CFS	0,165	50	75	230,0	3500	10,0
M6	CFS	0,22	50	65	230,0	3500	9,5
M7	CFS	0,22	50	150	230,0	3500	16,2
M8	CFS	0,11	50	700	230,0	3500	10,0
C100 50A	CFRP	1,25	50	100	17000	2,5	17,3
C200 50A	CFRP	1,25	50	200	17000	2,5	27,5
C300 50A	CFRP	1,25	50	300	17000	2,5	35,1
C400 50A	CFRP	1,25	50	400	17000	2,5	26,9

Table B.21: Single and Double shear test data collected from literature (Chen et al. [16]).Specimens C1-C16 are from Chajes et al.(1996). Specimens M1-M8 are from Bizindavy and Neale (1999). Specimens C100-C400 are from Taljsten (1997).

sizes were used. Half of the specimens in Series III and V used 100× 150 × 350 mm concrete prisms so that a desired range of b_{frp}/b ratios could be achieved. All other specimens used 150 × 150× 350mm concrete prims. GFRP was used in specimens III-7 and III-8 while CFRP was used in all others. The nominal thickness for the CFRP and GFRP strips were 0,165 and 1,27mm respectively, the former being roughly the fibre sheet thickness before resin impregnation with the latter being similar to the thickness of the cured FRP strip. The FRP strips were bonded to the concrete prisms following the manufacturer's instructions. FRP composites were bonded to the concrete prims with epoxy resins.

Fifty-six out of the 72 specimens failed due to debonding in concrete adjacent to the adhesive-concrete interface in which a thin layer of concrete is attached to the FRP strip after failure. Eight specimens failed by debonding at the adhesive-concrete interface where much less concrete is attached to the FRP strip after failure. The remaining eight specimens failed in the concrete prim by the formation of a fracture plane that starts at the far end of the FRP strip and extends to the top of the support block.

Twelve specimens were tested by Toutanji et al. (2007) [62] to study the influence of concrete strength and the amount of FRP on the ultimate load capacity of a FRP-concrete bond under direct shear.

The pull test specimens consisted of a concrete prism bonded with FRP strips by an inorganic epoxy. Three batches of plain concrete were cast into rectangular plywood molds. The prisms acted as the substrate for bonding the carbon fiber sheets. The surface used to bond FRP has a dimension of 200×200mm with a thickness of 130mm. Concrete cylinders made from the same batches were cast and tested at the same time as the series of specimens. The average modulus of concrete E_c was obtained as 33,5GPa.

The thickness of each layer of the carbon fiber is 0,165mm. Yarn fiber-type T300C, 3K was used.

The prepared surface was primed with inorganic epoxy. The carbon fiber sheet was also impregnated with the epoxy and was placed on the marked bonding area of 50× 100mm. The specimens were bonded with three, four, five and six layer of carbon fiber sheets. Each layer of the fiber sheet had the same length.

The specimens were tested under direct shear. Tests were conducted on a 100kN MTS closed-loop electrohydraulic universal testing machine.

In Tab.B.23, the specimens were divided into three groups, namely, Groups I, II and III, according to the concrete compressive strength. Groups I, II and III had concrete compressive strength of 17,0MPa, 46,2MPa and 61,5MPa, respectively. Further specimens in each group were numbered based on the layers of carbon fiber sheet.

A significant increase in ultimate load was noted with an increase of the con-

Specimen name	b_{frp} (mm)	f'_c (MPa)	L (mm)	P_{exp} (kN)	Specimen name	b_{frp} (mm)	f'_c (MPa)	L (mm)	P_{exp} (kN)
III-7	25,3	27,7	100	4,8	III-8	50,6	27,7	100	8,0
I-1	25,0	23,0	75	4,7	IV-2	25,0	18,9	95	5,9
I-2	25,0	23,0	85	5,7	IV-3	25,0	19,8	95	5,4
I-3	25,0	23,0	95	5,8	IV-4	25,0	19,8	95	5,8
I-4	25,0	23,0	95	5,8	IV-5	25,0	18,9	95	5,0
I-5	25,0	23,0	95	6,2	IV-6	25,0	19,8	95	7,1
I-6	25,0	23,0	115	6,0	IV-7	25,0	18,9	95	5,5
I-7	25,0	23,0	145	5,9	IV-8	25,0	19,8	95	5,9
I-8	25,0	23,0	190	6,7	IV-9	25,0	18,9	95	5,4
I-9	25,0	23,0	190	6,3	IV-10	25,0	19,8	95	6,6
I-10	25,0	23,0	95	6,2	IV-11	25,0	18,9	95	5,5
I-11	25,0	23,0	75	5,7	IV-12	25,0	19,8	95	5,7
I-12	25,0	23,0	85	6,0	IV-13	25,0	18,9	95	6,3
I-13	25,0	23,0	95	6,1	IV-14	25,0	19,8	95	6,2
I-14	25,0	23,0	115	6,2	V-1	15,0	21,1	95	3,8
I-15	25,0	23,0	145	6,3	V-2	15,0	21,1	95	4,4
I-16	25,0	23,0	190	7,0	V-3	25,0	21,1	95	6,3
II-1	25,0	22,9	95	5,2	V-4	50,0	21,1	95	12,2
II-2	25,0	22,9	95	6,7	V-5	75,0	21,1	95	14,3
II-3	25,0	22,9	95	5,5	V-6	100,0	21,1	95	15,6
II-4	25,0	22,9	190	7,0	VII-1	25,0	24,9	95	6,8
II-5	25,0	22,9	190	7,1	VII-2	25,0	24,9	95	6,8
II-6	25,0	22,9	190	7,0	VII-3	25,0	24,9	145	7,3
III-1	25,0	27,1	100	5,9	VII-4	25,0	24,9	145	6,5
III-2	50,0	27,1	100	11,7	VII-5	25,0	24,9	190	7,1
III-3	75,0	27,1	100	14,6	VII-6	25,0	24,9	190	7,4
III-4	100,0	27,1	100	19,1	VII-7	25,0	24,9	240	7,2
IV-1	25,0	18,9	95	5,9	VII-8	25,0	24,9	240	6,2

Table B.22: Specimen tests (Yao et al. [65]). b=t=150mm; t_{GFRP}=1,27mm and E_{GFRP}=22,5GPa; t_{CFRP}=0,165mm and E_{CFRP}=256GPa.

n. specimen	f'_c (MPa)	n.of layers	P_u (kN)	n. specimen	f'_c (MPa)	n.of layers	P_u (kN)
I-1	17,0	3	8,5	II-3	46,2	5	9,3
I-2	17,0	4	9,9	II-4	46,2	6	11,2
II-3	17,0	5	10,6	III-1	61,5	3	8,1
I-4	17,0	6	10,6	III-2	61,5	4	12,8
II-1	46,2	3	10,5	III-3	61,5	5	11,9
II-2	46,2	4	9,0	III-4	61,5	6	11,6

Table B.23: Ultimate load for specimen. For all specimens L_{frp}=100mm, b_{frp}=50mm.(Toutanji et al. [62])

crete strength. The major failure modes observed were concrete shearing and fiber delamination. For specimens I-1 and I-2, a thin layer of concrete was attached to the FRP after failure and no epoxy or fiber was left on the concrete substrate. This failure occurred inside the concrete substrate and is termed concrete shearing".

An analysis of all existing experimental push-pull test data available in the open literature was undertaken by Seracino et al. (2007) [49]. Of this population set, only the subset of data where the bonded length L was greater than the critical bonded length L_{crit} was considered. In the first instance, the critical bond length was predicted using the model recommended in Teng et al.(2002) [58]. A database of 55 tests is available which includes thin externally bonded plate of carbon fiber-reinforced polymer (Chajes et al., 1996 [15]; Taljsten, 1997 [57]; Yao et al., 2005 [65]) and glass fiber-reinforced polymer. For the Yao et al.'s tests (2005) [65] manufactured using the wet lay-up technique, $(EA)_{frp}$ was determined using Young's modulus and effective thickness of the CFRP sheet.

A series of tests to idealize the plate end failures of RC beams strengthened in flexure by CFRP plate is presented by Lee (2003) in Tab.B.24 and reported by Camata et al. (2004) [12]. Unlike the simplified bond test, in this case there are no boundary conditions along the free surface but only a concentrated force. A crack normal to the FRP plate opens at the plate end and then propagates at an inclined angle until it becomes horizontal. The specimens consist of two separate concrete blocks attached only by two FRP strips. The author considered three different bond lengths: 50, 75, 93mm. All the specimens are loaded up to complete failure of the bond system. As expected, an increase in the bonded length increases the failure load.

Thirty-six specimens were tested by Nakaba et al. (2001) [35] with a double-face shear type bond test. The specimens consisted of a concrete prism (100×100×600mm) cracked at the center using a hammer on the notch after reinforcing with FRP lami-

name of specimen	Bond Length, L (mm)	Concrete strength, f'_c (MPa)	Peak load, P_u (kN)
B50	50	28,9	21,2
B75	75	29,0	26,2
B97	93	28,1	33,9

Table B.24: Ultimate load for specimen tests (Lee [12]).

nates. The two steel bars also hade no connection, which means that the two prims were connected only through the FRP laminates. The FRP system used in this research consisted of fiber impregnated with epoxy resins, with the primary preparation of the concrete substrate using primer and putty. Putty is a thickened epoxy paste used to fill voids and smooth surface discontinuities. FRP laminates were bonded at two opposite sides of the specimen. One of the sides of the specimen was reinforced with a confinement FRP allowing the occurrence of delamination of the laminate only on the opposite side, where the strain gages were set. The laminate width chosen for this research was 50mm for all specimens and the bond length was set to 300mm.

Carbon (standard and high stiffness) and aramid fiber were used. To verify the influence of the quality of the substrate, the specimens were made by concrete and mortar. Three specimens were made for each combination concrete/mortar-fiber. In addition, the influence of the concrete strength (50 and 24MPa) was verified.

Each specimen was set in a universal testing machine, and submitted to pure tensile force, causing direct shear to be placed on the laminates. The speed used for load application was 1mm/min in the heads speed.

Identification of specimen	Load (kN)	Identification of specimen	Load (kN)	Identification of specimen	Load (kN)
C5-SCFH(1)	25,6	M5-SCFH1	20,6	C2-SCF1	13,9
C5-SCFH(2)	25,3	M5-SCFH2	22,3	C2-SCF2	12,8
C5-SCFH(3)	27,2	M5-SCFH3	23,2	C2-SCF3	14,9
C5-SCF(2)	15,2	M5-SCF1	15,2	C2P-SCF1	14,2
C5-SCF(3)	16,6	M5-SCF2	16,9	C2P-SCF2	14,8
C5-SCFL(1)	11,9	M5-SCF3	16,3	C2P-SCF3	12,6
C5-SCFL(3)	12,2	M5-SCFL1	8,7		
C5-HCF(1)	18,9	M5-SCFL2	8,1		
C5-HCF(3)	16,2	M5-SCFL3	10,0		
C5-ARF(1)	12,8	M5-HCF2	14,6		
C5-ARF(2)	12,5	M5-HCF3	12,6		
C5-ARF(3)	10,9	M5-ARF1	12,0		
		M5-ARF2	11,7		
		M5-ARF3	13,9		

Table B.25: Test results (Nakaba et al. [35]). C5: f'_c=57,6MPa; M5: f'_c=50,0MPa; C2: f'_c=23,8MPa; SCF: t_{frp}=0,167mm, f_{frp}=4200MPa, E_{frp}=261,1GPa; HCF-LCF: t_{frp}=0,165mm, f_{frp}=4400MPa, E_{frp}=425,1GPa; ARF: t_{frp}=0,193mm, f_{frp}=2800MPa, E_{frp}=124,5GPa.

In Tab.B.25 are reported the failure load of beams tested by Nakaba et al. [35].

Sharma et al. (2006) [51] tested thirty-six specimens using metallic and FRP plates with elastic modulus ranging from 32 to 300GPa, having ultimate tensile strength ranging between 50 and 300mm. The prims measuring 100×100×500mm were fabricated consisting a concrete mix by mass with the ratio: 1:1,3:3,5 (ordinary Portland cement:sand:coarse aggregate of 10mm maximum size)and a water-cement ratio 0,4. Plates of six different categories, GFRP with an elastic modulus (E_{frp}) of 32,7GPa, aluminium with E_{frp}=74,85GPa, steel of E_{frp}=208GPa and three types of CFRP plates with elastic moduli 165, 210 and 300GPa were used in the study. The epoxy resin used for bonding the plates had a compressive and tensile strengths of 80 and 17,8MPa.

The direct single shear tests, reported in Tab.B.26 have shown that the debonding in reinforced concrete prims, retrofitted with bonded FRP plate is always caused due to the initiation of the cracks in the vicinity of the most stressed end. The tensile strength of the plate has an effect on both the ultimate bond strength and critical bond length. These critical parameters are found to depend on elastic modulus, tensile strength, width, and thickness of the plate, as well as tensile strength of

Specimen reference	Bond length L_{frp} (mm)	Ultimate load P_u (kN)	Specimen reference	Bond length L_{frp} (mm)	Ultimate load P_u (kN)
G32,7-100	100	12,5	C210-150	150	30,4
G32,7-150	150	17,7	C210-180	180	34,0
G32,7-175	175	20,5	C210-190	190	36,0
G32,7-200	200	20,6	C210-200	200	36,0
G32,7-250	250	20,4	C210-230	230	37,0
G32,7-300	300	20,3	C210-255	255	36,8
C165-100	100	18,2	C300-160	160	38,0
C165-130	130	24,5	C300-180	180	41,1
C165-150	150	28,4	C300-200	200	46,3
C165-175	175	32,0	C300-250	250	45,5
C165-200	200	34,2	C300-300	300	45,9
C165-250	250	33,1			
C165-300	300	34,2			

Table B.26: Results from tests (Sharma et al. [51]). The size (width and thickness) of the specimens is 100×100mm. G32,7: f'_c=35,8MPa, E_{frp}=32,7GPa, f_{frp}=384MPa; C165: f'_c=29,7MPa, E_{frp}=165GPa, f_{frp}=2800MPa; C210: f'_c=35,8MPa, E_{frp}=210GPa, f_{frp}=2400MPa; C300: f'_c=29,7MPa, E_{frp}=300GPa, f_{frp}=1300MPa;

concrete and width factor.

In Ramos' bond tests (2006) [41], the specimens consists in two 150×150×275mm prisms which are separated 50mm but connected by a steel hinge placed in the center of the span, at 115mm from the bottom. The carbon fiber reinforcing system are applied to the bottom of the specimen. Eight prismatic specimens were set up for each type of fiber. The mean compressive strength of the concrete was 45MPa at 28 days (150×300mm cylinder test), and the steel reinforcement's characteristic yield stress was f_y=500MPa. the steel reinforcement placed in each block is comprised of eight longitudinal bars, four bars of 8mm diameter and four bars of 6mm diameter, and five shear stirrups of 6mm separated 45mm. The maximum size of aggregate was 12mm and the water/cement ratio=0,58. A superplasticizer was also added to concrete.

The load is applied at 50mm from both edges of the hinge, by means of two steel rollers. The specimen was supported by two steel rollers leaving a free span of 500mm, at a distance of 50mm from the end of the specimen. Sixteen specimens

	TFC	CFK
Width (mm)	80,0	100,0
Length (mm)	450,0	450,0
Thickness (mm)	0,4	1,4

Table B.27: Dimension of the CFRP in the bond tests (Ramos et al. [41]); TFC is a structural reinforcement system that consists of the adhesion of carbon fibers to a binding matrix, a bicomponent epoxy resin; the CFK procedure consists of using unidirectional carbon fiber plates impregnated in an epoxy resin and partially prestressed.

	ε_{uf}	σ_{uf}
TFC	0,0049 cov=12%	504,7 cov=6%
CFK	0,0028 cov=8%	417,2 cov=6%

Table B.28: Bond test results (Ramos et al. [41])

were tested, eight with each type of carbon fiber. The carbon fiber characteristic are described in Tab.B.27

The failure mechanism observed in these test series is known as “peeling”. The process starts when the flexure at the center of the specimen generates a tensile stress concentration in the concrete, in the zone next to the joint. In a first stage, diagonal cracks are generated and concrete separation occurs. The mechanism continues with the propagation of the crack along the concrete-fiber interface toward both sides of the element, leading to the complete debonding of the CFRP (Tab.B.28).

Appendix C

Collected databases

C.1 Database of beams failed for end debonding

The complete database used in this work, was reported as follow. Each experimental work was explained in the second chapter. It was collected 161 beams tests from 34 testing programs, divided in: 90 beams reinforced by wet lay-up carbon sheets, 57 beams reinforced by prepeg carbon plates, 7 beams reinforced by wet lay-up glass sheets, 7 beams reinforced by prepeg glass plates.

	Beam	b	h	d	d'	a	B	L	f'_c	E_s	f_{ys}	A_s	Reo	E'_s	f'_y	A'_s
		[mm]	[mm]	[mm]	[mm]	[mm]	[mm]	[mm]	[MPa]	[GPa]	[MPa]	[mm²]	[tension]	[GPa]	[MPa]	[mm²]
Ahmed et al. (1999)	AF3	125	225	193	32	100	500	1500	46,0	185	568	101	2-8	195	553	57
	CF2-1	125	225	193	32	100	500	1500	46,0	185	568	129	2-8,1-6	195	553	57
	CF3-1	125	225	193	32	100	500	1500	46,0	185	568	151	3-8	195	553	57
	CF4-1	125	225	193	32	100	500	1500	46,0	183	586	207	2-10,1-8	195	553	57
	DF.2	125	225	193	32	50	500	1500	46,0	185	568	151	3-8	195	553	57
	DF.3	125	225	193	32	50	500	1500	46,0	185	568	151	3-8	195	553	57
	DF.4	125	225	193	32	50	500	1500	46,0	185	568	151	3-8	195	553	57
Ahmed et al. (2000)	AF.2	125	225	196	25	200	500	-	41,0	200	568	101	-8	200	568	57
	AF.2-1	125	225	196	25	150	500	-	41,0	200	568	101	-8	200	568	57
	AF.4	125	225	196	25	50	500	-	41,0	200	568	101	-8	200	568	57
	DF.1	125	225	196	25	50	500	-	42,0	200	568	151	-8	200	568	57
	BF.2-1	125	225	196	25	50	500	-	41,0	200	568	101	-8	200	568	57
	BF.3-1	125	225	196	25	50	500	-	41,0	200	568	101	-8	200	568	57
	EF.1-1	125	225	196	25	50	500	-	46,0	200	568	151	-8	200	568	57
	EF.3-1	125	225	196	25	50	500	-	38,0	200	568	151	-8	200	568	57
	EF.4-1	125	225	196	25	50	500	-	33,0	200	568	151	-8	200	568	57
	FF.2-3	125	225	196	25	70	700	-	39,5	200	568	151	-8	200	568	57
Arduini et al. (1997)	A4	200	200	163	30	150	700	-	33,0	200	540	308	-14	200	540	308
	A5	200	200	163	30	150	700	-	33,0	200	540	308	-14	200	540	308
	B2	300	400	349,5	44	100	1100	-	30,0	200	340	398	-13	200	340	266
	B3	300	400	349,5	44	100	1100	-	30,0	200	340	398	-13	200	340	266
Beber et al. (1999)	VR5	120	250	214	34	75	783	2350	33,6	200	565	157	2-10	200	738	57
	VR6	120	250	214	34	75	783	2350	33,6	200	565	157	2-10	200	738	57
	VR7	120	250	214	34	75	783	2350	33,6	200	565	157	2-10	200	738	57
	VR8	120	250	214	34	75	783	2350	33,6	200	565	157	2-10	200	738	57
	VR9	120	250	214	34	75	783	2350	33,6	200	565	157	2-10	200	738	57
	VR10	120	250	214	34	75	783	2350	33,6	200	565	157	2-10	200	738	57
Benjeddou et al. (2007)	RB1	120	150	120	30	50	600	1800	21,0	200	400	157	2-10	200	400	157
	RB2	120	150	120	30	50	600	1800	21,0	200	400	157	2-10	200	400	157
	RB3	120	150	120	30	50	600	1800	21,0	200	400	157	2-10	200	400	157
	RB4	120	150	120	30	50	600	1800	21,0	200	400	157	2-10	200	400	157
	RB5	120	150	120	30	50	600	1800	21,0	200	400	157	2-10	200	400	157
	RB6	120	150	120	30	50	600	1800	38,0	200	400	157	2-10	200	400	157

Figure C.1: Database of beams failed for end debonding. Ahmed et al. [53], Ahmed et al. [18], Arduini et al. [18], Beber et al. [53], Benjeddou et al. [6].

	Beam	E_{vv}	f_{vv}	A_{sw}	s	E_a	t_a	Type	E_{frp}	f_{frp}	t_{frp}	b_{frp}	V_{exp}
		[GPa]	[MPa]	[mm²]	[mm]	[MPa]	[mm]	[-]	[GPa]	[MPa]	[mm]	[mm]	[kN]
Ahmed et al. (1999)	AF3	195	553	57	71	7200	-	C-W	240,00	3500	0,334	75	48,30
	CF2-1	195	553	57	71	7200	-	C-W	240,00	3500	0,334	75	52,40
	CF3-1	195	553	57	71	7200	-	C-W	240,00	3500	0,334	75	59,10
	CF4-1	195	553	57	71	7200	-	C-W	240,00	3500	0,334	75	70,10
	DF.2	195	553	57	100	7200	-	C-W	240,00	3500	0,334	75	60,30
	DF.3	195	553	57	100	7200	-	C-W	240,00	3500	0,501	75	60,00
	DF.4	195	553	57	100	7200	-	C-W	240,00	3500	0,668	75	62,80
Ahmed et al. (2000)	AF.2	200	553	57	71	-	-	C-W	240,00	3500	0,3	75	41,50
	AF.2-1	200	553	57	71	-	-	C-W	240,00	3500	0,3	75	42,90
	AF.4	200	553	57	71	-	-	C-W	240,00	3500	0,3	75	55,50
	DF.1	200	553	57	100	-	-	C-W	240,00	3500	0,2	75	59,00
	BF.2-1	200	553	57	167	-	-	C-W	240,00	3500	0,3	75	45,00
	BF.3-1	200	553	57	100	-	-	C-W	240,00	3500	0,3	75	52,00
	EF.1-1	200	553	57	100	-	-	C-W	240,00	3500	0,3	75	65,90
	EF.3-1	200	553	57	100	-	-	C-W	240,00	3500	0,3	75	59,50
	EF.4-1	200	553	57	100	-	-	C-W	240,00	3500	0,3	75	60,30
	FF.2-3	200	553	57	100	-	-	C-W	240,00	3500	0,5	75	53,00
Arduini et al. (1997)	A4	200	540	57	150	-	-	C-W	167,00	2906	1,3	150	55,00
	A5	200	540	57	150	-	-	C-W	167,00	2906	2,6	150	45,00
	B2	200	340	101	100	-	-	C-W	400,00	3000	0,2	300	85,00
	B3	200	340	101	100	-	-	C-W	400,00	3000	0,5	300	114,00
Beber et al. (1999)	VR5	200	738	57	110	8500	-	C-P	230,00	3400	0,22	120	51,10
	VR6	200	738	57	110	8500	-	C-P	230,00	3400	0,22	120	50,30
	VR7	200	738	57	110	8500	-	C-P	230,00	3400	0,22	120	62,10
	VR8	200	738	57	110	8500	-	C-P	230,00	3400	0,22	120	62,00
	VR9	200	738	57	110	8500	-	C-P	230,00	3400	0,22	120	64,80
	VR10	200	738	57	110	8500	-	C-P	230,00	3400	0,22	120	68,50
Benjeddou et al. (2007)	RB1	200	235	28	10	12800	-	C-P	165,00	2800	1,2	100	20,06
	RB2	200	235	28	10	12800	-	C-P	165,00	2800	1,2	100	18,83
	RB3	200	235	28	10	12800	-	C-P	165,00	2800	1,2	100	16,05
	RB4	200	235	28	10	12800	-	C-P	165,00	2800	1,2	100	15,38
	RB5	200	235	28	10	12800	-	C-P	165,00	2800	1,2	50	15,05
	RB6	200	235	28	10	12800	-	C-P	165,00	2800	1,2	100	18,69

Figure C.2: Database of beams failed for end debonding. Ahmed et al. [53], Ahmed et al. [18], Arduini et al. [18], Beber et al. [53], Benjeddou et al. [6].

	Beam	b [mm]	h [mm]	d [mm]	d' [mm]	a [mm]	B [mm]	L [mm]	f'_c [MPa]	E_s [GPa]	f_{ys} [MPa]	A_s [mm²]	Reo [tension]	E'_s [GPa]	f'_y [MPa]	A'_s [mm²]
Breña et al. (2004)	A1-I	102	102	89	13	25	330	812	42,2	200	435	71	1-9,5	200	435	71
	A1-II	102	102	89	13	25	330	812	42,2	200	435	142	2-9,5	200	435	142
	A2-I	102	102	89	13	25	330	812	42,2	200	435	71	1-9,5	200	435	71
	A2-II	102	102	89	13	25	330	812	42,2	200	435	142	2-9,5	200	435	142
	A3-I	102	102	89	13	25	330	812	53,3	200	435	71	1-9,5	200	435	71
	A3-II	102	102	89	13	25	330	812	53,3	200	435	142	2-9,5	200	435	142
	A4-I	102	102	89	13	25	330	812	53,3	200	435	71	1-9,5	200	435	71
	A4-II	102	102	89	13	25	330	812	53,3	200	435	142	2-9,5	200	435	142
	A5-I	102	102	89	13	25	330	812	53,3	200	435	71	1-9,5	200	435	71
	A5-II	102	102	89	13	25	330	812	53,3	200	435	142	2-9,5	200	435	142
	A6-I	102	102	89	13	25	330	812	47,7	200	435	71	1-9,5	200	435	71
David et al. (1999)	P_2	150	300	257	-	200	933	2800	40,0	200	500	308	2-14	-	-	-
	P_3	150	300	257	-	200	933	2800	40,0	200	500	308	2-14	-	-	-
	P_4	150	300	257	-	200	933	2800	40,0	200	500	308	2-14	-	-	-
	P_5	150	300	257	-	200	933	2800	40,0	200	500	308	2-14	-	-	-
Esfahani et al. (2006)	B3-12D-2L	150	200	166	25	100	600	1600	25,2	200	400	226	2-12	200	365	157
	B3-12D-3L	150	200	166	25	100	600	1600	25,2	200	400	226	2-12	200	365	157
Fanning et al. (2001)	F5	155	240	209	31	385	1100	2800	66,4	204	460	339	3-12	204	460	226
	F6	155	240	209	31	385	1100	2800	66,4	204	460	339	3-12	204	460	226
	F7	155	240	209	31	462	1100	2800	66,4	204	460	339	3-12	204	460	226
	F8	155	240	209	31	462	1100	2800	66,4	204	460	339	3-12	204	460	226
	F9	155	240	209	31	550	1100	2800	66,4	204	460	339	3-12	204	460	226
	F10	155	240	209	31	550	1100	2800	66,4	204	460	339	3-12	204	460	226
Garden et al. (1997)	$1A_u$	100	100	84	16	20	300	900	47,3	215	350	85	3-6	215	350	57
	$2A_u$	100	100	84	16	20	340	900	47,3	215	350	85	3-6	215	350	57
	$3A_u$	100	100	84	16	20	400	900	47,3	215	350	85	3-6	215	350	57
	$1B_u$	100	100	84	16	20	300	900	47,3	215	350	85	3-6	215	350	57
	$2B_u$	100	100	84	16	20	340	900	47,3	215	350	85	3-6	215	350	57
	$3B_u$	100	100	84	16	20	400	900	47,3	215	350	85	3-6	215	350	57
	$1B_{2u}$	100	100	84	16	20	300	900	47,3	215	350	85	3-6	215	350	57

Figure C.3: Database of beams failed for end debonding. Breña et al. [9], David et al. [53], Esfahani et al. [22], Fanning et al. [23], Garden et al. [53].

	Beam	E_{vv}	f_{vv}	A_{sw}	s	E_a	t_a	Type	E_{fm}	f_{fm}	t_{fm}	b_{fm}	V_{exp}
		[GPa]	[MPa]	[mm²]	[mm]	[MPa]	[mm]	[-]	[GPa]	[MPa]	[mm]	[mm]	[kN]
Breña et al. (2004)	A1-I	200	420	28	51	3035	0,4	C-W	230,00	3790	0,165	51	13,95
	A1-II	200	420	28	51	3035	0,4	C-W	230,00	3790	0,165	51	20,10
	A2-I	200	420	28	51	3035	0,8	C-W	230,00	3790	0,33	51	15,70
	A2-II	200	420	28	51	3035	0,8	C-W	230,00	3790	0,33	51	22,25
	A3-I	200	420	28	51	3035	1,2	C-W	230,00	3790	0,495	51	19,50
	A3-II	200	420	28	51	3035	1,2	C-W	230,00	3790	0,495	51	24,00
	A4-I	200	420	28	51	3035	0,8	C-W	230,00	3790	0,33	76	18,40
	A4-II	200	420	28	51	3035	0,8	C-W	230,00	3790	0,33	76	26,25
	A5-I	200	420	28	51	3035	0,4	C-W	230,00	3790	0,165	102	17,60
	A5-II	200	420	28	51	3035	0,4	C-W	230,00	3790	0,165	102	24,45
	A6-I	200	420	28	51	4480	1,6	C-P	155,00	2400	1,19	51	17,40
David et al. (1999)	P_2	200	500	57	140	8500	1,0	C-P	150,00	2400	1,2	100	68,00
	P_3	200	500	57	140	8500	1,0	C-P	150,00	2400	1,2	100	71,10
	P_4	200	500	57	140	8500	1,0	C-P	150,00	2400	2,4	100	78,00
	P_5	200	500	57	140	8500	1,0	C-P	150,00	2400	2,4	100	79,50
Esfahani et al. (2006)	B3-12D-2L	200	350	50	80	-	-	C-W	237,00	2845	0,176	150	35,47
	B3-12D-3L	200	350	50	80	-	-	C-W	237,00	2845	0,176	150	37,22
Fanning et al (2001)	F5	198	250	28	125	-	-	C-P	155,00	2400	1,2	120	50,00
	F6	198	250	28	125	-	-	C-P	155,00	2400	1,2	120	51,50
	F7	198	250	28	125	-	-	C-P	155,00	2400	1,2	120	48,75
	F8	198	250	28	125	-	-	C-P	155,00	2400	1,2	120	32,00
	F9	198	250	28	125	-	-	C-P	155,00	2400	1,2	120	31,00
	F10	198	250	28	125	-	-	C-P	155,00	2400	1,2	120	41,00
Garden et al (1997)	$1A_u$	215	350	14	51	11560	2,0	C-P	111,00	1273	0,5	90	19,80
	$2A_u$	215	350	14	51	11560	2,0	C-P	111,00	1273	0,5	90	19,30
	$3A_u$	215	350	14	51	11560	2,0	C-P	111,00	1273	0,5	90	19,50
	$1B_u$	215	350	14	51	11560	2,0	C-P	111,00	1273	0,7	65	18,30
	$2B_u$	215	350	14	51	11560	2,0	C-P	111,00	1273	0,7	65	17,00
	$3B_u$	215	350	14	51	11560	2,0	C-P	111,00	1273	0,7	65	17,30
	$1B_{2u}$	215	350	14	51	11560	2,0	C-P	111,00	1273	0,7	65	18,20

Figure C.4: Database of beams failed for end debonding. Breña et al. [9], David et al. [53], Esfahani et al. [22], Fanning et al. [23], Garden et al. [53].

	Beam	b	h	d	d'	a	B	L	f'_c	E_s	f_{ys}	A_s	Reo	E'_s	f_v	A'_s
		[mm]	[mm]	[mm]	[mm]	[mm]	[mm]	[mm]	[MPa]	[GPa]	[MPa]	[mm²]	[tension]	[GPa]	[MPa]	[mm²]
Garden et al (1997)	$1C_u$	100	100	84	16	20	300	900	47,3	215	350	85	3-6	215	350	57
	$2C_u$	100	100	84	16	20	340	900	47,3	215	350	85	3-6	215	350	57
	$3C_u$	100	100	84	16	20	400	900	47,3	215	350	85	3-6	215	350	57
Garden et al (1998)	B1u,1.0	100	100	84	16	20	300	900	43,2	215	350	85	3-6	215	350	57
	B2u,1.0	100	100	84	16	20	300	900	43,2	215	350	85	3-6	215	350	57
	B1u,2.3	130	230	206	25	20	844	2200	37,6	220	556	236	3-10	220	556	101
	B3U1.0	100	100	87	10	20	340	-	44,8	215	350	85	-6	215	350	57
	B4U1.0	100	100	87	10	20	400	-	44,8	215	350	85	-6	215	350	57
	B5U1.0	100	100	87	10	20	400	-	44,8	215	350	85	-6	215	350	57
	B1U4.5	145	230	214	15	40	1525	-	39,0	220	556	236	-12	220	556	111
Grace et al. (2005)	Bb1	152	254	228,6	25,4	152,5	864	2540	31,0	200	414	397	3-15,9	200	414	142
	Bb2	152	254	228,6	25,4	152,5	864	2540	31,0	200	414	397	3-15,9	200	414	142
	Bb3	152	254	228,6	25,4	152,5	864	2540	31,0	200	414	397	3-15,9	200	414	142
	Bb4	152	254	228,6	25,4	152,5	864	2540	31,0	200	414	397	3-15,9	200	414	142
Hau et al. (1999)	2	150	250	205	45	350	500	1500	35,4	231	537	157	2-10	231	537	157
	4	150	250	205	45	200	500	1500	36,2	231	537	157	2-10	231	537	157
	5	150	250	205	45	50	500	1500	40,6	231	537	157	2-10	231	537	157
	6	150	250	205	45	200	500	1500	39,9	231	537	157	2-10	231	537	157
	7	150	250	205	45	350	500	1500	37,6	231	537	157	2-10	231	537	157
Juvandes et al. (1998)	B7	75	150	131	22	10	650	1500	37,0	200	190	14	2-3	200	470	151
	B.11	75	150	128,5	20	200	650	-	36,0	200	190	14	-3	200	190	151
Matthys (2000)	BF2	200	450	409	-	70	1250	-	36,5	200	590	804	-16	200	590	-
	BF3	200	450	409	-	70	1250	-	34,9	200	590	804	-16	200	590	-
	BF4	200	450	409	-	70	1250	-	30,8	200	590	804	-16	200	590	-
	BF5	200	450	409	-	70	1250	-	37,4	200	590	804	-16	200	590	-
	BF8	200	450	409	-	71	1251	-	39,4	200	590	402	-16	200	590	-
	BF9	200	450	409	-	71	1251	-	33,7	200	590	402	-16	200	590	-
Nguyen et al (2001)	A950	120	150	120	34	190	440	1330	25,7	200	384	236	3-10	200	400	57
	A1100	120	150	120	34	115	440	1330	25,7	200	384	236	3-10	200	400	57
	A1150	120	150	120	34	90	440	1330	25,7	200	384	236	3-10	200	400	57
	B2	120	150	120	34	115	440	1330	25,7	200	384	236	3-10	200	400	57
Pham et al. (2006)	E1a	140	260	220	40	150	700	2300	53,7	205	551	339	3-12	205	551	226

Figure C.5: Database of beams failed for end debonding. Garden et al. [53], Garden et al. [27], Grace et al. [28], Hau et al. [53], Juvandes et al. [18], Matthys [18], Nguyen et al. [36], Pham et al. [39].

	Beam	E_{rv} [GPa]	f_{rv} [MPa]	A_{sv} [mm²]	s [mm]	E_a [MPa]	t_a [mm]	Type [-]	E_{fm} [GPa]	f_{fm} [MPa]	t_{fm} [mm]	b_{fm} [mm]	V_{exp} [kN]
Garden et al. (1997)	$1C_u$	215	350	14	51	11560	2,0	C-P	111,00	1273	1	45	16,00
	$2C_u$	215	350	14	51	11560	2,0	C-P	111,00	1273	1	45	17,80
	$3C_u$	215	350	14	51	11560	2,0	C-P	111,00	1273	1,0	45	15,40
Garden et al. (1998)	B1u,1.0	215	350	14	51	8600	2,0	C-P	111,00	1414	0,82	67	18,30
	B2u,1.0	215	350	14	51	8600	2,0	C-P	111,00	1414	0,82	67	16,00
	B1u,2.3	215	350	57	150	8600	2,0	C-P	115,00	1284	1,28	90	50,20
	B3U1.0	215	350	14	50	-	-	C-W	111,00	1414	0,8	67	17,00
	B4U1.0	215	350	14	50	-	-	C-W	111,00	1414	0,8	67	17,30
	B5U1.0	215	350	14	50	-	-	C-W	111,00	1414	0,8	67	17,30
	B1U4.5	220	350	57	150	-	-	C-W	115,00	1284	1,3	90	30,00
Grace et al. (2005)	Bb1	200	414	142	102	2140	-	C-W	138,00	2070	1,2	152	68,30
	Bb2	200	414	142	102	2140	-	C-W	138,00	2070	1,2	152	68,30
	Bb3	200	414	142	102	2140	-	C-P	227,00	2758	0,4	152	66,75
	Bb4	200	414	142	102	2140	-	C-P	227,00	2758	0,4	152	66,75
Hau et al. (1999)	2	231	537	157	100	3260	0,4	G-W	19,72	259	1,32	150	53,00
	4	231	537	157	100	3260	0,4	G-W	19,72	259	1,3	150	65,40
	5	231	537	157	100	3260	0,4	G-W	19,72	259	2,6	150	79,40
	6	231	537	157	100	3260	0,4	G-W	19,72	259	1,32	150	63,10
	7	231	537	157	100	3260	0,4	G-W	19,72	259	1,32	150	53,90
Juvandes et al. (1998)	B7	200	190	14	60	10250	2,5	C-P	150,00	2400	1,2	50	12,50
	B.11	200	190	14	60	-	-	C-W	150,00	2400	1,2	50	6,70
Matthys (2000)	BF2	200	560	101	100	-	-	C-W	159,00	3200	1,2	100	185,00
	BF3	200	560	101	100	-	-	C-W	159,00	3200	1,2	100	186,00
	BF4	200	560	101	100	-	-	C-W	159,00	3200	1,2	100	184,20
	BF5	200	560	101	100	-	-	C-W	159,00	3200	1,2	100	177,00
	BF8	200	560	101	100	-	-	C-W	159,00	3200	1,2	100	111,30
	BF9	200	560	101	100	-	-	C-W	159,00	3200	0,2	100	95,80
Nguyen et al. (2001)	A950	200	400	57	50	12800	1,5	C-P	181,00	3140	1,2	80	28,10
	A1100	200	400	57	50	12800	1,5	C-P	181,00	3140	1,2	80	28,70
	A1150	200	400	57	50	12800	1,5	C-P	181,00	3140	1,2	80	29,50
	B2	200	400	57	50	12800	1,5	C-P	181,00	3140	1,2	80	65,10
Pham et al. (2006)	E1a	204	334	79	125	3500	-	C-W	209,00	3900	1,056	100	35,35

Figure C.6: Database of beams failed for end debonding. Garden et al. [53], Garden et al. [27], Grace et al. [28], Hau et al. [53], Juvandes et al. [18], Matthys [18], Nguyen et al. [36], Pham et al. [39].

	Beam	b [mm]	h [mm]	d [mm]	d' [mm]	a [mm]	B [mm]	L [mm]	f'_c [MPa]	E_s [GPa]	f_{ys} [MPa]	A_s [mm²]	Reo [tension]	E'_s [GPa]	f_y [MPa]	A'_s [mm²]
Pham et al. (2006)	E1b	140	260	220	40	150	700	2300	53,7	205	551	339	3-12	205	551	226
	E2a	140	260	220	40	350	700	2300	53,7	205	551	339	3-12	205	551	226
	E2b	140	260	220	40	350	700	2300	53,7	205	551	339	3-12	205	551	226
	E3a	140	260	220	40	150	700	2300	53,7	205	551	339	3-12	205	551	226
	E3b	140	260	220	40	150	700	2300	53,7	205	551	339	3-12	205	551	226
	E4a	140	260	220	40	150	700	2300	53,7	205	551	339	3-12	205	551	226
	E4b	140	260	220	40	150	700	2300	53,7	205	551	339	3-12	205	551	226
	E5a	140	260	220	40	150	700	2300	53,7	205	551	339	3-12	205	551	226
	E5b	140	260	220	40	150	700	2300	53,7	205	551	339	3-12	205	551	226
	E3b2	140	260	220	40	150	700	2300	53,7	205	551	226	2-12	205	551	226
Quantrill el al. (1996)	B2	100	100	84	16	20	300	900	42,4	215	350	85	3-6	215	350	57
	B3	100	100	84	16	20	300	900	42,4	215	350	85	3-6	210	350	57
	B4	100	100	84	16	20	300	900	42,4	215	350	85	3-6	215	350	57
	B6	100	100	84	16	20	300	900	42,4	215	350	85	3-6	215	350	57
Rahimi et al. (2001)	A4	200	150	120	30	85	750	2100	41,5	210	575	157	2-10	210	575	101
	A5	200	150	120	30	85	750	2100	41,5	210	575	157	2-10	210	575	101
	A6	200	150	120	30	85	750	2100	41,5	210	575	157	2-10	210	575	101
	A7	200	150	120	30	85	750	2100	41,5	210	575	157	2-10	210	575	101
	A8	200	150	120	30	85	750	2100	41,5	210	575	157	2-10	210	575	101
	A9	200	150	120	30	85	750	2100	41,5	210	575	157	2-10	210	575	101
	A10	200	150	120	30	85	750	2100	41,5	210	575	157	2-10	210	575	101
	A11	200	150	120	30	85	750	2100	41,5	210	575	157	2-10	210	575	101
Ritchie et al (1991)	C	152	305	251	-	203	914	2438	39,8	200	414	253	2-12.7	-	-	-
	D	152	305	251	-	203	914	2438	39,8	200	414	253	2-12.7	-	-	-
	G	152	305	251	-	0	914	2438	43,0	200	414	253	2-12.7	-	-	-
	I	152	305	251	-	203	914	2438	39,8	200	414	253	2-12.7	-	-	-
	M	152	305	251	-	0	914	2438	43,0	200	414	253	2-12.7	-	-	-
Ross et al. (1999)	1B	200	200	152	48	1	914	2742	54,8	200	410	143	2-9.5	200	410	143
	1C	200	200	152	48	1	914	2742	54,8	200	410	143	2-9,5	200	410	143
	2B	200	200	152	48	1	914	2742	54,8	200	410	253	2-12,7	200	410	143
	2C	200	200	152	48	1	914	2742	54,8	200	410	253	2-12,7	200	410	143
	2D	200	200	152	48	1	914	2742	54,8	200	410	253	2-12,7	200	410	143

Figure C.7: Database of beams failed for end debonding. Pham et al. [39], Quantrill et al. [53], Rahimi et al. [40], Ritchie et al. [44], Ross et al. [45].

	Beam	E_{vv}	f_{vv}	A_{sw}	s	E_a	t_a	Type	E_{fm}	f_{fm}	t_{fm}	b_{fm}	V_{exp}
		[GPa]	[MPa]	[mm²]	[mm]	[MPa]	[mm]	[-]	[GPa]	[MPa]	[mm]	[mm]	[kN]
Pham et al. (2006)	E1b	204	334	79	125	3500	-	C-W	209,00	3900	1,056	100	37,30
	E2a	204	334	79	125	3500	-	C-W	209,00	3900	1,056	100	25,70
	E2b	204	334	79	125	3500	-	C-W	209,00	3900	1,056	100	26,70
	E3a	204	334	79	125	3500	-	C-W	209,00	3900	1,056	100	33,00
	E3b	204	334	79	125	3500	-	C-W	209,00	3900	1,056	100	32,60
	E4a	204	334	79	125	3500	-	C-W	209,00	3900	1,056	100	39,50
	E4b	204	334	79	125	3500	-	C-W	209,00	3900	1,056	100	30,60
	E5a	204	334	79	125	3500	-	C-W	209,00	3900	1,584	100	31,65
	E5b	204	334	79	125	3500	-	C-W	209,00	3900	1,584	100	31,60
	E3b2	204	334	79	125	3500	-	C-W	209,00	3900	1,056	100	30,00
Quantrill et al. (1996)	B2	215	350	14	50	11560	2,0	G-P	49,00	1078	1,2	80	17,00
	B3	215	350	14	50	11560	2,0	G-P	49,00	1078	1,2	30	12,30
	B4	215	350	14	50	11560	2,0	G-P	49,00	1078	1,6	60	17,50
	B6	215	350	14	50	11560	2,0	C-P	118,50	987	1,2	80	20,40
Rahimi et al. (2001)	A4	210	575	28	150	7000	2,0	C-W	127,00	1532	0,8	150	30,95
	A5	210	575	28	150	7000	2,0	C-W	127,00	1532	0,8	150	31,60
	A6	210	575	28	150	7000	2,0	C-W	127,00	1532	1,2	150	29,70
	A7	210	575	28	150	7000	2,0	C-W	127,00	1532	1,2	150	35,30
	A8	210	575	28	150	7000	2,0	C-W	127,00	1532	0,8	150	32,60
	A9	210	575	28	150	7000	2,0	C-W	127,00	1532	0,8	150	31,95
	A10	210	575	28	150	7000	2,0	C-W	127,00	1532	0,8	150	33,75
	A11	210	575	28	150	7000	2,0	C-W	127,00	1532	0,8	150	34,70
Ritchie et al (1991)	C	200	414	99	102	8500	2,0	G-P	11,72	161	4,76	152	55,40
	D	200	414	99	102	8500	2,0	G-P	11,72	161	4,76	151	59,60
	G	200	414	99	102	8500	2,0	G-P	10,34	184	4,19	152	62,90
	I	200	414	99	102	8500	2,0	C/G-P	27,58	319	4,06	150	50,60
	M	200	414	99	102	8500	2,0	C-P	117,91	1489	1,27	152	72,10
Ross et al. (1999)	1B	200	410	143	102	8500	2,0	C-P	138,00	2206	0,5	200	40,10
	1C	200	410	143	102	8500	2,0	C-P	138,00	2206	0,5	200	35,60
	2B	200	410	143	102	8500	2,0	C-P	138,00	2206	0,5	200	49,00
	2C	200	410	143	102	8500	2,0	C-P	138,00	2206	0,5	200	35,60
	2D	200	410	143	102	8500	2,0	C-P	138,00	2206	0,5	200	40,10

Figure C.8: Database of beams failed for end debonding. Pham et al. [39], Quantrill et al. [53], Rahimi et al. [40], Ritchie et al. [44], Ross et al. [45].

	Beam	b [mm]	h [mm]	d [mm]	d' [mm]	a [mm]	B [mm]	L [mm]	f'_c [MPa]	E_s [GPa]	f_{ys} [MPa]	A_s [mm²]	Reo [tension]	E'_s [GPa]	f'_y [MPa]	A'_s [mm²]
Ross et al. (1999)	3B	200	200	152	48	1	914	2742	54,8	200	410	396	2-15,9	200	410	143
	4B	200	200	150,5	40	0	914	-	54,8	200	410	567	-19	200	410	142
	5B	200	200	149	40	0	914	-	54,8	200	410	774	-22	200	410	142
	6B	200	200	147	40	0	914	-	54,8	200	410	1019	-26	200	410	142
	3C	200	200	152	48	1	914	2742	54,8	200	410	396	2-15,9	200	410	143
	3D	200	200	152	48	1	914	2742	54,8	200	410	396	2-15,9	200	410	143
Saadatmanesh et al. (1991)	B	205	455	400	55	155	1983	4575	35,0	200	456	1013	2-25.4	200	456	253
Sharif et al. (1994)	P2	150	150	114	36	75	393	1180	37,7	200	450	157	2-10	200	450	57
	P3	150	150	114	36	75	393	1180	37,7	200	450	157	2-10	200	450	57
Spadea et al. (1997)	A1.1	140	300	262	30	50	1800	-	24,9	200	435	402	-16	200	435	402
	A3.1	140	300	262	30	50	1800	-	24,9	200	435	402	-16	200	435	402
Tan et al. (1999)	A00	100	150	124	21	-	600	-	28,6	200	500	157	-10	200	500	57
	A15	100	150	124	22	-	600	-	31,4	200	500	157	-11	200	500	57
	A25	100	150	124	23	-	600	-	29,7	200	500	157	-12	200	500	57
	A40	100	150	124	24	-	600	-	31,4	200	500	157	-13	200	500	57
	A60	100	150	124	25	-	600	-	28,6	200	500	157	-14	200	500	57
	A75	100	150	124	26	-	600	-	28,5	200	500	157	-15	200	500	57
	A90	100	150	124	27	-	600	-	30,1	200	500	157	-16	200	500	57
Täljsten et al. (1999)	SB1	200	300	252	48	150	1300	3600	51,2	200	527	402	2-16	200	527	402
	SB2	200	300	252	48	200	1300	3600	52,0	200	527	402	2-16	200	527	402
	SB3	200	300	252	48	300	1300	3600	52,0	200	527	402	2-16	200	527	402
	MB1	200	300	252	48	150	1300	3600	56,0	200	527	402	2-16	200	527	402
	HB1	200	300	252	48	150	1300	3600	56,0	200	527	402	2-16	200	527	402
	FB1	200	300	252	48	150	1300	3600	51,2	200	527	402	2-16	200	527	402
Teng and Yao (2007)	CS	150,2	252,7	221,7	31	50	500	1500	25,5	199	536	157	2-10	199	536	157
	CS-L3	151,1	253	222	31	50	500	1500	27,3	199	536	157	2-10	199	536	157
	CS-W100	150,6	254	218,5	35,5	50	500	1500	31,4	199	536	157	2-10	199	536	157
	CP	151,1	252,8	222,8	30	50	500	1500	30,7	199	536	157	2-10	199	536	157
	CS-C10	151,1	252,7	240,7	12	50	500	1500	22,7	199	536	157	2-10	199	536	157
Triantafillou et al. (1992)	4	76	127	111	16	75	305	1220	44,7	200	517	33	2-4.6	-	-	-
	5	76	127	111	16	75	305	1220	44,7	200	517	33	2-4.6	-	-	-
	6	76	127	111	16	75	305	1220	44,7	200	517	33	2-4.6	-	-	-

Figure C.9: Database of beams failed for end debonding. Ross et al. [45], Saadamanesh et al. [46], Sharif et al. [50], Spadea et al. [54], Tan et al. [18], Tälijsten et al. [55], Teng and Yao [61], Triantafillou et al. [64].

	Beam	E_{vv} [GPa]	f_{vv} [MPa]	A_{sv} [mm²]	s [mm]	E_a [MPa]	t_a [mm]	Type [-]	E_{fm} [GPa]	f_{fm} [MPa]	t_{fm} [mm]	b_{fm} [mm]	V_{exp} [kN]
Ross et al. (1999)	3B	200	410	143	102	8500	2,0	C-P	138,00	2206	0,5	200	54,50
	4B	200	410	142	102	-	-	C-W	138,00	2206	0,5	200	53,80
	5B	200	410	142	102	-	-	C-W	138,00	2206	0,5	200	73,40
	6B	200	410	142	102	-	-	C-W	138,00	2206	0,5	200	84,50
	3C	200	410	143	102	8500	2,0	C-P	138,00	2206	0,5	200	54,10
	3D	200	410	143	102	8500	2,0	C-P	138,00	2206	0,5	200	54,30
Saadatmanesh et al. (1991)	B	200	456	253	150	8500	1,5	G-P	37,23	400	6,0	152	125,00
Sharif et al. (1994)	P2	200	450	28	60	-	1,0	G-W	14,90	170	2	100	34,00
	P3	200	450	28	60	-	1,0	G-W	14,90	170	3	100	33,00
Spadea et al. (1997)	A1.1	200	435	57	150	-	-	C-W	152,00	2400	1,2	80	43,40
	A3.1	200	435	25	150	-	-	C-W	152,00	2400	1,2	80	37,40
Tan et al. (1999)	A00	200	500	57	75	-	-	C-W	230,00	3400	0,2	100	27,50
	A15	200	500	57	75	-	-	C-W	230,00	3400	0,2	100	24,70
	A25	200	500	57	75	-	-	C-W	230,00	3400	0,2	100	24,30
	A40	200	500	57	75	-	-	C-W	230,00	3400	0,2	100	24,70
	A60	200	500	57	75	-	-	C-W	230,00	3400	0,2	100	26,00
	A75	200	500	57	75	-	-	C-W	230,00	3400	0,2	100	21,90
	A90	200	500	57	75	-	-	C-W	230,00	3400	0,2	100	19,80
Täljsten et al. (1999)	SB1	200	527	157	75	8500	2,1	C-P	155,00	2400	1,4	120	71,40
	SB2	200	527	157	75	8500	2,4	C-P	155,00	2400	1,4	120	75,50
	SB3	200	527	157	75	8500	3,0	C-P	155,00	2400	1,4	120	73,90
	MB1	200	527	157	75	8500	2,4	C-P	210,00	2000	1,4	120	79,60
	HB1	200	527	157	75	8500	2,1	C-P	300,00	1400	1,4	100	80,10
	FB1	200	527	157	75	8500	0,4	C-W	95,00	1800	2,4	150	74,40
Teng and Yao (2007)	CS	199	536	157	100	-	2,0	C-W	256,00	4114	1,74	148	81,50
	CS-L3	199	536	157	100	-	2,0	C-W	256,00	4114	2,63	148	78,50
	CS-W100	199	536	157	100	-	2,0	C-W	256,00	4114	1,95	100	80,80
	CP	199	536	157	100	-	2,0	C-P	165,00	2800	1,2	148	76,00
	CS-C10	199	536	157	100	-	2,0	C-W	256,00	4114	1,86	148	99,40
Triantafillou et al. (1992)	4	200	517	17	40	-	-	C-W	186,00	1450	0,7	63	14,78
	5	200	517	17	40	-	-	C-W	186,00	1450	0,7	63	15,25
	6	200	517	17	40	-	-	C-W	186,00	1450	0,9	63	13,95

Figure C.10: Database of beams failed for end debonding. Ross et al. [45], Saadamanesh et al. [46], Sharif et al. [50], Spadea et al. [54], Tan et al. [18], Tälijsten et al. [55], Teng and Yao [61], Triantafillou et al. [64].

Beam	b	h	d	d'	a	B	L	f'_c	E_s	f_{ys}	A_s	Reo	E'_s	f'_y	A'_s
	[mm]	[mm]	[mm]	[mm]	[mm]	[mm]	[mm]	[MPa]	[GPa]	[MPa]	[mm²]	[tension]	[GPa]	[MPa]	[mm²]
Triantafillou et al. (1992) 7	76	127	111	16	75	305	1220	44,7	200	517	33	2-4.6	-	-	-
8	76	127	111	16	75	305	1220	44,7	200	517	33	2-4.6	-	-	-
Tumialan et al. (1999) A3	150	300	250	-	-	1065	2130	51,7	207	427	792	4-15.9	-	-	-
A8	150	300	250	-	-	1065	2130	51,7	207	427	792	4-15.9	-	-	-
C2	150	300	250	-	-	1065	2130	51,7	207	427	792	4-15.9	-	-	-

Beam	E_{vv}	f_{vv}	A_{sv}	s	E_a	t_a	Type	E_{fm}	f_{fm}	t_{fm}	b_{fm}	V_{exp}
	[GPa]	[MPa]	[mm²]	[mm]	[MPa]	[mm]	[-]	[GPa]	[MPa]	[mm]	[mm]	[kN]
Triantafillou et al. (1992) 7	200	517	17	40	-	-	C-W	186,00	1450	0,9	63	12,80
8	200	517	17	40	-	-	C-W	186,00	1450	1,9	64	18,67
Tumialan et al. (1999) A3	207	427	143	125	2000	-	C-W	230,00	3400	0,495	150	86,10
A8	207	427	143	125	2000	-	C-W	230,00	3400	0,99	75	98,20
C2	207	427	143	250	2000	-	C-W	230,00	3400	0,495	150	79,30

Figure C.11: Database of beams failed for end debonding. Triantafillou et al. [64], Tumialan et al. (1999) [53].

C.2 Database of prism tests

The complete database used in this work, was reported as follow. Each experimental work was explained in the second chapter. It was collected 176 shear or pull-out tests from 11 testing programs, divided in: 131 prisms with wet lay-up carbon sheets, 6 prisms with prepeg carbon plates, 31 prisms with wet lay-up glass sheets, 2 prisms with prepeg glass plates and 6 prisms with wet lay-up aramid sheets.

		b [mm]	h [mm]	t [mm]	f'_c [MPa]	E_s [MPa]	t_s [mm]	Type [k]	E_{frp} [GPa]	f_{frp} [MPa]	t_{frp} [mm]	b_{frp} [mm]	L_{frp} [mm]	P_u [kN]
Bizindavyi et al. (1999)	B-1	150	400	150	43,6	3304	1,1	G-W	29,20	472,0	1,0	25,4	135,0	11,40
	B-2	150	400	150	43,6	3304	1,1	G-W	29,20	472,0	1,0	25,4	145,0	11,40
	B-3	150	400	150	43,6	3304	1,1	G-W	29,20	472,0	1,0	25,4	150,0	11,40
	B-4	150	400	150	43,6	3304	1,1	G-W	29,20	472,0	1,0	25,4	155,0	11,40
	B-5	150	400	150	43,6	3304	1,1	G-W	29,20	472,0	2,0	25,4	120,0	21,40
	B-6	150	400	150	43,6	3304	1,1	G-W	29,20	472,0	2,0	25,4	210,0	21,40
	B-7	150	400	150	43,6	3304	1,1	G-W	29,20	472,0	2,0	25,4	220,0	21,40
	B-8	150	400	150	43,6	3304	1,1	G-W	29,20	472,0	2,0	25,4	240,0	21,40
	B-9	150	400	150	43,6	3304	1,1	G-W	29,20	472,0	2,0	25,4	240,0	21,40
	B-10	150	400	150	43,6	-	1,1	C-W	75,70	1014,0	0,3	25,4	50,0	8,50
	B-11	150	400	150	43,6	-	1,1	C-W	75,70	1014,0	0,7	25,4	100,0	15,10
	B-12	150	400	150	43,6	-	1,1	C-W	75,70	1014,0	0,7	25,4	120,0	15,10
	B-13	150	400	150	43,6	-	1,1	C-W	75,70	1014,0	0,7	25,4	160,0	15,10
	B-14	150	400	150	43,6	-	1,1	C-W	75,70	1014,0	0,7	25,4	220,0	15,10
Casas et al. (2007)	TFC-2	150	225	150	40,0	2338	0,5	C-W	105,00	1400,0	0,4	80	18,9	5,42
	CFK2-2	150	225	150	40,0	10920	0,5	C-P	150,00	2200,0	1,4	100	39,4	12,60
	CFK2-4	150	225	150	40,0	10920	0,5	C-P	150,00	2200,0	1,3	100	26,3	13,13
Chajes et al. (1996)	C1	228,6	-	152,4	36,1	5172	-	G-W	108,48	1655	1,016	25,4	76,2	8,46
	C2	228,6	-	152,4	47,1	5172	-	G-W	108,48	1655	1,016	25,4	76,2	9,93
	C3	228,6	-	152,4	47,1	5172	-	G-W	108,48	1655	1,016	25,4	76,2	10,64
	C4	228,6	-	152,4	47,1	5172	-	G-W	108,48	1655	1,016	25,4	76,2	10,64
	C5	228,6	-	152,4	43,6	2207	-	G-W	108,48	1655	1,016	25,4	76,2	10,53
	C6	228,6	-	152,4	43,6	234	-	G-W	108,48	1655	1,016	25,4	76,2	8,96
	C7	228,6	-	152,4	43,6	234	-	G-W	108,48	1655	1,016	25,4	76,2	9,61
	C8	228,6	-	152,4	43,6	1584	-	G-W	108,48	1655	1,016	25,4	76,2	10,52
	C9	228,6	-	152,4	24,0	1584	-	G-W	108,48	1655	1,016	25,4	76,2	11,20
	C10	228,6	-	152,4	28,9	1584	-	G-W	108,48	1655	1,016	25,4	76,2	9,87
	C11	228,6	-	152,4	43,7	1584	-	G-W	108,48	1655	1,016	25,4	76,2	9,34
	C12	228,6	-	152,4	36,4	1584	-	G-W	108,48	1655	1,016	25,4	76,2	11,20
	C13	228,6	-	152,4	36,4	1584	-	G-W	108,48	1655	1,016	25,4	50,8	8,09
	C14	228,6	-	152,4	36,4	1584	-	G-W	108,48	1655	1,016	25,4	101,6	12,81
	C15	152,4	-	152,4	36,4	1584	-	G-W	108,48	1655	1,016	25,4	152,4	11,92
	C16	152,4	-	152,4	36,4	1584	-	G-W	108,48	1655	1,016	25,4	203,2	11,57

Figure C.12: Database for prism tests. Bizindavyi et al. (1999) [7], Casas and Pascual [13], Chajes et al. [15].

		b [mm]	h [mm]	t [mm]	f_c' [MPa]	E_s [MPa]	t_s [mm]	Type [k]	E_{fm} [GPa]	f_{fm} [MPa]	t_{fm} [mm]	b_{fm} [mm]	L_{dm} [mm]	P_u [kN]
Kamiharako (2006)	S1-4	100	-	100	36,3	-	-	C-W	270,00	-	0,1	20	175	8,78
	S1-5	100	-	100	34,9	-	-	C-W	270,00	-	0,1	30	100	12,89
	S1-7	100	-	100	38,8	-	-	C-W	270,00	-	0,1	30	250	12,83
	S1-9	100	-	100	41,5	-	-	C-W	270,00	-	0,1	70	175	29,84
	S1-10	100	-	100	41,5	-	-	C-W	270,00	-	0,1	90	175	29,38
Lee et al. (2003)	B50	100	-	100	28,9	12800	1,0	C-W	165,00	-	1,5	42	50,0	10,60
	B75	100	-	100	29,0	12800	1,0	C-W	165,00	-	1,5	42	75,0	13,10
	B97	100	-	100	28,1	12800	1,0	C-W	165,00	-	1,5	42	93,0	16,95
Maeda et al. (1997)	M1	100	-	100	40,8	5000	-	CFS-	230,00	3500	0,11	50	75	5,80
	M2	100	-	100	40,8	5000	-	CFS-	230,00	3500	0,11	50	150	9,20
	M3	100	-	100	43,3	5000	-	CFS-	230,00	3500	0,11	50	300	11,95
	M4	100	-	100	42,4	5000	-	CFS-	230,00	3500	0,165	50	75	10,00
	M6	100	-	100	42,7	5000	-	CFS-	230,00	3500	0,22	50	65	9,50
	M7	100	-	100	42,7	5000	-	CFS-	230,00	3500	0,22	50	150	16,25
	M8	100	-	100	44,7	5000	-	CFS-	230,00	3500	0,11	50	700	10,00
Nakaba et al. (2001)	C5-SCFH1	100	300	100	57,6	-	-	C-W	261,10	4200	0,2	50	300	25,63
	C5-SCFH2	100	300	100	57,6	-	-	C-W	261,10	4200	0,2	50	300	25,33
	C5-SCFH3	100	300	100	57,6	-	-	C-W	261,10	4200	0,2	50	300	27,24
	C5-SCF2	100	300	100	57,6	-	-	C-W	261,10	4200	0,2	50	300	15,24
	C5-SCF3	100	300	100	57,6	-	-	C-W	261,10	4200	0,2	50	300	16,57
	C5-SCFL1	100	300	100	57,6	-	-	C-W	261,10	4200	0,2	50	300	11,94
	C5-SCFL3	100	300	100	57,6	-	-	C-W	261,10	4200	0,2	50	300	12,23
	C5-HCF1	100	300	100	57,6	-	-	C-W	425,10	4400	0,2	50	300	18,88
	C5-HCF3	100	300	100	57,6	-	-	C-W	425,10	4400	0,2	50	300	16,25
	C5-ARF1	100	300	100	57,6	-	-	A-W	124,50	2800	0,2	50	300	12,76
	C5-ARF2	100	300	100	57,6	-	-	A-W	124,50	2800	0,2	50	300	12,50
	C5-ARF3	100	300	100	57,6	-	-	A-W	124,50	2800	0,2	50	300	10,89
	M5-SCFH1	100	300	100	50,0	-	-	C-W	261,10	4200	0,2	50	300	20,64
	M5-SCFH2	100	300	100	50,0	-	-	C-W	261,10	4200	0,2	50	300	22,29
	M5-SCFH3	100	300	100	50,0	-	-	C-W	261,10	4200	0,2	50	300	23,20
	M5-SCF1	100	300	100	50,0	-	-	C-W	261,10	4200	0,2	50	300	15,25
	M5-SCF2	100	300	100	50,0	-	-	C-W	261,10	4200	0,2	50	300	16,86
	M5-SCF3	100	300	100	50,0	-	-	C-W	261,10	4200	0,2	50	300	16,29

Figure C.13: Database for prism tests. Kamiharako [32], Lee et al. [12], Maeda et al. [16], Nakaba et al. [35].

		b [mm]	h [mm]	t [mm]	f'_c [MPa]	E_s [MPa]	t_s [mm]	Type [k]	E_{fm} [GPa]	f_{fm} [MPa]	t_{fm} [mm]	b_{fm} [mm]	L_{fm} [mm]	P_u [kN]
Nakaba et al. (2001)	M5-SCFL1	100	300	100	50,0	-	-	C-W	261,10	4200	0,2	50	300	8,75
	M5-SCFL2	100	300	100	50,0	-	-	C-W	261,10	4200	0,2	50	300	8,06
	M5-SCFL3	100	300	100	50,0	-	-	C-W	261,10	4200	0,2	50	300	9,99
	M5-HCF2	100	300	100	50,0	-	-	C-W	425,10	4400	0,2	50	300	16,25
	M5-HCF3	100	300	100	50,0	-	-	C-W	425,10	4400	0,2	50	300	14,64
	M5-ARF1	100	300	100	50,0	-	-	A-W	124,50	2800	0,2	50	300	12,57
	M5-ARF2	100	300	100	50,0	-	-	A-W	124,50	2800	0,2	50	300	11,98
	M5-ARF3	100	300	100	50,0	-	-	A-W	124,50	2800	0,2	50	300	11,70
	C2-SCF1	100	300	100	23,8	-	-	C-W	261,10	4200	0,2	50	300	13,91
	C2-SCF2	100	300	100	23,8	-	-	C-W	261,10	4200	0,2	50	300	12,81
	C2-SCF3	100	300	100	23,8	-	-	C-W	261,10	4200	0,2	50	300	14,95
	C2P-SCF1	100	300	100	23,8	-	-	C-W	261,10	4200	0,2	50	300	14,22
	C2P-SCF2	100	300	100	23,8	-	-	C-W	261,10	4200	0,2	50	300	14,79
	C2P-SCF3	100	300	100	23,8	-	-	C-W	261,10	4200	0,2	50	300	12,62
Sharma et al. (2006)	GFRP-32.7-100	100	500	100	35,8	-	-	G-W	32,70	384	4,0	30	100	12,50
	GFRP-32.7-150	100	500	100	35,8	-	-	G-W	32,70	384	4,0	30	150	17,74
	GFRP-32.7-175	100	500	100	35,8	-	-	G-W	32,70	384	4,0	30	175	20,50
	GFRP-32.7-200	100	500	100	35,8	-	-	G-W	32,70	384	4,0	30	200	20,60
	GFRP-32.7-250	100	500	100	35,8	-	-	G-W	32,70	384	4,0	30	250	20,40
	GFRP-32.7-300	100	500	100	35,8	-	-	G-W	32,70	384	4,0	30	300	14,98
	C165-100	100	500	100	29,7	-	-	C-W	165,00	2800	1,2	50	100	18,25
	C165-130	100	500	100	29,7	-	-	C-W	165,00	2800	1,2	50	130	24,50
	C165-150	100	500	100	29,7	-	-	C-W	165,00	2800	1,2	50	150	28,44
	C165-175	100	500	100	29,7	-	-	C-W	165,00	2800	1,2	50	175	32,00
	C165-200	100	500	100	29,7	-	-	C-W	165,00	2800	1,2	50	200	34,22
	C165-250	100	500	100	29,7	-	-	C-W	165,00	2800	1,2	50	250	33,14
	C165-300	100	500	100	29,7	-	-	C-W	165,00	2800	1,2	50	300	34,24
	C210-150	100	500	100	35,8	-	-	C-W	210,00	2400	1,2	50	150	30,40
	C210-180	100	500	100	35,8	-	-	C-W	210,00	2400	1,2	50	180	34,00
	C210-190	100	500	100	35,8	-	-	C-W	210,00	2400	1,2	50	190	36,00
	C210-200	100	500	100	35,8	-	-	C-W	210,00	2400	1,2	50	200	36,02
	C210-230	100	500	100	35,8	-	-	C-W	210,00	2400	1,2	50	230	37,02
	C210-255	100	500	100	35,8	-	-	C-W	210,00	2400	1,2	50	255	36,80

Figure C.14: Database for prism tests. Nakaba et al. [35], Sharma et al. [51].

		b [mm]	h [mm]	t [mm]	f_c' [MPa]	E_s [MPa]	t_s [mm]	Type [k]	E_{frp} [GPa]	f_{frp} [MPa]	t_{frp} [mm]	b_{frp} [mm]	L_{frp} [mm]	P_u [kN]
Sharma et al. (2006)	C300-160	100	500	100	29,7	-	-	C-W	300,00	1300	1,2	50	160	38,02
	C300-180	100	500	100	29,7	-	-	C-W	300,00	1300	1,2	50	180	41,15
	C300-200	100	500	100	29,7	-	-	C-W	300,00	1300	1,2	50	200	46,35
	C300-250	100	500	100	29,7	-	-	C-W	300,00	1300	1,2	50	250	45,50
	C300-300	100	500	100	29,7	-	-	C-W	300,00	1300	1,2	50	300	45,95
Täljsten et al (1997)	C100 50A	200	-	200	54,1	6700	-	C-P	170,00	2497,0	1,25	50	100	17,30
	C200 50A	200	-	200	59,8	6700	-	C-P	170,00	2497,0	1,25	50	200	27,50
	C300 50A	200	-	200	65,8	6700	-	C-P	170,00	2497,0	1,25	50	300	35,10
	C400 50A	200	-	200	65,8	6700	-	C-P	170,00	2497,0	1,25	50	400	26,90
Toutanji et al. (2007)	I-1	200	200	130	17,0	4100	-	C-W	110,00	660	0,495	50	100	7,56
	I-2	200	200	130	17,0	4100	-	C-W	110,00	660	0,66	50	100	9,29
	I-3	200	200	130	17,0	4100	-	C-W	110,00	660	0,825	50	100	11,64
	I-4	200	200	130	17,0	4100	-	C-W	110,00	660	0,99	50	100	12,86
	II-1	200	200	130	46,2	4100	-	C-W	110,00	660	0,495	50	100	12,55
	II-2	200	200	130	46,2	4100	-	C-W	110,00	660	0,66	50	100	14,25
	II-3	200	200	130	46,2	4100	-	C-W	110,00	660	0,825	50	100	17,72
	II-4	200	200	130	46,2	4100	-	C-W	110,00	660	0,99	50	100	18,86
	III-1	200	200	130	61,5	4100	-	C-W	110,00	660	0,495	50	100	13,24
	III-2	200	200	130	61,5	4100	-	C-W	110,00	660	0,66	50	100	15,17
	III-3	200	200	130	61,5	4100	-	C-W	110,00	660	0,825	50	100	18,86
	III-4	200	200	130	61,5	4100	-	C-W	110,00	660	0,99	50	100	19,03
Yao et al. (2005)	III-7	150	-	150	27,7	-	-	G-P	22,50	351,0	1,3	25,3	100,0	4,78
	III-8	150	-	150	27,7	-	-	G-P	22,50	351,0	1,3	50,6	100,0	8,02
	I1	150	-	150	23,0	-	-	C-W	256,00	4114,0	0,2	25	75,0	4,75
	I2	150	-	150	23,0	-	-	C-W	256,00	4114,0	0,2	25	85,0	5,69
	I3	150	-	150	23,0	-	-	C-W	256,00	4114,0	0,2	25	95,0	5,76
	I4	150	-	150	23,0	-	-	C-W	256,00	4114,0	0,2	25	95,0	5,76
	I5	150	-	150	23,0	-	-	C-W	256,00	4114,0	0,2	25	95,0	6,17
	I6	150	-	150	23,0	-	-	C-W	256,00	4114,0	0,2	25	115,0	5,96
	I7	150	-	150	23,0	-	-	C-W	256,00	4114,0	0,2	25	145,0	5,95
	I8	150	-	150	23,0	-	-	C-W	256,00	4114,0	0,2	25	190,0	6,68
	I9	150	-	150	23,0	-	-	C-W	256,00	4114,0	0,2	25	190,0	6,35
	I10	150	-	150	23,0	-	-	C-W	256,00	4114,0	0,2	25	95,0	6,17

Figure C.15: Database for prism tests. Sharma et al. [51], Täljsten et al. [16], Toutanji et al. [62], Yao et al. [65].

		b [mm]	h [mm]	t [mm]	f'_c [MPa]	E_a [MPa]	t_a [mm]	Type [k]	E_{frp} [GPa]	f_{frp} [MPa]	t_{frp} [mm]	b_{frp} [mm]	L_{frp} [mm]	P_u [kN]
Yao et al. (2005)	I11	150	-	150	23,0	-	-	C-W	256,00	4114,0	0,2	25	75,0	5,72
	I12	150	-	150	23,0	-	-	C-W	256,00	4114,0	0,2	25	85,0	6,00
	I13	150	-	150	23,0	-	-	C-W	256,00	4114,0	0,2	25	95,0	6,14
	I14	150	-	150	23,0	-	-	C-W	256,00	4114,0	0,2	25	115,0	6,19
	I15	150	-	150	23,0	-	-	C-W	256,00	4114,0	0,2	25	145,0	6,27
	I16	150	-	150	23,0	-	-	C-W	256,00	4114,0	0,2	25	190,0	7,03
	II-1	150	-	150	22,9	-	-	C-W	256,00	4114,0	0,2	25,0	95,0	5,20
	II-2	150	-	150	22,9	-	-	C-W	256,00	4114,0	0,2	25	95,0	6,75
	II-3	150	-	150	22,9	-	-	C-W	256,00	4114,0	0,2	25	95,0	5,51
	II-4	150	-	150	22,9	-	-	C-W	256,00	4114,0	0,2	25	190,0	7,02
	II-5	150	-	150	22,9	-	-	C-W	256,00	4114,0	0,2	25	190,0	7,07
	II-6	150	-	150	22,9	-	-	C-W	256,00	4114,0	0,2	25	190,0	6,98
	III-1	150	-	150	27,1	-	-	C-W	256,00	4114,0	0,2	25	100,0	5,94
	III-2	150	-	150	27,1	-	-	C-W	256,00	4114,0	0,2	50	100,0	11,66
	III-3	150	-	150	27,1	-	-	C-W	256,00	4114,0	0,2	75	100,0	14,63
	III-4	150	-	150	27,1	-	-	C-W	256,00	4114,0	0,2	100	100,0	19,07
	IV-1	150	-	150	18,9	-	-	C-W	256,00	4114,0	0,2	25	95,0	5,86
	IV-2	150	-	150	18,9	-	-	C-W	256,00	4114,0	0,2	25	95,0	5,90
	IV-3	150	-	150	19,8	-	-	C-W	256,00	4114,0	0,2	25	95,0	5,43
	IV-4	150	-	150	19,8	-	-	C-W	256,00	4114,0	0,2	25	95,0	5,76
	IV-5	150	-	150	18,9	-	-	C-W	256,00	4114,0	0,2	25	95,0	5,00
	IV-6	150	-	150	19,8	-	-	C-W	256,00	4114,0	0,2	25	95,0	7,08
	IV-7	150	-	150	18,9	-	-	C-W	256,00	4114,0	0,2	25	95,0	5,50
	IV-8	150	-	150	19,8	-	-	C-W	256,00	4114,0	0,2	25	95,0	5,93
	IV-9	150	-	150	18,9	-	-	C-W	256,00	4114,0	0,2	25	95,0	5,38
	IV-10	150	-	150	19,8	-	-	C-W	256,00	4114,0	0,2	25	95,0	6,60
	IV-11	150	-	150	18,9	-	-	C-W	256,00	4114,0	0,2	25	95,0	5,51
	IV-12	150	-	150	19,8	-	-	C-W	256,00	4114,0	0,2	25	95,0	5,67
	IV-13	150	-	150	18,9	-	-	C-W	256,00	4114,0	0,2	25	95,0	6,31
	IV-14	150	-	150	19,8	-	-	C-W	256,00	4114,0	0,2	25	95,0	6,19
	V-1	150	-	150	21,1	-	-	C-W	256,00	4114,0	0,2	15	95,0	3,81
	V-2	150	-	150	21,1	-	-	C-W	256,00	4114,0	0,2	15	95,0	4,41
	V-3	150	-	150	21,1	-	-	C-W	256,00	4114,0	0,2	25	95,0	6,26

Figure C.16: Database for prism tests. Yao et al. [65].

		b [mm]	h [mm]	t [mm]	f'_c [MPa]	E_a [MPa]	t_a [mm]	Type [k]	E_{frp} [GPa]	f_{frp} [MPa]	t_{frp} [mm]	b_{frp} [mm]	L_{frp} [mm]	P_u [kN]
Yao et al. (2005)	V-4	150	-	150	21,1	-	-	C-W	256,00	4114,0	0,2	50	95,0	12,22
	V-5	150	-	150	21,1	-	-	C-W	256,00	4114,0	0,2	75	95,0	14,29
	V-6	150	-	150	21,1	-	-	C-W	256,00	4114,0	0,2	100	95,0	15,58
	VII-1	150	-	150	24,9	-	-	C-W	256,00	4114,0	0,2	25	95,0	6,80
	VII-2	150	-	150	24,9	-	-	C-W	256,00	4114,0	0,2	25	95,0	6,80
	VII-3	150	-	150	24,9	-	-	C-W	256,00	4114,0	0,2	25	145,0	7,33
	VII-4	150	-	150	24,9	-	-	C-W	256,00	4114,0	0,2	25	145,0	6,49
	VII-5	150	-	150	24,9	-	-	C-W	256,00	4114,0	0,2	25	190,0	7,07
	VII-6	150	-	150	24,9	-	-	C-W	256,00	4114,0	0,2	25	190,0	7,44
	VII-7	150	-	150	24,9	-	-	C-W	256,00	4114,0	0,2	25	240,0	7,16
	VII-8	150	-	150	24,9	-	-	C-W	256,00	4114,0	0,2	25	240,0	6,24

Figure C.17: Database for prism tests. Yao et al. [65].

C.3 Database of beams failed for I-C induced debonding

The intermediate crack induced debonding database includes 187 beam tests from 38 experimental works. Here, the data without information on resin's characteristics were reported. It was composed by 125 beams reinforced by carbon sheets, 4 beams reinforced by glass sheets and 32 beams reinforced by aramid sheets. They did not use for the models comparison but only to examine the code limitations. The database with resin characteristics was reported in the sixth chapter.

		b	h	a	B	L	d	d'	f'c	Es	fys	As	E's	fy	A's	Type	Efrp	ffrp	tfrp	bfrp	Vexp	type
		[mm]	[mm]	[mm]	[mm]	[mm]	[mm]	[mm]	[MPa]	[GPa]	[MPa]	[mm²]	[GPa]	[MPa]	[mm²]	[-]	[GPa]	[MPa]	[mm]	[mm]	[kN]	of test
Beber et al. (1999)	VR5	120	250	75	783	2349	214	34	33,6	200	565	157	200	565	57	C-	230,0	3400	0,44	120	51,1	f.p.b.t.
	VR6	120	250	75	783	2349	214	34	33,6	200	565	157	200	565	57	C-	230,0	3400	0,44	120	50,3	f.p.b.t.
	VR7	120	250	75	783	2349	214	34	33,6	200	565	157	200	565	57	C-	230,0	3400	0,77	120	62,1	f.p.b.t.
	VR8	120	250	75	783	2349	214	34	33,6	200	565	157	200	565	57	C-	230,0	3400	0,77	120	62	f.p.b.t.
	VR9	120	250	75	783	2349	214	34	33,6	200	565	157	200	565	57	C-	230,0	3400	1,1	120	64,8	f.p.b.t.
	VR10	120	250	75	783	2349	214	34	33,6	200	565	157	200	565	57	C-	230,0	3400	1,1	120	68,5	f.p.b.t.
Benjamin (2005)	L1	152	254	-	2269	4537	229	25	23,3	200	429	398	200	429	157	C-	155,1	2792	1,4	25	39,9	3.p.b.t.
	H1	152	254	-	2269	4537	229	25	23,3	200	429	398	200	429	157	C-	155,1	2792	1,4	25	37,7	3.p.b.t.
	L2	152	254	-	2269	4537	229	25	23,3	200	429	398	200	429	157	C-	155,1	2792	1,4	51	44,3	3.p.b.t.
	L2x1	152	254	-	2269	4537	229	25	23,3	200	429	398	200	429	157	C-	155,1	2792	1,4	51	45,5	3.p.b.t.
	H2	152	254	-	2269	4537	229	25	23,3	200	429	398	200	429	157	C-	155,1	2792	1,4	51	43,5	3.p.b.t.
	H2x1	152	254	-	2269	4537	229	25	23,3	200	429	398	200	429	157	C-	155,1	2792	1,4	51	45,1	3.p.b.t.
	L4	152	254	-	2269	4537	229	25	23,3	200	429	398	200	429	157	C-	155,1	2792	1,4	102	51,8	3.p.b.t.
	H4	152	254	-	2269	4537	229	25	23,3	200	429	398	200	429	157	C-	155,1	2792	1,4	102	49,2	3.p.b.t.
Bonacci & Maalej (2000)	B2	270	400	101	1300	3650	350,2	44,8	22,6	201	485	900	201	485	143	C-	230,0	3400	0,3	250	148	f.p.b.t.
Chan et al. (2001)	B2	250	470	50	1600	4600	430	40	42,4	200	505	628	200	505	402	C-	181,0	3180	1,2	150	142,5	f.p.b.t.
	B3	250	470	50	1600	4600	430	40	42,4	200	505	943	200	505	402	C-	181,0	3180	1,2	150	176	f.p.b.t.
	B6	250	470	50	1600	4600	430	40	42,4	200	505	628	200	505	402	C-	181,0	3180	1,2	150	129	f.p.b.t.
	B8	250	470	50	1600	4600	430	40	42,4	200	505	1257	200	505	402	C-	181,0	3180	1,2	150	220	f.p.b.t.
Chan and Li (2000)	S6-50-0	330	100	-	850	2500	76	-	53,4	200	677	113	200	-	-	C-	165,0	2940,0	1,2	50	14,9	f.p.b.t.
	S8-50-0	330	100	-	850	2500	76	-	53,4	200	653	201	200	-	-	C-	165,0	2940,0	1,2	50	17,9	f.p.b.t.
	S8-50-0F	330	100	-	850	2500	76	-	53,4	200	653	201	200	-	-	C-	165,0	2940,0	1,2	50	16,45	f.p.b.t.
Delaney (2006)	R_UC_C1	150	200	50	820	1800	160	40	49,1	190	477	266	190	477	266	C-	50,5	817	1,4	150	44,4	f.p.b.t.
	R_UC_C2	150	200	50	820	1800	160	40	50,1	190	477	266	190	477	266	C-	50,5	817	1,4	150	49,5	f.p.b.t.
	R_UC_C3	150	200	50	820	1800	160	40	50,2	190	477	266	190	477	266	C-	50,5	817	1,4	150	45,3	f.p.b.t.
	R_UC_C4	150	200	50	820	1800	160	40	50,4	190	477	266	190	477	266	C-	50,5	817	1,4	150	48,5	f.p.b.t.
Esfahani et al. (2006)	B11-20D-1L	150	200	-	600	1600	162	25	24,1	200	350	628	200	365	157	C-W	237,0	2845	0,176	150	54,46	f.p.b.t.
Gao et al. (2004)	A0	150	200	150	500	1500	162	27	35,7	200	531	157	200	531	101	C-	235,0	4200	0,2	75	40,35	f.p.b.t.
	A10	150	200	150	500	1500	162	27	35,7	200	531	157	200	531	101	C-	235,0	4200	0,2	75	39,35	f.p.b.t.
	A20	150	200	150	500	1500	162	27	35,7	200	531	157	200	531	101	C-	235,0	4200	0,2	75	43,95	f.p.b.t.
Kishi et al. (1998)	A200-1	150	250	50	1050	2600	210	40	24,8	206	378	402	206	378	402	A-	126,5	2480	0,1	130	37	f.p.b.t.
	A200-2	150	250	50	1050	2600	210	40	24,8	206	378	402	206	378	402	A-	126,5	2480	0,1	130	38	f.p.b.t.
	A415-1	150	250	50	1050	2600	210	40	24,8	206	378	402	206	378	402	A-	126,5	2480	0,3	130	41,7	f.p.b.t.
	A623-1	150	250	50	1050	2600	210	40	24,8	206	378	402	206	378	402	A-	126,5	2480	0,4	130	39,5	f.p.b.t.

Figure C.18: Intermediate crack induced debonding. Type of test: f.p.b.t.=four point bending test; c.b.t.=cantilever beam test; 3.p.b.t=three point bending test. Beber et al. [68], Benjamin [68], Bonacci and Maalej [8], Chan et al. [68], Chan and Li [68], Delaney (2006) [68], Esfahani et al. [22], Gao et al. [26], Kishi et al. [68]

		b [mm]	h [mm]	a [mm]	B [mm]	L [mm]	d [mm]	d' [mm]	f_c' [MPa]	E_s [GPa]	f_{ys} [MPa]	A_s [mm²]	E_s' [GPa]	f_y [MPa]	A_s' [mm²]	Type [-]	E_{fm} [GPa]	f_{fm} [MPa]	t_{fm} [mm]	b_{fm} [mm]	V_{exp} [kN]	type of test
Kishi et al. (1998)	A623-2	150	250	50	1050	2600	210	40	24,8	206	378	402	206	378	402	A-	126,5	2480	0,4	130	40,25	f.p.b.t.
	C300-1	150	250	50	1050	2600	210	40	24,8	206	378	402	206	378	402	C-	230,5	4070	0,2	130	39,6	f.p.b.t.
	C300-2	150	250	50	1050	2600	210	40	24,8	206	378	402	206	378	402	C-	230,5	4070	0,2	130	37,5	f.p.b.t.
	C445-1	150	250	50	1050	2600	210	40	24,8	206	378	402	206	378	402	C-	230,5	4070	0,2	130	42	f.p.b.t.
	C445-2	150	250	50	1050	2600	210	40	24,8	206	378	402	206	378	402	C-	230,5	4070	0,2	130	41,4	f.p.b.t.
Kishi et al. (2003)	A-250-1	150	250	100	1050	2600	210	40	29,6	210	406	402	210	406	402	A-	118,0	2060	0,3	130	42,1	f.p.b.t.
	A-400-2	150	400	100	1050	2600	360	40	29,6	210	406	402	210	406	402	A-	118,0	2060	0,6	130	80	f.p.b.t.
Kotynia (2005)	B-08/S1	150	300	150	800	3000	270	30	33,8	195	490	339	195	490	157	C-	172,0	2915	1,2	80	90	f.p.b.t.
	BF-040.5S	150	300	150	1500	3000	270	30	33,0	199	421	157	199	421	157	C-	172,0	2915	1,2	40	48	3.p.b.t.
	BF-06'S	150	300	150	1500	3000	270	30	32,5	195	490	226	195	490	157	C-	172,0	2915	1,2	80	86	3.p.b.t.
	B-08/M	150	300	75	1400	4200	270	30	37,3	220	436	339	220	436	157	C-	220,0	2742	1,4	120	70	f.p.b.t.
	B-08/S2	150	300	75	1400	4200	270	30	32,3	220	436	339	220	436	157	C-	172,0	2915	1,2	50	47	f.p.b.t.
	B-083m	150	300	75	1400	4200	270	30	34,4	220	436	339	220	436	157	C-	170,0	2915	0,4	150	46	f.p.b.t.
Kurihashi et al. (1999)	B0-A	150	250	100	1100	2200	200	50	23,9	206	364	266	206	364	266	A-	126,5	2480	0,3	80	56,1	3.p.b.t.
	B40-A	150	250	100	1100	2600	200	50	23,9	206	364	266	206	364	266	A-	126,5	2480	0,3	80	26,15	f.p.b.t.
	B0-C	150	250	100	1100	2200	200	50	23,9	206	364	266	206	364	266	C-	126,5	4070	0,2	80	55,1	3.p.b.t.
Kurihashi et al. (2000)	R7-2	150	250	100	1450	3400	210	40	28,2	206	378	402	206	378	402	A-	126,5	2480	0,6	130	34,95	f.p.b.t.
	R6-2	150	250	100	1260	3020	210	40	28,2	206	378	402	206	378	402	A-	126,5	2480	0,6	130	41,3	f.p.b.t.
	R5-2	150	250	100	1050	2600	210	40	28,2	206	378	402	206	378	402	A-	126,5	2480	0,6	130	46,5	f.p.b.t.
	R4-2	150	250	100	840	2180	210	40	28,2	206	378	402	206	378	402	A-	126,5	2480	0,6	130	58,6	f.p.b.t.
	R3-2	150	250	100	650	1800	210	40	28,2	206	378	402	206	378	402	A-	126,5	2480	0,6	130	77,55	f.p.b.t.
Leung (2004)	B11	300	800	800	2400	7200	740	60	41,5	200	526	2513	200	526	1030	C-	235,0	4200	0,9	300	508,8	f.p.b.t.
	B12	300	800	800	2400	7200	740	60	41,5	200	526	2513	200	526	1030	C-	235,0	4200	0,9	300	516,5	f.p.b.t.
	B21	150	400	400	1200	3600	370	30	41,5	200	535	603	200	535	226	C-	235,0	4200	0,4	150	137,2	f.p.b.t.
	B22	150	400	400	1200	3600	370	30	41,5	200	535	603	200	535	226	C-	235,0	4200	0,4	150	136,3	f.p.b.t.
	B31	75	200	200	600	1800	170	30	41,5	200	599	157	200	599	101	C-	235,0	4200	0,2	75	32,1	f.p.b.t.
	B32	75	200	200	600	1800	170	30	41,5	200	599	157	200	599	101	C-	235,0	4200	0,2	75	32,15	f.p.b.t.
	B41	75	200	200	600	1800	185	15	41,5	200	599	157	200	599	101	C-	235,0	4200	0,2	75	34,8	f.p.b.t.
	B42	75	200	200	600	1800	185	15	41,5	200	599	157	200	599	101	C-	235,0	4200	0,2	75	37,85	f.p.b.t.
	NB1-8	300	800	60	2400	7200	740	60	29,0	200	519	2513	200	519	1030	C-	235,0	4200	0,9	300	512	f.p.b.t.
	NB1-16	300	800	60	2400	7200	740	60	29,0	200	519	2513	200	519	1030	C-	235,0	4200	1,8	300	548,5	f.p.b.t.
	NB2-2	150	400	30	1200	3600	370	30	29,0	200	521	603	200	521	226	C-	235,0	4200	0,2	150	108,1	f.p.b.t.
	NB2-4	150	400	30	1200	3600	370	30	29,0	200	521	603	200	521	226	C-	235,0	4200	0,4	150	119,6	f.p.b.t.

Figure C.19: Intermediate crack induced debonding. Type of test: f.p.b.t.=four point bending test; c.b.t.=cantilever beam test; 3.p.b.t=three point bending test. Kishi et al. [68], Kishi et al. [68], Kotynia [68], Kurihashi et al. [68], Kurihashi et al. [68], Leung [68].

		b	h	a	B	L	d	d'	f_c'	E_s	f_{ys}	A_s	E_s'	f_y	A_s'	Type	E_{frp}	f_{frp}	t_{frp}	b_{frp}	V_{exp}	type
		[mm]	[mm]	[mm]	[mm]	[mm]	[mm]	[mm]	[MPa]	[GPa]	[MPa]	[mm²]	[GPa]	[MPa]	[mm²]	[-]	[GPa]	[MPa]	[mm]	[mm]	[kN]	of test
Leung (2004)	NB2-6	150	400	30	1200	3600	370	30	29,0	200	521	603	200	521	226	C-	235,0	4200	0,7	150	127,6	f.p.b.t.
	NB2-8	150	400	30	1200	3600	370	30	29,0	200	521	603	200	521	226	C-	235,0	4200	0,9	150	138	f.p.b.t.
	NB3-2	75	200	15	600	1800	185	15	29,0	200	599	157	200	599	101	C-	235,0	4200	0,2	75	34,45	f.p.b.t.
	NB3-4	75	200	15	600	1800	185	15	29,0	200	599	157	200	599	101	C-	235,0	4200	0,4	75	37,2	f.p.b.t.
Maalej and Leong (2005)	A3	115	146	25	500	1500	120	26	42,8	180	547	236	180	547	157	C-	235,0	3550	0,2	108	38,75	f.p.b.t.
	A4	115	146	25	500	1500	120	26	42,8	180	547	236	180	547	157	C-	235,0	3550	0,2	108	37,75	f.p.b.t.
	A5	115	146	25	500	1500	120	26	42,8	180	547	236	180	547	157	C-	235,0	3550	0,3	108	43,7	f.p.b.t.
	A6	115	146	25	500	1500	120	26	42,8	180	547	236	180	547	157	C-	235,0	3550	0,3	108	42,9	f.p.b.t.
	B3	230	292	50	1000	3000	240	52	42,8	183	544	943	183	544	628	C-	235,0	3550	0,3	216	131,8	f.p.b.t.
	B4	230	292	50	1000	3000	240	52	42,8	183	544	943	183	544	628	C-	235,0	3550	0,3	216	130,2	f.p.b.t.
	B5	230	292	50	1000	3000	240	52	42,8	183	544	943	183	544	628	C-	235,0	3550	0,7	216	147,4	f.p.b.t.
	B6	230	292	50	1000	3000	240	52	42,8	183	544	943	183	544	628	C-	235,0	3550	0,7	216	142,2	f.p.b.t.
	C3	368	467,2	80	1600	4800	384	83,2	42,4	181	552	2413	181	552	1609	C-	235,0	3550	0,5	368	326,5	f.p.b.t.
	C4	368	467,2	80	1600	4800	384	83,2	42,4	181	552	2413	181	552	1609	C-	235,0	3550	0,5	368	334,7	f.p.b.t.
Maeda et al. (2001)	SP-C	200	200	30	750	1800	165	35	35,0	200	360	266	200	360	266	C-	236,0	4120	0,2	200	39,15	f.p.b.t.
	SP-C2	200	200	30	750	1800	165	35	35,0	200	360	266	200	360	266	C-	236,0	4120	0,3	200	54,5	f.p.b.t.
Matthys (2000)	BF2	200	450	70	1250	3800	409	-	36,5	200	590	804	200	-	-	C-	159,0	3200	1,2	100	185	f.p.b.t.
	BF3	200	450	70	1250	3800	409	-	34,9	200	590	804	200	-	-	C-	159,0	3200	1,2	100	186	f.p.b.t.
	BF8	200	450	70	1250	3800	409	-	39,4	200	590	402	200	-	-	C-	159,0	3200	1,2	100	111,3	f.p.b.t.
	BF9	200	450	70	1250	3800	409	-	33,7	200	590	402	200	-	-	C-	233,0	3200	0,2	100	95,8	f.p.b.t.
M'Bazaa et al. (1996)	P111	200	300	50	1000	3000	240	-	44,3	200	439	157	200	-	-	C-	82,0		0,9	167	49,9	f.p.b.t.
Mikami et al. (1999)	A-140	150	250	100	1500	3000	200	50	23,9	200	364	266	200	364	266	C-	126,5	2480	0,3	80	40,2	3.p.b.t.
Niu et al. (2006)	A1	960	203	475	2100	4200	168	-	31,6	192	452	861	192	-	-	C-	184,0	2446	1,3	200	127,8	3.p.b.t.
	A2	960	203	475	2100	4200	168	-	33,4	192	452	861	192	-	-	C-	195,0	2384	1,2	200	130,4	3.p.b.t.
	A3	960	203	475	2100	4200	168	-	35,2	192	452	861	192	-	-	C-	80,4	724	1,4	300	102,7	3.p.b.t.
	A4	960	203	475	2100	4200	168	-	34,4	192	452	861	192	-	-	C-	108,5	859	2,6	300	133,7	3.p.b.t.
	A5	960	203	475	2100	4200	168	-	35,9	192	452	861	192	-	-	C-	108,5	859	2,6	200	107,4	3.p.b.t.
	A6	960	203	475	2100	4200	168	-	35,1	192	452	861	192	-	-	C-	80,4	724	1,4	200	93,7	3.p.b.t.
	B1	960	203	475	1600	4200	168	-	35,2	192	452	861	192	-	-	C-	184,0	2446	1,3	200	71,85	f.p.b.t.
	B2	960	203	475	1600	4200	168	-	34,5	192	452	861	192	-	-	C-	80,4	724	1,4	300	56,7	f.p.b.t.
	B3	960	203	475	1600	4200	168	-	34,7	192	452	861	192	-	-	C-	80,4	724	1,4	200	54,15	f.p.b.t.
	C2	960	203	475	2100	4200	168	-	33,3	196	446	896	196	-	-	C-	184,0	2446	1,3	200	133,8	3.p.b.t.
	C3	960	203	475	2100	4200	168	-	34,1	196	446	896	196	-	-	C-	80,4	724	1,4	300	107,2	3.p.b.t.

Figure C.20: Intermediate crack induced debonding. Type of test: f.p.b.t.=four point bending test; c.b.t.=cantilever beam test; 3.p.b.t=three point bending test. Leung [68], Maalej and Leong [68], Maeda et al. [68], Matthys [68], M'Bazaa et al. [68], Mikami et al. [68], Niu et al [37].

		b [mm]	h [mm]	a [mm]	B [mm]	L [mm]	d [mm]	d' [mm]	f_c' [MPa]	E_s [GPa]	f_{ys} [MPa]	A_s [mm²]	E_s' [GPa]	f_y' [MPa]	A_s' [mm²]	Type [-]	E_{fm} [GPa]	f_{fm} [MPa]	t_{fm} [mm]	b_{fm} [mm]	V_{exp} [kN]	type of test
Niu et al. (2006)	C4	960	203	475	2100	4200	168	-	34,5	196	446	896	196	-	-	C-	80,4	724	1,4	200	90,5	3.p.b.t.
Seim et al. (2001)	S11	480	102	100	1015	2030	81	-	33,2	205	462	214	205	-	-	C-	198,0	2270	1,2	100	40,8	3.p.b.t.
	S12	480	102	100	1015	2030	81	-	33,2	205	462	214	205	-	-	C-	198,0	2270	1,2	100	42,5	3.p.b.t.
	S5	480	102	100	1015	2030	81	-	33,2	205	462	214	205	-	-	C-	198,0	2270	1,2	100	43,2	3.p.b.t.
	S1m	480	102	285	1015	2030	81	-	33,2	205	462	214	205	-	-	C-	198,0	2270	1,2	100	41,9	3.p.b.t.
	C12	480	102	100	1015	2030	81	-	33,2	205	462	214	205	-	-	G-	63,8	675	1,1	480	80,8	3.p.b.t.
	C21	480	102	100	1015	2030	81	-	33,2	205	462	214	205	-	-	G-	91,5	724	1,2	480	71,3	3.p.b.t.
Spadea et al. (2001)	A1.1	140	300	50	1800	4800	261	39	27,4	200	435	402	200	435	402	G-	152,0	2300	1,2	80	43,4	f.p.b.t.
	A3.1	140	300	50	1800	4800	263	37	28,5	200	435	402	200	435	402	C-	152,0	2300	1,2	80	37,4	f.p.b.t.
Takahashi and Sato (2003)	F1	200	300	50	700	1600	250	50	35,8	200	371	573	200	371	63	C-	230,0	3480	0,2	200	113,5	f.p.b.t.
	F2	200	300	50	700	1600	250	50	40,2	200	371	573	200	371	63	C-	230,0	3480	0,3	200	122	f.p.b.t.
	F3	200	300	50	700	1600	250	50	39,0	200	371	573	200	371	63	C-	230,0	3480	0,5	200	135	f.p.b.t.
	F5	200	300	50	700	1600	250	50	50,3	200	371	573	200	371	63	C-	230,0	3480	0,3	200	139	f.p.b.t.
	F6	200	300	50	700	1600	250	50	49,5	200	371	573	200	371	63	C-	230,0	3480	0,5	200	155,5	f.p.b.t.
Takeo et al. (1999)	No.2	160	260	70	1000	2000	225	35	31,3	200	356	266	200	356	266	C-	230,0	3480	0,2	140	33,85	3.p.b.t.
	No.3	160	260	70	800	2000	225	35	31,3	200	356	266	200	356	266	C-	230,0	3480	0,2	140	38,35	f.p.b.t.
	No.4	160	260	70	700	2000	225	35	31,3	200	356	266	200	356	266	C-	230,0	3480	0,2	140	43,5	f.p.b.t.
	No.5	160	260	70	550	2000	225	35	39,0	200	356	266	200	356	266	C-	230,0	3480	0,2	140	66	f.p.b.t.
	No.6	160	260	70	1000	2000	225	35	39,0	200	356	266	200	356	266	C-	230,0	3480	0,2	140	78,6	3.p.b.t.
	No.7	160	260	70	1000	2000	225	35	39,0	200	356	266	200	356	266	C-	230,0	3480	0,2	140	85,6	3.p.b.t.
Teng and Yao (2007)	CS-W50	150,6	255,3	50	500	1500	222,8	32,5	32,8	199	536	157,1	199	536	157,1	C-W	256,0	4114	2,01	50	71,3	f.p.b.t.
	GS	151,1	252,2	50	500	1500	217,7	34,5	32,3	199	536	157,1	199	536	157,1	G-W	22,5	351	1,67	148	82	f.p.b.t.
Wu et al. (1999)	H-s CFRP	150	200	50	600	1800	150	50	33,8	210	390	402	210	390	266	C-	230,0	4200	0,3	150	68,25	f.p.b.t.
	H-m CFRP	150	200	50	600	1800	150	50	33,8	210	390	402	210	390	266	C-	290,0	4000	0,3	150	78,45	f.p.b.t.
Wu et al. (2000)	RC-1	150	200	50	900	1800	160	40	30,2	210	360	402	210	360	266	C-	230,0	3200	0,1	140	65	3.p.b.t.
	RC-2	150	200	50	900	1800	160	40	30,2	210	360	402	210	360	266	C-	230,0	3200	0,1	140	68,9	3.p.b.t.
	RCS-1	150	200	50	900	1800	160	40	34,6	210	360	402	210	360	266	C-	230,0	3200	0,222	140	73,5	3.p.b.t.
Yao et al. (2005)	CP4	304,5	150,3	100	1000	1100	120,2	-	46,2	208	343	157	208	-	-	C-	165,0	2800	1,2	50	13,5	c.b.t.
	II-1	303	153	100	1000	1100	117,5	-	25,6	208	349	157	208	-	-	C-	257,0	4519	0,2	30	7.2	c.b.t.
	I-2	305	149	100	1000	1100	116,5	-	25,3	208	332	157	208	-	-	C-	257,0	4519	0,2	50	8,4	c.b.t.
	II-3	305	150	100	1000	1100	117,5	-	30,2	208	332	157	208	-	-	C-	257,0	4519	0,2	70	8,9	c.b.t.
	II-4	302	150	100	1000	1100	118,7	-	21,9	208	332	157	208	-	-	C-	257,0	4519	0,2	90	10,2	c.b.t.
	II-8	203,5	152	100	1000	1100	114,5	-	23,8	208	364	157	208	-	-	C-	257,0	4519	0,2	50	8,4	c.b.t.

Figure C.21: Intermediate crack induced debonding. Type of test: f.p.b.t.=four point bending test; c.b.t.=cantilever beam test; 3.p.b.t=three point bending test. Niu et al. [37], Seim et al. [48], Spadea et al. [54], Takahashi and Sato [68], Takeo et al. [68], Teng and Yao [61], Wu et al. [68], Wu et al. [68],Yao et al. [66]

		b [mm]	h [mm]	a [mm]	B [mm]	L [mm]	d [mm]	d' [mm]	f_c' [MPa]	E_s [GPa]	f_{ys} [MPa]	A_s [mm²]	E'_s [GPa]	f_y [MPa]	A'_s [mm²]	Type [-]	E_{fm} [GPa]	f_{fm} [MPa]	t_{fm} [mm]	b_{fm} [mm]	V_{exp} [kN]	type of test
Yao et al. (2005)	II-9	320	151	100	1000	1100	117	-	22,2	208	332	157	208	-	-	C-	257,0	4519	0,2	30	6,9	c.b.t.
	III-1	203	155	100	1000	2000	121	-	22,5	208	346	157	208	-	-	C-	257,0	4519	0,2	50	15	3.p.b.t.
	III-2	199	156,5	100	1000	2000	122,5	-	21,2	210	373	157	210	-	-	C-	257,0	4519	0,2	100	21,4	3.p.b.t.
	III-4	150,1	153,5	100	1000	2000	122	-	22,4	206	351	157	206	-	-	C-	257,0	4519	0,2	50	18,4	3.p.b.t.
Zarniç et al. (1999)	1	200	300	100	960	2900	270	30	25,0	205	450	339	205	450	226	C-	150,0	2400	1,2	50	58,4	f.p.b.t.
	2	800	120	100	960	2900	105	15	25,0	205	450	339	205	450	156	C-	150,0	2400	1,2	100	31,5	f.p.b.t.
Zhang et al. (2005)	A-1	150	340	100	1200	3000	300	40	31,5	210	407	402	210	407	402	A-	118,0	2060	0,6	130	63,35	f.p.b.t.
	A-2	150	340	100	1200	3000	300	40	31,5	210	407	402	210	407	402	A-	118,0	2060	0,6	130	63,5	f.p.b.t.
	A-3	150	340	100	1200	3000	300	40	31,5	210	407	402	210	407	402	A-	118,0	2060	0,6	130	63,1	f.p.b.t.
	A-4	150	340	100	1200	3000	300	40	31,5	210	407	402	210	407	402	A-	118,0	2060	0,6	130	65,8	f.p.b.t.
	A-5	150	340	100	1200	3000	300	40	31,5	210	407	402	210	407	402	A-	118,0	2060	0,6	130	62,15	f.p.b.t.
	A-6	150	340	100	1200	3000	300	40	31,5	210	407	402	210	407	402	A-	118,0	2060	0,6	130	62,1	f.p.b.t.
	B-2	150	250	100	1050	2600	210	40	31,5	210	407	402	210	407	402	C-	230,0	3400	0,2	130	40,45	f.p.b.t.
	B-3	150	250	100	1050	2600	210	40	31,5	210	407	402	210	407	402	A-	118,0	2060	0,3	130	42,1	f.p.b.t.
	B-4	150	250	100	1050	2600	210	40	31,5	210	407	402	210	407	402	A-	78,5	2350	0,4	130	41,05	f.p.b.t.
	B-6	150	400	100	1050	2600	360	40	31,5	210	407	402	210	407	402	C-	230,0	3400	0,3	130	78,15	f.p.b.t.
	B-7	150	400	100	1050	2600	360	40	31,5	210	407	402	210	407	402	A-	118,0	2060	0,6	130	79,6	f.p.b.t.
	B-8	150	400	100	1050	2600	360	40	31,5	210	407	402	210	407	402	A-	78,5	2350	0,8	130	78,1	f.p.b.t.
	C-1	150	235	100	650	1800	210	40	31,5	210	407	402	210	407	402	A-	118,0	2060	0,6	130	74,95	f.p.b.t.
	C-2	150	250	100	650	1800	210	40	31,5	210	407	402	210	407	402	A-	118,0	2060	0,6	130	75,95	f.p.b.t.
	C-4	150	235	100	1050	2600	210	40	31,5	210	407	402	210	407	402	A-	118,0	2060	0,6	130	45,25	f.p.b.t.
	C-5	150	250	100	1050	2600	210	40	31,5	210	407	402	210	407	402	A-	118,0	2060	0,6	130	47,2	f.p.b.t.
	C-6	150	270	100	1050	2600	205	40	31,5	210	407	402	210	407	402	A-	118,0	2060	0,6	130	48,5	f.p.b.t.
	C-7	150	235	100	1450	3500	210	40	31,5	210	407	402	210	407	402	A-	118,0	2060	0,6	130	34,4	f.p.b.t.
	C-8	150	250	100	1450	3500	210	40	31,5	210	407	402	210	407	402	A-	118,0	2060	0,6	130	34	f.p.b.t.
	C-9	150	270	100	1450	3500	205	40	31,5	210	407	402	210	407	402	A-	118,0	2060	0,6	130	35,4	f.p.b.t.

Figure C.22: Intermediate crack induced debonding. Type of test: f.p.b.t.=four point bending test; c.b.t.=cantilever beam test; 3.p.b.t=three point bending test. Yao et al. [66], Zaniç et al. [68], Zhang et al. [68]